AMBRA1 as a Biomarker and its Functional Crosstalk with Autophagy and Epidermal Differentiation in Cutaneous Squamous Cell Carcinoma Tumourigenesis

Michael Hugh Alexander

Thesis submitted in partial fulfilment of the requirements for the degree of

Doctor of Philosophy

Translational and Clinical Research Institute

Faculty of Medical Science

Newcastle University

December 2021

Abstract.

AMBRA1 as a Biomarker and its Functional Crosstalk with Autophagy and Epidermal Differentiation in Cutaneous Squamous Cell Carcinoma Tumourigenesis

Abstract

Cutaneous Squamous Cell Carcinoma (cSCC) is a skin cancer with an increasing worldwide incidence. While most patients have an excellent prognosis, a subset of patients develop disease recurrence/metastasis, emphasising the need for novel reliable prognostic biomarkers, as well as an improved understanding of the cellular signalling mechanisms underlying cSCC tumourigenesis and progression. Autophagy is essential for cellular homeostasis and keratinocyte differentiation, with the deregulation of both processes being associated with cSCC tumourigenesis. As a key protein to both autophagy and keratinocyte differentiation, the aim of the current study was to define crosstalk between AMBRA1 and the deregulation of these processes in cSCC development and progression and its potential, together with the associated autophagy cargo protein SQSTM1 (p62), as prognostic biomarkers. Biomarker assay development and analysis in a cohort of primary cSCC tumours revealed that loss of cytoplasmic AMBRA1 expression in the tumour growth front, in combination with loss of cytoplasmic p62 expression in the peritumoural epidermis, as putative prognostic biomarkers for cSCC reoccurrence and metastasis, independent of tumour differentiation status. Importantly, the combined loss of these proteins also identified moderately/poorly differentiated primary cSCC tumours at high risk of metastasis. Studies of the potential contribution of cullin E3 ligase-mediated degradation or TGF-β2-mediated downregulation of AMBRA1 in cSCC cell lines revealed only increased levels of TGF-β2 secretion correlated with loss of AMBRA1 expression. Furthermore, although chemical inhibition of TGF-β signalling inhibited cSCC cell proliferation *in vitro*, no effect on AMBRA1 expression levels was observed, suggesting an undefined TGF-β2 independent-mediated mechanism of AMBRA1 loss in cSCC. Studies investigating AMBRA1 involvement in keratinocyte differentiation and autophagy further demonstrated AMBRA1 expression in keratinocytes initially relies on autophagy activation but is later maintained by epidermal differentiation-related calcium signalling. Additional studies also revealed that this calcium-signalling mediated regulation of AMBRA1 expression is lost during cSCC tumourigenesis, likely resulting in the maintenance of a dedifferentiated cell phenotype, facilitating sustained tumour cell proliferation. This further highlights that loss of AMBRA1 expression as a key event in the uncoupling of autophagy and keratinocyte differentiation in cSCC development.

Collectively these data highlight the tumour suppressive role of AMBRA1 in cSCC and its loss of expression in the tumour growth front, in combination with the loss of peritumoural epidermal p62 expression, as a novel prognostic biomarker for cSCC reoccurrence and metastasis.

Declaration

This thesis is submitted for the degree of Doctor of Philosophy at Newcastle University. The research was performed in the Translational and Clinical Research Institute in the Faculty of Medical Science under the primary supervision of Professor Penny Lovat. This thesis is my own work unless otherwise stated within the test. I certify that none of the material offered in this thesis has been submitted by me for a degree or any other qualification at this, or any other university.

Dedication

This thesis is dedicated to my dear sister

Kristen Alexander

Who has always been smarter and stronger than me.

Acknowledgements

The work presented in this thesis was gratefully funded by the European Regional Development Fund, Northern Powerhouse and AMLo Biosciences Ltd.

I would first and foremost like to thank my primary supervisor, Professor Penny Lovat. Since meeting her during my maters project, she has continuously advocated for my personal and professional development. Whilst I believe she only employed me because I had the cleanest bench in the laboratory, I am still incredibly grateful for the opportunities she provided me. During my PhD, she has volunteered much of her own time to help me at every stage of this project and has also afforded me many additional opportunities to grow as a scientist. I will fondly remember the final few months of my PhD, where she ruthlessly excised much of the 'waffle' in my thesis, making it far easier to read.

I would also like to thank Dr Marie Labus. As CEO of AMLo Biosciences ltd. she has given me valuable insight into the operations of a biosciences company and I look forward to watching AMLo grow and succeed under her and Penny's stewardship.

I am also grateful to Professor Guillermo Velasco, and his PhD student, Estibaliz Gabicagogeascoa-Corta, for allowing me to spend five weeks working with them at the Complutense University of Madrid.

All studies in primary cutaneous squamous cell carcinoma tissue were made possible by Dr Niki Stefanos (Addenbrookes Hospital, Cambridge). Not only did she work tireless to source the material that made this work possible but she also sat with me for countless hours to teach me histopathology. During these sessions, she never lost her enthusiasm for my project, purposed countless ideas and provided me some much needed encouragement.

I have had the pleasure to start and complete my PhD within 'Dermatological Sciences' at Newcastle University. Whilst not an official department, this group of scientists have been a pleasure to work with. I would specifically like to thank Dr Ashleigh McConnell, who was both a wonderful mentor and a true friend throughout my PhD. I would also like to thank Dr Tom Ewen, Dr Ioana Cosgarea-McHugh, Grant Richardson, Will Cousins and Krishan Mistry, who have tolerated my presence better than most over the last four years.

I would like to thank my friends. Emily, Moa, and Patrick, who have provided me constant love and support, even when I disappeared for months at a time. I am lucky to have such friends that continue to care for me after all these years.

Finally, and most of all, I would like to thank my mother, Janet, my father, Bob and my sister, Kristen. I love you all and I would not be here without you.

Contents

List of Figures

List of Tables

Abbreviations

ADP – Adenosine Diphosphate

AJCC – American Joint Committee on Cancer

AK – Actinic Keratosis

AKT – Protein Kinase B

ALK – Anaplastic Lymphoma Kinase

AMBRA1 – Activating Molecule in Beclin-1-Regualted Autophagy

AMP - Adenosine Monophosphate

AMPK - Adenosine Monophosphate-Activated Protein Kinase

ANOVA – Analysis of Variance

ATF – Activating Transcription Factor

ATG – Autophagy Associated Gene

ATP - Adenosine Triphosphate

BMP-1 – Bone Morphogenetic Protein 1

BNIP3 - BCL2 Interacting Protein 3

BWH - Brigham and Women's Hospital

CAMKKβ - Calcium/Calmodulin-Dependent Protein Kinase

CaSR – Calcium-sensing Receptor

CCDN1 - Cyclin D1

CD133 - Prominin-1

CDKN2A - Cyclin Dependent Kinase Inhibitor 2A

CI – Confidence Interval

cm – Centimetre

CO_2 – Carbon Dioxide

CQ – Chloroquine

cSCC – Cutaneous Squamous Cell Carcinoma

DAB - 3,3’-Diaminobenzidin

DDB1 - DNA Damage-Binding Protein 1

ddH_2O – Double Distilled Water

DEPTOR - DEP Domain-containing mTOR-interacting Protein

DMEM – Dulbecco’s Modified Eagle Medium

DMSO – Dimethyl Sulfoxide

DNA - Deoxyribonucleic Acid

ECM – Extracellular Matrix

EDTA - Ethylenediaminetetraacetic Acid

EGFR - Epidermal Growth Factor Receptor

EMT – Epithelial-to-Mesenchymal Transition

ER – Endoplasmic Reticulum

ERK – Extracellular Signal-related Kinase

FAB – Fragment Antigen-Binding

Fat1 - Protocadherin FAT1

FBS – Fetal Bovine Serum

FFPE – Formalin-fixed Paraffin-embedded

FGFR – Fibroblast Growth Factor Receptor

FIP200 – Focal Adhesion Kinase Family Interacting Protein of 200 kDa

FKBP12 – FK506-binding Protein

GAPDH - Glyceraldehyde-3-phosphate Dehydrogenase

GPCR – G-protein Coupled Receptor

Grb2 – Growth Factor Receptor-bound Protein 2

hEGF – Human Epithelial Growth Factor

HEPES - 4-(2-hydroxyethyl)-1-piperazineethanesulfonic Acid

HIF1α - Hypoxia-inducible Factor 1-alpha

HKGS – Human Keratinocyte Growth Serum

HPV – Human Papillomavirus

HuCAL – Human Combinatorial Antibody Library

IKK - Inhibitor of Nuclear Factor-κB (IκB) Kinase

INPP5A - Inositol Polyphosphate-5-Phosphatase A

IP3 - Inositol Trisphosphate

LC3 - Microtubule-associated Protein 1A/1B-light Chain 3

LKB1 - Serine/threonine Kinase 11

LLC – Large Latent Complex

LTBP - Latent TGF-β Binding Protein

MAPK – Mitogen-activated Protein Kinase

miR - microRNA

mL - Millilitre

mM - Millimolar

MMP2 – Matrix Metallopeptidase 2

MPa – Megapascal Pressure Unit

mTOR – Mammalian Target of Rapamycin

MYC - MYC Proto-Oncogene, BHLH Transcription Factor

N – Normality

NF-κB - Nuclear Factor Kappa-light-chain-enhancer of Activated B Cells

ng – Nanogram

NICD1 – NOTCH Intracellular Domain

nm – nanometre

NRF2 - Nuclear factor erythroid 2-related Factor 2

OCT – Optimal Cutting Temperature

OPSCC - Oropharyngeal Squamous Cell Carcinoma

p300 – Transcriptional Coactivator p300

PBS - Phosphate-buffered Saline

PBS-T - Phosphate-buffered Saline Tween Solution

PD1 – Programmed Cell Death-1

pg – Picogram

pH – Potential of Hydrogen

PI3K - Phosphoinositide 3-kinase

PKC – Protein Kinase C

PLC - Phospholipase C

PSA – Prostate Specific Antigen

PtdIns-3P - Phosphatidylinositol 3-phosphate

PVDF - Polyvinylidene Fluoride

Rag – Rag GTPase

RAS – Rat Sarcoma Virus GTPase

RB1 - Retinoblastoma Protein

RB1CC1 - RB1 Inducible Coiled-Coil 1

RDEB - Recessive Dystrophic Epidermolysis Bullosa

REDD1 - Regulated in Development and DNA Damage Responses 1

Rheb - Ras Homolog Enriched in Brain

RNF - Ring Finger Protein

ROC - Receiver Operating Characteristic

SD – Standard Deviation

SDS - Sodium Dodecyl Sulphate

SDS-PAGE - Sodium Dodecyl Sulphate-Polyacrylamide Gel Electrophoresis

ShcA - Schizandrin A

SOS - Son of Sevenless

SOX2 - SRY-Box Transcription Factor 2

SQSTM1 (p62) - Sequestosome 1

TAK1 - Mitogen-Activated Protein Kinase Kinase Kinase 7

TBS – Tris-buffered Saline

TBS-T - Tris-buffered Saline Tween Solution

TERT - Telomerase Reverse Transcriptase

TGFBR – Transforming Growth Factor-β Receptor

TGF-β - Transforming Growth Factor-β

TNM – Tumour-node-metastasis Staging

TP53 – Tumour Protein p53

TP63 – Tumour Protein p63

TRP - Tryptophan

TSC - Tuberous Sclerosis Complex

ULK1 - Unc-51 like Autophagy Activating Kinase

UPR – Unfolded Protein Response

UV – Ultraviolet

v/v – volume per volume

VEGF – Vascular Endothelial Growth Factor

VSP – Voltage Sensitive Phosphatase

µL – Microliter

µm – Micrometre

µM – Micron

Chapter 1. Introduction

Table of Contents

1.1. Normal Skin

1.1.1. Principle Function, Evolution and Structure

The skin represents the largest organ of the human body whose principle function is as a protective barrier. This barrier can broadly be split into two functions, an inside-out barrier (preventing escape from the body) and an outside-in barrier (preventing entry to the body), with the latter being produced by several sub-barriers such as low permeability, immune protection and UV radiation shielding (Basler et al., 2016).

Whilst principally composed of two layers, the dermis and the epidermis, the initial barrier of the skin is conferred by corneocytes and secreted lipid lamellae structures, which are present in the upper layers of the epidermis, the stratum corneum and stratum granulosum (Elias, 2005). Through the interlacing of these corneocytes and lipids, a tortuous route of entry to the body by any foreign organism or molecule is produced. The natural hydrophobicity of both the secreted lamellar bodies and the lipids present in the cornified envelope of the stratum corneum further serve to provide a barrier to water or hydrophilic molecules. Additionally, the release of lamellar bodies at the border of the stratum granulosum and corneum, as well as the many tight junctional complexes within the stratum granulosum provide an additional defence to water penetration or loss (Menon et al., 2012).

However, lamellar bodies do not only serve as a hydrophobic barrier, as their secretion also releases a variety of antimicrobial compounds and cytokines that are able to destroy invading pathogens. These chemicals alongside, the presence of Langerhans cells in the epidermis, provide an effect barrier to pathogen invasion. (Matsui and Amagai, 2015).

In addition to its barrier function the skin also provides a vital role as a sensory organ, interpreting and transmitting signals from the external environment to the central nervous system (Owens and Lumpkin, 2014), as well as functioning as an endocrine organ in its capacity as the primary site of vitamin D production (Reichrath et al., 2017).

Human skin forms during the third trimester of pregnancy but development begins much earlier (Schempp et al., 2009), originating from both the ectoderm, which produces the epidermis (Lawrence F. Eichenfield, 2001), as well as the mesoderm, which produces the dermis (Arda et al., 2014).

It's also important to appreciate that skin is not a static structure of cells but a dynamic piece of tissue, that is not only able to relay information about an individual's external environment

but also able to move and stretch to facilitate everyday movement. It's only when the skin loses this ability, e.g. from the formation of scar tissue for example, that the vital function of skin becomes observable (Wong et al., 2016).

As discussed above, skin is essentially organised into the epidermis and dermis, with an additional layer named the hypodermis present beneath. The structure and principle function of these layers can be summarised as follows (Figure 1.1).

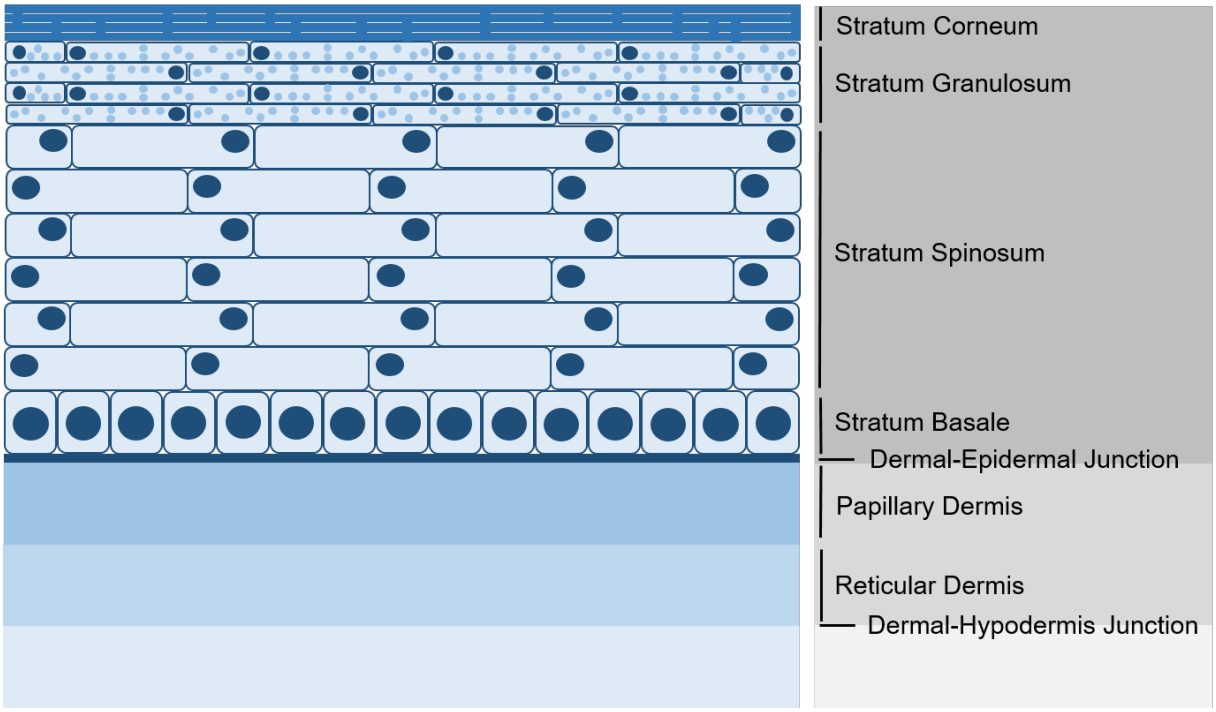

FIGURE 1. 1. STRUCTURE OF NORMAL SKIN
A schematic diagram of the various strata of the epidermis, the subdivisions of the dermis and the hypodermis, with the separating structures also shown.

Hypodermis; Located immediately beneath the dermis, the hypodermis consists of connective tissue and a high number of adipose cells. This adipose tissue, and the fat stored within, serve to reduce the potential of internal injury by reducing force transmission through the skin while also acting as a nutrient store. In addition the hypodermis acts as a thermo-regulator of the body and also facilitates connections to the underlying deep fascia, the aponeurosis and periosteum (Arda et al., 2014). This area also contains a large amount of proteoglycans and glycosaminoglycans, which act to draw in water, ensuring this area has a mucous like consistency (Wong et al., 2016).

Dermis-Hypodermis Junction; the boundary between the dermis and hypodermis but a clear dividing membrane is not present (Arda et al., 2014).

Dermis; Typically 2 mm thick the dermis is principally comprised of fibroblasts, which function to produce an extracellular matrix composed of collagen I/III, elastin, fibrillin and other structural proteins lined with a variety of proteoglycans and glycoproteins. Other cells and structures present include mast cells, plasma cells, dendritic cells, histiocytes, capillaries and nerve terminal structures (Lai-Cheong and McGrath, 2009). The dermis binds to both the epidermis and hypodermis and acts to provide nutrients to both areas (Arda et al., 2014). The dermis is also responsible for the mechanical resistance of the skin, being able to resist force of up to 27 MPa (Wong et al., 2016).
Structurally, the dermis is subdivided into two separate layers, the papillary dermis and reticular dermis, which arise from two different mesenchymal origins, giving them distinct ECM architectures and protein distributions.

Papillary Dermis; the superficial subdivision of the dermis that is in direct contact with the epidermis, comprising dermal projections at the dermal-epidermal interface, termed dermal papillary. These projections, in combination with anchoring fibrils that contact the basement membrane, give the dermis its tensile strength (Driskell et al., 2013). Due to its close association with the epidermis, it's this subdivision of the dermis that is innervated with both blood supply and nerve fibres.

Reticular Dermis; a subsection of the dermis in contact with the hypodermis (Lai-Cheong and McGrath, 2009), containing dense connective tissue housing the eccrine, sebaceous and apocrine glands of the skin (Cui and Schlessinger, 2015, Hoover and Krishnamurthy, 2019, Murphrey and Vaidya, 2019). A variety of nerve fibres innervations are also present, specialised to interpret signals from the external environment (Arda et al., 2014).

Dermal-Epidermal Junction; a 200 nm thick basement membrane (Lai-Cheong and McGrath, 2009) that separates the epidermis and dermis and comprising glycoproteins and proteins that provides a solid structure for epidermal and dermal cells to adhere to via keratin and collagen filaments and which is actively involved in transmitting cellular signals between these two areas.

Epidermis; The epidermis, the uppermost layer of the skin, varying typically between 75 to 150 µm thick, but which may be as thick as 600 µm on the palms of the hands and soles of the feet (Wong et al., 2016). This layer is predominantly composed of keratinocytes (95%), with melanocytes (pigmentation), Langerhans (immune system) and Merkel cells (mechanoreceptors) making up the remaining 5% (Menon, 2002). Conferring barrier function, the epidermis is formed and replenished through the continuous differentiation (Menon, 2002) of keratinocytes as they move from the basal layer to the outermost stratum corneum, in response to an increasing calcium gradient. Stratified into four or five layers, depending on the body sight; the stratum basale, stratum spinosum, stratum granulosum, stratum lucidum (only present in areas of thick skin) and the stratum corneum, the organisation and morphology of these layers is outlined as follows;

Stratum Basale; the lowest level of the epidermis, comprising keratinocytes undergoing constant division, either dividing horizontally to replenish the epidermis by providing cells that are pushed superficially (Baroni et al., 2012), or dividing laterally to replace lost epidermal stem cells (Arda et al., 2014). Cells within this epidermal layer appear columnar with a high nuclear-to-cytoplasm ratio and attach directly to the basement membrane separating the epidermis and dermis. This attachment is facilitated by tonofilaments, which connect to the basement membrane via hemidesmosomes present in the basal membrane, thus preventing movement towards the surface of skin. These cells also attach to the cells around them, both laterally and horizontally via desmosomes (Pappas, 2015). Interestingly, studies into the circadian clock present in stratum basale cells have also demonstrated that mitotic activity is restricted to night hours (Matsui et al., 2016), with activity occurring in four to five hourly cycles and genes involved in skin protection upregulated during daylight hours while genes involved in cell proliferation are upregulated during night time hours (Antonioli et al., 2014). This pattern of activity limits UV induced damage of DNA during cell mitosis, reducing the potential for mutant cell expansion (Matsui et al., 2016).

Stratum Spinosum; directly above the stratum basale, the stratum spinosum is the thickest section of the epidermis and is where keratinocyte differentiation begins (Arda et al., 2014). The keratinocytes compromising this layer are characterised by many interconnecting desmosome junctions and cytoplasmic projections that give them a histologically recognisable

polyhedral shape (Pappas, 2015). The tonofilaments/desmosome that facilitate interdigitating between cells allows for a reinforced structure of stratum and direct cell-to-cell communication. Morphologically cells appears flattened and elongated and the production of lamellar bodies can be seen histologically (Menon, 2002).

Stratum Granulosum; sited above the stratum spinosum, the stratum granulosum is further divided into three sub layers; SG3, SG2 and SG1 (Matsui and Amagai, 2015). Typically ten to eighteen cells thick, cell undergo extensive differentiation in this sub layer, accumulating cytoplasmic keratohyalin granules, which stain darkly in the cytosol (Menon, 2002).
The accumulation of lamellar bodies peaks within this sublayer and the granulosum cells form additional tight barrier junctions aiding barrier function (Elias et al., 1998).
Terminal keratinocyte differentiation occurs at the interface between SG1 and the stratum corneum, a process named cornification. This includes the mass secretion of the lamellar bodies, which fuse in the extracellular space to fully occlude the area, aiding barrier function. The cornified envelope also forms in this epidermal layer, a protein-structure that forms around the cell aiding barrier function (Menon, 2002).

Stratum Lucidum; this epidermal sub layer is only present in the skin of the soles and palms. Approximately five cells thick, these cells are highly refractive and eosinophilic and due to the absence of nuclei, this stratum is typically characterised as a subdivision of the stratum corneum (Arda et al., 2014).

Stratum Corneum; Representing the upper most superficial stratum of the epidermis, the stratum corneum is approximately fifteen to twenty one cells thick. Keratinocytes within this sub layer are characterised by their flattened and elongated morphology which occurs as part of their cornification process and also their 'brick and mortar' structure (Arda et al., 2014). The brick and mortar structure describes the organisation of the corneocytes or 'bricks' embedded in the lamellar sheets or 'mortar' (Steinert, 1999). It's this interlacing that provides the strong barrier function to external pathogens. Additional alterations occurring in the stratum corneum also include the conversion of desmosomes to corneodesmosomes; tight junctional complexes with increased adhesion compared to their previous counterparts (Menon, 2002), later broken down to aid cell separation and desquamation (Matsui and Amagai, 2015).

1.1.2. Epidermal Differentiation

Integral to the formation and integrity of the component strata, with their distinct morphology, is the process of epidermal differentiation. Highly regulated, this process involves a series of gene expression changes that ultimately produce a terminally differentiated keratinocyte, key to epidermal barrier function.

The principle driver of epidermal differentiation in keratinocytes is the presence of an epidermal calcium gradient, with low calcium concentrations ensuring ongoing proliferation and replenishment of the epidermis, while higher calcium concentrations trigger cellular differentiation and the production of a functioning epidermal barrier. The extracellular calcium gradient in the epidermis is low at the stratum basale, with concentrations as low as 3 μM, that steadily increase towards the stratum granulosum, eventually reaching >20 μM and then reducing to concentrations <3 μM in the stratum corneum (Celli et al., 2010). However, the extracellular calcium gradient only partially contributes to calcium gradient present in the epidermis, with intracellular concentrations of calcium being the principle source of the gradient. The rise in external calcium, from the stratum basale to granulosum, is interpreted by the G-protein coupled receptor Calcium Sensing Receptor (CaSR), which leads to the production of inositol phosphates via activating phospholipase C (PLC), which in turn activates the inositol trisphosphate (IP3) receptor (Elsholz et al., 2014). The activation of this IP3 receptor then causes calcium influx as a result of both the intake of calcium from the extracellular space, through TRP channels, and the release from intracellular stores (Bikle et al., 2012). This rise in intracellular calcium, promoted by the cell-to-cell adhesion complexes, leads to the activation of protein kinase C (PKC) (Tu and Bikle, 2013).

PKC activation in turn induces a variety of genes involved in epidermal differentiation, some activated by calcium sensitive promoters, via transcription factors such as activator protein 1 (AP1), with others induced via induction of the 'epidermal differentiation complex,' a 2 mega base pair region located at 1q21 (Kypriotou et al., 2012). It's this sequence of rising extracellular calcium, leading to a rise in intracellular calcium, inducing signalling events and gene activation that ultimately produces keratinocyte differentiation.

The result of calcium induced gene expression is the gradual differentiation of keratinocytes as they move superficially through the epidermis. During this process, keratinocytes also

undergo a variety of protein expression changes that result in a terminally differentiated cell that is perfectly suited to reinforce and maintain the epidermal barrier.

The differentiation process of keratinocytes begins with the cells present in the basal layer escaping the cell cycle and detaching from the basement membrane and entering the superficial strata (Segre, 2003).

One of the clearest examples of this change in protein expression is the alteration in keratin expression; cells present in the stratum basale express keratin 5 and 14 but upon moving superficially and forming the stratum spinosum, a change in expression to the expression of keratin 1 and 10 occurs. Keratin 1 and 10 are continuously expressed until differentiating keratinocytes cells reach the stratum granulosum, where expression is lost (Elsholz et al., 2014).

Other key proteins involved in epidermal differentiation and cornification are only expressed by keratinocytes within specific strata (Figure 1.2); for example, involucrin and transglutaminase expression is induced in the stratum spinosum, while loricrin and profilaggrin are induced in the stratum granulosum (Bikle et al., 2012). Changes also occur to the expression of cell junction proteins. In the stratum basale, the dominant proteins in desmosomes are desmogleins 2 and 3 and desmocollins 2 and 3. However, when entering the stratum spinosum, desmoglein 2 and desmocollin 2 become the dominant proteins involved in desmosomes (Delva et al., 2009) while in the stratum granulosum/corneum, desmoglein 1 and desmocollin 1 are the predominant proteins (Bikle et al., 2012). This change in expression reflects the change in function that occurs during keratinocyte differentiation, desmoglein 3 has been shown to be involved in cell proliferation while desmoglein 1 expression is vital to barrier function in the upper layers of the epidermis.

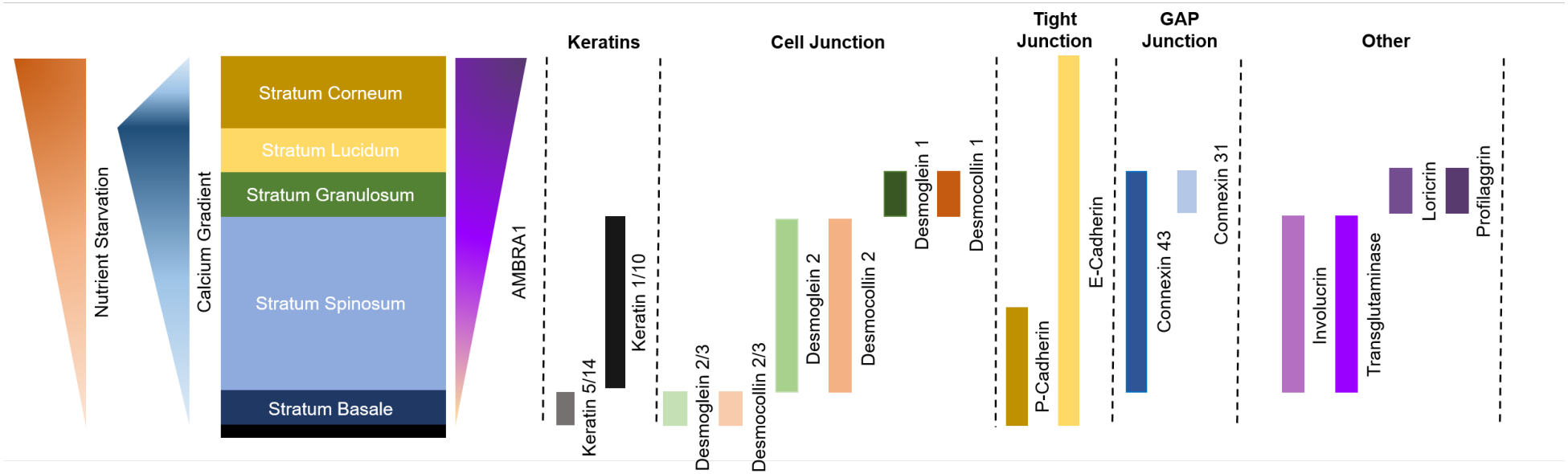

FIGURE 1. 2. Protein Expression during Keratinocyte Differentiation.
A schematic diagram demonstrating the alterations to the expression of AMBRA1, keratins, cell junction proteins, tight junctional proteins and other key differentiation proteins that occur as keratinocytes undergo differentiation. Also shown is the calcium gradient and nutrient starvation pressure present in the epidermis.

In terms of tight junctions in the epidermis, both P- and E-cadherin are found in the tight junction complexes. This changes as the cells move superficially with the tight junctional complexes becoming dominated by E-cadherin, while P-cadherin is no longer expressed. E-cadherin is assisted in tight junction formation by claudins and occludins, whose expression is initiated in the stratum spinosum (Bikle et al., 2012).

Interestingly, recent studies have shown that AMBRA1, a pro-autophagy regulatory protein also acts as an epidermal differentiation protein, its expression increasing from the stratum basale to the stratum corneum and its loss associated with hyper-proliferation and impaired epidermal differentiation (Ellis et al., 2020, Cosgarea et al., 2021)

These gradual changes during the process of epidermal differentiation lead to terminal differentiation, or cornification, which occurs at the interface between the stratum granulosum and stratum corneum. During this process, several cellular changes occur, including the formation of the cornified cell envelope, produced by the cross-linking of involucrin, loricrin, small proline rich proteins, desmoplakin and other proteins that provides a solid structural encasing of the cell that is resistant to mechanical and chemical disruption (Elias, 2005). Profilaggrin is also processed to filaggrin, which is then distributed across the cell and accumulates additional keratin filaments, which aid structural rigidity (Eckhart et al., 2013). A coordinated secretion of the lamellar bodies also occurs during terminal differentiation. The contents of these lamellar disc organelles fuse to form lamellar sheets which fill and occlude the extracellular space around the terminally differentiated keratinocytes (Bouwstra and Honeywell-Nguyen, 2002). This process occurs during organelle and nuclei degradation, resulting in the elongation and further flattening of cell morphology.

Given the suggested role of AMBRA1 in epidermal differentiation, and the need to remove the organelles present in the keratinocyte during this process, autophagy has been shown to play a key role in epidermal differentiation. Supporting this function, recent studies have demonstrated increased basal autophagy in the epidermis, as evidenced by the presence of increased levels of LC3-II expression, a marker of autophagic flux, in the granular layer (Haruna et al., 2008). Further studies also suggest while not vital for epidermal barrier function, autophagy is key to cellular remodelling during cornification; skin grafts of Atg7 deficient mice showing defective skin formation leading to acanthosis and hyperkeratosis following initial

transplantation (Yoshihara et al., 2015). Follow on studies in an epidermal-Atg7-deficient mouse model also reveal a thicker stratum corneum, suggesting a failure of organelle degradation. (Rossiter et al., 2013). Furthermore differentiating keratinocytes, encounter both calcium mediated stress and nutrient deprivation, stress responses required for differentiation that lead to UPR-induced ATF6 signalling, and the induction of lysosome formation and autophagy signalling, independent of mTOR, a regulator of autophagy (Mahanty et al., 2019). Taken together, these studies suggest that whilst the attenuation of autophagy does not affect barrier formation of the epidermis, likely due to multiple redundancies, it contributes to the process of keratinocyte cornification. The intimate role of autophagy within keratinocyte differentiation nevertheless, remains poorly defined.

Collectively this body of evidence demonstrates the numerous and complex cell processes, including autophagy and differentiation, that must act in unison to ensure replenishment of epidermal cells to produce fully differentiated cells and ensure the barrier function of the skin is operational. As such, any disruption to these processes has the potential to become pathological and produce epidermal originating malignancies.

1.2. Cutaneous Squamous Cell Carcinoma

1.2.1. Incidence, Characteristics and Risk Factors

Cutaneous squamous cell carcinoma (cSCC) is a cutaneous malignancy that arises from the transformation of keratinocytes that appear squamous in appearance, and commonly classified as a non-melanoma skin cancer. Incidence continues to rise worldwide, with the UK incidence reported to be 77 per 100,000 people (Venables et al., 2019b) and with the highest incidence in Australia, at 499 per 100,000 persons (Staples et al., 2006). The growing worldwide incidence of cSCC thus places enormous pressure on healthcare services, estimated to be around £36 million by 2020, in the UK alone.

The major risk factor identified linked to the development of cSCC is UV radiation, with both UV-A and UV-B able to promote keratinocyte tumourigenesis. UV-B is able to directly induce DNA mutations via directing C-to-T substitutions, whilst UV-A acts to produce ROS species that go on to induce cancerous transformations. Whilst exposure to UV is highly associated with

cSCC development, numerous other factors contribute to tumour development (Dotto and Rustgi, 2016). These include fair skin, an age of >60yrs (Xiang et al., 2014), and sex (men being at greater risk of cSCC development (Venables et al., 2019b, Andersson et al., 2011, Rogers et al., 2015, Staples et al., 2006). Immunodeficiency/suppression, both within organ transplant patients and patients with immune cell based cancer is also strongly associated with cSCC development (Jensen et al., 2000, Hartevelt et al., 1990, Omland et al., 2016, Velez et al., 2014, Mehrany et al., 2005), as well as, albeit to a minimal degree, the presence of premalignant lesions such as actinic keratoses (AK) (Ratushny et al., 2012).

Both cSCC development and progression pose a significant health care burden. Risk factors for cSCC progression include the physical dimension of the primary tumour; a Breslow depth >2 mm or a tumour diameter >20 mm being associated with a significant risk of local disease recurrence (Brantsch et al., 2008, Que et al., 2018, Thompson et al., 2016). Differentiation status is also linked to disease progression; a poorly differentiated phenotype being associated with both a high risk of local recurrence as well as tumour metastasis (Thompson et al., 2016, Que et al., 2018). However, it is worth noting that whilst differentiation status may have some prognostic potential, this criterion has been removed from more recent AJCC staging criteria. Further physical factors contributing to the risk of local recurrence and metastasis also include invasion below subcutaneous fat and perineural invasion (Martinez et al., 2003, Thompson et al., 2016, Harris et al., 2017, Carter et al., 2013).

Key to the development and progression of cSCC is the accumulation of genetic mutations, including mutations in TP53 (Missero and Antonini, 2014), CDKN2A/RB1, CCDN1, MYC, tyrosine kinase receptors (EGFR and FGRF), RAS/MAPK and PI3K signalling, TP63, SOX2, NRF2 as well as epidermal differentiation genes such as Notch and Fat1 (Dotto and Rustgi, 2016). More recently, mutations in AMBRA1 have also been linked with cSCC. A study of 39 patients demonstrated a mutational rate of 25%, with the mutations being typically missense in nature. Patients with AMBRA1 mutations had a median survival of 25 months, in comparison to 124.9 months in patients without this mutation, suggesting that loss of AMBRA1 function is a risk factor in developing more aggressive cSCC disease (Pickering et al., 2014) and highlighting the potential importance of this protein in tumourigenesis and progression.

1.2.2. Current cSCC Staging and Management

cSCC can be staged according to the 8th edition of the American Joint Committee on Cancer Staging for SCC, which in turn may guide treatment stratification. This classification uses the TNE staging system, with various clinical criteria for the primary tumour (T), shown in Table 1.1, criteria for regional lymph nodes (N), shown in Table 1.2 and criteria for distant metastasis, shown in Table 1.3, all being used together to stage an cSCC tumour (Califano, 2017) into 4 different stages, named I-IV, shown in Table 1.4. Stage I represents the presence of a small single primary tumour (<2cm), Stage II represents a moderate single primary tumour (>2 cm but <4 cm), Stage III represents a large primary tumour (>4 cm) and can also indicate the presence in a single ipsilateral lymph node while Stage IV represents a variety of primary tumour sizes with different degrees of lymph node involvement and can also include the presence of distant metastasis. However, it has also been suggested that this system overly stratifies patients into poor outcome groups when compared to the Brigham and Women's Hospital (BWH) staging system (Table 1.5) (Ruiz et al., 2019). However, the BWH staging system has also been heavily criticised for not including multivariate analysis or additional risk factors, such as immunosuppression or tumour location, which have been well documented to impact on cSCC progression (Mina N Le, 2017). Despite several revisions of the AJCC staging system, the criterion within this system are still unable to reliably predict the risk of disease progression (Mina N Le, 2017), leaving an acute unmet need for reliable prognostic biomarkers

T Category	T Criteria
TX	Primary tumour cannot be identified
Tis	Carcinoma in-situ
T1	Tumour <2 cm in its greatest dimension
T2	Tumour is >2 cm but <4 cm in its greatest dimension
T3	Tumour is >4 cm in a clinical diameter or Minor bone erosion or Perineural invasion or Deep invasion
T4	Tumour with gross cortical bone/marrow invasion or skull bone invasion or skull base foramen invasion
T4a	Tumour with Gross cortical bone/marrow invasion
T4b	Tumour with skull bone invasion or Skull base foramen invasion

TABLE 1. 1. THE TUMOUR CRITERIA FOR THE STAGING OF CSCC AS DEFINED BY THE 8TH EDITION OF THE AMERICAN JOINT COMMITTEE ON CANCER STAGING.
Adapted from (Califano, 2017).

N Category	N Criteria for Pathologic N
NX	Regional lymph nodes cannot be assessed
N0	No regional lymph nodes metastasis
N1	Metastasis in a single ipsilateral lymph node, <3 cm in its greatest dimension and ENE-
N2	Metastasis in a single ipsilateral lymph node <3 cm in greatest dimension and ENE+ or >3 cm but not >6 cm in greatest dimension and ENE- or metastases in multiple ipsilateral lymph nodes, none >6 cm in greatest dimension and ENE- or in bilateral or contralateral lymph nodes, none >6 cm in greatest dimension and ENE-
N2a	Metastasis in a single ipsilateral lymph node <3 cm in greatest dimension and ENE+ or >3 cm but not >6 cm in greatest dimension and ENE-
N2b	Metastases in multiple ipsilateral lymph nodes, none >6 cm in greatest dimension and ENE-
N2c	In bilateral or contralateral lymph nodes, none >6 cm in greatest dimension and ENE-
N3	Metastasis in a lymph node >6 cm in greatest dimension and ENE- or in a single ipsilateral node >3 cm in greatest dimension and ENE+ or multiple ipsilateral, contralateral, or bilateral nodes, any with ENE+
N3a	Metastasis in a lymph node >6 cm in greatest dimension and ENE-
N3b	Metastasis in a single ipsilateral node >3 cm in greatest dimension and ENE+ or multiple ipsilateral, contralateral, or bilateral nodes, any with ENE+

TABLE 1. 2. THE REGIONAL LYMPH NODE CRITERIA FOR THE STAGING OF CSCC AS DEFINED BY THE 8TH EDITION OF THE AMERICAN JOINT COMMITTEE ON CANCER STAGING.
Adapted from (Califano, 2017).

M Category	M Criteria
M0	No distant metastasis
M1	Distant metastasis

TABLE 1. 3. THE METASTATIC CRITERIA FOR THE STAGING OF CSCC AS DEFINED BY THE 8TH EDITION OF THE AMERICAN JOINT COMMITTEE ON CANCER STAGING.
Adapted from (Califano, 2017).

Combined SCC Staging Criteria			
Stage	**T Criteria**	**N Criteria**	**M Criteria**
0	TIS	N0	M0
I	T1	N0	M0
II	T2	N0	M0
III	T3	N0 or N1	M0
IV	T1 and T2	N1	M0
	T1, T2 and T3	N2	M0
	Any T	N3	M0
	T4	Any N	M0
	Any T	Any N	M1

TABLE 1. 4. THE TNE CRITERIA FOR THE STAGING OF CSCC AS DEFINED BY THE 8TH EDITION OF THE AMERICAN JOINT COMMITTEE ON CANCER STAGING.
Adapted from (Califano, 2017).

Stage	No. of High-Risk Factors
T1	0
T2a	1
T2b	2-3
T3	>4

TABLE 1. 5. THE STAGING CRITERIA FOR THE BRIGHAM AND WOMEN'S HOSPITAL (BWH).
High-risk factors are defined as a tumor diameter ≥2 cm, poorly differentiated histology, perineural invasion ≥0.1 mm or tumor invasion beyond fat (excluding bone invasion). Adapter from (Karia et al., 2014)

Current treatment options for cSCC depend on disease stage, incorporating surgical and non-surgical options (Potenza et al., 2018). Tumours are classically removed by surgical excision, including the provision of clinical margins, which may be combined with adjuvant therapy, to further prevent the risk of local reoccurrence and metastasis (Brodland and Zitelli, 1992, Breuninger et al., 2013). Mohs micrographic surgery is another surgical option, which can be used if the site of primary tumour development has aesthetic impacts upon its removal. This technique comprises surgical removal of the tumour and a series of horizontal sections around the tumour margin and then examining each section histologically for tumour cells. If the presence of tumour cells are detected, further sections are taken. This technique has shown success in the treatment of cSCC, reducing the rate of tumour recurrence to as little as 3% (Neville et al., 2007, Nguyen and Ho, 2002).

If there is evidence for cSCC disease spread then additional broad spectrum treatments including radiotherapy are adopted (Bonerandi et al., 2011) while for metastatic disease classical chemotherapy treatments incorporate the use of capecitabine (Oliveira et al., 2016, Endrizzi et al., 2013), cisplatin (Khansur and Kennedy, 1991) and paclitaxel (Lewis et al., 2004). In some rarer occasions, electrochemotherapy can be utilised (Oliveira et al., 2016). The limited success of these therapeutic approaches for metastatic disease has more recently led to the development of a plethora of more targeted therapies. These include the use of immunotherapies and biological response modifiers, such as retinoids and interferons, which act to induce immune antitumor activity (Lewis et al., 2012). Others include EGFR inhibitors (Maubec et al., 2011), Herbacetin (Kim et al., 2017), the PD1 inhibitor cemiplimab (Blum et al., 2018, Ogata and Tsuchida, 2019) and autophagy modulatory therapies (Yun and Lee, 2018). Nevertheless, despite some success with the use of these agents either alone or in combination, there are still no consistently beneficial treatments, emphasising the acute need for novel therapeutic strategies for metastatic disease to accompany more reliable prognostic and companion biomarkers.

1.3. Autophagy

1.3.1. Function and Forms of Autophagy

Autophagy is often described as the self-eating process, which is used by cells to sequester cytoplasmic components and organelles for degradation and recycling to maintain cell homeostasis. The cell can employ three distinct mechanism to achieve this, named chaperone mediated autophagy, microautophagy and macroautophagy. Whilst all three processes lead to the degradation of intracellular components, the mechanisms they employ to achieve this are vastly different (Figure 1.3). The best characterised process is macroautophagy (Feng et al., 2014). This form of autophagy involves the formation of a double membrane vesicles around target substrates, with the resultant vesicle then trafficked to the lysosome, where it fuses, allowing the target substrate to be degraded by lysosomal enzymes. Microautophagy, differs from macroautophagy as it utilises lysosomal membrane invaginations and extensions to surround target substrates and absorb them into the lysosome (Li et al., 2012, Kunz et al., 2004, Mijaljica et al., 2011) while chaperone mediated autophagy is a highly selective process that traffics individual proteins to the lysosome for degradation (Kaushik and Cuervo, 2018, Li et al., 2019, Majeski and Dice, 2004). This process of individual protein sequestering is unique to chaperone mediated autophagy, as both micro and macroautophagy sequester their target substrates in bulk.

The process of mammalian macroautophagy can be broken down into clearly defined stages and is facilitated by a large group of autophagy-related proteins (ATG proteins) that form distinct complexes, collectively named the ‘core autophagy machinery’. The process is summarised in Figure 1.4.

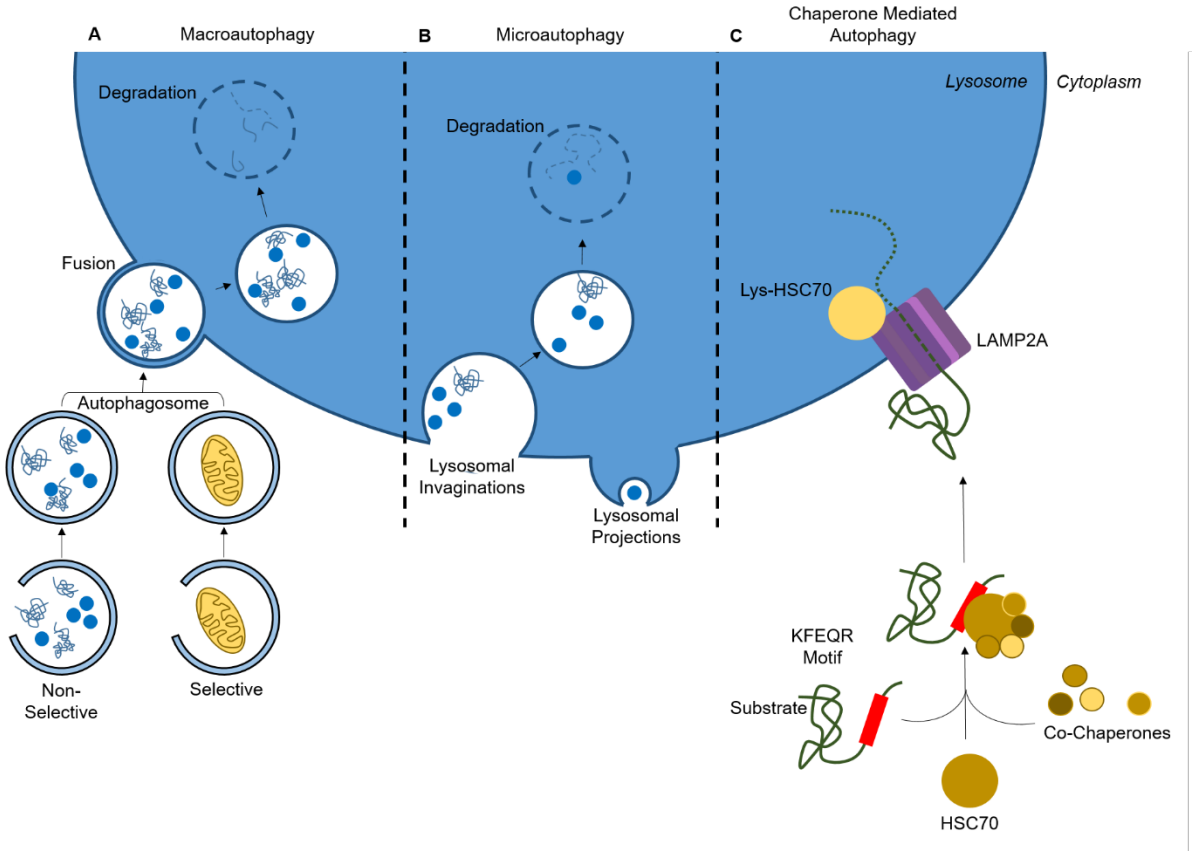

FIGURE 1. 3. THE THREE FORMS OF AUTOPHAGY.
A schematic diagram demonstrating the mechanisms of action for the three major forms of autophagy. (A) Macroautophagy involves the enclosing of the autophagosome around the substrate/organelles and then trafficking those components to the lysosome, where it fuses and is degraded. This relies on the core autophagy machinery to form the phagophore. (B) Microautophagy involves the projection and invagination of the lysosomal membrane to sequester substrates for degradation. (C) Chaperone mediated autophagy involves the translocation of the substrate via KFEGR mediated HSC70 association to the lysosome. Here, it is passed through the oligomerized LAMP2A receptor, aided by lys-HSC70, and into the lumen of the lysosome for degradation. Adapted from (Kaushik and Cuervo, 2018).

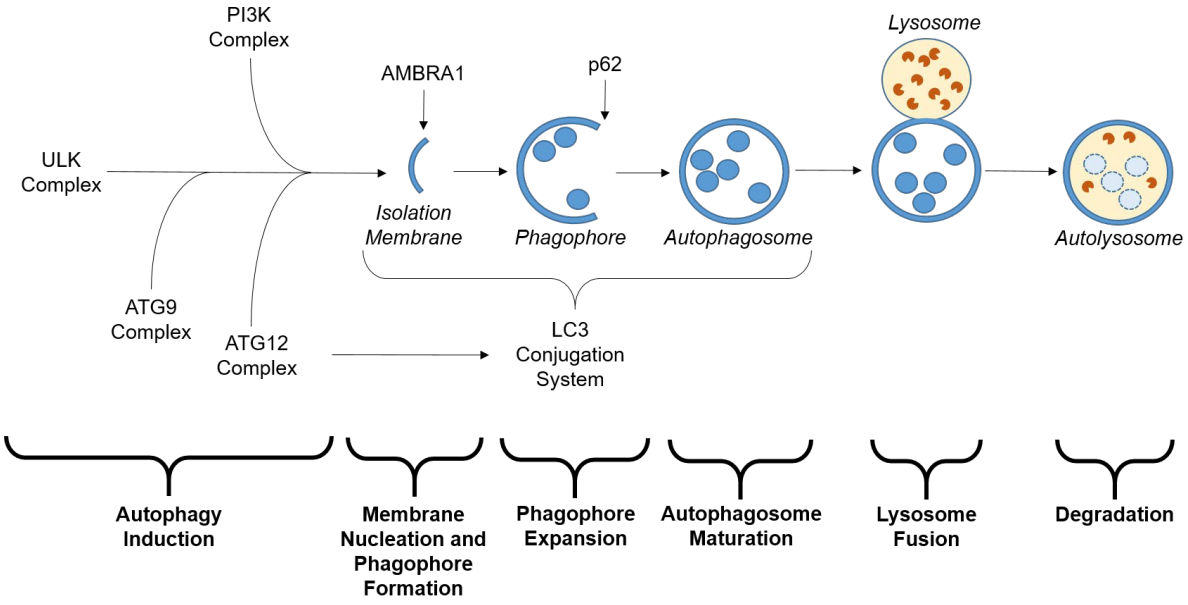

FIGURE 1. 4. THE MECHANISM OF MACROAUTOPHAGY.
Autophagy is induced following the formation of ULK complex puncta. This leads to the recruitment of further core autophagy machinery, the PI3K complex, the ATG9 complex and the ATG12 complex. Through the production of lipids by the PI3K complex, this leads to membrane nucleation and the formation of the phagophore. Following this, the action of membrane donation by ATG9 and the action of the LC3 conjugation system, aided by the ATG12 ubiquitination like complex, phagophore expansion and autophagosome maturation occurs. The completed autophagosome is then trafficked to the lysosome, where the two organelles fuse, allowing for degradation of the intracellular components. Adapted from (Sun et al., 2013).

The first of these stages is 'initiation', the process which marks the site of formation of the double membrane vesicle named the 'phagophore.'. Initiation of autophagy is marked by the formation of ULK1 puncta. Under nutrient rich conditions ULK1 appears to be scattered through the cytosol but upon nutrient loss and the induction of autophagy, ULK1 is activated by the loss of mTOR mediated inhibition and AMPK-mediated activation (discussed further in Section.1.2.2). The resultant formation of the ULK1 complex containing ULK1 (serine/threonine kinase), ATG13 (regulatory protein) and RB1CC1/FIP200 (scaffold protein) then leads to the recruitment of other core autophagy machinery involved in the nucleation and elongation of the phagophore.

The second stage of macroautophagy is 'phagophore nucleation,' mediated by the VPS34 complex, comprising VPS34 (phosphoinositide 3-Kinase (PI3K)), VPS13 (serine/threonine kinase), Beclin-1 and ATG14 (regulatory protein). Upon the interaction of the regulatory protein AMBRA1 with this complex, the production of phosphatidylinositol 3-phosphate (PtdIns-3P) is triggered and thus, membrane nucleation begins and further autophagy-related proteins are recruited. (Axe et al., 2008, Carlsson and Simonsen, 2015, Karanasios et al., 2013).

Once nucleation has been facilitated, the next stage of macroautophagy is phagophore elongation. This process is partly facilitated by the ATG9 complex, comprising ATG9, (transmembrane protein), ATG18 (PtdIns-3P binding protein) and ATG2 (ATG18 interacting protein) which functions to tether and incorporate lipid membrane structures into the phagophore, causing its elongation and expansion. This process is also facilitated by the ubiquitin-like protein, LC3 complex, which cooperates with the ATG12 complex in the processing of LC3, from proLC3 to LC3-I and its subsequent conjugation to phosphatidylethanolamine (PE) to form LC3-II, which serves to aid elongation of the phagophore (Knaevelsrud et al., 2013, Dooley et al., 2014, Xie et al., 2008). As a dynamic process, LC3-II can be deconjugated from PE to reform LC3-I, where it can then leave the phagophore and recruit further membranes (Feng et al., 2014). Another key protein involved in this process is the receptor SQSTM1 (p62), which is a scaffold protein that is able to interact with ubiquitinated proteins and then shuttle them into the growing phagophore by associating with LC3-II. This allows the autophagosome to surround the selected cargo and ultimately ensure its degradation. This interaction between p62 and LC3-II does lead to the degradation

of p62 by the same lysosomal hydrolases that degrade the ubiquitinated cargo (Lamark et al., 2017, Pankiv et al., 2007).

The membrane expansion and LC3-induced curvature of the phagophore continues until an entire vesicle is nearly formed, when the fourth and final process occurs, named 'autophagosome maturation.' (Zhao and Zhang, 2019, Takahashi et al., 2018). Once the autophagosome has formed, it and its contents are then trafficked to a lysosome, where both vesicle structures fuse to form an 'autolysosome' where cytosolic components are degraded by lysosomal hydrolases present in the lumen, allowing the sequestered contents to be further broken down. This completes the process of macroautophagy and is collectively termed autophagic flux (Yu et al., 2018).

1.3.2. Autophagy Regulation

Macroautophagy is principally regulated by nutrient sensing signals acting on mammalian target of rapamycin (mTOR), an autophagy repressor, and AMPK, an autophagy activator (Figure 1.5) (Laplante and Sabatini, 2012).

mTOR is active during times of high nutrient availability and represses autophagy by interacting directly with ULK and other proteins in the ULK complex. mTOR induces inhibitory phosphorylations on the ULK complex, acting on ATG13 and ULK directly and also on the VPS34 complex, by phosphorylating ATG14 (Kim et al., 2011, Yeh et al., 2011). These inhibitory phosphorylations prevent the interaction of these protein complexes and thus prevent their coordinated action in autophagy induction. However, in times of nutrient starvation, oxidative or cellular stress, the inactivation of mTOR occurs, triggering the induction of autophagy.

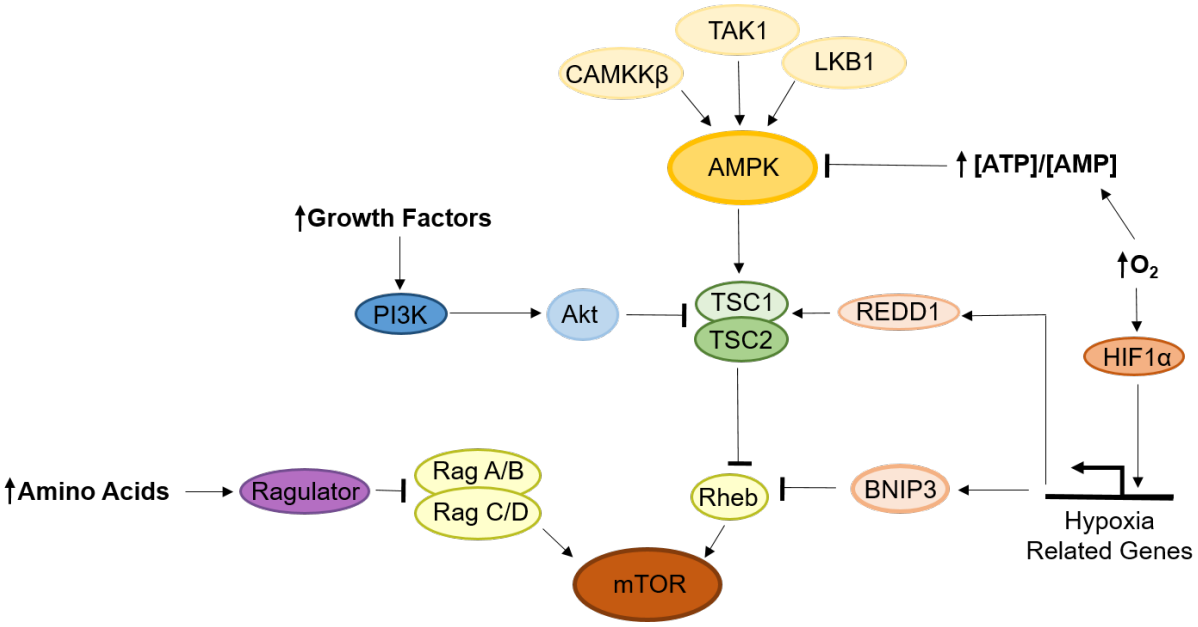

FIGURE 1. 5. OVERVIEW OF THE REGULATION OF MTOR BY NUTRIENT SENSING.
A schematic diagram demonstrating the many form of regulation that occurs on mTOR. An increase in amino acid concentration is able to signal to the Ragulator complex to mediate the activating interaction between Rag A/B, Rag C/D and mTOR. The signalling of growth factor receptors at the cell surface is able to activate the PI3K pathway and the activation of Akt, leading to the inhibition of the TSC1/2 complex. This causes the TSC1/2 complex to be unable to inhibit Rheb, allowing it to activate mTOR. A loss of oxygen in the cell leads to the HIF1α mediated induction of hypoxia related genes, including BNIP3 and REDD1. BNIP is able to directly inhibit the mTOR activator Rheb and REDD1 is also able to inhibit Rheb indirectly, by acting on TSC1/2. Low oxygen or a high metabolic rate causes the accumulation of AMP and ADP, which are able to activate AMPK. AMPK can also be activated by TAK1, LKB1 and CAMKKβ. This activation leads to the activation of the TSC1/2 complex, causing Rheb inhibition, preventing the activation of mTOR and inhibition of autophagy. Adapted from (Russell et al., 2014).

Whilst inhibition of mTOR is vital to the process of autophagy induction, the reactivation of mTOR is vital to autophagy termination once nutrient levels in the cell have returned to normal levels. This reinhibition prevents autophagy induced cell death (Antonioli et al., 2017).

The pro-autophagy serine/threonine kinase (AMPK) is also key to autophagy regulation, where it principally functions to monitor intracellular ratios of ATP:ADP:AMP (Hardie, 2011). As ATP is the metabolic driver of the cell, a shift in the ratio leading to an accumulation of ADP and AMP leads to activation of AMPK by several regulatory proteins, such as CAMKKβ, LKB1 and TAK1 (Russell et al., 2014). AMPK is able to activate autophagy by removing the inhibitory

action on ULK imposed by mTOR, by inducing the activating phosphorylation on TSC1 and TSC2 and by directly inhibiting mTOR. (Gwinn et al., 2008). In addition to its role in mTOR inhibition, AMPK can also directly activate autophagy through ULK1 (Kim et al., 2013a). Further, ULK1 is also able to directly phosphorylate beclin1-regulated autophagy (AMBRA1). Under nutrient rich conditions, AMBRA1 stops the action of Beclin-1 and VSP34 by sequestering the two proteins into a complex on dynein. Upon ULK1 phosphorylation, AMBRA1 releases both Beclin-1 and VSP34 from complex, facilitating autophagy induction (Nazio and Cecconi, 2017). AMBRA1 itself also has further roles in promoting autophagy, being able to promote TRAF6 association with mTOR, causing mTOR ubiquitination of mTOR, stopping its action (Nazio and Cecconi, 2017).

AMBRA1 itself is regulated to ensure autophagy activation is not indefinite and resulting in excessive cell death. Under normal conditions, AMBRA1 is bound to the Cullin adapter DDB1, marking the protein for degradation by Cullin 4A and 4B, which stops its proautophagy signalling. However, upon nutrient deprivation, AMBRA1 loses this interaction and binds to Elongin B. When unbound to AMBRA1, Elongin B degrades the mTOR inhibitor protein DEPTOR, but upon its association with AMBRA1, this action is prevented. This allows the stabilisation of DEPTOR expression, which then acts to inhibit mTOR and allow the induction of autophagy. Thus AMBRA1 is able to establish a strong positive feedback loop on mTOR, ensuring the continuation of active autophagy. This switch in binding partner induced by the activation of autophagy is slowly reversed, causing the degradation of both AMBRA1 and DEPTOR. This stops the feedback system and allows autophagy to be reduced. (Antonioli et al., 2014, Cianfanelli et al., 2015b).

Bioinformatic studies (Corazzari and Lovat unpublished data) of the AMBRA1 promotor have also identified TGF-β signalling responsive elements with recent data highlighting secretion of TGF-β2 by high risk melanomas leads to the transcriptional down regulation of AMBRA1 in the epidermal microenvironment (Cosgarea et al., 2021). This suggests an additional novel regulation of AMBRA1 by TGF-β signalling, further discussed below.

1.3.3. Autophagy in Cancer

Whilst the mechanism and regulation of autophagy has been well elucidated in normal cells, autophagy has been shown to have a paradoxical role in cancer. (Kim and Lee, 2014, Johnson and Tee, 2017). A blockade of autophagy in early stage cancers such as shown in prostate, ovarian and breast cancer with monoallelic loss of Beclin-1 promotes tumorigenesis (Liang et al., 1999, Choi et al., 2013, Aita et al., 1999). Mouse models with loss of ATG5 and ATG7 are also susceptible to tumour development, further supporting the notion that loss of autophagy is genotoxic, resulting in DNA damage and the initiation of cancer development (White et al., 2015). On the other hand, in later stages of carcinogenesis, autophagy can act as a tumour promotor; in solid tumours such as melanoma, when in a nutrient deprived environment, autophagy can actively promote tumour cell survival (Tang et al., 2016, Mathew and White, 2011).

It has also been shown that autophagy is linked to angiogenesis. Tumour cells promote angiogenesis by producing VEGF, which binds to and acts on endothelial cells and initiates signalling cascades that causes the growth of new blood vessels into the tumour. Autophagy thus acts to limit the damage oxidative stress causes the tumour cell, ensuring cancer cells can survive for a limited time without an oxygen or nutrient supply (Cavallaro and Christofori, 2000). However, autophagy can also be utilised to inhibit angiogenesis, as it is involved in the degradation of gastrin, a pro-angiogenesis molecule (Kim et al., 2013b). Again, this highlights the paradoxical role of autophagy in cancer, being able to both promote and suppress angiogenesis during cancer progression.

Given autophagy's diverse role in carcinogenesis, considerable interest in the last decade has explored autophagy as both a biomarker and a therapeutic target (Levy et al., 2017, Bortnik and Gorski, 2017). As a principle autophagy regulatory protein, studies have looked at the endogenous expression of LC3 as a potential biomarker in cancer (Lazova et al., 2012), with studies in cSCC suggesting its increased expression is associated with more aggressive tumours (Giatromanolaki et al., 2010). However due to the lack of cyclic processing of LC3 and the dynamic nature of autophagic flux, its expression does not accurately reflect the level of autophagy within a tumour cell (Soengas and Lowe, 2003).

Pilot data leading to the present study have also shown loss of immunohistochemical expression of AMBRA1 in poorly, compared to well-differentiated primary cSCC tumours. However, AMBRA1 expression appears to be retained in premalignant lesions such as AK and Bowens disease (Green, 2021), further supporting a potential tumour suppressive role for AMBRA1, as well as its potential as a diagnostic/prognostic biomarker for cSCC.

p62 as a autophagy cargo protein has also shown potential as a prognostic biomarker in cutaneous malignancy. Its expression closely aligns with the paradoxical role of autophagy in cancer, where an increase in p62 expression has been observed in early stage localised melanomas, compared to reduced expression in later stages of melanoma progression, consistent with the activation of pro-survival autophagy (Ellis et al., 2014). In the context of cSCC, pilot data has also shown in line with a loss of AMBRA1 expression, poorly differentiated cSCC display a concurrent reduction in p62 expression (Lovat et al unpublished data). It is possible that AMBRA1 and/or p62 will therefore display potential as biomarkers of cSCC development or progression.

The modulation of autophagy for therapeutic benefit is also a growing area of interest in the cancer field, including for cSCC. One of the best examples of this has been the use of the anti-malarial, chloroquine, shown to have inhibitory actions on autophagy in several cancer types. However, chloroquine is not a specific inhibitor autophagy and may lead to detrimental effects on kidney function (Kimura et al., 2013) and prompting the use of specific autophagy inhibitors, such as those to VPS34. In fact, the use of VPS34 inhibitors has already been shown to overcome autophagy-induced drug resistance in breast cancer cells, as well as in mouse models of melanoma (Dyczynski et al., 2018, Verykiou et al., 2019).

Considering a blockade of autophagy is protumorigenic, it is nevertheless possible that clinical inhibition of autophagy in cancer may lead to secondary tumourigenesis (Marinkovic et al., 2018). This possibility that has led to the recent alternative strategy of promoting cytotoxic autophagy with agents such as therapeutic cannabinoids, including in the context of cutaneous malignancy (Armstrong et al., 2015, Blazquez et al., 2006).

In the context of cSCC, studies have shown the inhibition of autophagy with chloroquine in cSCC cell lines promotes the efficacy of AKT inhibitor targeted therapy, resulting in the significant enhancement of tumour apoptosis (Claerhout et al., 2010), (Wright et al., 2013). Additional studies reporting the inhibition of autophagy with lycopene (carotenoid), also inhibits cSCC progression *in vitro* (Bi et al., 2019). Further studies also report the potential for

autophagy exacerbation by lapatinib (an EGFR inhibitor) as a means through which to inhibit mTOR and promote the inhibition of cSCC proliferation as well as increase apoptosis (Yao et al., 2017). Furthermore studies in vitro have shown treatment of cSCC cells with ALA-PDT (a combination of photodynamic therapy and 5-aminolevulinic acid) leads to increased basal autophagy and apoptosis, mediated by an increase in the lncRNA TINCR (Zhou et al., 2019).

1.4. TGF-β Signalling

1.4.1. TGF-β Signalling Family and Network

The secreted peptide members of the Transforming Growth Factor-β (TGF-β) superfamily have been widely studied, and whilst initially characterised as aiding early embryonic development, members of this family have been shown to be central regulators of both cellular homeostasis, autophagy and pathogenesis (Derynck and Zhang, 2003, Ding and Choi, 2014). The TGF-β ligands themselves are produced from 33 distinct and conserved genes and are categorised into distinct families, named TGF-β, BMPs and activins, among others (Morikawa et al., 2016). Whilst differences exist between the ligand families, generally newly synthesised nascent TGF-β molecules are initially severely inhibited in function by several mechanisms, including disulphide bond formation connecting an inactivating prodomain to the active component, latency inducing N-terminal glycosylation and dimerization of immature molecules (Robertson and Rifkin, 2016, Miyazono and Heldin, 1989). The production of these pro-TGF-β molecules ensures that the manufacturing cell does not respond to its own TGF-β synthesis directly. Following production, these inactive molecules undergo disulphide bond-mediated association with the latent TGF-β binding protein (LTBP) within the ER lumen, with the resultant complex commonly referred to as the large latent complex (LLC) (Hinck et al., 2016). This complex than traverses the cis- and trans-Golgi network, during which proteases cleave the connecting disulphide bond between the prodomain and active domain of the pro-TGF-β proteins present in the dimer. This action results in the separation of these domains, a preparatory step before full activation, whilst still preventing unintended internal signalling events (Tzavlaki and Moustakas, 2020). The LLC is then localised to secretory vesicles, eventually travelling to the cell membrane where they undergo exocytosis into the extracellular space. The resultant complex can then be readily activated or associate with numerous extracellular proteins, delaying activation.

These two different timings of LLC activation has been explained by the action of two different mechanisms. Firstly, recent work by Dong et al. has illustrated that if the LLC associates with the complex network of ECM related proteins present in the extracellular space, such as fibronectin and fibrillin, the beginning step of activation is the enzyme elastase frees the LLC from this entrapment through ECM protein cleavage. The LLC complex is then free to associate with cell type specific integrin receptors, through RGD residues (arginine, glycine and aspartic acid peptides) present within the prodomain of the pro-TGF-β molecule. A unique mechanism of ligand activation then pursues whereby the cytoskeletal-mediated physical force on these receptors causes the separation of the prodomain of TGF-β molecule from the active ligand (Dong et al., 2017). Alternatively reports have suggested the pro-TGF-β molecule is initially separated from the LTBP through the action of tolloid-like proteases, such as BMP-1 (Ge and Greenspan, 2006a). The resultant latent complex then undergoes a final cleavage, mediated by the matrix metalloprotease MMP2, which ensures complete separation of the prodomain from the mature TGF-β ligand (Ge and Greenspan, 2006b).

However activated, the secreted TGF-β ligand then associates with a four-component oligomer of ATP-dependent serine/threonine kinase receptors. The component receptors are separated into two distinct families, named TGF-β Receptor Type 1 (TGFBRI) and TGF-β Receptor Type 2 (TGFBRII type II). Currently, seven TGFBRI and five TGFBRII have been identified, but family member expression is typically cell specific (Heldin and Moustakas, 2016). These receptors however need to be activated in order to undergo full oligomerization. Upon presentation, the TGF-β ligand initially interacts with a TGFBRII homodimer, leading to an increased affinity for TGFBRI homodimers (Groppe et al., 2008). This affinity results in an oligomerization event leading to the interaction of the four TGF-β receptors and the associated ligand. This induced interaction between TGFBRI and TGFBRII homodimers causes the phosphorylation and activation of a juxtamembrane domain in the TGFBRI, leading to the dissociation of the negative regulator FKBP12 and allosteric conformational change, prompting the activation of downstream signalling components (Wrana et al., 1994). This pathway is summarised in Figure 1.6.

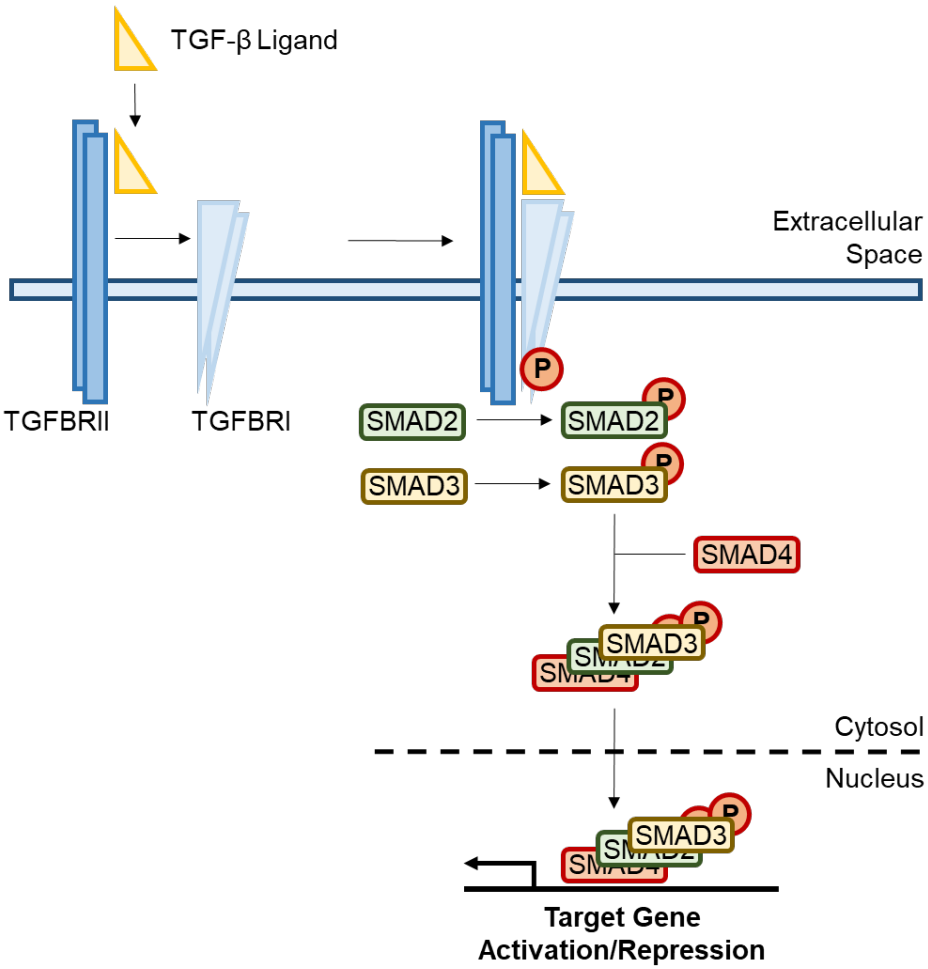

FIGURE 1. 6. BROAD MECHANISM OF TGF-B SIGNALLING ACTIVATION.
TGF-β ligands initially bind to a TGFBRII homodimer, which facilitates TGFBRI homodimer interaction. This ligand/receptor oligomer results in allosteric conformational change of the TGFBRI, causing the activation of downstream R-SMADs, such as SMAD2 and SMAD3. Upon interaction with the co-SMAD SMAD4, this resultant trimer translocates to the nucleus and promotes target gene activation or repression. Adapted from (Tzavlaki and Moustakas, 2020)

These two TGF-β receptors however are not the only receptors involved in this signalling pathway, with multiple receptors now also identified that either act on TGFBRI/II or are able to directly bind to TGF-β ligands to cause unique cellular actions. The transmembrane receptor betaglycan, the glycoprotein endoglin and the glycosylphosphatidylinositol-anchored protein Cripto, have been shown to have complex impacts on TGF-β function, being able to either promote, direct or reduce ligand activity (López-Casillas et al., 1994, Barbara et al., 1999, Yan et al., 2002).

The downstream elements acted on by these receptors are collectively termed R-SMAD proteins, with specific ligand-receptor interactions driving specific R-SMAD activation (Wrana and Attisano, 2000). Generally, SMAD2 and SMAD3 are activated following the binding of TGF-β ligands, with SMAD1, SMAD5 and SMAD8 being activated by BMP ligands (Derynck and Budi, 2019). However, members of all TGF-β ligand families have shown capability of activating all SMAD proteins. In addition to these proteins, co-SMADs act post R-SMAD activation to either mediate or repress downstream effects. A critical co-SMAD is the mediator SMAD4, which is able to interact with phosphorylated R-SMAD proteins through the MH2 domain on its L3 loop (Chacko et al., 2004, Souchelnytskyi et al., 1997). SMAD4 most commonly binds to two activated R-SMADs, facilitating their trafficking and downstream effects. However, trimeric R-SMAD complexes can also be formed that exclude any co-SMADs and can also be produced from any combination of R-SMADs, regardless of activating ligand (Lucarelli et al., 2018). These differing oligomers of R-SMADs and co-SMADs results in finely tuned gene responses specific to signalling and cell contexts.

The resultant SMAD complexes, in whatever composition produced, translocate to the nucleus, where they interact with chromatin remodelling and transcription factors, resulting in the activation or repression of TGF-β specific response genes (Mullen et al., 2011).

1.4.2. TGF-β Signalling in Cell Differentiation, Proliferation and Autophagy

Initial studies of TGF-β revealed its predominant functional role was in the process of embryogenesis (Asashima et al., 1990, Hemmati-Brivanlou et al., 1994). However, research has now shown many additional roles, with two of the critical functions being the coordination of cell differentiation and proliferation. Evidence has shown that TGF-β ligands direct differentiation of neuronal, blood and immune cells (Li and Flavell, 2008, Blank and Karlsson, 2015, Krieglstein et al., 2011). Additionally genetic interference in mice models has further shown that a reduction in TGF-β production, whilst not preventing formation, causes significant defects in multiple bone structures, the central nervous system and critical organs such as the heart, lung and eye (Morikawa et al., 2016). Critical to the present study, TGF-β signalling activity has also been shown to regulate formation of the epidermis, directing embryonic gastrulation and facilitating epithelial-to-mesenchymal transition (EMT) of epiblast tissue, which results in the formation of the mesoderm and endoderm (Robertson, 2014). Later, when the epidermis begins to fully form in the third trimester, TGF-β ligands have been shown to direct formation of several epidermal structures, including the

interfollicular epidermis, hair follicles, sebaceous glands and sweat glands (Blanpain and Fuchs, 2014). Specifically, previous work has demonstrated TGF-β activity as a prominent regulator of epidermal formation through its structural control of keratinocyte proliferation; TGF-β1 overexpression in mice models driven by the *Krt1* promoter arrests the keratinocyte cell cycle, ultimately preventing hyperproliferation of the epidermis (Sellheyer et al., 1993). Interestingly however, overexpression of TGF-β1 driven by the *Krt10* promoter may also lead to increased proliferation of epidermal cells (Cui et al., 1995). Given the strata difference in the expression of these keratins, it is likely that TGF-β activity acts to ensure controlled growth of epidermal stem cell pools but promotes keratinocyte proliferation in higher-level strata to ensure the formation of a functioning epidermis.

TGF-β signalling has also been associated with a regulation of autophagy. However, this interaction has only been reported in disease states. Most notably, TGF-β signalling has been shown to promote fibrosis of both the lung and kidney through direct regulation of autophagy (Racanelli et al., 2018, Ding and Choi, 2014). Specifically, studies have shown TGF-β1 promotes both autophagy and the unfolded protein response in human lung fibroblasts of idiopathic pulmonary fibrosis patients, resulting in the accumulation of collagen and fibronectin, further promoting the fibrosis (Ghavami et al., 2018). Interestingly, TGF-β has also been shown to regulate autophagic activity in the context of cancer with emerging evidence showing TGF-β-induced autophagy allows for the escape of growth inhibition signals, preventing the induction of apoptotic cell death and promotion of cell invasion (Kiyono et al., 2009, Ding et al., 2010, Zhang et al., 2017a).

1.4.3. Overview of TGF-β Signalling in Cancer and cSCC

Beyond its regulation of autophagy, TGF-β has been widely investigated in the broader context of cancer. However, even with multiple decades of study, the specific tumour suppressive or promoting role of TGF-β is still being debated and defined.

Several context specific roles of TGF-β signalling in cancer progression have been proposed reviewed by, (Akhurst and Derynck, 2001).

Firstly, it is widely accepted that the transformation of a normal cell to a pre-lesional cell can be prevented through the inhibitory action of TGF-β signalling (Cui et al., 1996). If this is unsuccessful in preventing tumourigenesis, there are generally two recognised mechanisms of TGF-β signalling, that subsequently influence cancer metastasis. The first arises from genetic mutations that inhibit TGF-β signalling, such as inactivating mutations in either TGFBRI or TGFBRII (Markowitz et al., 1995). Given the well-documented growth inhibitory role of TGF-β1, especially within epidermal stem cell pools, that acts to prevent cell growth and induce apoptosis, the loss of this proliferative control leads to increased cell division. This uncontrolled cell division increases the chances of acquired mutations, leading to tumourigenesis (Massagué et al., 2000). In contrast, and identified more broadly and frequently in numerous cancers, alteration to active TGF-β signalling through interference in SMAD signalling pathway may lead to the acquisition of pro-cancerous characteristics such as increased plasticity and invasive capacity (Akhurst and Derynck, 2001).

Beyond these generally agreed routes to metastasis, growing evidence points towards the crosstalk between TGF-β signalling and other pathways involved in cancer progression and metastasis. Several pathways have been extensively linked to TGF-β signalling, such as MAPK, ERK and AKT pathways (Zhao et al., 2018) . The MAPK pathway, which has been shown to drive cell behaviour changes including reduced differentiation, increased proliferation and resistance to apoptosis has been shown to be activated by TGF-β signalling (Javelaud and Mauviel, 2005). Additionally, cell growth and proliferation associated ERK and AKT pathway activation has also been linked with TGF-β signalling. The activation of the ERK pathway requires TGFBRI activation of the ShcA/Grb2/SOS complex, which can rapidly induce cell survival signals (Lee et al., 2007). Complicating this relationship however, multiple SMAD elements within TGF-β downstream pathways have shown the potential for negative regulation by ERK action (Kretzschmar et al., 1999). PI3K activation of AKT leads to increased cell proliferation and apoptosis inhibition, with TGF-β1 signalling being shown in epithelial cell

lines to bypass PI3K and activation AKT directly (Bakin et al., 2000). Again interestingly, TGF-β1 is commonly seen as tumour suppressor protein further highlighting the role of TGF-β signalling as cell type and cell context specific and the likely differing functional roles within different cancers at different stages of progression.

Within the specific context of cSCC, again the specific role of TGF-β signalling in cancer progression is still debated. Recent work by Siljamäki et al. has suggested that TGF-β secretion by fibroblasts in the cSCC microenvironment leads to the H-Ras dependent accumulation of laminin-332 in cSCC cells, which prompts invasion and metastasis (Siljamäki et al., 2020). However, contrasting work by Rose et al. has shown broad loss or inactivating mutations of TGF-β can be observed in model systems of cSCC tumourigenesis. However, even within this study, activating mutations of TGF-β receptors and the tumour promoting roles of TGF-β ligands were also identified (Rose et al., 2017, Rose et al., 2018). Given these contradictory studies, an improved understanding of TGF-β signalling in cSCC is clearly warranted.

1.5. Hypothesis, Aims and Objectives

Given the importance of AMBRA1 in epidermal differentiation and autophagy and its potential as a biomarker for cutaneous malignancy, the central hypothesis was that loss of AMBRA1 expression leads to the deregulation of epidermal differentiation and autophagy driving cSCC tumourigenesis and progression.

To test this hypothesis, the specific aims of the present study were to:

- Determine the potential of AMBRA1 expression, alone or in combination with the autophagy cargo protein SQSTM1 (p62) in primary cSCC as a prognostic biomarker.
- Investigate the potential mechanisms mediating loss of AMBRA1 expression in cSCC tumourigenesis and specifically the potential contribution of increased ubiquitin-mediated degradation of TGF-β-mediated transcriptional downregulation of AMBRA1.
- Determine the relationship between AMBRA1, autophagy and epidermal differentiation in normal keratinocytes and cSCC in vitro.
- Harness results derived from the present study to inform the commercial development of a novel prognostic test for cSCC.

Chapter 2. Materials and Methods

Table of Contents

2.1. Growth and maintenance of human keratinocyte cell line CCD1106

The human immortalised keratinocyte cell line CCD1106 (immortalised by HPV-16 E6/E7, ATCC, UK) was cultured and maintained in EpiLife medium (ThermoFisher Scientific, USA), supplemented with human keratinocyte growth supplement (HKGS) (ThermoFisher Scientific, USA) and 5% antibiotic antimycotic solution (PSA) (Lonza, Belgium) in T25/T75/T175 cell culture flasks (Corning, USA) and maintained in a humidified atmosphere of 5% CO_2 in air at 37°C. Upon reaching 70-90% confluence, cells were passaged by washing with sterile Dulbecco's phosphate-buffered saline (PBS) (Sigma-Aldrich, USA) twice and detached using Trypsin/EDTA solution (Sigma-Aldrich, USA) for 5-10 minutes as previously described (Verykiou et al., 2019). Once detached, Dulbecco's Modified Eagles Medium (DMEM) with 10% FBS was added to the flask to terminate Trypsin/EDTA induced surface protein cleavage, before between 0.5 – 3.0 mls of detached cells were transferred to new tissue culture flasks in complete EpiLife medium and culture continued for up to a maximum of 10 passages. New cells stored at a low passage number in freezing medium, composed of 90% foetal bovine serum (FBS) (Sigma-Aldrich, USA) and 10% DMSO (Fisher Scientific, USA), in liquid nitrogen, were then revived for further culture up to 10 passages. For all experiments CCD1106 cells were used between 70-90% confluency.

CCD1106 cells were routinely screened for mycoplasma infection using a MycoStrip-Mycoplasma Detection Kit (InvivoGen, USA) according to the manufacturer's specifications and authenticated as cells of a keratinocyte origin by the expression of epithelial specific antigen, detected via immunofluorescence (Gudjonsson et al., 2002).

2.2. Growth and maintenance of human squamous cell carcinoma cell lines

The human cutaneous squamous cell carcinoma isogenic cell lines PM1, MET1 and MET4 (kindly supplied by Prof Mark Birch Machin, Newcastle University) were derived from a patient at different stages of cSCC malignant transformation. PM1, derived from dysplastic forehead skin, MET1, derived from the primary cutaneous tumour and MET4, derived from a distant metastasis, were cultured and maintained in complete RM+ medium. Stock RM+ medium comprised 375 mL of DMEM medium (Lonza, Belgium) and 125 mL of F12 medium (ThermoFisher Scientific, USA) supplemented with 10% foetal bovine serum (FBS) (Sigma-Aldrich, USA), 5 mL antibiotic antimycotic solution (PSA) (Sigma-Aldrich, USA), 0.4 µg/mL Hydrocortisone (Sigma-Aldrich, USA), 8.5 ng/mL Cholera Toxin (Sigma-Aldrich, USA), 26.9

fg/mL Triiodo-L-Thyronine (Sigma-Aldrich, USA), 48.6 ng/mL Adenine (Sigma-Aldrich, USA), 5 µg/mL Insulin (Sigma-Aldrich, USA), 20 pg/mL hEGF (Sigma-Aldrich, USA) and 5 µg/mL Transferrin (Sigma-Aldrich, USA).

The human cutaneous squamous cell carcinoma cell lines IC1, IC1-MET and IC12 (Cancer Research Technologies, UK) were derived from cSCC patients at different stages of cSCC malignant transformation. IC1 and IC1-MET are isogenic cell lines, with IC1 cells derived from a primary cSCC tumour and IC1-MET cells derived from a distant metastasis. These cell lines were cultured and maintained in complete DMEM medium. Stock complete DMEM was comprised of 500 mL DMEM medium (Lonza, Belgium) supplemented with 10% FBS (Sigma-Aldrich, USA) and 5 mL antibiotic antimycotic solution (PSA) (Sigma-Aldrich, USA).

All cells were maintained in a humidified atmosphere of 5% CO2 at 37°C and passaged at 70-90% confluence, as described for CCD1106 cells in section 2.1, for up to a maximum of 50 passages. Frozen stocks of each cell line were stored at a low passage number in freezing medium, as described in section 2.1, in liquid nitrogen, prior to thawing for routine cell culture. For all experiments PM1, MET1, MET4, IC1 and IC1-MET cells were used between 70-90% confluency.

PM1, MET1, MET4, IC1 and IC1-MET cells were routinely screened for mycoplasma infection using a MycoStrip-Mycoplasma Detection Kit (InvivoGen, USA) according to the manufacturer's specifications and authenticated as cSCC cells by the expression of keratin 8 and 18, detected by immunofluorescence (Proby et al., 2000).

2.3. Pilot cohort of well and poorly differentiated cutaneous squamous cell carcinoma

An initial primary cohort of 13 well or poorly differentiated formalin-fixed paraffin-embedded (FFPE) primary cutaneous squamous cell carcinomas (cSCC) were obtained from the Department of Pathology, Royal Victoria Infirmary, Newcastle Upon Tyne Hospitals NHS Foundation Trust, Newcastle upon Tyne, UK.

Full ethical permission for all studies was granted through the Newcastle University Dermatology Biobank (North-East-Newcastle and North Tyneside 1 Research Ethics committee, REF (08/H0906195+5_Lovat).

2.4 Discovery cohort of well, moderately and poorly differentiated cutaneous squamous cell carcinoma

A discovery retrospective cohort of 106 primary, locally recurrent or metastatic formalin-fixed paraffin-embedded (FFPE) cutaneous squamous cell carcinomas (cSCC), which were either well, moderately or poorly differentiated, were obtained from Dr Niki Stefanos (Consultant Histopathologist, Department of Histopathology, Addenbrookes Hospital, Cambridge University Hospitals NHS Foundation Trust, Cambridge, UK (Table 2.1.)

Addenbrookes Hospital Cambridge cSCC Cohort	
Localised Primary cSCC Tumours	
Well-differentiated	22
Moderately-differentiated	24
Poorly-differentiated	19
Recurrent/Metastatic Primary cSCC Tumours	
Well-differentiated	12
Moderately-differentiated	18
Poorly-differentiated	10

TABLE 2. 1. DETAILS OF PRIMARY CSCC TUMOURS IN THE ADDENBROOKES HOSPITAL CAMBRIDGE CSCC COHORT.

Time to disease reoccurrence for each primary tumour was extrapolated from pathology reports, detailing the date of surgical removal of both the primary cSCC tumour and the local recurrence/metastasis.

Full ethical permission for all studies was again obtained through the Newcastle Dermatology Biobank (REC REF 08/H0906195+5_Lovat) and a material transfer agreement with Addenbrookes Hospital Cambridge.

2.5. Chemical and drug treatments

ALX-270-445 (ALX-270-445, Enzo, USA), a selective ATP-competitive inhibitor of the ALK5 receptor, was dissolved in DMSO to reach a concentration of 100 µM. 1 mL aliquots of this stock solution were stored at -20 °C or used to treat cells before defrosting and added to cell culture medium to achieve a final concentration of 50 nM, with an equal volume of vehicle control used as a treatment negative control.

Chloroquine diphosphate salt (hereby referred to as chloroquine), (C6628, Sigma-Aldrich, USA), an inhibitor of autophagosome-lysosomal fusion which acts by increasing lysosomal pH,

was dissolved in sterile double distilled water (ddH_20) to a concentration of 10 mM and stored at room temperature, away from direct light. For all experiments, chloroquine was added to cells for the final 2 hours of treatment at a final concentration of 10 µM.

2.6. Calcium-induced differentiation and nutrient starvation-induced autophagy of CCD1106 or cSCC cell lines.

The switch of culture of keratinocytes from culture in low calcium chloride 60 µM to culture in 1.3 mM calcium chloride was used as a standard model of keratinocyte differentiation (Seo et al., 2005). Calcium chloride dihydrate (C3306, Sigma-Aldrich, USA), was dissolved in sterile ddH_20 to a concentration of 300 mM and stored at room temperature, away from direct light. To induce cellular differentiation, CCD1106 or cSCC cell lines were switched from culture in either EpiLife medium containing 60 µM calcium chloride or RM+ medium containing 1.4 mM calcium chloride to medium containing 1.3 mM calcium chloride for 72 hours.

To model autophagy induction through nutrient deprivation (Pan et al., 2019) all cells were deprived of all growth supplements contained in their respective cell culture medium, i.e. for cSCC cell lines removing, foetal bovine serum, Hydrocortisone , Cholera Toxin Triiodo-L-Thyronine, Adenine, insulin, hEGF and Transferrin and for CCD1106 cells depriving them human epithelial growth factor (serum equivalent) for either 24 or 72 hours. As a reference to nutrient deprivation throughout this thesis, the term serum starvation is used in all figures, legends and text.

2.7. MTS Cell Viability Assay

MET1 cells were seeded at a density of 5.0×10^3, in 100 µL of cell culture medium, into each well of a 96-well cell culture plate (Starstedt, Germany) in at least 3 technical replicates within each experiment and allowed to adhere overnight at 37°C before treatment with either 50 nM or 10 µM of ALX-270-445 for a period of either 24 or 48 hours.

Cell viability was determined by the addition of 20 µL of CellTiter 96® AQ_{ueous} One Solution Cell Proliferation Assay (MTS Reagent) (Promega, UK) for the final 2 hours of treatment incubation, and absorbance measured at 490 nm using a Spectra Max 250 plate reader (Molecular Devices, USA).

2.8. ELISA Assays

TGF-β2 and TGF-β3 secretion by cSCC cell lines was determined using commercial ELISA assays from abcam, UK and Elabscience, USA respectively. Cell culture supernatants from 1.0 x10^5 cSCC cell lines (PM1, MET1 and MET4) cultured in 1.5 mL RM+ medium per well of a 6 well tissue culture plate for 4 days were extracted into a 1.5 mL eppendorf microfuge tubes before centrifugation at 1000 g for 20 minutes at 4°C. Supernatants were then subjected to TGF- β2 or TGF- β3 activation, through the addition of 12.5 µL 1 N hydrochloric acid (VWR Chemicals, USA) and incubation for 10 minutes at room temperature and subsequent neutralisation by the addition of 12.5 µL 1.2 N Sodium Hydroxide (Fisher, USA) with 0.5 M HEPES (Sigma-Aldrich, USA) solution. The ELISA was then carried out according to manufactures specification with TGF-β2 or TGF- β3 concentrations determined at 450 nm using a SpectraMAX 250 plate reader as compared with a standard curve on a log-log graph.

2.9 Cell Lysis

Adhered CCD1106, PM1, MET1, MET4, IC1, IC1-MET and IC12 cells were directly lysed in 150 µL of lysis buffer 100 mM trizma hydrochloride pH 7.4 (Sigma-Aldrich, USA), 100 mM sodium chloride (VWR Chemicals, USA) 25mM sodium fluoride (Sigma-Aldrich, USA), 1 mM benzamine (Sigma-Aldrich, USA), 2 mM EDTA (Sigma-Aldrich, USA), 0.1 mM sodium orthovanadate (Sigma-Aldrich, USA), 0.1% Triton x100 (Fisher, USA) containing 15% v/v protease inhibitor cocktail (Promega, UK) and dislodged using a 1.7 cm blade cell scrapper (Sarstedt, Germany) before transfer to a 1.5 mL eppendorf tube and incubation on ice for 30 minutes. Cell lysates were then either processed directly for Western blotting of stored prior to use at -20°C

2.10. Western blotting

Cell lysates were sonicated for 2×5 second pulses at an amplitude of 7 µm, using a Soniprep 150 probe sonicator (MSE, UK), and protein concentration determined using a Bradford protein quantification assay (ThermoFisher Scientific, USA), according to the manufactures instructions. Protein absorption was determined at 595 nm using a SpectraMAX 250 plate reader (Molecular Devices Ltd, UK). 10 µg of protein was diluted 3:4 in 4x sample buffer (250 mM trizma hydrochloride (pH 8) (Sigma-Aldrich, USA), 8% sodium dodecyl sulphate (SDS) (Fisher, USA), 40% glycerol (Fisher, USA) and bromophenol blue (Sigma-Aldrich, USA) with 10% β-mercaptoethanol (Sigma-Aldrich, USA) and separated using 4-20% pre-cast tris-glycine gels

(Bio-Rad, USA), alongside a prestained protein ladder (Invitrogen, UK) by sodium dodecyl sulphate polyacrylamide gel electrophoresis (SDS-PAGE) in 25 mM trizma base (Sigma-Aldrich, USA), 190 mM glycine (Fisher, USA) and 0.1% sodium dodecyl sulphate (SDS) (Fisher, USA) running buffer. Resultant gels were then transferred onto PVDF membrane (Bio-Rad, USA) using a Turbo-Blotter (Bio-Rad, USA). Membranes were subsequently incubated at room temperature for 60 minutes in 5% milk (OXOID, UK) diluted in tris-buffered saline and 0.1% tween (TBS-T) blocking solution. Membranes were then incubated in primary antibodies (Table 2.2), diluted in either 5% milk (OXOID, UK) or 5% bovine serum albumin (BSA) (2BScientific, UK) in TBS-T solution, overnight at 4°C. Following three washes in TBS-T, membranes were then incubated with secondary antibodies (Table 2.3), diluted in a 5% milk (OXOID, UK) in TBS-T solution, for 60 minutes at room temperature. After a further three washes in TBS-T antibody binding was revealed using Clarity Western ECL-Substrate (Bio-Rad, USA) according to the manufacturer's instructions and visualised and quantified by densitometry using a Licor Odyssey Fc (Licor, USA). Protein expression was normalised against GAPDH loading control and compared to the average densitometry value for the experimental replicate to produce a relative expression value.

Antibody Target	Host Species	Clonality	Dilution Ratio	Product Code	Supplier
AMBRA1	Rabbit	Polyclonal	1:1000	26190002	Novus
AMBRA1	Rabbit	Polyclonal	1:1000	24907	Cell Signalling Technology
AMBRA1	Rabbit	Polyclonal	1:1000	ABC131	Millipore
c-Myc	Rabbit	Polyclonal	1:1000	9402	Cell Signalling Technology
Cullin 4A	Rabbit	Polyclonal	1:1000	A300-739A	Bethyl Laboratories
GAPDH	Rabbit	Monoclonal	1:10000	2118S	Cell Signalling Technology
LC3B	Rabbit	Polyclonal	1:1000	2775S	Cell Signalling Technology
Loricrin	Rabbit	Polyclonal	1:10,000	Poly19051	BioLegend
p62 (SQSTM1)	Mouse	Monoclonal	1:1000	sc-28359	Santa Cruz
P-SMAD1/5/9	Rabbit	Monoclonal	1:1000	13820	Cell Signalling Technology
P-SMAD2	Rabbit	Polyclonal	1:1000	3101	Cell Signalling Technology
P-SMAD2	Rabbit	Monoclonal	1:1000	3108	Cell Signalling Technology
P-SMAD3	Rabbit	Monoclonal	1:1000	ab52903	Abcam
TGF-β2	Rabbit	Polyclonal	1:10,000	AB-12-NA	R&D Systems
TGF-β3	Goat	Polyclonal	1:500	AB-244-NA	R&D Systems
Total SMAD1	Rabbit	Polyclonal	1:1000	9743	Cell Signalling Technology
Total SMAD2	Rabbit	Monoclonal	1:1000	5339	Cell Signalling Technology
Total SMAD3	Rabbit	Monoclonal	1:1000	9523	Cell Signalling Technology
Total SMAD5	Rabbit	Monoclonal	1:1000	12534S	Cell Signalling Technology

TABLE 2. 2. PRIMARY ANTIBODIES USED IN WESTERN BLOTTING.

Antibody Target	Host Species	Format	Dilution Ratio	Product Code	Supplier
Peroxidase Labelled Anti-Goat IgG	Goat	Concentrate	1:2500	PI-1000	Vector Laboratories
Peroxidase Labelled Anti-Mouse IgG	Horse	Concentrate	1:2500	PI-2000	Vector Laboratories
Peroxidase Labelled Anti-Rabbit IgG	Horse	Concentrate	1:2500	PI-9500	Vector Laboratories

TABLE 2. 3. SECONDARY ANTIBODIES USED IN WESTERN BLOTTING.

2.11. Generation of recombinant antibodies to p62 using HuCAL technology

Novel recombinant p62 antibody clones were generated by Bio-Rad, USA on the behalf of AMLo Biosciences ltd, UK. using their HuCAL antibody generation service. HuCAL antibody development employs CysDisplay technology to screen billions of potential antibody genes for high-affinity recognition of an immobilised antigen, for this study SQSTM1 (p62). 13 high performing clones were produced for use in this study (Table 2.5).

Antibody Target	Host Species/ Conjugated Species/ Conjugated Region	Clonality	Dilution Ratio	Product Code	Supplier
p62 (SQSTM1)	HuCAL - FLAG	Monoclonal	1:10 – 1:10,000	AbD34896.1	AMLo Biosciences
p62 (SQSTM1)	HuCAL - FLAG	Monoclonal	1:10 – 1:10,000	AbD34897.1	AMLo Biosciences
p62 (SQSTM1)	HuCAL - FLAG	Monoclonal	1:10 – 1:10,000	AbD34898.1	AMLo Biosciences
p62 (SQSTM1)	HuCAL - FLAG	Monoclonal	1:10 – 1:10,000	AbD34899.1	AMLo Biosciences
p62 (SQSTM1)	HuCAL - FLAG	Monoclonal	1:10 – 1:10,000	AbD34900.1	AMLo Biosciences
p62 (SQSTM1)	HuCAL - FLAG	Monoclonal	1:10 – 1:10,000	AbD34901.1	AMLo Biosciences
p62 (SQSTM1)	HuCAL - FLAG	Monoclonal	1:10 – 1:10,000	AbD34902.1	AMLo Biosciences
p62 (SQSTM1)	HuCAL - FLAG	Monoclonal	1:10 – 1:10,000	AbD34903.1	AMLo Biosciences
p62 (SQSTM1)	HuCAL - FLAG	Monoclonal	1:10 – 1:10,000	AbD34904.1	AMLo Biosciences
p62 (SQSTM1)	HuCAL - FLAG	Monoclonal	1:10 – 1:10,000	AbD34905.1	AMLo Biosciences
p62 (SQSTM1)	HuCAL - FLAG	Monoclonal	1:10 – 1:10,000	AbD34906.1	AMLo Biosciences
p62 (SQSTM1)	HuCAL - FLAG	Monoclonal	1:10 – 1:10,000	AbD34907.1	AMLo Biosciences
p62 (SQSTM1)	HuCAL - FLAG	Monoclonal	1:10 – 1:10,000	AbD34908.1	AMLo Biosciences
p62 (SQSTM1)	HuCAL - Mouse	Monoclonal	1:10 – 1:10,000	AbD34907.1	AMLo Biosciences
p62 (SQSTM1)	HuCAL - Mouse	Monoclonal	1:10 – 1:10,000	AbD34908.1	AMLo Biosciences

TABLE 2. 4. LIST OF PRIMARY ANTIBODIES GENERATED USING HUCAL TECHNOLOGY.

2.12. Manual immunohistochemistry for detection of AMBRA1 and p62 expression in FFPE and OCT embedded tissue sections.

Slides with 4 µm FFPE fixed tissue were deparaffinised by submersion in Histo-Clear II (National Diagnostics, USA) for 20 minutes at room temperature, followed by 100% , 75% and 50% ethanol (Fisher, USA) each for 5 seconds before a final rinse in dH2O.

Both these deparaffinised FFPE sections and 4 µm frozen sections in optimal cutting temperature (OCT) compound were then subjected to antigen retrieval.

Antigen retrieval was performed by heating slides in a microwave (Sharp, Japan) for 5 minutes twice in 10 mM tris hydrochloric acid solution (pH 9.0), before cooling at room temperature for 15 minutes. Once cooled, sections were marked around with a hydrophobic pen, washed in PBS with 1 % tween (Fisher, USA) (PBS-T) and permeabilised in 0.2% Triton x100 (Fisher, USA) solution for 10 minutes at room temperature. Endogenous peroxidase activity was then blocked by incubating tissue sections in 3% hydrogen peroxide solution (Sigma-Aldrich, USA) for 3 minutes, before washing in PBS-T and blocking endogenous avidin binding sites by incubation in avidin solution (Vector, USA) for 15 minutes. Following a further three washes in PBS-T, sections were then incubated in 2% serum, appropriate to the subsequent primary antibody for 20 minutes before two washes in PBS and incubation with primary antibodies (Table 2.5), diluted in the appropriate 2% serum/PBS solution, for 60 minutes at room temperature. Following 3 PBS-T washes, primary antibody binding was then detected using secondary antibodies (Table 2.6), diluted in the appropriate 2% serum/PBS solution, for 60 minutes at room temperature. Sections were then washed twice in PBS-T before incubation with ABC reagent (Vector, USA) for 30 minutes at room temperature. Following this, sections were washed again in PBS-T before incubation with 3,3'-diaminobenzidine substrate (DAB) (Vector, USA) for 2 minutes at room temperature, washing in tap water for 10 minutes and counterstaining with Meyer's Haemalum (ThermoFisher Scientific, USA) for 30 seconds. Sections were finally washed for 10 minutes in tap water, with multiple changes, dehydrated by submersing the solution in 75% ethanol for 5 seconds and then 100% ethanol for 5 seconds and Histo-Clear II for 2 minutes and mounting with a coverslip in DPX (ThermoFisher Scientific, USA). Image analysis was performed using a Licor Aperio AT2 slide scanner (Licor, USA).

Antibody Target	Host Species/ Conjugated Species/ Conjugated Region	Clonality	Dilution Ratio	Product Code	Supplier
AMBRA1	HuCAL - Mouse	Monoclonal	1:60	AbD33473	AMLo Biosciences
p62 (SQSTM1)	Mouse	Monoclonal	1:50	sc-28359	Santa Cruz
p62 (SQSTM1)	HuCAL - FLAG	Monoclonal	1:10 – 1:10,000	AbD34896.1	AMLo Biosciences
p62 (SQSTM1)	HuCAL - FLAG	Monoclonal	1:10 – 1:10,000	AbD34897.1	AMLo Biosciences
p62 (SQSTM1)	HuCAL - FLAG	Monoclonal	1:10 – 1:10,000	AbD34898.1	AMLo Biosciences
p62 (SQSTM1)	HuCAL - FLAG	Monoclonal	1:10 – 1:10,000	AbD34899.1	AMLo Biosciences
p62 (SQSTM1)	HuCAL - FLAG	Monoclonal	1:10 – 1:10,000	AbD34900.1	AMLo Biosciences
p62 (SQSTM1)	HuCAL - FLAG	Monoclonal	1:10 – 1:10,000	AbD34901.1	AMLo Biosciences
p62 (SQSTM1)	HuCAL - FLAG	Monoclonal	1:10 – 1:10,000	AbD34902.1	AMLo Biosciences
p62 (SQSTM1)	HuCAL - FLAG	Monoclonal	1:10 – 1:10,000	AbD34903.1	AMLo Biosciences
p62 (SQSTM1)	HuCAL - FLAG	Monoclonal	1:10 – 1:10,000	AbD34904.1	AMLo Biosciences
p62 (SQSTM1)	HuCAL - FLAG	Monoclonal	1:10 – 1:10,000	AbD34905.1	AMLo Biosciences
p62 (SQSTM1)	HuCAL - FLAG	Monoclonal	1:10 – 1:10,000	AbD34906.1	AMLo Biosciences
p62 (SQSTM1)	HuCAL - FLAG	Monoclonal	1:10 – 1:10,000	AbD34907.1	AMLo Biosciences
p62 (SQSTM1)	HuCAL - FLAG	Monoclonal	1:10 – 1:10,000	AbD34908.1	AMLo Biosciences
p62 (SQSTM1)	HuCAL - Mouse	Monoclonal	1:10 – 1:10,000	AbD34907.1	AMLo Biosciences
p62 (SQSTM1)	HuCAL - Mouse	Monoclonal	1:10 – 1:10,000	AbD34908.1	AMLo Biosciences

TABLE 2. 5. PRIMARY ANTIBODIES USED IN MANUAL IMMUNOHISTOCHEMISTRY.

Antibody Target	Host Species	Clonality/ Format	Dilution Ratio	Product Code	Supplier
Anti-FLAG M2-Peroxidase	Mouse	Monoclonal	1:200	A8592	Sigma Aldrich
Peroxidase Labelled Anti-Mouse IgG	Horse	Concentrate	1:200	PI-2000	Vector Laboratories

TABLE 2. 6. SECONDARY ANTIBODIES USED IN MANUAL IMMUNOHISTOCHEMISTRY.

2.13. Automated immunohistochemistry for AMBRA1 and p62 expression in FFPE tissue sections

Automated immunohistochemical staining of 4 μm FFPE sections of cSCC tissue on glass slides derived from either the Newcastle or Cambridge cohorts of cSCC for AMBRA1 and p62 expression (Table 2.7) was performed using a Ventana Benchmark (Ventana Medical Systems, USA) automated staining instrument by the Department of Pathology, Royal Victoria Infirmary, Newcastle Upon Tyne Hospitals NHS Foundation Trust, Newcastle upon Tyne, UK. All slides were counterstained with either 3,3'-diaminobenzidine substrate (DAB) or Fast Red substrate and Haemalum. Whole slide digital images (X40 magnification) of AMBRA1 or p62 staining were then obtained using an Aperio AT2 Slide Scanner (Leica Biosystems, UK).

Antibody Target	Host Species/ Conjugated Species/ Conjugated Region	Clonality	Dilution Ratio	Product Code	Supplier
AMBRA1	HuCAL - Mouse	Monoclonal	1:60	AbD33473	AMLo Biosciences
p62 (SQSTM1)	Mouse	Monoclonal	1:50	sc-28359	Santa Cruz

TABLE 2. 7. PRIMARY ANTIBODIES USED IN AUTOMATED IMMUNOHISTOCHEMISTRY.

2.14. Digital H-score quantification of AMBRA1 and p62 expression in cSCC stained tissue sections.

All digital H-score quantification was undertaken using the Aperio ImageScope Software (V12.4.2.5010, Leica Biosystems, UK). For each cSCC tumour, four regions of interest were identified; the normal epidermis, peritumoural epidermis, tumour mass and tumour growth front. 2 areas of normal/peritumoural epidermis and 5 areas of tumour mass/tumour growth front were annotated for each tumour, prior to H-score analysis. All cytoplasmic expression was analysed using the cytoplasmic V2 algorithm and the nuclear expression was analysed using the nuclear V9 algorithm, with both algorithms pre-optimised for analysis of primary keratinocytes and cSCC cells (Figure 2.1 and Figure 2.2). The mean H score was derived for all representative staining in either the 2 normal/peritumoural epidermal regions or 5 annotated area of tumour mass/tumour growth front.

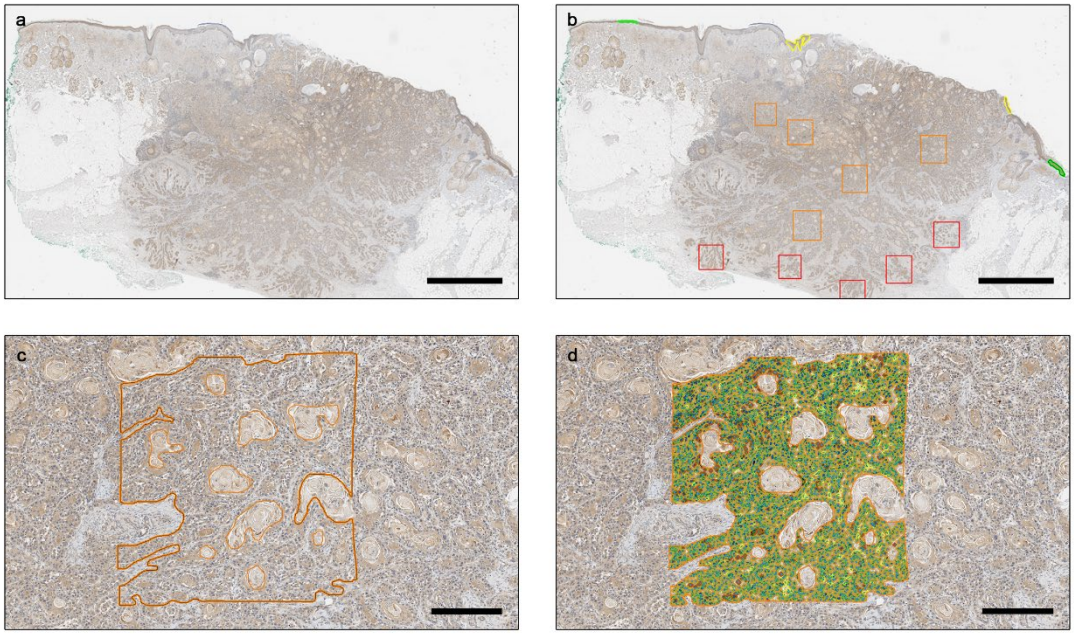

FIGURE 2. 1. REPRESENTATIVE IMAGES DEMONSTRATING THE DIGITAL CYTOPLASMIC H-SCORE QUANTIFICATION METHODOLOGY.

(a) *Representative image of a cSCC tumour pre-analysis**.*** *Scale bar = 3 mm.* ***(b)*** *Representative image of a cSCC tumour with the key areas identified. Green annotations depict normal epidermis, yellow annotations depict peritumoural epidermis, orange annotations depict tumour mass and red annotation depict tumour growth front. Scale bar = 3 mm.* ***(c)*** *Representative image of the detailed annotations of one area of tumour mass. Area within solid line depicts viable tumour cells and area within dashed line depicts non-viable areas, such as highly keratinised regions. Scale bar = 300 µm.* ***(d)*** *Representative image of a detailed annotation of one area of tumour mass analysed with the cytoplasmic V2 algorithm. Individual cell cytoplasm -s assigned a colour based on staining intensity. Yellow represents negative staining, orange represents weak positive staining, brown represents moderate positive staining and red represents strong positive staining. Scale bar = 300 µm.*

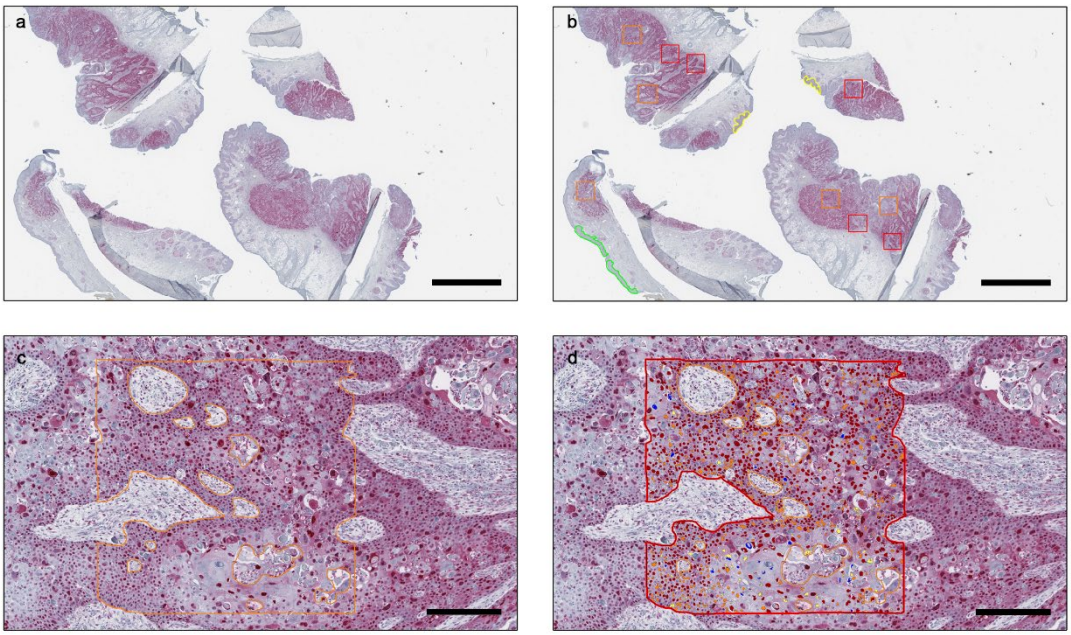

FIGURE 2. 2. REPRESENTATIVE IMAGES DEMONSTRATING THE DIGITAL NUCLEAR H-SCORE QUANTIFICATION METHODOLOGY. ***(a)*** *Representative image of a cSCC tumour pre-analysis****.*** *Scale bar = 4 mm.* ***(b)*** *Representative image of a cSCC tumour with the key areas identified. Green annotations depict normal epidermis, yellow annotations depict peritumoural epidermis, orange annotations depict tumour mass and red annotation depict tumour growth front. Scale bar = 4 mm.* ***(c)*** *Representative image of the detailed annotations of one area of tumour mass. Area within solid line depicts viable tumour cells and area within dashed line depicts non-viable areas, such as highly keratinised regions. Scale bar = 300 µm.* ***(d)*** *Representative image of a detailed annotation of one area of tumour mass analysed with the nuclear V9 algorithm. Individual cell nucleuses are assigned a colour based on staining intensity. Blue represents negative staining, yellow represents weak positive staining, orange represents moderate positive staining and red represents strong positive staining. Scale bar = 300 µm.*

2.15. Statistical Analysis

Data throughout this thesis were analysed using the statistical software Prism 9 (Graph Pad, USA). All data were accessed for normal distribution with a Shapiro-Wilk test. If data had insufficient individual points or wasn't normally distributed, the appropriate nonparametric test was used. Statistical significance is indicated by P values of *P<0.05, **P<0.01, ***P<0.001 and ****P<0.0001. Statistical tests that resulted in P>0.05 were deemed as non-significant (ns).

Protein bands produced by western blotting were quantified using the Image Studio Software (Licor, USA). Relative protein expression was calculated by densitometry, comparing the protein of interest to either a loading control or inactivated form of the protein, and was expressed as a mean ± SD of three independent experiments (N=3). These data were then tested for significance using one-way analysis of variance (ANOVA) with Tukey's post-hoc correction.

TGF-β2 and TGF-β3 concentrations in the cSCC cell line supernatants analysed by ELISA assay were expressed as the mean ± SD of three independent experiments (N=3). These data were then tested for significance using one-way analysis of variance (ANOVA) with Tukey's post-hoc correction.

Cell viability assays were analysed by normalising test conditions to control conditions, with resultant values expressed as a mean ± SD of three independent experiments (N=3). These data were then tested for significance using one-way analysis of variance (ANOVA) with Tukey's post-hoc correction.

The cytoplasmic and nuclear expression of AMBRA1 and p62 in the normal epidermis, peritumoural epidermis, tumour mass and growth front of cSCC tumours were quantified using digital methodology (described in section 2.13) to derive a mean H-score for expression in each designated region. cSCCs were categorised according to their metastatic and differentiation status with the mean ± SD of each area of cSCC tumour compared between these categories, and with significance tested using one-way analysis of variance (ANOVA) with Tukey's post-hoc correction.

The prognostic potential of cytoplasmic and nuclear expression of AMBRA1 and p62 in in the normal epidermis, peritumoural epidermis, tumour mass and growth front of cSCC tumours

was accessed using ROC curve analysis, with area under the curve (AUC) values closest to 1 indicating the best prognostic potential.

The ability of cytoplasmic and nuclear expression of AMBRA1 and p62 in in the normal epidermis, peritumoural epidermis, tumour mass and growth front of cSCC tumours to predict survival was analysed using Kaplan-Meier survival analysis, with Log-rank (Mantel-Cox) test used to determine significant separation of populations.

Chapter 3. Defining the potential of AMBRA1 and p62 as prognostic biomarkers for high -risk cutaneous squamous cell carcinoma

Table of Contents

3.1. Introduction

The global incidence of cSCC is increasing worldwide and is a considerable health care burden (Venables et al., 2019b, Lomas et al., 2012, Goon et al., 2017, Cust, 2017). While surgical excision of the primary tumour has a high likelihood of being a curable event (Simonacci et al., 2018, van Lee et al., 2019) the prognosis however, for patients who develop advanced disease is poor (Brodland and Zitelli, 1992, Tokez et al., 2021, Schmults et al., 2013). Coupled with the inability of current clinical parameters to accurately predict metastatic risk (Weinberg et al., 2007) there is hence an urgent unmet need for the development of reliable and consistent biomarkers able to identity subsets of patients with cSCC at risk of disease recurrence or metastasis.

Given the high degree of genetic heterogeneity and variety in sub-clonal populations within primary cSCC tumours (Ji et al., 2020, Inman et al., 2018) a genetic driven approach to the identification of biomarkers for cSCC progression is unlikely to succeed. However, protein biomarkers may offer a more effective approach (Azimi et al., 2020a, Azimi et al., 2020b).
The deregulation of autophagy has been shown to be a key event in cancer development and progression (Singh et al., 2018) and in this context several biomarkers reflecting the paradoxical role of this key signalling pathway have been proposed, including and importantly in the context of cutaneous malignancy, AMBRA1 (Tang et al., 2016, Ellis et al., 2020) and SQSTM1 (p62) (Ellis et al., 2014).

Supported by studies in the melanoma microenvironment AMBRA1 plays a key role in keratinocyte differentiation with its loss in the epidermis overlying primary early AJCC stage melanomas being a prognostic biomarker (Cosgarea et al., 2021, Ellis et al., 2020),and suggesting its potential as a biomarker for cSCC.

SQSTM1 (p62), as an autophagy cargo protein has also been proposed as a prognostic biomarker in cutaneous malignancy. This again reflects the paradoxical role of autophagy and hence its accumulated expression in cells where autophagy is blocked driving genotoxicity, while lower levels of expression reflect active autophagy as seen in solid tumour cells

undergoing oxidative stress (Li et al., 2021, Yan et al., 2019, Kim et al., 2019, Lei et al., 2020, Ellis et al., 2014).

These observations, combined with pilot data leading to the current study demonstrating an association between the change in the level and subcellular localisation of p62 expression and cSCC differentiation status, suggest p62 expression may also act as a prognostic biomarker for cSCC progression.

To investigate the potential of both AMBRA1 and p62 as prognostic biomarkers for cSCC, the aims of the present chapter were therefore to:

- ***Evaluate AMBRA1 expression and cellular localisation in well, moderately or poorly differentiated primary cSCCs and any association/correlation with disease outcome.***
- ***Evaluate p62 expression and cellular localisation in well, moderately or poorly differentiated cSCC tumourigenesis and any association/correlation with disease outcome.***
- ***Determine the potential for AMBRA1 and/or p62 expression as prognostic biomarkers for cSCC patient progression.***
- ***Validate a novel anti-p62 antibody for use in future cSCC prognostic biomarker validation studies for the sponsoring company of the present study, AMLo Biosciences Ltd.***

3.2. Results

3.2.1. Loss of AMBRA1 expression occurs in well and poorly differentiated primary cSCC tumours

Pilot studies leading to the current thesis suggested AMBRA1 expression was associated with the differentiation status of primary cSCC tumours; well-differentiated primary cSCC tumours maintained cytoplasmic expression, whilst expression was reduced in poorly differentiated primary cSCC tumours compared to expression in the normal epidermis (Ellis, Husain and Lovat unpublished data). This difference in expression, coupled with published data indicating a poorly differentiated phenotype is associated with increased risk of cSCC progression (Que et al., 2018), suggested AMBRA1 as a potential prognostic biomarker for cSCC progression.

To further probe a potential relationship between AMBRA1 expression and differentiation status in primary cSCC tumours, automated immunohistochemical staining for AMBRA1 expression was carried out in a pilot cohort of 13 FFPE primary Newcastle derived cSCC tumours. In contrast to initial observations, results demonstrated variable expression of AMBRA1 in both well and poorly differentiated primary cSCC tumours (Figure 3.1A), with expression of AMBRA1 extensively reduced (Figure 3.1A a and d), partially reduced (Figure 3.1A b and e) as well as being retained in both cSCC tumour subsets. (Figure 3.1A c and f). Moreover, there was notable heterogeneity in AMBRA1 expression (Figure 3.1B) within tumours, where expression in some tumour areas was notably absent, (Figure 3.1B a), partially lost (Figure 3.1B b) or retained (Figure 3.1B c).

In contrast to the initial hypothesis that AMBRA1 expression correlates with tumour differentiation status, collectively, these data suggest AMBRA1 expression between and within cSCC tumours of differing cellular differentiation status is more complex. A more thorough investigation of AMBRA1 expression in a larger primary cSCC tumour cohort with defined clinical follow up was therefore subsequently undertaken in order to test its potential as a prognostic biomarker for cSCC progression.

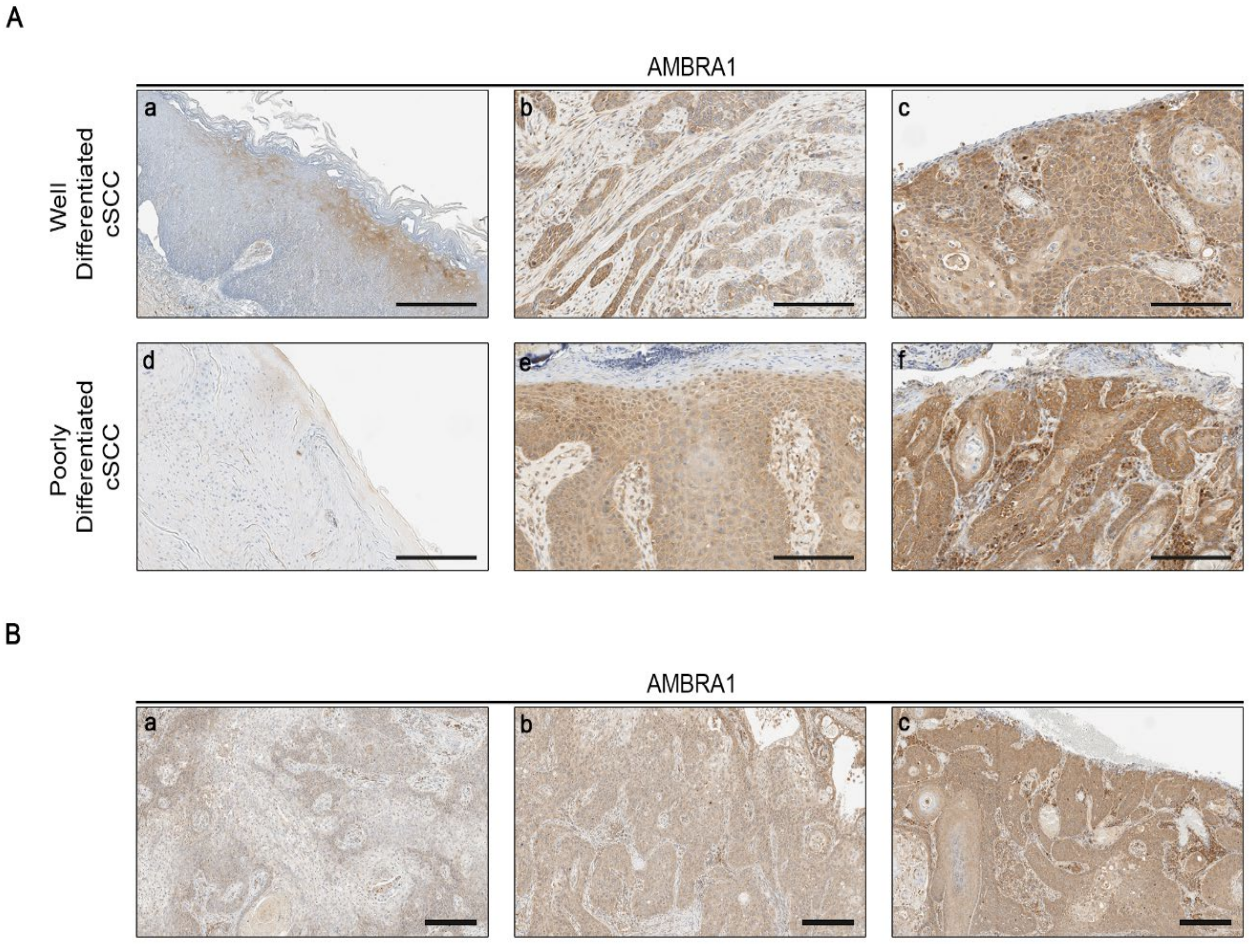

FIGURE 3. 1. AMBRA1 EXPRESSION IN BOTH WELL AND POORLY DIFFERENTIATED PRIMARY CSCC TUMOURS WITH SOME DISPLAYING LARGE HETEROGENEITY

*(**A**) Representative photomicrograph images of AMBRA1 expression in (**a-c**) 3 well differentiated cSCC and (**d-f**) 3 poorly differentiated cSCC. Visible staining was achieved via automated immunohistochemistry with a DAB counterstain. Images were taken using bright field microscopy at a magnification of 13.4x. Scale bar = 200 µm. (**B**) Representative photomicrograph images of AMBRA1 staining in three areas of a primary cSCC representing (**a**) low level of expression, (**b**) moderate level of expression and (**c**) high level of AMBRA1 expression. Visible staining was achieved via automated immunohistochemistry with a DAB counterstain. Images were taken using bright field microscopy at a magnification of 8.6x. Scale bar = 300 µm.*

3.2.2. Increased cytoplasmic and nuclear p62 expression is observed in well and poorly differentiated primary cSCC tumours

Additionally, to the observations between cSCC differentiation status and AMBRA1 expression, previous studies also investigated the relationship between p62 expression and cSCC tumourigenesis. Results suggested that p62 expression changes from a nuclear to a cytoplasmic subcellular location during cSCC tumourigenesis and invasion into deeper tissue compartments (Ellis, Husain and Lovat unpublished data). To further interrogate this result, the present study incorporated the automated immunohistochemical analysis of p62 expression in the same pilot cohort of 13 FFPE primary cSCC tumours (Figure 3.2). In contrast to observations made in previous studies, results demonstrated an increase in p62 expression in both the nuclear (Figure 3.2 a-c) and cytoplasmic (Figure 3.2 a-b) subcellular locations during cSCC tumourigenesis and invasion. However, similarly to observations with AMBRA expression, this differential p62 expression was only observed in a few of the 13 pilot cohort of primary cSCC tumours, prompting further studies in a larger discovery cohort of cSCC tumours of differing cellular differentiations status with full clinical follow up, in order to further define the relationship between cSCC tumourigenesis and p62 expression and the potential for p62 as a prognostic biomarker for cSCC.

Taken together, these data nevertheless demonstrate a change in both p62 expression and subcellular localisation may be linked to cSCC tumourigenesis and progression.

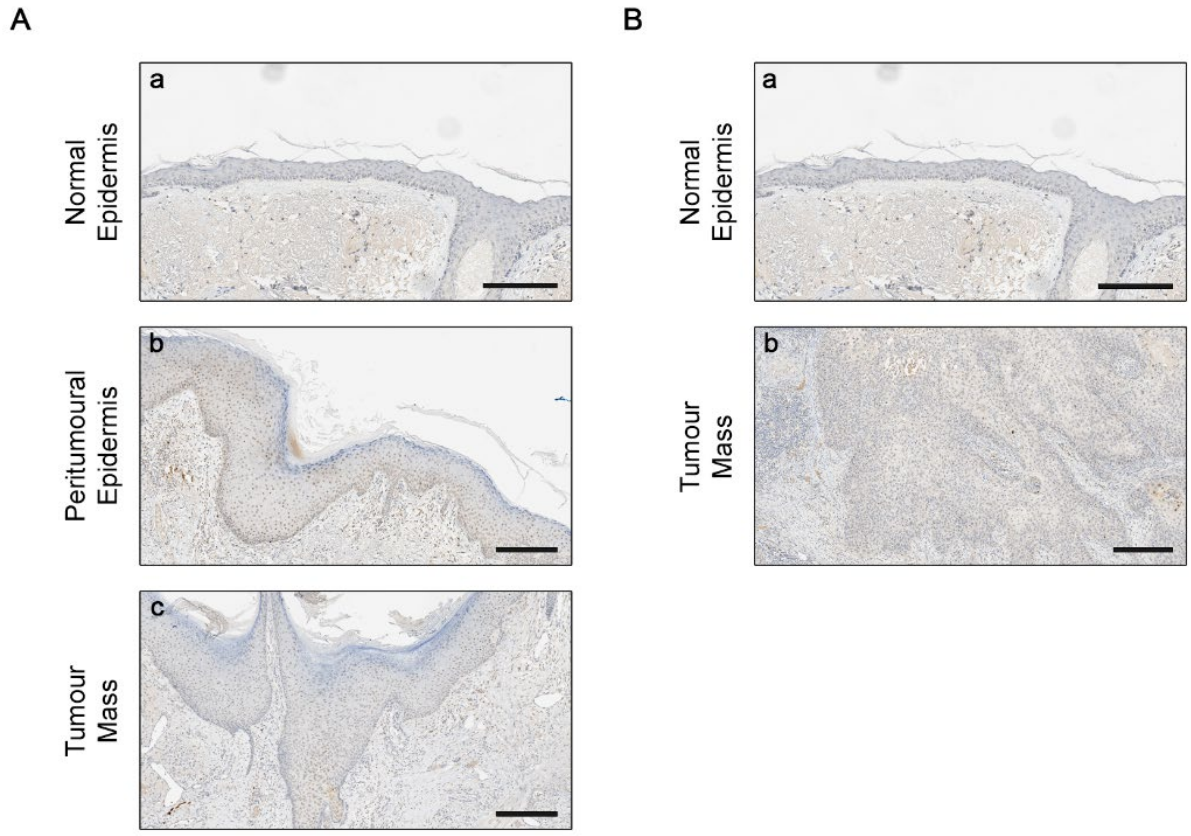

FIGURE 3. 2. CYTOPLASMIC AND NUCLEAR P62 EXPRESSION INCREASES DURING CSCC TUMOURIGENESIS
*(**A**) Representative photomicrograph images of p62 expression in a primary cSCC in the (**a**) normal epidermis, (**B**) peritumoural epidermis and (**c**) tumour mass. Visible staining was achieved via immunohistochemistry with a DAB counterstain. Image **a** was taken using bright field microscopy at a magnification of 15.0x. Scale bar = 200 µm. Images **b** and **c** were taken using bright field microscopy at a magnification of 8.0x. Scale bar = 300 µm. (**B**) Representative photomicrograph images of p62 staining in a primary cSCC in the (**a**) normal epidermis and the (**b**) tumour mass. Visible staining was achieved via immunohistochemistry with a DAB counterstain. Image **a** was taken using bright field microscopy at a magnification of 15.0x. Scale bar = 200 µm. Image **b** taken using bright field microscopy at a magnification of 8.0x. Scale bar = 300 µm*

3.2.3. Qualitative analysis of AMBRA1 and p62 expression in a discovery cohort of localised and recurrent/metastatic primary cSCC tumours reveals loss of tumoural AMBRA1 expression and a gain of nuclear and cytoplasmic p62 expression is associated with cSCC tumourigenesis

To enable the analysis of AMBRA1 and p62 expression as potential prognostic biomarkers for cSCC patients, a discovery cohort of 108 primary cSCC tumours with known clinical follow-up and differentiation status was sourced from Dr Niki Stefanos, Addenbrookes Hospital (As described in Section 2.4). All tissue sections derived from this tumour cohort were subjected to automated immunohistochemistry for both AMBRA1 and p62 expression.

Consistent with analysis of expression in the pilot cohort of 13 cSCCs derived from Newcastle, results revealed, regardless of differentiation status or disease outcome, AMBRA1 expression was consistently lost in primary cSCC tumours when compared to expression in the normal epidermis (Figure 3.3A). This suggests that the loss of AMBRA1 expression, and the subsequent deregulation of both keratinocyte differentiation and autophagy, is key to cSCC tumourigenesis.

Secondly, results revealed an increase in p62 expression during cSCC tumourigenesis and progression, as evidenced by increased expression in tumour cells which had invaded into deeper tissue compartments (Figure 3.3 B). Keratinocytes present in peritumoural regions (i.e. epidermal regions lying directly next to the site of cSCC tumour) also exhibited an increased level of nuclear p62 expression as compared with expression in the keratinocytes present in normal epidermis (Figure 3.3B a-b). Interestingly, within cSCC tumour cells an increase in both cytoplasmic and nuclear p62 expression was also observed (Figure 3.3 c).

Given the apparent complexity of AMBRA1 and p62 expression and subcellular localisation in cSCC progression, a digital approach was subsequently developed to quantify AMBRA1 and p62 (both nuclear and cytoplasmic) in differing regions of primary cSCCs and in their tumour microenvironment using the Cambridge discovery cohort of primary localised or recurrent/metastatic cSCCs.

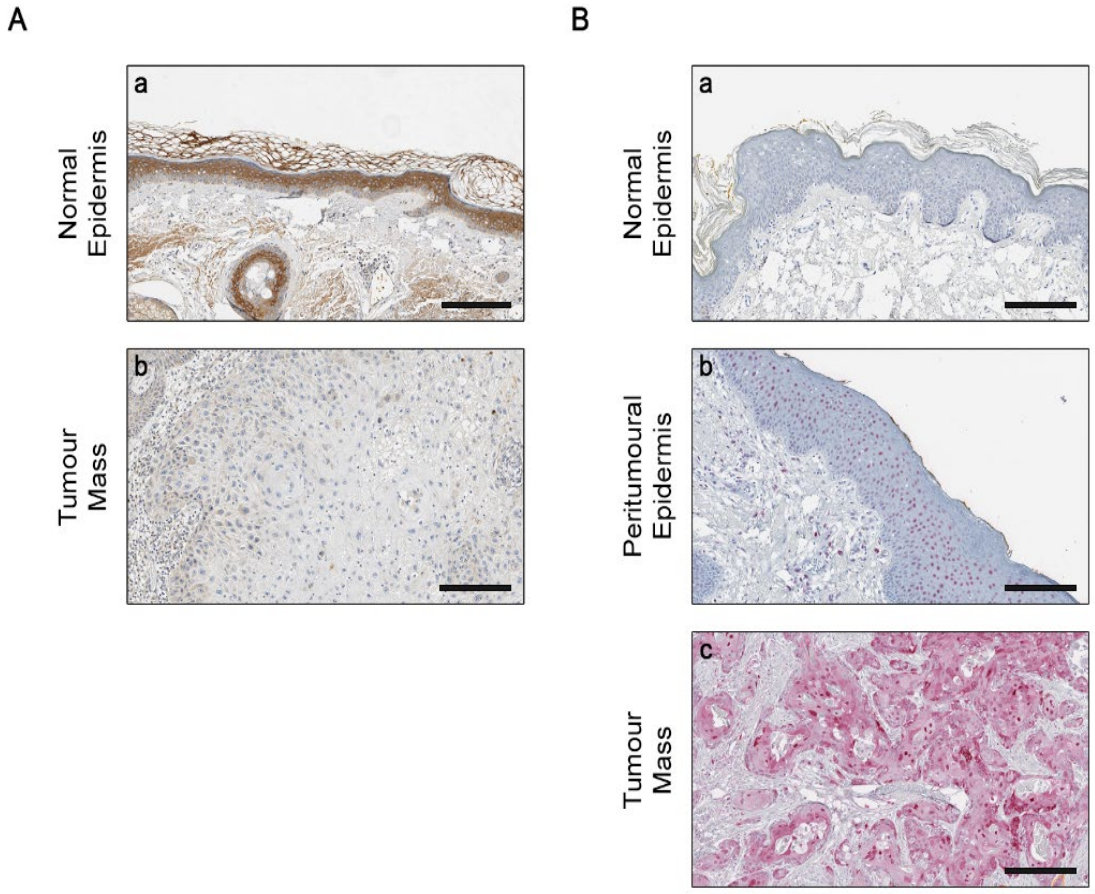

FIGURE 3. 3. LOSS OF AMBR1 EXPRESSION AND AN INCREASE IN BOTH CYTOPLASMIC AND NUCLEAR P62 EXPRESSION OCCURS IN CSCC TUMOURIGENESIS

*(**A**) Representative photomicrograph images of AMBRA1 expression in a primary cSCC in the (**a**) normal epidermis and (**b**) tumour mass. Visible staining was achieved via automated immunohistochemistry with a DAB counterstain. Image**s** were taken using bright field microscopy at a magnification of 15.4x. Scale bar = 200 µm. (**B**) Representative photomicrograph images of p62 staining in primary cSCCs in the (**a**) normal epidermis, (**b**) peritumoural epidermis and (**c**) tumour mass. Visible staining was achieved via automated immunohistochemistry with a fast red counterstain. Images were taken using bright field microscopy at a magnification of 15.4x. Scale bar = 200 µm.*

3.2.4. Development of a digital quantification method to analyse AMBRA1 or p62 expression in the growth front, tumour mass, peritumoural or normal epidermal environment of primary cSCCs

Automated immunohistochemistry for the expression of AMBRA1 and p62 was performed in all tissue sections derived from the Cambridge Addenbrookes Hospital discovery cohort of cSCCs. Following the acquisition of digital images (40 X magnification), four key regions of interest were identified (Figure 3.4):

- ***the 'normal epidermis,' defined as an epidermal region distant to the primary tumour***
- ***the peritumoural epidermis, defined as the epidermis directly alongside the primary tumour***
- ***the 'tumour mass,' defined as the principle tumour area (and not at the deepest aspect of the tumour or displaying an invasive phenotype)***
- ***tumour growth front,' defined as the tumour regions at the deepest aspect or the region displaying a invasive phenotype.***

The normal epidermis served as an internal control for AMBRA1 and p62 expression in keratinocytes in homeostatic conditions. The 'peritumoural epidermis,' on the other hand, represented keratinocytes that had either been exposed to the same tumorigenic field effect as the cells that had become transformed and/or cells that were subjected to the same signalling environment as the tumour. As such, keratinocytes in this environment are a good representation of cells that, whilst not fully functioning under homeostatic conditions, have not undergone full carcinogenic transformation. The area of the tumour growth front was analysed independently of cellular expression in the tumour mass as cells in this region had likely been through several additional mutagenic events, acquired pro-survival mechanisms and were beginning to exhibit a metastatic phenotype.

Digital images were annotated using the annotating tool within the Aperio ImageScope software, marking 2 X 1.00 mm^2 square boxes each for the normal and peritumoural epidermis and 5 representative areas/ 1.00 mm^2 square boxes each for the tumour mass and tumour growth front (Figure 3.4). The number of square boxes used for each region was determined based on the observed variability within primary cSCC tumours. As there was little or no variability between the normal epidermis and peritumoural epidermis only two 1.00 mm^2 square boxes, one either side of the site of the primary tumour were annotated. However,

since qualitative analysis of both AMBRA1 and p62 showed a high degree of intratumoural variability within primary cSCC tumours, multiple representative areas (x 5) were selected to best encompass this variability. Further annotation was then undertaken within each box of interest ensuring all keratinocytes within recognisable epidermal structures in normal and peritumoural epidermal regions and all tumour cells for the annotated tumour mass and tumour growth front regions were captured (Figure 3.4). The collaborating study histopathologist, Dr Niki Stefanos, confirmed annotations of all cases.

Following this, all annotated areas of interest were subjected to digital H score analysis using Aperio ImageScope software analysis with a pre-optimised cytoplasmic or nuclear algorithm. The H score from each representative area of interest defined the level of staining intensity of either AMBRA1 or p62 (as described in Section 2.14) which was used to derive the mean H score value and correlate with clinical follow up data.

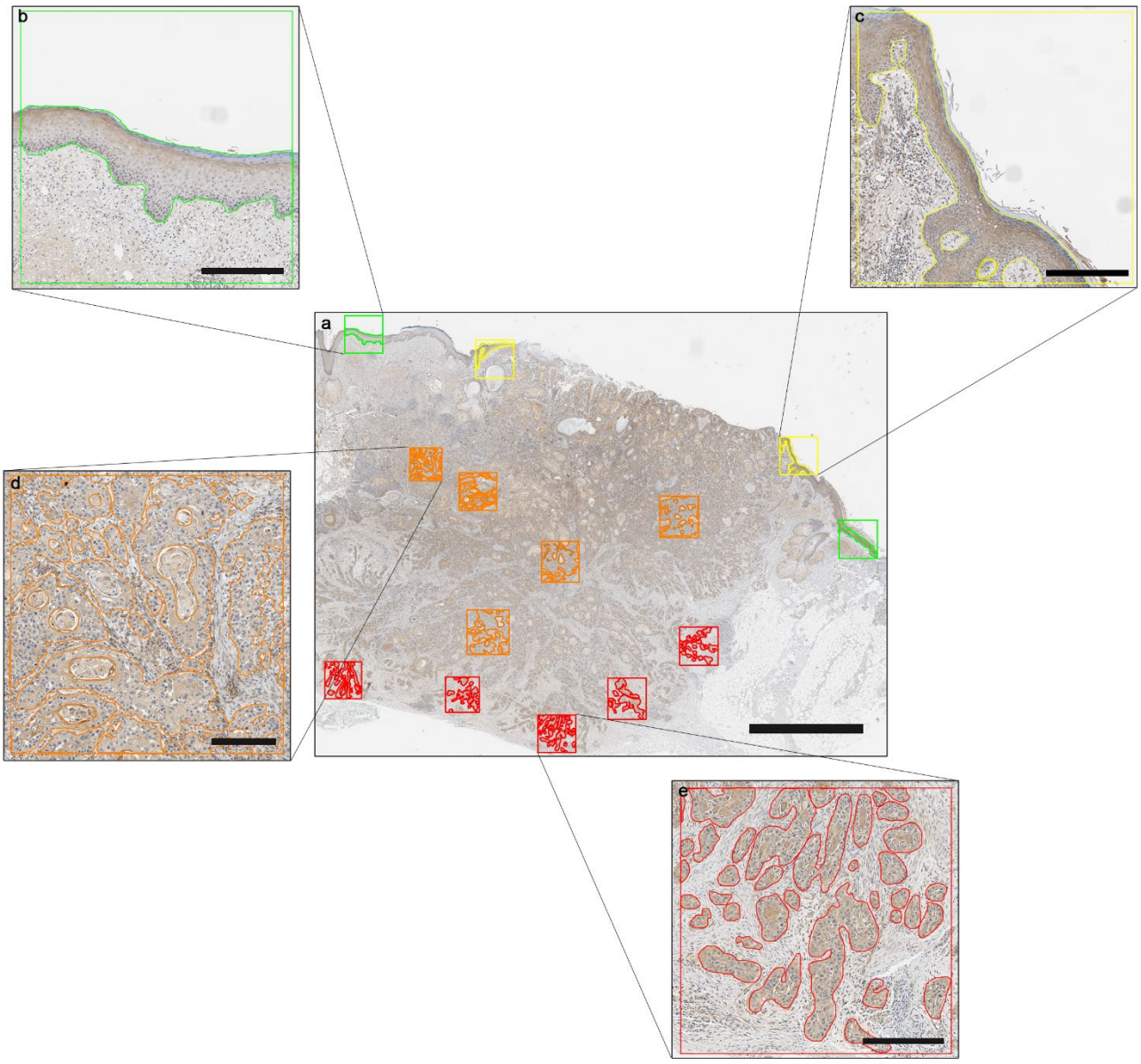

FIGURE 3. 4. ANNOTATION METHODOLOGY USED TO ANALYSE EXPRESSION OF AMBRA1 AND P62 IN PRIMARY CSCC TUMOURS.

*(**a**) Representative photomicrograph images of a cSCC tumour stained for AMBRA1 with completed annotations for the normal epidermis region (green), peritumoural epidermis region (yellow), tumour mass region (orange) and tumour growth front region (red). (**b**) Enlarged photomicrograph image of the normal epidermis annotated region of the cSCC tumour. (**c**) Enlarged photomicrograph image of the peritumoural epidermis annotated region of the cSCC tumour. (**d**) Enlarged photomicrograph image of the tumour mass annotated region of the cSCC tumour. (**e**) Enlarged photomicrograph image of the tumour growth front annotated region of the cSCC tumour. Visible staining was achieved via immunohistochemistry with a DAB counterstain. Image **a** was taken using bright field microscopy with a magnification of 0.8x. Scale bar = 3 mm. Image **b**, **d** and **e** were taken using bright field microscopy with a magnification of 9.5x. Scale bar = 300 µm. Image **c** was taken using bright field microscopy with a magnification of 10.3x. Scale bar = 200 µm*

3.2.5. Loss of AMBRA1 occurs in primary cSCC tumours regardless of cellular differentiation status and disease outcome

Mean H-scores for cytoplasmic AMBRA1 expression in the normal epidermis, peritumoural epidermis, tumour mass and tumour growth front regions were compared within localized and recurrent/metastatic primary cSCC tumours derived from the Cambridge cohort (Figure 3.5). Results in localised primary cSCC tumours revealed a significant loss of cytoplasmic AMBRA1 expression between the normal and peritumoural epidermis, tumour mass and tumour growth front regions ($P<0.0001$, Figure 3.5). Additionally, a significant loss of cytoplasmic AMBRA1 expression was also observed between the peritumoural epidermis and the tumour mass ($P<0.01$, Figure 3.5) and tumour growth front regions ($P<0.05$, Figure 3.5). Similarly, analysis of cytoplasmic AMBRA1 expression in recurrent/metastatic cSCC tumours revealed a significant loss of expression between the normal and peritumoural epidermis ($P<0.05$, Figure 3.5), and the tumour mass ($P<0.0001$, Figure 3.5) as well as the tumour growth front regions ($P<0.0001$, Figure 3.5). In contrast to results derived from AMBRA1 expression analysis in the localised primary cSCC tumours however, there was no significant difference in expression between the peritumoural epidermis region and the tumour mass or growth front regions.

Comparison of AMBRA1 expression in the four regions between localised and recurrent/metastatic cSCC tumours further confirmed no significant difference in expression in any region between these two groups (Appendix Figure A.1), collectively suggesting AMBRA1 expression is lost is cSCC tumorigenesis regardless of disease outcome.

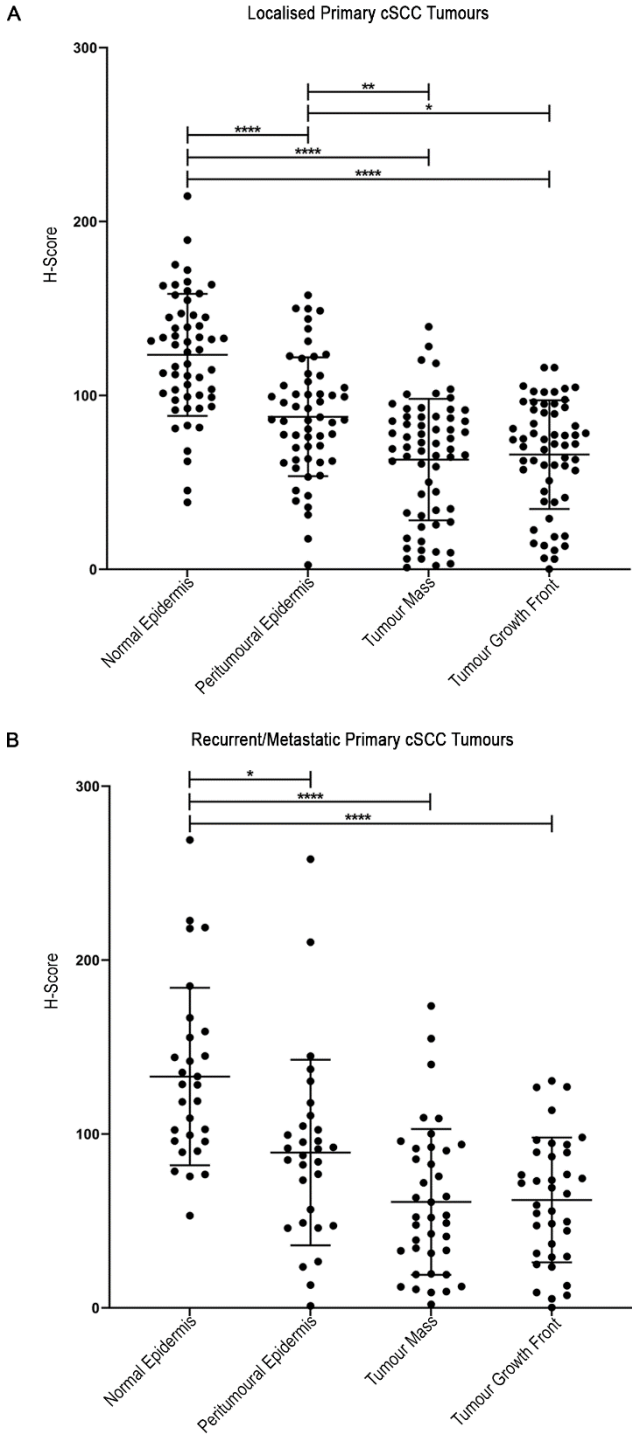

FIGURE 3. 5. CYTOPLASMIC AMBRA1 EXPRESSION DECREASES WITH CSCC TUMORIGENESIS.
*(**A**) Scatter graph representing the mean cytoplasmic AMBRA1 H-score in the normal epidermis (n=55), peritumoural epidermis (n=56), tumour mass (n=62) and tumour growth front (n=58) of 62 localised primary cSCC tumours. Horizontal bars represent the mean ± SD H-score for each group. Statistics acquired by Kruskal-Wallis test with Dunn's post hoc correction. (*P<0.05) (**P<0.01) (****P<0.0001). (**B**) Scatter graph representing the mean cytoplasmic AMBRA1 H-score in the normal epidermis (n=29), peritumoural epidermis (n=30), tumour mass (n=39) and tumour growth front (n=37) of 39 recurrent/metastatic primary cSCC tumours. Horizontal bars represent the mean ± SD H-score for each group. Statistics acquired by Kruskal-Wallis test with Dunn's post hoc correction. (*P<0.05) (****P<0.0001).*

Additional sub-cohort analysis of AMBRA1 expression in all localised and recurrent/metastatic cSCC tumours was also performed on the basis of tumour differentiation status ie in well, moderately or poorly differentiated tumour subsets (Appendix Figures A.2-A.7).

Compared to expression in the normal epidermis, results revealed a trend wise loss in AMBRA1 expression in the peritumoural epidermis with a further reduction in expression in the tumour mass and growth front in either localised or recurrent/metastatic well, moderately or poorly differentiated primary cSCC tumours (Appendix Figure A.2-A.4).

Comparison of AMBRA1 expression in the normal or peritumoural epidermis, the tumour mass or growth front in localised or recurrent/metastatic primary cSCC tumours stratified by differentiation status also revealed no significant difference in the mean H score for AMBRA1 expression (Appendix Figure A.5-A.7) in any region between localised or recurrent/metastatic well, moderately or poorly differentiated cSCCs, further suggesting AMBRA1 loss in localised or recurrent/metastatic cSCCs occurs regardless of tumour differentiation status.

3.2.6. Nuclear and cytoplasmic p62 expression is increased in primary cSCC tumours regardless of tumour differentiation status or disease outcome

Comparative expression analysis of both cytoplasmic and nuclear p62 was also carried out in the normal and peritumoural epidermis as well as in the tumour mass and tumour growth front regions of localised and recurrent/metastatic primary tumours included in the Cambridge cSCC cohort. Results revealed a significant increase in the level of cytoplasmic p62 expression in the tumour mass or growth front of localised primary cSCC tumours compared to expression levels in either the normal epidermis or peritumoural epidermis ($P<0.0001$, Figure 3.6). A similar trend was also seen in recurrent/metastatic primary cSCC tumours, with a significant increase in cytoplasmic p62 expression observed between the peritumoural epidermis and the tumour mass ($P<0.01$, Figure 3.6) or tumour growth front regions ($P<0.05$, Figure 3.6). However, whilst there was a significant increase in cytoplasmic p62 expression in the tumour mass compared to the normal epidermis of recurrent/metastatic tumours ($P<0.05$, Figure 3.6), there was no significant difference in expression between the normal epidermis and the tumour growth front.

Comparative analysis of cytoplasmic p62 expression between localised and recurrent/metastatic primary cSCC tumours in the four regions also revealed no significant difference (Appendix Figure A.8). Taken together these data suggest that there is an increase

in cytoplasmic p62 expression during cSCC tumourigenesis, although expression may be lost in cells at deeper, more invasive aspects of tumours that reoccur/metastasise.

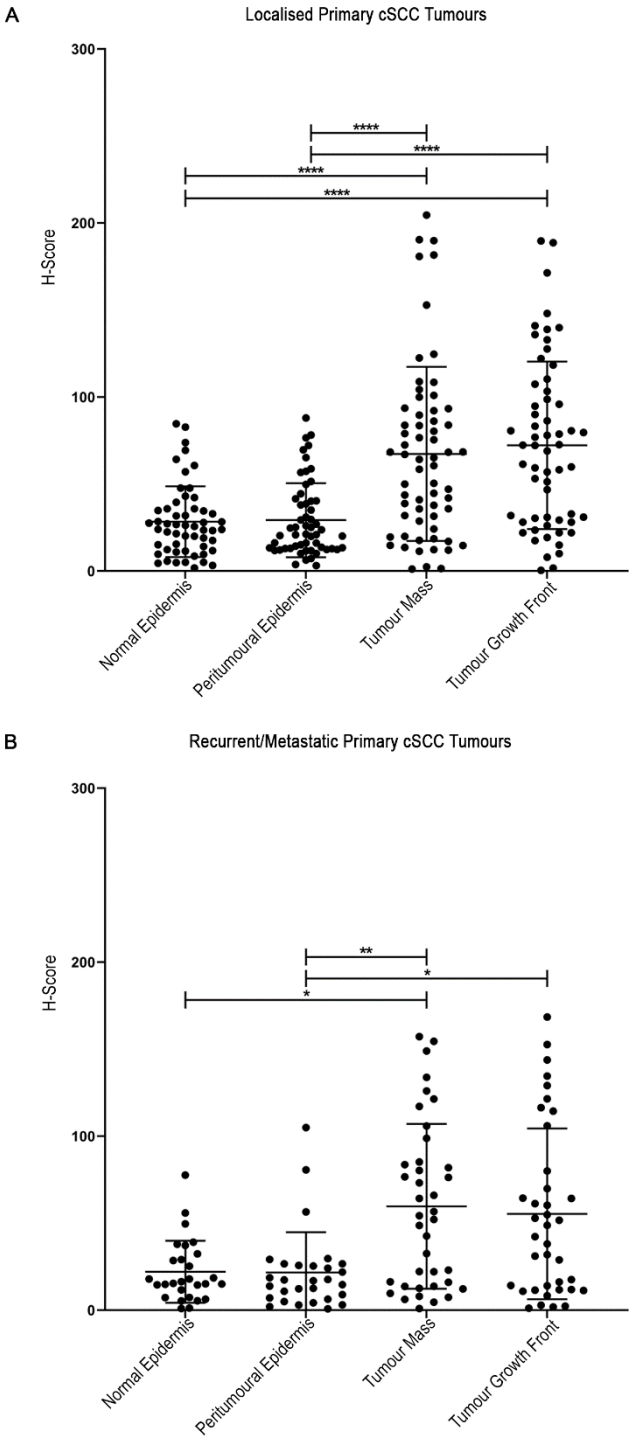

FIGURE 3. 6. CYTOPLASMIC P62 EXPRESSION INCREASES WITH CSCC PROGRESSION IN ALL PRIMARY CSCC TUMOURS REGARDLESS OF DISEASE OUTCOME.

*(**A**) Scatter graph representing the mean cytoplasmic p62 H-score in the normal epidermis (n=54), peritumoural epidermis (n=56), tumour mass (n=63) and tumour growth front (n=59) of 63 localised primary cSCC tumours. Horizontal bars represent the mean ± SD H-score for each group. Statistics acquired by Kruskal-Wallis test with Dunn's post hoc correction. (****P<0.01). (**B**) Scatter graph representing the mean cytoplasmic p62 H-score in the normal epidermis (n=28), peritumoural epidermis (n=29), tumour mass (n=39) and tumour growth front (n=38) of 39 recurrent/metastatic primary cSCC tumours. Horizontal bars represent the mean ± SD H-score for each group. Statistics acquired by Kruskal-Wallis test with Dunn's post hoc correction. (*P<0.05) (**P<0.01).*

Sub cohort analysis of p62 expression was also undertaken in well, moderately and poorly differentiated cSCCs. Results again revealed increased cytoplasmic expression of p62 in the tumour mass and growth front of all tumours regardless of differentiation status but with no significant difference in expression between the normal or peritumoural epidermis or the tumour mass or growth front of localised or recurrent/metastatic tumours (Appendix Figures A.9-A.11). Although increased in the tumour mass and growth front of well, moderately and poorly differentiated tumours, notably cytoplasmic p62 expression was only significantly increased in these regions of localised cSCCs. This observation is perhaps reflective however, of the small number of recurrent/metastatic primary cSCC tumours when stratifying by differentiation status.

Additional sub cohort analysis of cytoplasmic p62 expression in the normal or peritumoural epidermis or tumour mass or growth front of localised or recurrent/metastatic cSCC tumours stratified by differentiation status again revealed no significant difference in expression in any region in either well, moderately or poorly differentiated tumours (Appendix Figures A.12-A.14). Collectively these data suggest that the increase in cytoplasmic p62 expression in the tumour mass/growth front of primary cSCC tumours occurs regardless of differentiation status or disease outcome.

Analysis of nuclear p62 expression in the normal or peritumoural epidermis or the tumour mass or growth front of localised primary cSCC tumours, revealed a significant increase in expression between the normal epidermis and peritumoural epidermis and the tumour mass or tumour growth front regions ($P<0.0001$, Figure 3.7A). This significant increase in nuclear p62 expression between the normal epidermis and the tumour mass and tumour growth front ($P<0.0001$, Figure 3.7B) and between expression in peritumoural epidermis and the tumour mass or tumour growth front ($P<0.01$, Figure 3.B) was also observed in recurrent/metastatic primary cSCC tumours. Comparative analysis of nuclear p62 expression between localised and recurrent/metastatic primary cSCC tumours in the four differing regions however, revealed no significant difference between localised and recurrent/metastatic primary cSCC tumour (Appendix Figure A.15). Taken together these data suggest that there is an increase in nuclear p62 expression during cSCC tumourigenesis regardless of differentiation status or disease outcome.

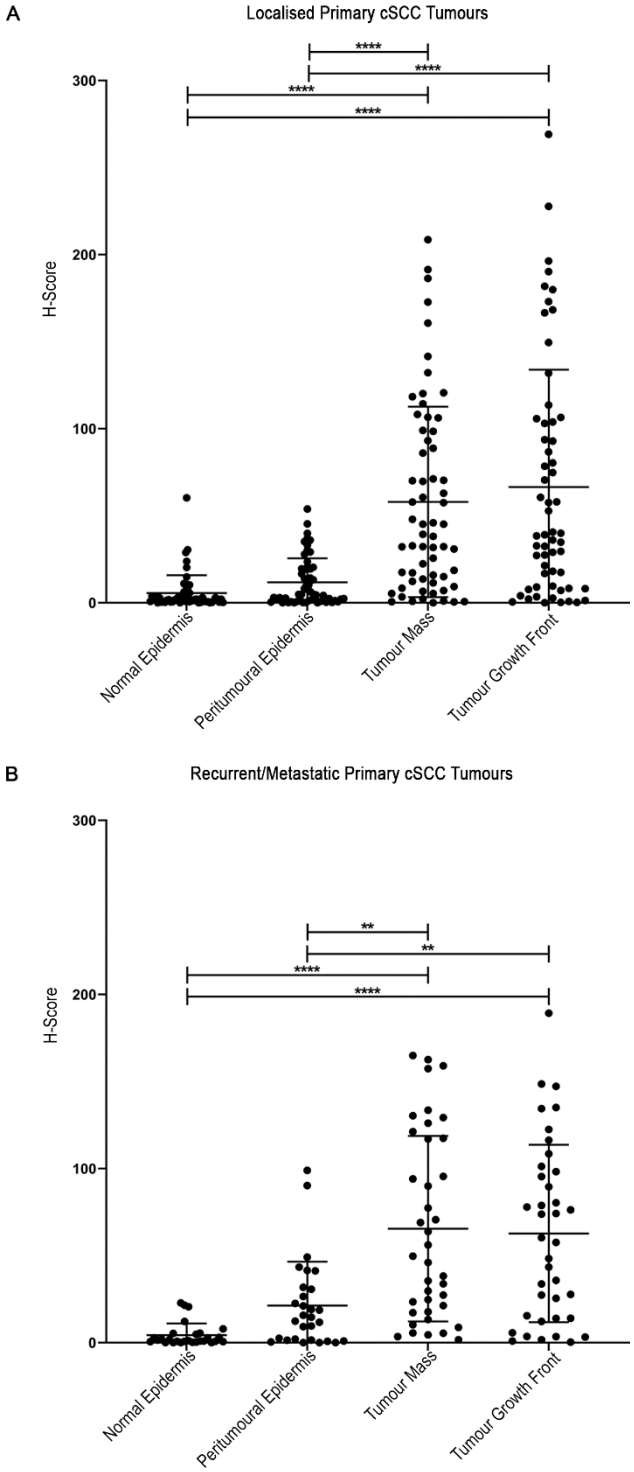

FIGURE 3. 7. NUCLEAR P62 EXPRESSION INCREASES WITH CSCC PROGRESSION.

*(**A**) Scatter graph representing the mean nuclear p62 H-score in the normal epidermis (n=54), peritumoural epidermis (n=56), tumour mass (n=63) and tumour growth front (n=59) of 63 localised primary cSCC tumours. Horizontal bars represent the mean ± SD H-score for each group. Statistics acquired by Kruskal-Wallis test with Dunn's post hoc correction. (****P<0.0001). (**B**) Scatter graph representing the mean nuclear p62 H-score in the normal epidermis (n=28), peritumoural epidermis (n=29), tumour mass (n=39) and tumour growth front (n=38) of 39 recurrent/metastatic primary cSCC tumours. Horizontal bars represent the mean ± SD H-score for each group. Statistics acquired by Kruskal-Wallis test with Dunn's post hoc correction. (**P<0.01) (****P<0.0001).*

Further sub-cohort analysis of nuclear p62 expression in primary cSCC tumours revealed a significant increase in nuclear p62 expression between normal epidermis and peritumoural epidermis and the tumour mass and tumour growth front regions (Appendix Figure A.16-A.18) in localised tumours with a well, moderately or poorly differentiated phenotype. However, regardless of whether well, moderately of poorly differentiated, the only consistent significant increase in nuclear p62 expression observed was between the normal epidermis and the tumour mass and tumour growth front regions of recurrent/metastatic primary cSCC tumours (Appendix Figure A.16-A.18). Collectively these data suggest nuclear p62 expression in the peritumoural epidermis of cSCC tumours is influenced by disease outcome. However, when the level of nuclear p62 expression in the peritumoural epidermis region was directly compared between well, moderately or poorly differentiated localised or recurrent/metastatic primary cSCC tumours, there was no significant difference in expression or indeed any significant difference in nuclear p62 expression levels between tumours (Appendix Figure A.19-A.21). Taken together these data suggest, that like cytoplasmic p62 expression, there is a significant increase in nuclear p62 expression with cSCC tumourigenesis.

3.2.7. Loss of cytoplasmic AMBRA1 expression at the cSCC tumour growth front, in combination with loss of cytoplasmic, peritumoural epidermal p62 expression is a putative prognostic biomarker for cSCC disease progression

ROC curve analysis was used to define the prognostic potential of cytoplasmic AMBRA1 or nuclear or cytoplasmic p62 expression for cSCC, where the greatest potential is given by the area under the curve (AUC) value, closest to 1.00.

ROC curve analysis of all primary cSCC tumours within the Cambridge cohort revealed cytoplasmic AMBRA1 expression in the tumour growth front region (as opposed to expression in the peritumoural epidermis or tumour mass, Appendix Figure A.22), with an AUC value of 0.5622 and cytoplasmic p62 expression in the peritumoural epidermis (as opposed to expression in the tumour mass or growth front (Appendix A.26) or nuclear expression in any region of interest, (Appendix Figure A.30), with an AUC of 0.6178 as the regions with greatest prognostic potential (Figure 3.8). Within the tumour growth front region, a mean AMBRA1 H-score value of <59.740 (Figure 3.8A) had the highest sensitivity and specificity while for cytoplasmic p62 an H-score value <20.010 (Figure 3.8B) had the highest sensitivity and specificity for identifying primary cSCC tumours at risk of disease recurrence or metastasis.

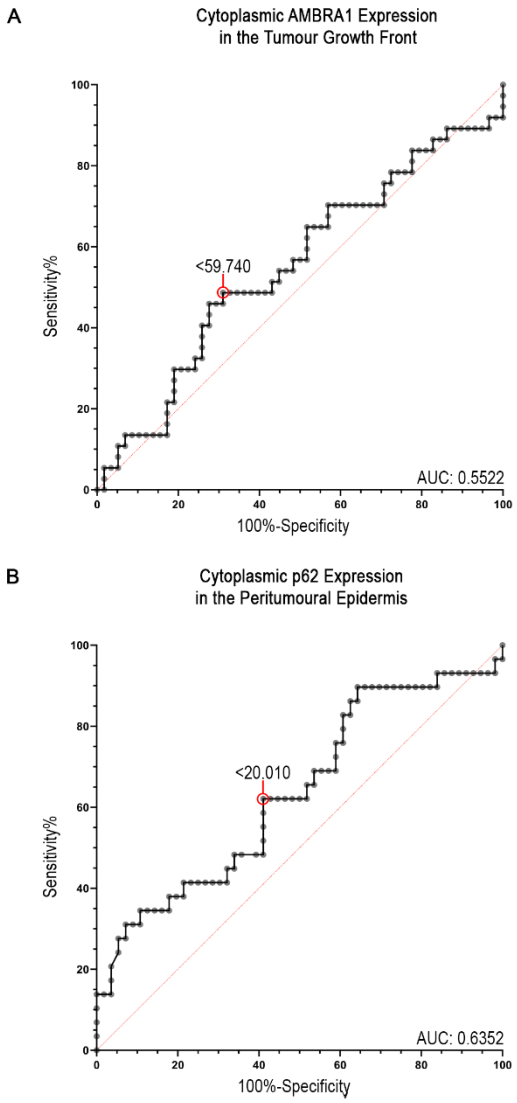

FIGURE 3. 8. LOSS OF CYTOPLASMIC AMBRA1 EXPRESSION IN THE TUMOUR GROWTH FRONT REGION AND LOSS OF CYTOPLASMIC P62 EXPRESSION IN THE PERITUMOURAL EPIDERMIS BEST PREDICT CSCC RECURRENCE OR METASTASIS.
*(**A**) Receiver operating characteristic (ROC) curve for prediction of either cSCC reoccurrence or metastasis based on the cytoplasmic AMBRA1 H-score in the tumour growth front of all primary cSCC tumours (n=95). The AMBRA1 H-score with the highest specificity and sensitivity is highlighted by a red circle. AUC = area under the curve. (**B**) Receiver operating characteristic (ROC) curve for prediction of a cSCC event (reoccurrence/metastasis) based on the cytoplasmic p62 H-score in the peritumoural epidermis of all primary cSCC tumours (n=85). The p62 H-score with the highest specificity and sensitivity is highlighted by a red circle. AUC = area under the curve.*

ROC curve analysis of cytoplasmic AMBRA1 expression in the peritumoural epidermis, and the tumour mass and growth front was also undertaken in sub-cohorts of well, moderately and poorly differentiated primary cSCC tumours (Appendix Figures A.23-A.25). Regardless of cellular differentiation status, cytoplasmic AMBRA1 expression in the tumour growth front region was consistently the region with the highest AUC value (Appendix Figure A.23-A.25).

However, for expression of p62, ROC curve analysis in sub cohorts of well, moderately or poorly differentiated cSCCs identified different regions in which cytoplasmic or nuclear expression corresponded with the highest prognostic potential. For well-differentiated cSCCs loss of cytoplasmic p62 expression in the peritumoural epidermis gave the highest prognostic potential, (Appendix Figure A.27), while in moderately differentiated cSCCs, loss of cytoplasmic p62 expression in the tumour growth front (Appendix Figure A.28) or in poorly-differentiated cSCCs the increase in nuclear p62 expression in the peritumoural epidermis gave the highest prognostic potential (Appendix Figure A.33).

Taken together, these data demonstrate that regardless of tumour differentiation status, the loss of cytoplasmic AMBRA1 expression in the tumour growth front region and the loss of cytoplasmic p62 expression in the peritumoural epidermis have the highest potential to identify cSCCs at risk of disease recurrence or metastasis.

Having determined the optimal expression levels of AMBRA1 in the tumour growth front and p62 in the peritumoural epidermis with greatest prognostic potential, survival curve analysis was then performed to determine the potential or either marker or the combined prognostic potential of these two putative biomarkers. Initial analysis based on cytoplasmic AMBRA1 expression in the tumour growth front region alone and a cut off H-score of <59.740 to define a high-risk tumour revealed no significant difference in predicting disease progression in high or low risk subsets; 73.59% of tumours defined as low-risk and 57.58% of tumours defined as high-risk had no disease event within 60 months (Figure 3.9), collectively indicating the unsuitability of AMBRA1 expression in the tumour growth front alone as a prognostic biomarker for cSCC.

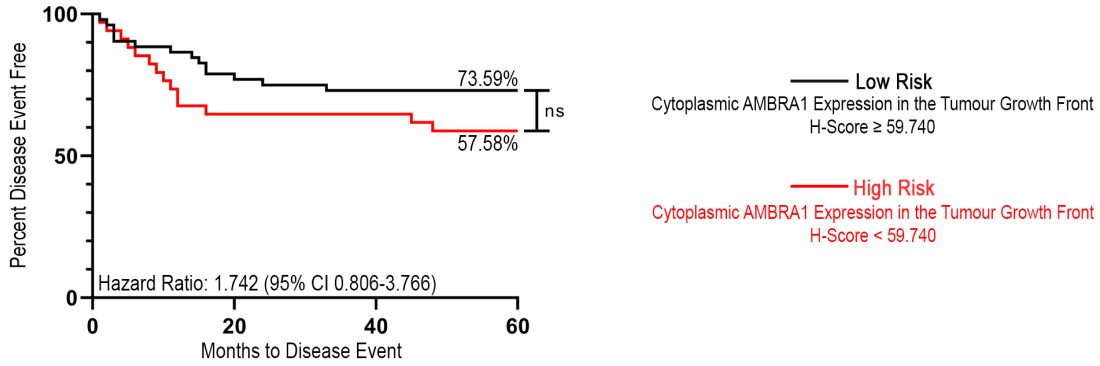

FIGURE 3. 9. CYTOPLASMIC AMBRA1 EXPRESSION IN THE TUMOUR GROWTH FRONT ALONE IS NOT A PROGNOSTIC BIOMARKER FOR CSCC.
Kaplan-Meier survival analysis representing 60-month disease event free rate in 86 primary cSCC tumours stratified as low risk (n=52) and high risk (n=34) groups based on cytoplasmic AMBRA1 expression in the tumour growth front region. Statistics acquired by Mantel-Cox log-rank test and Mantel-Haenszel test (ns=non-significant).

Additional Kaplan-Meier survival analysis of AMBRA1 expression in the tumour growth front of sub-cohorts of either well, moderately or poorly differentiated cSCCs also demonstrated the inability of this single marker to identify low and high risk tumour subsets (Appendix Figure A.34).

Kaplan-Meir survival analysis based on cytoplasmic p62 expression in the peritumoural epidermis alone and a cut off mean H-score of <20.01 to define a high risk sub set was also unable to define high risk cSCC subsets; 72.72% of tumours defined as low-risk and 69.57% tumours defined as high-risk had no disease event within 60 months (figure 3.10), again, collectively indicating the inability of p62 expression in the peritumoural epidermis alone as a prognostic biomarker for cSCC.

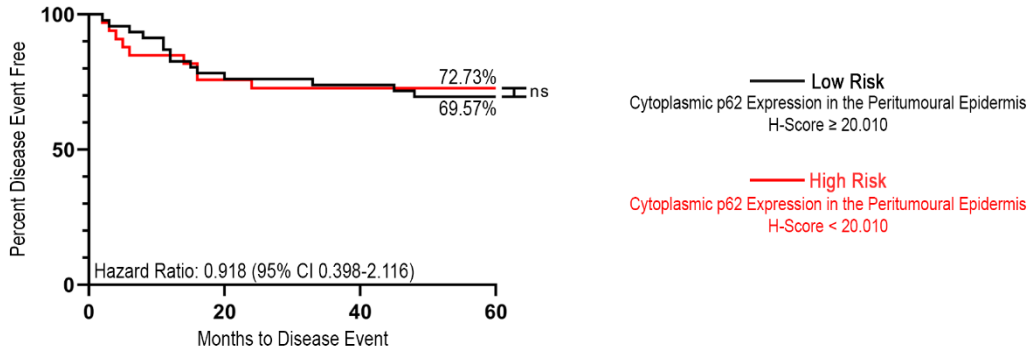

FIGURE 3. 10. CYTOPLASMIC P62 EXPRESSION IN THE PERITUMOURAL EPIDERMIS ALONE IS NOT A PROGNOSTIC BIOMARKER FOR CSCC.
Kaplan-Meier survival analysis representing 60-month disease event free rate in 79 primary cSCC tumours stratified as low risk (n=46) and high risk (n=33) groups based on cytoplasmic p62 expression in the peritumoural epidermis. Statistics acquired by Mantel-Cox log-rank test and Mantel-Haenszel test (ns=non-significant).

Similarly, to analysis of AMBRA1 in the tumour growth front of sub cohorts of primary cSCCs with differing differentiation status, Kaplan-Meier survival analysis based on both cytoplasmic and nuclear p62 expression was performed in well, moderately and poorly differentiated tumours. Whilst cytoplasmic p62 expression in the peritumoural epidermis of well and cytoplasmic p62 expression in the tumour growth front of moderately differentiated primary cSCCs had the greatest prognostic potential, neither marker was able to significantly distinguish between high and low risk tumour subsets. Nuclear p62 expression in the peritumoural epidermis, on the other hand was able to distinguish disease recurrence or metastasis in tumour subsets of poorly differentiated cSCCs (Appendix Figure A.35).

Given the limited ability of AMBRA1 expression in the growth front of cSCCs or the expression of cytoplasmic p62 in the peritumoural epidermis as single biomarkers, their capacity as combined prognostic biomarkers was evaluated in the entire Cambridge cohort of poorly, moderately or well differentiated localised or recurrent/metastatic cSCCs (Figure 3.11) as well as in individual sub cohorts of well, moderately or poorly differentiated tumours (Appendix Figure A. 36). A tumour with a cytoplasmic AMBRA1 H-score in the growth front region of <59.74 and a mean cytoplasmic p62 H score in the peritumoural epidermis of <20.010, was defined as being at high risk of a disease recurrence/metastasis, while a cytoplasmic AMBRA1

H-score in the tumour growth front ≥59.74 and/or a mean cytoplasmic p62 H score in the peritumoural epidermis of ≥20.010 was categorised as low risk.

Resultant Kaplan-Meier survival curve analysis revealed dual AMBRA1 expression in the tumour growth front and p62 expression in the peritumoural epidermis significantly distinguished between high and low risk tumour subsets (P<0.05, Figure 3.11); 78.57% of patients with low risk tumours were disease free at 60 months compared to only 46.15% of patients with high risk tumours. Furthermore, as a biomarker, the combined AMBRA1 tumour growth front and peritumoural epidermal p62 expression predicted recurrence /metastasis of primary cSCCs with a hazard ratio of 4.421 (95% CI 1.322-14.790), a negative predictive value of 75.38%, a positive predictive value of 53.85%, an assay specificity of 89.09% and sensitivity of 30.43%.

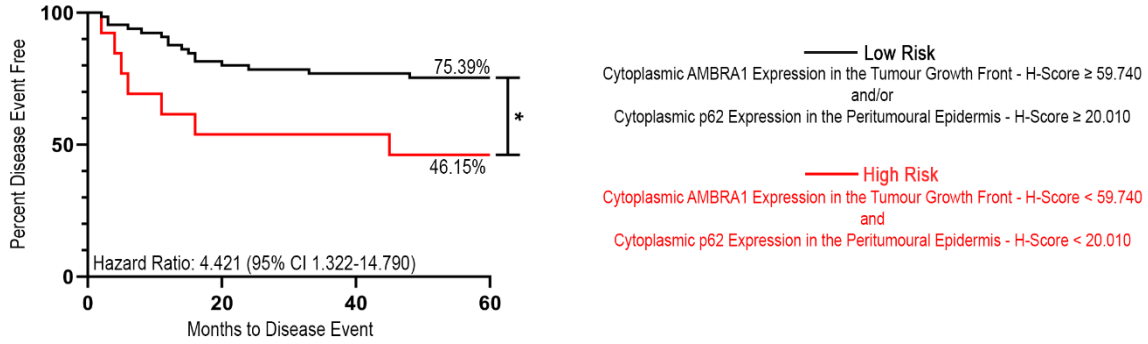

FIGURE 3. 11. CYTOPLASMIC AMBRA1 EXPRESSION IN THE TUMOUR GROWTH FRONT REGION AND CYTOPLASMIC P62 EXPRESSION IN THE PERITUMOURAL EPIDERMIS REGION ACT AS A PUTATIVE BIOMARKER FOR CSCC PATIENTS.
*Kaplan-Meier survival analysis representing 60-month disease event free rate in 79 primary cSCC tumours stratified as low risk (n=65) and high risk (n=13) groups based on cytoplasmic AMBRA1 expression in the tumour growth front region and cytoplasmic p62 expression in the peritumoural epidermis. Statistics acquired by Mantel-Cox log-rank test and Mantel-Haenszel test (*P<0.05).*

Kaplan-Meier survival curve analysis of combined AMBRA1 growth front and peritumoural epidermal p62 expression in well, moderately or poorly differentiated localised or recurrent/metastatic tumours also significantly distinguished between high and low risk subsets of moderately or poorly differentiated tumours although this was not significant in well differentiated tumours (Appendix Figure A.36).

In summary these data suggest the combined expression of cytoplasmic AMBRA1 in the tumour growth front and cytoplasmic p62 expression in the peritumoural epidermis as a novel putative prognostic biomarker for cSCC disease recurrence/metastasis.

3.2.8. Loss of cytoplasmic AMBRA1 expression at the cSCC tumour growth front, in combination with loss of cytoplasmic, peritumoural epidermal p62 expression is a putative prognostic biomarker for metastasis in moderately and poorly differentiated cSCC tumours

Having established the combined expression of cytoplasmic AMBRA1 in the tumour growth front and cytoplasmic p62 in the peritumoural epidermis is able to predict cSCC recurrence and metastasis, further sub cohort analysis was undertaken to evaluate the improved potential of this combined biomarker to predict metastasis with in well, moderately, poorly or moderately/poorly differentiated cSCCs. Results demonstrated combined cytoplasmic AMBRA1 expression in the tumour growth front and cytoplasmic p62 expression in the peritumoural epidermis was unable to significantly predict metastasis of well-differentiated cSCCs (Figure 3.12); 85.71% patients with low risk tumours did not have a metastatic event at 60 months compared to 100% of patients with high risk tumours, suggesting the unsuitability of this combined biomarker for prognosticating well-differentiated cSCCs.

The prognostic ability of AMBRA1 tumour growth front and p62 peritumoural epidermal expression was however significantly improved in moderately ($P<0.01$, Figure 3.13) and poorly-differentiated cSCCs ($P<0.05$, Figure 3.14) by removal of the recurrent tumour subsets. Specifically, metastasis at 60 months did not occur in 70.37% patients with low risk moderately differentiated primary cSCC tumours while all patients with high-risk tumours developed metastasis by 60 months (Figure 3.13). 82.35% of patients with poorly differentiated low risk primary cSCC tumours on the other hand did not develop metastatic disease at 60 months, while 66.67% of patients with high-risk tumours developed metastasis by 60 months (Figure 3.14). Collectively these data suggest combined AMBRA1 tumour growth front and peritumoural epidermal p62 expression as a viable prognostic biomarker of metastasis in moderately or poorly differentiated cSCCs.

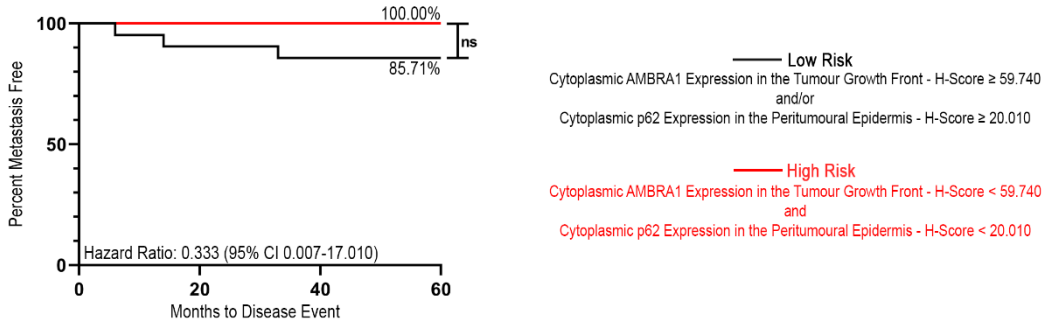

FIGURE 3. 12. CYTOPLASMIC AMBRA1 EXPRESSION IN THE TUMOUR GROWTH FRONT REGION AND CYTOPLASMIC P62 EXPRESSION IN THE PERITUMOURAL EPIDERMIS REGION DO NOT ACT AS A PROGNOSTIC BIOMARKER FOR DISEASE METASTASIS IN WELL-DIFFERENTIATED CSCC TUMOURS.

*Kaplan-Meier survival analysis representing 60-month metastasis free rate in 23 well-differentiated primary cSCC tumours stratified as low risk (n=21) and high risk (n=2) groups based on cytoplasmic AMBRA1 expression in the tumour growth front region and cytoplasmic p62 expression in the peritumoural epidermis. Statistics acquired by Mantel-Cox log-rank test and Mantel-Haenszel test (*P<0.05).*

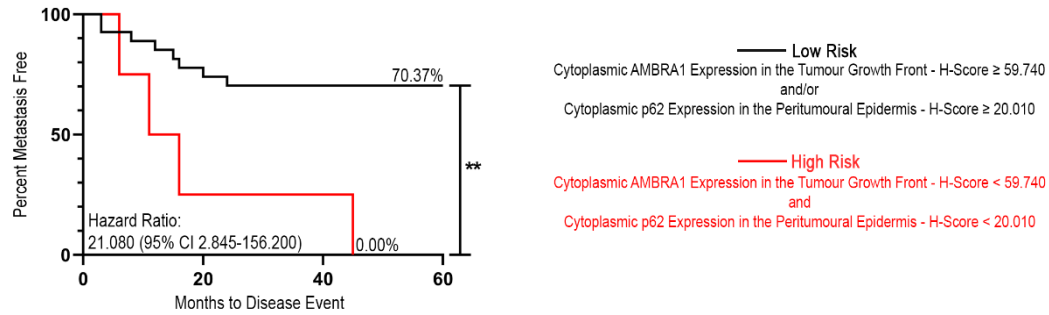

FIGURE 3. 13. CYTOPLASMIC AMBRA1 EXPRESSION IN THE TUMOUR GROWTH FRONT REGION AND CYTOPLASMIC P62 EXPRESSION IN THE PERITUMOURAL EPIDERMIS REGION DOES ACT AS A PROGNOSTIC BIOMARKER FOR DISEASE METASTASIS IN MODERATELY DIFFERENTIATED CSCC TUMOURS.

*Kaplan-Meier survival analysis representing 60-month disease event free rate in 31 moderately-differentiated primary cSCC tumours stratified as low risk (n=27) and high risk (n=4) groups based on cytoplasmic AMBRA1 expression in the tumour growth front region and cytoplasmic p62 expression in the peritumoural epidermis. Statistics acquired by Mantel-Cox log-rank test and Mantel-Haenszel test (*P<0.05).*

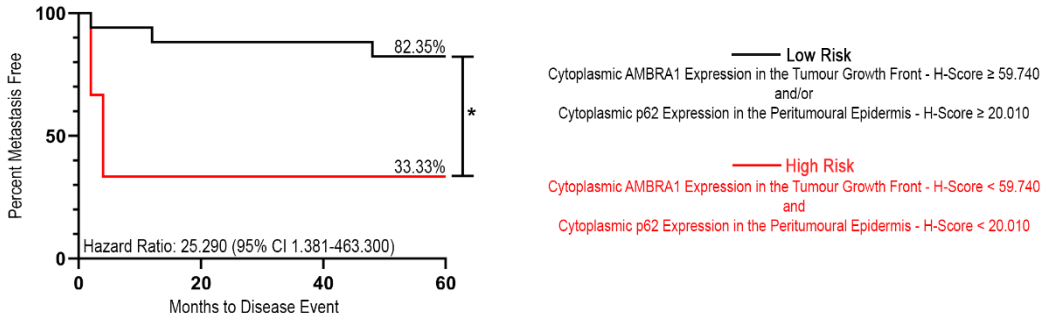

FIGURE 3. 14. CYTOPLASMIC AMBRA1 EXPRESSION IN THE TUMOUR GROWTH FRONT REGION AND CYTOPLASMIC P62 EXPRESSION IN THE PERITUMOURAL EPIDERMIS REGION DOES ACT AS A PROGNOSTIC BIOMARKER FOR DISEASE METASTASIS IN POORLY DIFFERENTIATED CSCC TUMOURS.
*Kaplan-Meier survival analysis representing 60-month disease event free rate in 20 poorly-differentiated primary cSCC tumours stratified as low risk (n=17) and high risk (n=3) groups based on cytoplasmic AMBRA1 expression in the tumour growth front region and cytoplasmic p62 expression in the peritumoural epidermis. Statistics acquired by Mantel-Cox log-rank test and Mantel-Haenszel test (*P<0.05).*

Clinically, primary cSCCs are more commonly categorised as moderately-to-poorly differentiated, rather than being categorised separately as either moderately or poorly differentiated. Further validating the potential for combined AMBRA1 tumour growth front and peritumoural epidermal p62 expression as a prognostic biomarker for disease metastasis in combined moderately/poorly differentiated cSCCs, Kaplan-Meier survival curve analysis revealed a significant increase in the ability to predict metastasis in these tumours (P<0.0001, Figure 3.15); 75.00% patients with low risk tumours did not develop metastasis at 60 months compared to 85.71% of patients with high risk tumours that developed metastatic disease. Furthermore as a biomarker, the combined AMBRA1 tumour growth front and peritumoural epidermal p62 expression predicts metastasis of moderately/poorly differentiated cSCCs with a hazard ratio of 30.07 (95% CI 5.48- 165), a negative predictive value of 75.00%, a positive predictive value of 85.71%, an assay specificity of 97.06% and sensitivity of 35.29%. Collectively this highlights the power and potential clinical impact of combined AMBRA1 tumour growth front and peritumoural epidermal p62 expression as a novel prognostic biomarker for moderately/poorly differentiated cSCC.

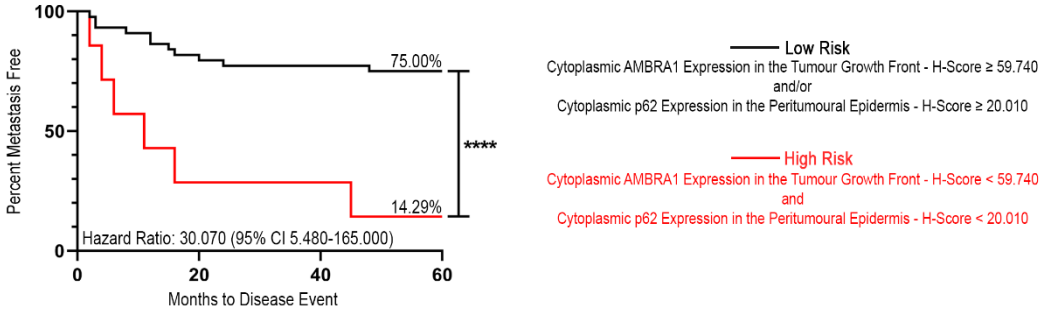

FIGURE 3. 15. CYTOPLASMIC AMBRA1 EXPRESSION IN THE TUMOUR GROWTH FRONT REGION AND CYTOPLASMIC P62 EXPRESSION IN THE PERITUMOURAL EPIDERMIS REGION DOES ACT AS A PROGNOSTIC BIOMARKER FOR DISEASE METASTASIS IN MODERATELY/POORLY DIFFERENTIATED CSCC TUMOURS.
*Kaplan-Meier survival analysis representing 60-month disease event free rate in 51 primary cSCC tumours separated into low risk (n=44) and high risk (n=7) groups based on cytoplasmic AMBRA1 expression in the tumour growth front region and cytoplasmic p62 expression in the peritumoural epidermis. Statistics acquired by Mantel-Cox log-rank test and Mantel-Haenszel test (*P<0.05).*

3.2.9. Post-viva data analysis of AMBRA1 and p62 as putative prognostic biomarkers

Following the initial submission of this thesis, and the subsequent viva examination, additional work was completed to refine and correct the analysis of the potential of cytoplasmic AMBRA1 expression in the tumour growth front and cytoplasmic p62 in the peritumoural epidermis region as a putative prognostic biomarker for cSCC. Further clinical feedback led to the removal of some tumours from the cohort, due to either clinical or quality control standard alterations. The remaining tumours were also subject to re-examination of their tumour differentiation status, with tumours being either completely reclassified and moderately-differentiated tumours additionally classified as either well-moderately or moderately-poorly differentiated tumours. This refined cohort was then subject to the same survival curve analysis as previous explained (Section 3.2.7.) to access the potential of AMBRA1 and p62 immunohistochemical expression as predictive markers of cSCC metastasis.

Resultant Kaplan-Meier curve analysis revealed that cytoplasmic AMBRA1 expression in the tumour growth front region and cytoplasmic p62 expression in the peritumoural epidermis region, whilst not significant, does still show some ability to distinguish between cSCC at a high or low risk of metastasising, regardless of differentiation status (Figure 3.16); 81.36% of 59 low risk tumours did not progress to metastatic disease, whilst 60.00% of 10 high risk tumours did experience metastatic disease. Additionally, analysis with a Mantel-Haenszel test revealed this classifying system had a hazard ratio of 3.85 (95% CI 0.82-18.08).

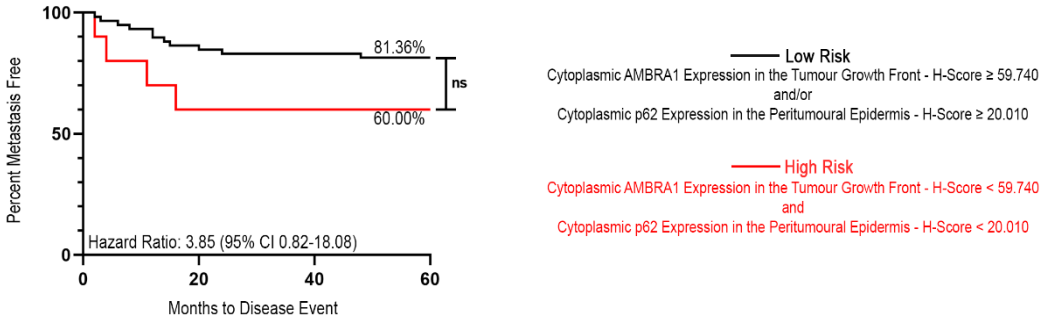

FIGURE 3. 16.CYTOPLASMIC AMBRA1 EXPRESSION IN THE TUMOUR GROWTH FRONT REGION AND CYTOPLASMIC P62 EXPRESSION IN THE PERITUMOURAL EPIDERMIS REGION IS ASSOCIATED WITH DECREASED METASTASIS FREE SURVIVAL IN CSCC TUMOURS REGARDLESS OF DIFFERENTIATION STATUS

Kaplan-Meier survival analysis representing 60-month disease event free rate in 69 primary cSCC tumours stratified as low risk (n=59) and high risk (n=10) groups based on cytoplasmic AMBRA1 expression in the tumour growth front region. Statistics acquired by Mantel-Cox log-rank test and Mantel-Haenszel test (ns=non-significant).

Subcohort analysis demonstrated that cytoplasmic AMBRA1 expression in the tumour growth front region and cytoplasmic p62 expression in the peritumoural epidermis region is still unable to identity well-differentiated cSCC patients at high risk of metastasis (Figure 3.17). Additionally, whilst the original analysis showed that this putative biomarker was able to identify high-risk patient subsets in both moderately- and poorly-differentiated cSCC tumours, this refined cohort subjected to the same survival curve analysis only showed capability of identifying high-risk poorly-differentiated cSCC patients (Figure 3.18 and 3.19, *P<0.05), with 81.25% of 14 low risk patients being metastasis-free after 60 months and only 33.33% of 5 high-risk cSCC patients not experiencing a metastasis, a hazard ratio of 20.52 (p5% CI 1.197-351.70), a PPV of 66.67%, NPV 81.25% and an assay sensitivity of 40.00% and specificity 92.86%.

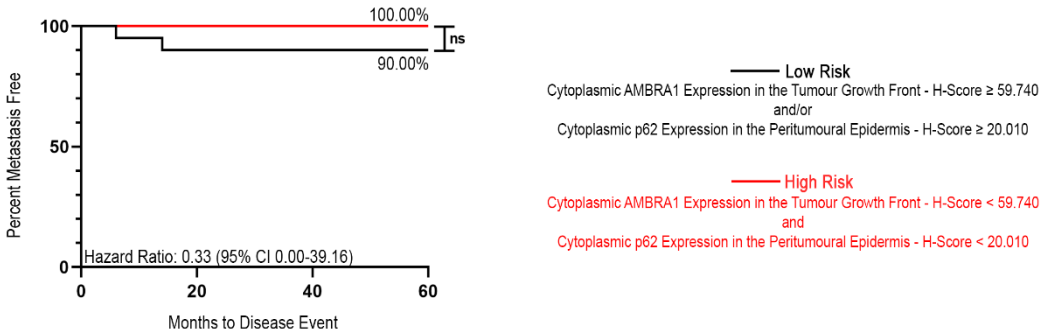

FIGURE 3. 17. CYTOPLASMIC AMBRA1 EXPRESSION IN THE TUMOUR GROWTH FRONT REGION AND CYTOPLASMIC P62 EXPRESSION IN THE PERITUMOURAL EPIDERMIS REGION IS NOT A PREDICTOR OF METASTASIS IN WELL-DIFFERENTIATED SCC TUMOURS

Kaplan-Meier survival analysis representing 60-month disease event free rate in 22 primary cSCC tumours stratified as low risk (n=22) and high risk (n=0) groups based on cytoplasmic AMBRA1 expression in the tumour growth front region. Statistics acquired by Mantel-Cox log-rank test and Mantel-Haenszel test (ns=non-significant).

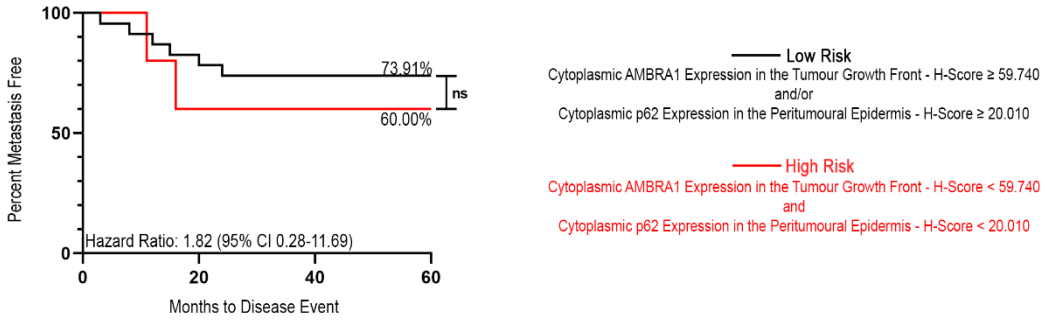

FIGURE 3. 18. CYTOPLASMIC AMBRA1 EXPRESSION IN THE TUMOUR GROWTH FRONT REGION AND CYTOPLASMIC P62 EXPRESSION IN THE PERITUMOURAL EPIDERMIS REGION IS NOT A PREDICTOR OF METASTASIS IN MODERATELY-DIFFERENTIATED SCC TUMOURS

Kaplan-Meier survival analysis representing 60-month disease event free rate in 28 primary cSCC tumours stratified as low risk (n=19) and high risk (n=8) groups based on cytoplasmic AMBRA1 expression in the tumour growth front region. Statistics acquired by Mantel-Cox log-rank test and Mantel-Haenszel test (ns=non-significant).

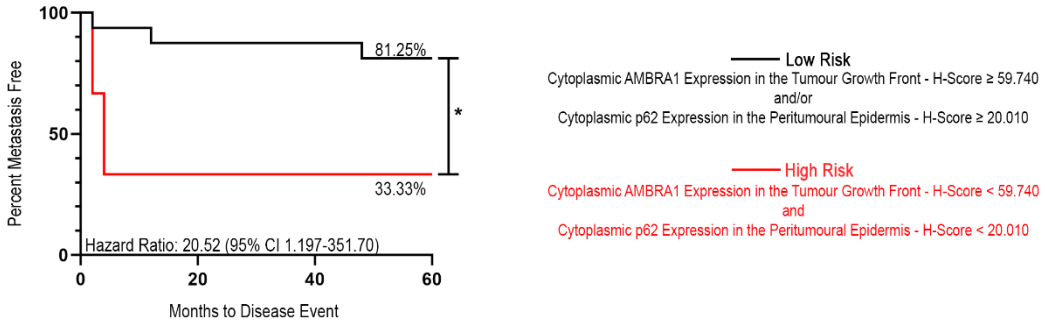

FIGURE 3. 19. CYTOPLASMIC AMBRA1 EXPRESSION IN THE TUMOUR GROWTH FRONT REGION AND CYTOPLASMIC P62 EXPRESSION IN THE PERITUMOURAL EPIDERMIS REGION IS A PREDICTOR OF METASTASIS IN POORLY-DIFFERENTIATED SCC TUMOURS

Kaplan-Meier survival analysis representing 60-month disease event free rate in 19 primary cSCC tumours stratified as low risk (n=14) and high risk (n=5) groups based on cytoplasmic AMBRA1 expression in the tumour growth front region. Statistics acquired by Mantel-Cox log-rank test and Mantel-Haenszel test (ns=non-significant).

In addition to these subcohorts, all cSCC tumours that were classified as poorly-differentiated where combined with all moderately-differentiated cSCC tumours that had at least one compartment that is trending towards a poorly-differentiated cSCC tumours, to access if cytoplasmic AMBRA1 expression in the tumour growth front region and cytoplasmic p62 expression in the peritumoural epidermis region was able to identity high-risk tumours that have a poorly-differentiated element. Results revealed that whilst not significant, this putative prognostic biomarker has some ability to identify high-risk cSCC patient subsets (Figure 3.20), with 76.19% of 31 low-risk patients not experiencing a metastatic event and 50.00% of 13 high-risk patients progressing to metastatic disease; with a hazard ratio of 3.34 (95% CI 0.56-19.72).

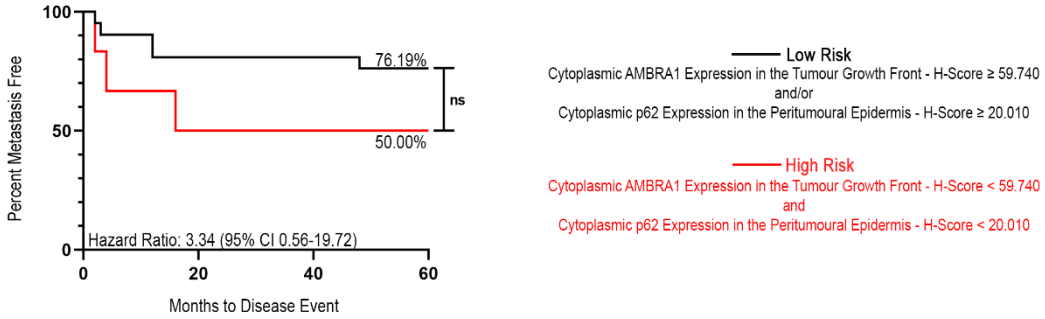

FIGURE 3. 20. CYTOPLASMIC AMBRA1 EXPRESSION IN THE TUMOUR GROWTH FRONT REGION AND CYTOPLASMIC P62 EXPRESSION IN THE PERITUMOURAL EPIDERMIS REGION IS ASSOCIATED WITH DECREASED METASTASIS FREE SURVIVAL IN SCC TUMOURS WITH A COMPONENT TRENDING TOWARDS A LESS-DIFFERENTIATED PHENOTYPE

Kaplan-Meier survival analysis representing 60-month disease event free rate in 44 primary cSCC tumours stratified as low risk (n=31) and high risk (n=13) groups based on cytoplasmic AMBRA1 expression in the tumour growth front region. Statistics acquired by Mantel-Cox log-rank test and Mantel-Haenszel test (ns=non-significant).

Collectively, these survival analyses on this refined cohort further demonstrates the potential and power of the joint use of cytoplasmic AMBRA1 expression in the tumour growth front region and cytoplasmic p62 expression in the peritumoural epidermis region as a prognostic biomarker for cSCC metastasis.

3.2.10. Development and validation of a novel p62 antibody for future cSCC biomarker studies

Results from the current study demonstrating the expression of AMBRA1 in the tumour growth front and p62 expression in the peritumoural epidermis of cSCCs as a putative prognostic biomarker were derived using a clinically validated antibody from AMLo Biosciences and a pre-optimised SQSTM1 p62 antibody from Santa Cruz. To develop a potential novel AMBRA1/p62 biomarker prognostic kit for cSCC an additional aim of the present study was to develop and pre validate a novel recombinant p62 antibody developed using the same technology used to generate the AMBRA1 antibody by the study sponsoring company, AMLo Biosciences Ltd. 13 anti-p62 HuCAL FAB antibody fragment clones were generated (BioRad in association with AMLo Biosciences Ltd) and screened by manual immunohistochemistry for their binding specificity in FFPE sections of normal human skin (Figure 3.16). The individual binding performance of each HuCAL FAB antibody was judged by comparison to the staining achieved by the commercially available research antibody to p62 from Santa Cruz (acting as a positive control). Results revealed strong and specific staining by 7 of the anti-p62 HuCAL FAB antibody fragment clones, specifically clones AbD34898, AbD34899, AbD34900, AbD34902, AbD34904, AbD34907 and AbD34908 when compared to

staining achieved using the Santa Cruz antibody (Figure 3.21). Positive p62 expression was observed in the cytoplasmic and nuclear cell sub compartments of both epidermal keratinocytes and dermal endothelial cells. A degree of non-specific background staining, localised to areas rich in dermal collagen, was also observed in both the anti-p62 HuCAL FAB antibody fragment clones and the positive control Santa Cruz.

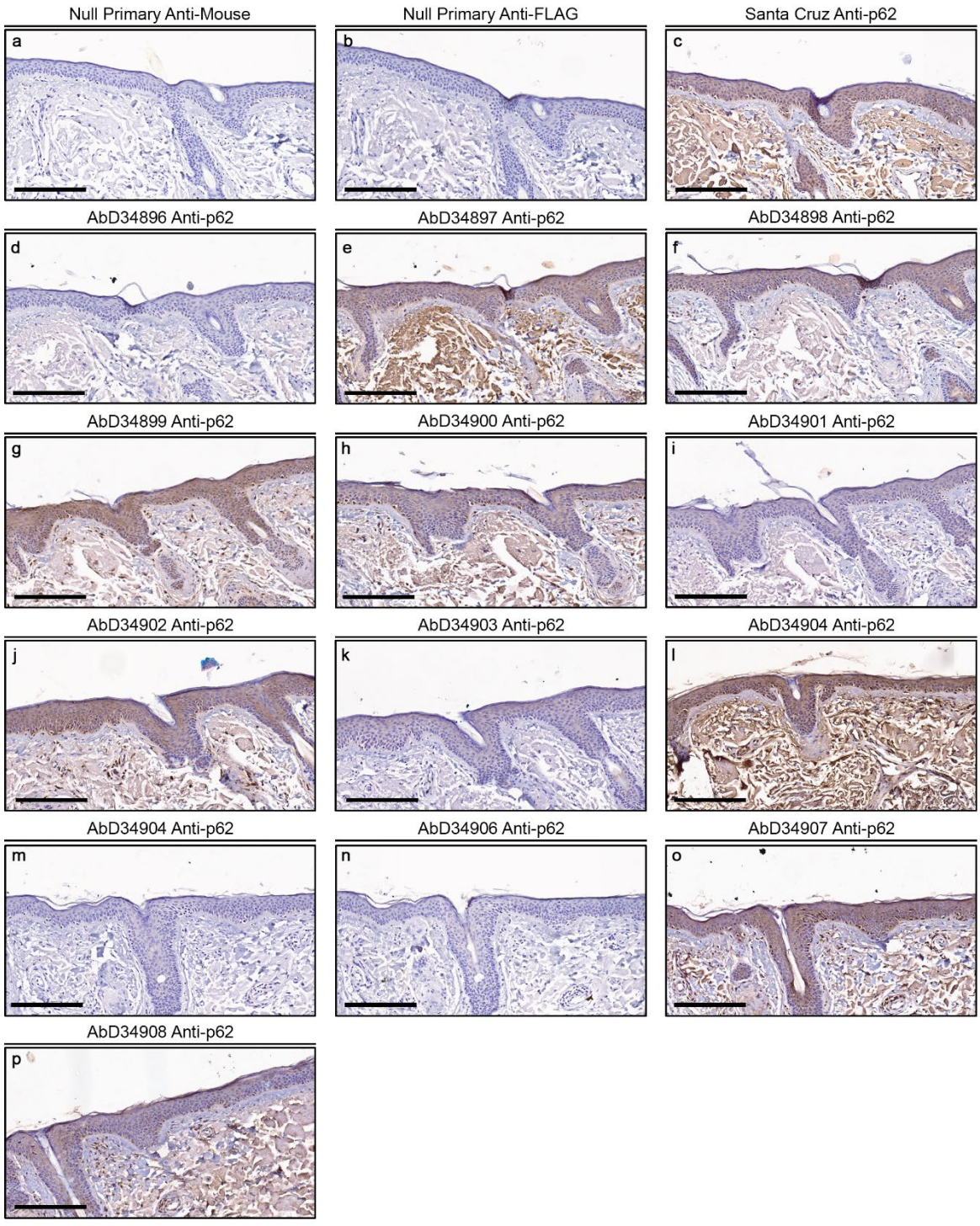

FIGURE 3. 21. THE RECOMBINANT ANTI-P62 HUCAL ANTIBODY CLONES ABD34898, ABD34899, ABD34900, ABD34902, ABD34904, ABD34907 AND ABD34908 HAVE THE HIGHEST COMPARABLE STAINING TO THE CURRENT RESEARCH STANDARD IN FFPE NORMAL SKIN TISSUE.

*Representative photomicrograph images of p62 staining in FFPE normal epidermis with (**a**) a null primary anti-mouse (negative control), (**b**) a null primary anti-FLAG (negative control), (**c**) a Santa Cruz p62 antibody (positive control) and each of the potential recombinant anti-p62 HuCAL antibody clones, (**d**) AbD34896, (**e**) AbD34897, (**f**) AbD34898, (**g**) AbD34899, (**h**) AbD34900, (**i**) AbD34901, (**j**) AbD34902, (**k**) AbD34903, (**l**) AbD34904, (**m**) AbD34905, AbD34906, (**n**) (**o**) AbD34907 and (**p**) AbD34908. Visible staining was achieved via immunohistochemistry with a DAB counterstain. Images taken using bright field microscopy at a magnification of 13.4x. Scale bar = 200 µm.*

To functionally validate the 7 best performing anti-p62 HuCAL FAB antibody fragment clones, western blotting was used to evaluate p62 expression in the CCD1106 keratinocyte cell line in response to starvation-induced autophagy, using the anti-p62 Santa Cruz antibody as a positive control (data not shown). In comparison to the GAPDH loading control, the Santa Cruz p62 antibody as well as the anti-p62 HuCAL FAB antibody fragment clones AbD34902, AbD34907 and AbD34908 demonstrated the expected autophagy-induced reduction in p62 in comparison to non-starved CCD1106 cells. As such, the anti-p62 HuCAL FAB antibody fragment clones AbD34902, AbD34907 and AbD34908 were taken forward for further validation.

The binding specificity of the HuCAL FAB antibody fragment clones AbD34902, AbD34907 and AbD34908 was next assessed via manual immunohistochemistry of FFPE sections derived from both well and poorly differentiated primary cSCC tumours. The anti-p62 HuCAL FAB antibody fragment clones AbD34907 and AbD34908 demonstrated the same staining pattern, albeit with a much higher staining intensity, as that observed by the positive control p62 antibody from Santa Cruz p62 (Figure 3.22). The p62 HuCAL FAB antibody fragment clone AbD34902 also appeared to show the same binding specificity at that of the positive control, but given the much weaker level of staining, was not taken forward for further validation. Positive p62 expression was observed consistently in the cytoplasmic of cSCC tumour cells, with occasional nuclear staining also detected. Additionally, to the staining observed in the cSCC tumour cells, cytoplasmic and nuclear p62 expression was again observed in dermal endothelial cells and also detected in infiltrating immune cells and glandular cells. Consistent with the observations made in the analysis of p62 staining in FFPE normal skin (Figure 3.16), dermal collagen demonstrated a high level of non-specific secondary binding.

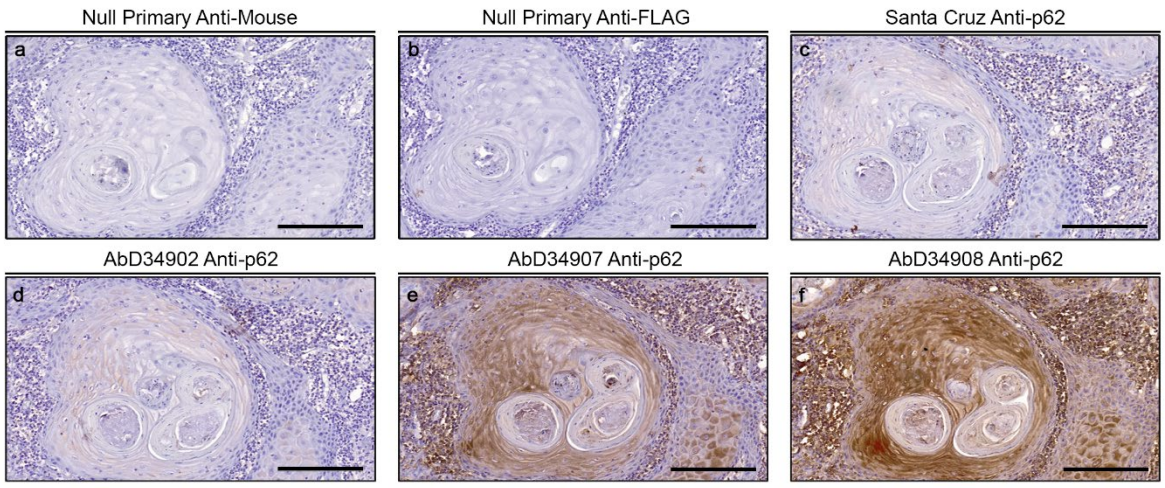

FIGURE 3. 22. THE RECOMBINANT ANTI-P62 HUCAL ANTIBODY CLONES ABD34907 AND ABD34908 HAVE THE HIGHEST COMPARABLE STAINING TO THE CURRENT RESEARCH STANDARD IN FFPE CSCC TISSUE.
*Representative photomicrograph images of p62 staining in FFPE cSCC with (**a**) a null primary anti-mouse (negative control), (**b**) a null primary anti-FLAG (negative control), (**c**) a Santa Cruz p62 antibody (positive control) and each of the potential recombinant anti-p62 HuCAL antibody clones, (**d**) AbD34902, (**e**) AbD34907 and (**f**) AbD34908. Visible staining was achieved via immunohistochemistry with a DAB counterstain. Images were taken using bright field microscopy at a magnification of 13.4x. Scale bar = 200 µm.*

Given the high staining intensity observed from the p62 HuCAL FAB antibody fragment clones AbD34907 and AbD34908 from manual immunohistochemistry in FFPE cSCC tumour sections, concentration optimisation of these antibody clones was performed in sections of FFPE normal skin. Primary concentrations of AbD34907 and AbD34908 at 20 µg/mL, 10 µg/mL, 5 µg/mL, 1 µg/mL and 0.1 µg/mL were used in manual immunohistochemistry and compared to the intensity and localisation of p62 expression achieved by the positive control anti-p62 Santa Cruz antibody, at the pre-optimised concentration of 4 µg/mL (Figure 3.23 and 3.24). Results revealed that using 0.5 µg/mL of either AbD34907 or AbD34908 had comparable staining intensity and cellular localisation of p62 expression as that derived from use of the Santa Cruz p62 antibody at its optimised concentration. This suggested that these p62 HuCAL FAB antibody fragment clones have the same binding specificity and intensity in FFPE material, at a 20-fold dilution rate, as that of the Santa Cruz antibody.

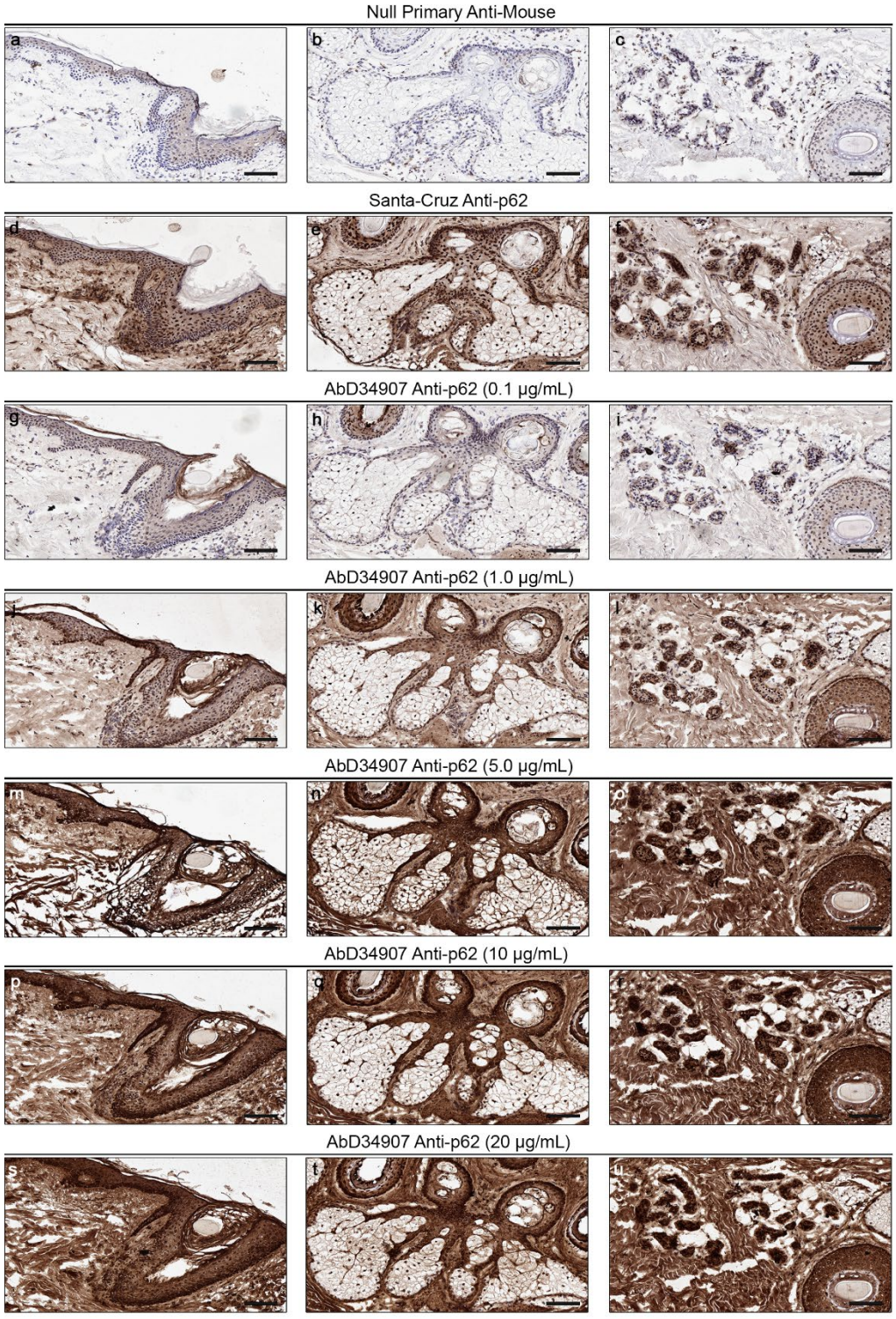

FIGURE 3. 23. A CONCENTRATION OF 1.0 MG/ML OF THE RECOMBINANT ANTI-P62 HUCAL ANTIBODY CLONE ABD34907 IS MOST COMPARABLE TO THE CURRENT RESEARCH STANDARD IN OCT NORMAL SKIN TISSUE.

*Representative photomicrograph images of p62 staining in three areas of OCT normal epidermis with (**a-c**) a null primary anti-mouse (negative control), (**d-f**) a Santa Cruz p62 antibody and the potential recombinant anti-p62 HuCAL antibody clone AbD34907 at the concentrations (**g-i**) 0.1 µg/mL, (**j-l**) 1 µg/mL, (**m-o**) 5 µg/mL, (**p-r**) 10 µg/mL and (**s-u**) 20 µg/mL. Visible staining was achieved via immunohistochemistry with a DAB counterstain. Images taken using confocal microscopy with a magnification of 13.4x. Scale bar = 200 µm.*

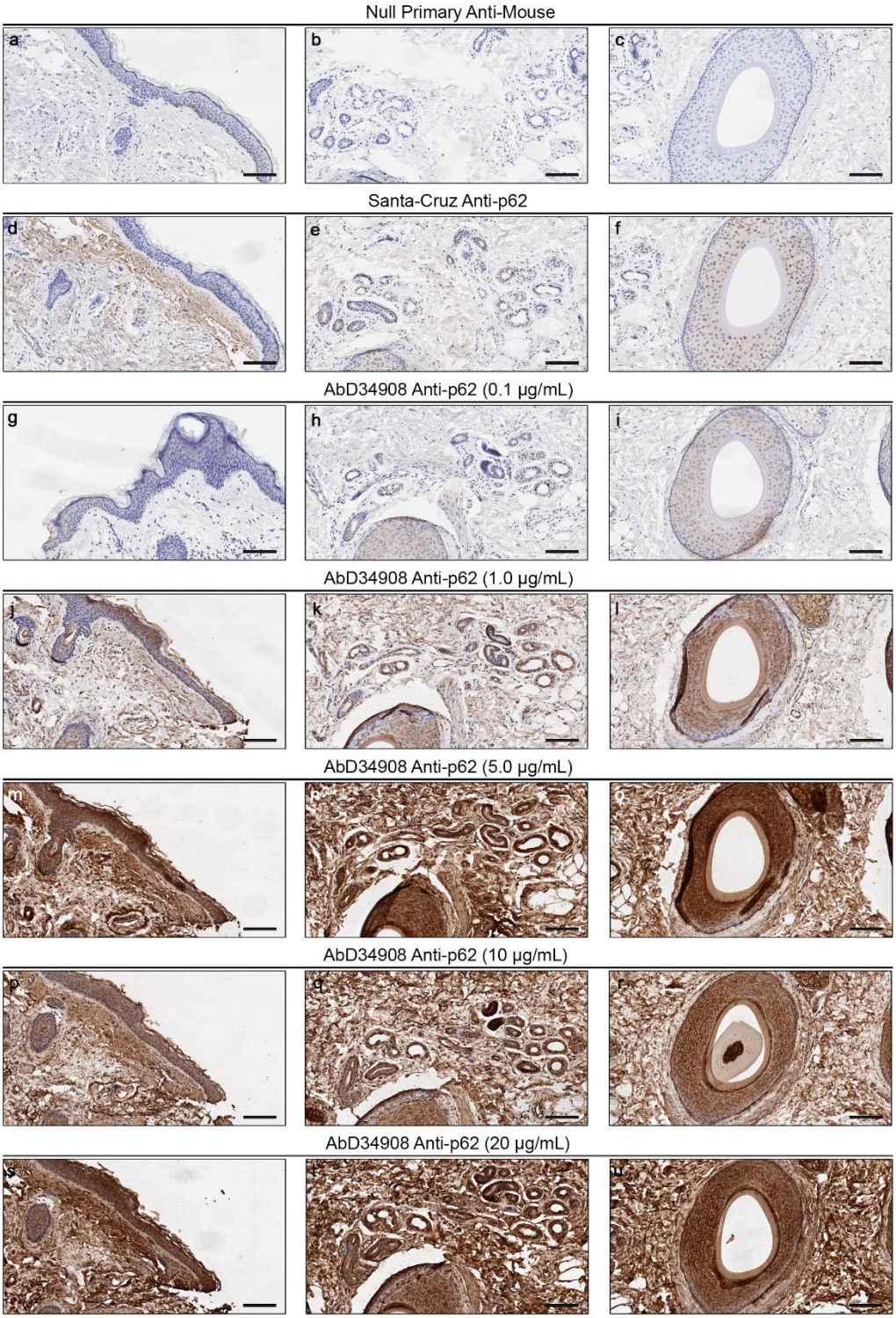

FIGURE 3. 24. CONCENTRATION OF 0.1 MG/ML OF THE RECOMBINANT ANTI-P62 HUCAL ANTIBODY CLONE ABD34908 IS MOST COMPARABLE TO THE CURRENT RESEARCH STANDARD IN FFPE NORMAL SKIN TISSUE.
*Representative photomicrograph images of p62 staining in three areas of FFPE normal epidermis with (**a-c**) a null primary anti-mouse (negative control), (**d-f**) a Santa Cruz p62 antibody and the potential recombinant anti-p62 HuCAL antibody clone AbD34908 at the concentrations (**g-i**) 0.1 µg/mL, (**j-l**) 1 µg/mL, (**m-o**) 5 µg/mL, (**p-r**) 10 µg/mL and (**s-u**) 20 µg/mL. Visible staining was achieved via immunohistochemistry with a DAB counterstain. Images taken using bright field microscopy with a magnification of 13.4x. Scale bar = 200 µm.*

Given the use of frozen tissue samples in diagnostic pathology, methodology optimisation was repeated in a series of OCT embedded normal skin sections. Anti-p62 HuCAL FAB antibody fragment clones AbD34907 and AbD34908 were used in manual immunohistochemistry at concentrations of 20 µg/mL, 10 µg/mL, 5 µg/mL, 1 µg/mL and 0.1 µg/mL and p62 expression compared to the staining derived from use of the positive control Santa-Cruz at its pre-optimised concentration. Results revealed similar staining intensity and localisation of p62 expression could be observed between the clone AbD34907 and AbD34908 when used at a concentration of 1 µg/mL as that derived from use of the positive control Santa Cruz antibody (Figure 3.25 and 3.26), suggesting p62 HuCAL FAB antibody fragment clones have the same binding specificity and intensity in OCT material, at a 4-fold dilution rate, as the Santa Cruz antibody.

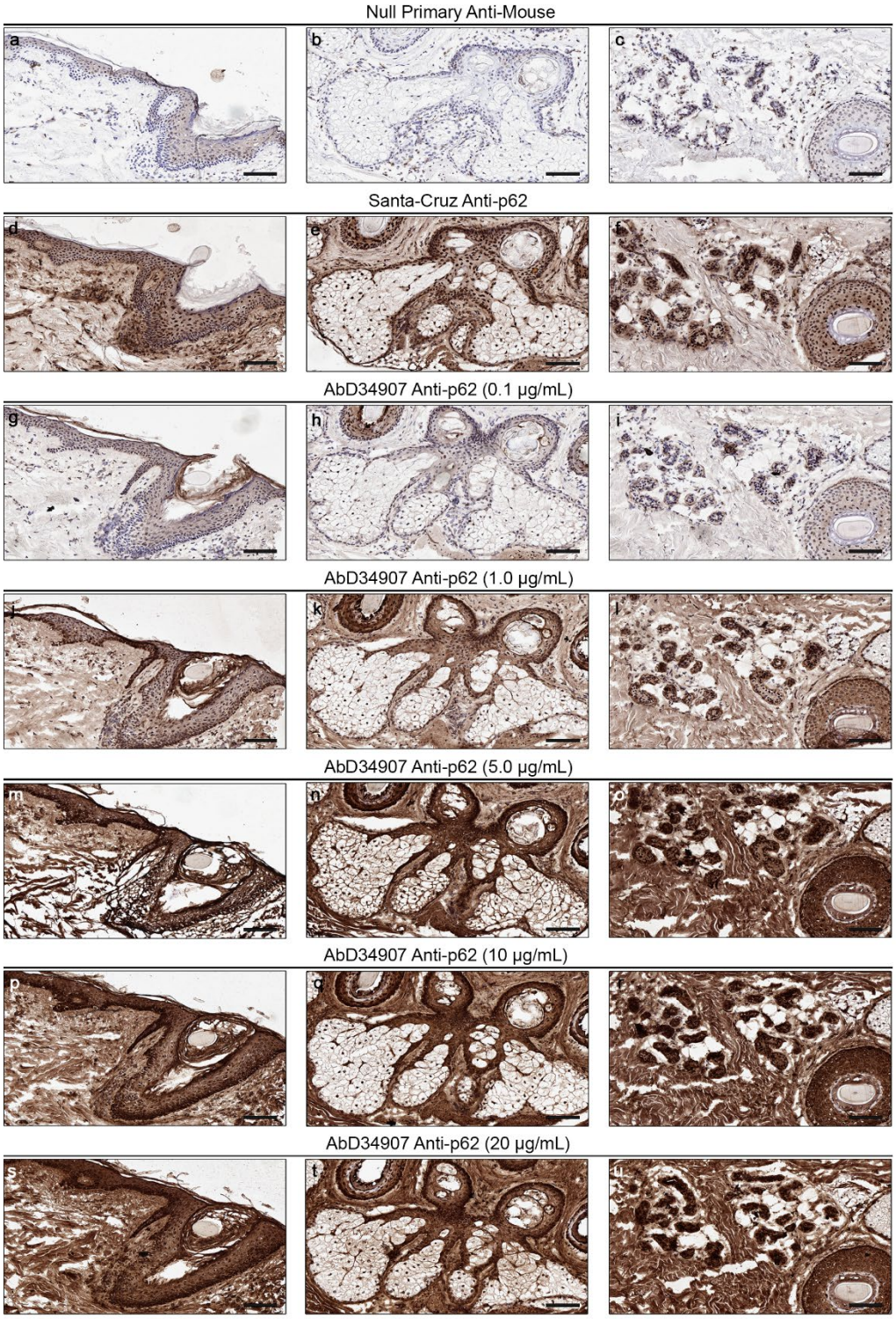

FIGURE 3. 25. A CONCENTRATION OF 1.0 MG/ML OF THE RECOMBINANT ANTI-P62 HUCAL ANTIBODY CLONE ABD34907 IS MOST COMPARABLE TO THE CURRENT RESEARCH STANDARD IN OCT NORMAL SKIN TISSUE.

*Representative photomicrograph images of p62 staining in three areas of OCT normal epidermis with (**a-c**) a null primary anti-mouse (negative control), (**d-f**) a Santa Cruz p62 antibody and the potential recombinant anti-p62 HuCAL antibody clone AbD34907 at the concentrations (**g-i**) 0.1 µg/mL, (**j-l**) 1 µg/mL, (**m-o**) 5 µg/mL, (**p-r**) 10 µg/mL and (**s-u**) 20 µg/mL. Visible staining was achieved via immunohistochemistry with a DAB counterstain. Images taken using confocal microscopy with a magnification of 13.4x. Scale bar = 200 µm.*

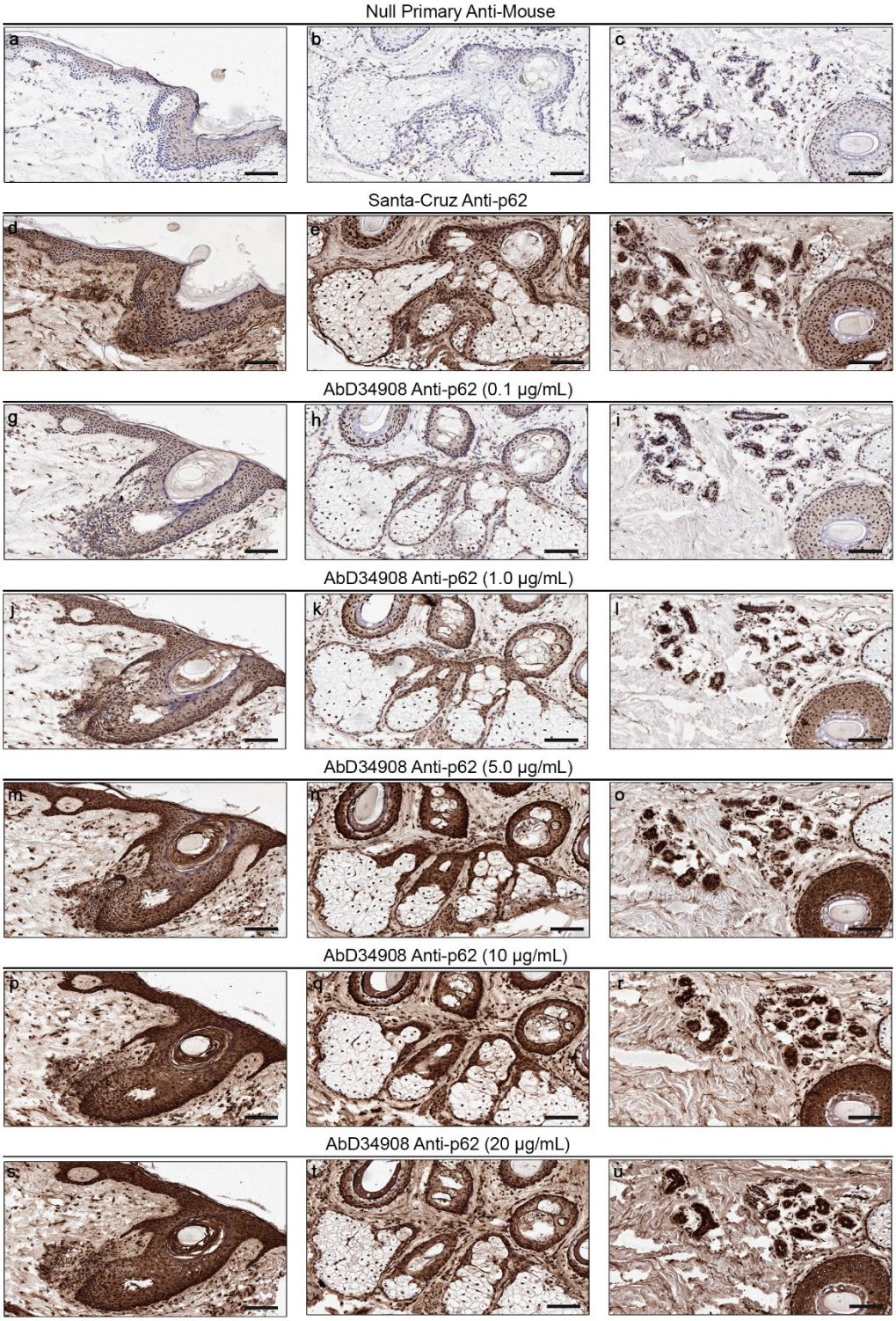

FIGURE 3. 26. A CONCENTRATION OF 1.0 MG/ML OF THE RECOMBINANT ANTI-P62 HUCAL ANTIBODY CLONE ABD34908 IS MOST COMPARABLE TO THE CURRENT RESEARCH STANDARD IN OCT NORMAL SKIN TISSUE.

*Representative photomicrograph images of p62 staining in three areas of OCT normal epidermis with (**a-c**) a null primary anti-mouse (negative control), (**d-f**) a Santa Cruz p62 antibody and the potential recombinant anti-p62 HuCAL antibody clone AbD34908 at the concentrations (**g-i**) 0.1 µg/mL, (**j-l**) 1 µg/mL, (**m-o**) 5 µg/mL, (**p-r**) 10 µg/mL and (**s-u**) 20 µg/mL. Visible staining was achieved via immunohistochemistry with a DAB counterstain. Images taken using confocal microscopy with a magnification of 13.4x. Scale bar = 200 µm.*

Taken together, these data indicated similar staining localisation and intensity for p62 expression in FFPE and OCT sections of human skin was derived using anti-p62 HuCAL FAB antibody fragment clones AbD34907 and AbD34908 HuCAL. However, non-specific background staining was observed at a higher level in sections stained with the AbD34907 clone when compared to the AbD34908 clone. As such the clone AbD34908 was selected to undergo the final validation.

The ability of AbD34908 to detect p62 expression in FFPE cSCC tumours was further assessed by manual IHC (Figure 3.27). Results revealed that, whilst staining was weaker, the anti-p62 HuCAL FAB antibody fragment clone AbD39408 performed equally well to the positive control Santa Cruz antibody, being able to detect cell-to-cell differences in p62 expression, in both cytoplasmic and nuclear regions, within the same cluster of cSCC cells.

Collectively these data validated the anti-p62 HuCAL FAB antibody fragment clone AbD34908 as a potential diagnostic antibody for use in combination with the current AMBRA1 antibody in the development of a novel prognostic biomarker IHC assay kit for cSCC.

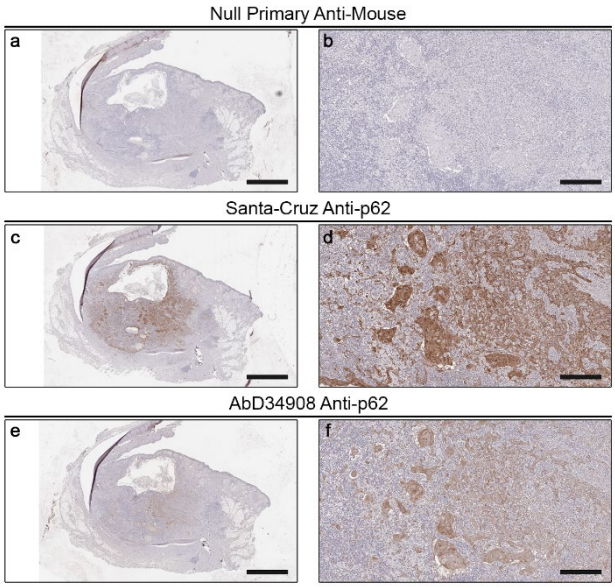

FIGURE 3. 27. THE RECOMBINANT ANTI-P62 HUCAL ANTIBODY CLONE ABD34908 IDENTIFIES THE SAME P62 EXPRESSION AS THE CURRENT RESEARCH STANDARD ANTIBODY IN FFPE CSCC TISSUE.
*Representative photomicrograph images of p62 expression in FFPE normal skin with (**a**-**b**) a null primary anti-mouse (negative control), (**c**-**d**) a Santa Cruz p62 antibody and (**e**-**f**) the potential recombinant anti-p62 HuCAL antibody clone AbD34908. Visible staining was achieved via immunohistochemistry with a DAB counterstain. Images **a**, **c** and **e** taken using bright field microscopy with a magnification of 0.8x. Scale bar = 3 mm. Images **b**, **d** and **f** taken using bright field microscopy with a magnification of 6.0x. Scale bar = 400 µm.*

3.3. Discussion

In the last decade, several systematic genomic and proteomic approaches have been undertaken in an attempt to identify prognostic biomarkers for cSCC (Wei et al., 2018, Shapanis et al., 2021). Those that have been identified include the expression of the glycoprotein podoplanin (Kreppel et al., 2013), the histone acetyltransferase p300 (Chen et al., 2015), TERT a catalytic subunit of telomerase (Campos et al., 2019), over expression of EGFR (Cañueto et al., 2017c), miR-205 expression (Cañueto et al., 2017b), expression of INPP5A and CD133 (Sekulic et al., 2010, Xu et al., 2016) and a 40-gene expression profile test proposed by Castle Biosciences Ltd (Wysong et al., 2020). However, the credible biomarker capacity of all is limited by their consistency, reliability, accuracy and/or feasibility.

Studies in podoplanin expression suggest its presence in tumour cells acts as a potential prognostic biomarker for cSCC with a univariate hazard ratio of 17.95 (95% CI: 3.85-83.66). (Kreppel et al., 2013, Cañueto et al., 2017a). However, expression was based on manual consensus scoring by pathologists, which is subjective and inconsistent, and again, to date no larger-scale patient validation studies with more detailed statistical analysis (i.e. PPV, NPV, sensitivity or specificity) have been described. Overexpression of the histone acetyltransferase p300 has also been suggested as a potential biomarker, but with a poor hazard ratio of 2.42 (95% CI: 1.32-4.42) and again with no detailed statistical analysis on test performance described (Chen et al., 2015). The mutation of the catalytic subunit of telomerase TERT, has been suggested to predict cSCC recurrence, with a hazard ratio of 8.41 (95% CI: 2.53-27.90), and metastasis with a hazard ratio of 15.60 (95% CI: 1.85-131.65). However, given the requirement to extract, amplify, sequence and analyse DNA from FFPE patient samples, this poses a significant cost and time commitment and hence questions the translation feasibility of this biomarker into standard clinical practice (Campos et al., 2019).

As with other cancers, EGFR overexpression has been linked to a poor outcome in cSCC. Immunohistochemical based biomarker analysis in a cohort of 94 cSCC patients showed some ability to predict cSCC TNM stage progression, however, as a biomarker it did not concur any advantage over tumour differentiation status. (Cañueto et al., 2017c). Further studies by Cañueto et al also investigated the prognostic potential of microRNA miR-205 expression. However, with a univariate hazard ratio of 6.552 (95% CI: 1.332–32.232) and high cost implications, this is unlikely to be a viable prognostic biomarker for cSCC (Cañueto et al., 2017b).

The proposed biomarkers INPP5A and CD133, both employ immunohistochemical expression analysis as the basis of a prognostic test for cSCC, the easiest methodology to integrate into standard clinical practice. However, with univariate hazard ratios predicting either recurrence or metastasis all below 5.00, their potential as accurate biomarkers is also limited (Maly et al., 2020, Cumsky et al., 2019, Xu et al., 2016).

Finally, Castle Biosciences have recently published their validation of a 40-gene expression profile test (Wysong et al., 2020). To date, this has been the most extensive study of a potential prognostic biomarker for cSCC, as discussed below, and making it perhaps the best candidate to compare against the prognostic potential of the proposed combined expression of AMBRA1 and p62. It should be noted however that this 40 gene test only reports the multivariate hazard ratio with no explanation underpinning the chosen 40-genes.

Collectively the various issues associated with the above proposed biomarkers emphasise the remaining unmet need for novel credible prognostic biomarkers to identify high-risk cSCC and prompting the current study aimed at defining the prognostic potential of AMBRA1 and p62 expression.

3.3.1. Loss of AMBRA1 expression occurs in cSCC tumourigenesis

Initial observations from immunohistochemical staining of AMBRA1 in both the pilot Newcastle and Cambridge discovery cohorts of primary cSCCs revealed a consistent loss of AMBRA1 expression in the tumour mass compared to control, maintained expression in the adjacent normal epidermis. Loss of AMBRA1 expression occurred regardless of either the cellular differentiation status of the tumour or the ultimate disease outcome (Figure 3.1 and Figure 3.3A), conflicting early preliminary data suggesting loss of AMBRA1 expression is associated with a poorly differentiated tumour phenotype (Lovat et al un published data) , a factor frequently associated with higher levels of disease recurrence and metastasis (Thompson et al., 2016, O'Hara et al., 2011, Samarasinghe et al., 2011, Friedman et al., 1985). However, multiple studies have shown disease recurrence and metastasis occurs in both well and poorly differentiated cSCC tumours, albeit at different rates (Rodriguez et al., 2021). Given this fact and the uniform loss of AMBRA1 in all primary cSCC tumours, if loss of AMBRA1 expression does influence cSCC disease outcome, it is more likely that loss of AMBRA1 expression occurs more often and to a greater extent in poorly differentiated tumours, and potentially explaining the differing progression rates in the present study sub-cohorts of cSCC.

Visual analysis of AMBRA1 expression in the pilot Newcastle cohort of cSCCs was consistent with its quantified expression in the normal epidermis, peritumoural epidermis, tumour mass and tumour growth front of all primary cSCC tumours within the Cambridge discovery cohort. Data further demonstrated a significant loss of AMBRA1 expression between the normal epidermis and all other regions of the primary cSCC tumours regardless of disease outcome (Figure 3.5). These results suggest that loss of AMBRA1 expression is universal in cSCC tumourigenesis, rather than aiding or being required for cSCC progression. The most likely explanation for this result comes from previous work, suggesting AMBRA1 is critical for the completion of keratinocyte differentiation, an additional function (Cosgarea et al., 2021) outside of its well-documented role in autophagy induction (Huang et al., 2018). Studies further examining the potential relationship between AMBRA1, keratinocyte differentiation and autophagy are described in chapter 5, but its loss of expression in cSCCs likely results in the maintenance of a more dedifferentiated cell state, preventing terminal differentiation and ensuring higher levels of proliferation (Dahl, 2012, Ghadially, 2012, Dallaglio et al., 2013). With this initial transformation complete, loss of AMBRA1 expression would thus further promote cSCC development by causing dysregulated autophagy that leads to an increase in the mutation rate of cancer cells, and ultimately the acquisition of pro-oncogenic functions, cSCC cell survival and progression (Rosenfeldt and Ryan, 2011, Qu et al., 2003, Liang et al., 1999).

Notably however, AMBRA expression differed between localised and recurrent/metastatic primary cSCC tumours, with no apparent loss in expression detected between the peritumoural epidermis and the tumour mass and growth front regions of recurrent/metastatic cSCCs (Figure 3.5B). These data suggest there is a greater decrease in AMBRA1 expression in the tumour epidermal environment of cSCCs that progress and potentially explained by two potential mechanisms.

Firstly the tumour-inducing field effect that led to cSCC initiation, most likely UV radiation, may have been chronic or concentrated enough to more severely impact on epidermal keratinocytes (Kuluncsics et al., 1999, Douki et al., 2003, Lochhead et al., 2015) resulting in the early acquisition of a larger number of pro-oncogenic mutations, including loss of AMBRA1 that allowed for more rapid tumour progression. This hypothesis could be tested by evaluating if the observed loss of AMBRA1 expression in the peritumoural epidermis is more frequently associated with a UV signature of carcinogenesis associated with a higher mutational burden (D'Errico et al., 2000, Liu-Smith et al., 2017). Alternatively, this greater loss of AMBRA1

expression in the peritumoural environment may be driven by increased paracrine signalling in primary cSCC tumours that reoccur or metastasise. It is possible that such tumours develop an early mutation leading to an increase in a signalling driver of reduced AMBRA1 expression. This secretion would impact nearby noncancerous epidermal cells as well as cSCC cells, explaining the greater loss of AMBRA1 expression. This hypothesis is additionally supported by recent studies indicating melanoma secretion of isoform specific TGF-β2 underpins both epidermal loss of AMBRA1 expression and a weakening in epidermal integrity, factors likely also critical in cSCC progression (Cosgarea et al., 2021). An investigation into the potential signalling mechanisms mediating loss of AMBRA1 expression in cSCCs is further explored in chapter 4.

Taken together, these data provide strong evidence for the loss of AMBRA1 expression in the tumour mass of all primary cSCC tumours regardless of their differentiation status or disease outcome. This lack of difference between AMBRA1 expression in the tumour mass of localised and recurrent/metastatic cSCC tumours suggests such loss may promote initial tumourigenesis rather than progression, dampening expectations that AMBRA1 expression has prognostic potential for cSCC.

3.3.2. Cytoplasmic and nuclear p62 expression increases in cSCC tumourigenesis

A similar characterisation of p62 expression changes in cSCC tumourigenesis was also conducted, examining the alterations to both cytoplasmic and nuclear p62 expression initially with simple visual assessment of p62 staining in immunohistochemically stained slides derived from the pilot Newcastle cohort of cSCCs but followed up with more detailed digital quantification analysis in the Cambridge cohort of cSCCs.

Initial results revealed, in both the pilot and discovery cohorts, an increase in both cytoplasmic and nuclear p62 expression in all primary cSCC tumours regardless of differentiation status or disease outcome (Figure 3.2 and 3.3B). These data conflicted previous studies, which suggested the observable change in subcellular localisation of p62 from a nuclear to a cytoplasmic subcellular compartment was associated with cSCC tumorigenesis and progression (Liu et al., 2014). However, digital quantification of p62 expression in both subcellular compartments of all primary cSCC tumours in the Cambridge discovery cohort demonstrated a significant increase in both cytoplasmic and nuclear p62 expression in the tumour mass and growth front regions, suggesting such translocation unlikely occurs (Figure 3.5 and 3.6).

The observed increase in both cytoplasmic and nuclear p62 has been linked to cancer through several different mechanisms in previous studies. In terms of cytoplasmic p62 expression, a higher level of p62 may play an active role in both aspects of the accepted paradoxical role of autophagy in cancer. Firstly, the accumulation of p62 could indicate defective autophagy in cancer, leading to an increased mutation rate (Huang et al., 2018). However, multiple studies have demonstrated p62 could also be supporting cell growth through its signalling-hub like activity that leads to the stimulation of mTORC1, thus allowing for continual tumour cell proliferation (Linares et al., 2013, Linares et al., 2015). p62 has also been shown to maintain aberrant expression of Nrf2 by interfering with the ubiquitin E3 ligase adapter protein Keap1, which normally acts to reduce Nrf2 under homeostatic conditions. This allows for greater protection of cancer cells against antioxidant stress and thus their resistance to apoptosis (Sun et al., 2016, Jain et al., 2010). Finally, cytoplasmic p62 expression could also be involved in preventing or reducing excessive activation of the NF-κB signalling pathway by either preventing the activation of the IKK complex indirectly (Zotti et al., 2014) or by activating RIP1, leading to the ubiquitin induced degradation of the IKK complex (Kanayama et al., 2015).

Nuclear p62 expression has been investigated chiefly as a central tumour microenvironment reprogramming protein but recent work has suggested it also promotes tumourigenesis. Work by Zhang et al. has shown that nuclear p62 expression leads to NICD1 and LC3-mediated degradation of NOTCH1, a critical differentiation protein in the epidermis and thus allowing for the preservation of a dedifferentiated phenotype (Zhang et al., 2018).

The numerous associations between p62 and cancer thus suggest the observed increase in both cytoplasmic and nuclear expression within the well, moderately or poorly differentiated cSCCs likely directly contributes to tumour progression. Noteworthy however, was the decline in increased cytoplasmic p62 expression levels in the tumour mass and growth front regions of all primary cSCCs upon sub cohort analysis of tumours stratified by differentiation status. Additionally, results also revealed no significant difference in cytoplasmic p62 expression between any region of well, moderately or poorly-differentiated recurrent/metastatic cSCC tumours (Appendix Figures A.9 – A.11). This result was surprising as studies in a wide range of cancers have suggested that an increase in p62 expression is correlated with a poor prognosis. Studies in colon, gastric, thyroid, lung and liver cancer have all demonstrated that a high level of p62 expression is consistent with a poor prognosis (Lei et al., 2020, Kim et al., 2019, Mao et al., 2021, Denk et al., 2019). Additionally, the expression of p62 has also been

shown to have prognostic potential in epithelial or squamous tumours where high expression is also associated with poor patient outcomes (Wang et al., 2020b, Ellis et al., 2014, Yoshihara et al., 2014, Liu et al., 2014). These consistent observations in the literature and the fact p62 accumulation was not observed in sub-cohort analysis but was observed in the pooled analysis of the Cambridge discovery cohort of cSCCs suggests that this cohort may have been under powered rather than a lack of p62 accumulation being attributed to a distinct biological mechanism.

A similar observation was seen for the distribution of nuclear p62 expression across differing regions analysed in sub cohorts of well, moderately or poorly cSCCs (Appendix Figure A.16-A.18). While nuclear p62 expression levels differed in well, moderately and poorly differentiated sub-cohorts of recurrent/metastatic primary cSCC tumours, particularly showing significant differences in expression between the normal epidermis/peritumoural epidermis regions and the tumour mass/tumour growth front regions, the pattern of expression was nevertheless inconsistent. Similarly, to the hypothesis proposed for cytoplasmic p62 expression analysis, this result may reflect the use of underpowered cSCC sub cohorts. Collectively these data suggest however, that cSCC tumourigenesis is associated with a significant increase in both cytoplasmic and nuclear p62 expression regardless of tumour differentiation status or disease outcome.

3.3.3. The combined loss of cytoplasmic AMBRA1 expression in the tumour growth front and loss of cytoplasmic p62 expression in the peritumoural epidermis is a putative prognostic biomarker for cSCC

Cytoplasmic AMBRA1, cytoplasmic p62 and nuclear p62 expression levels were compared in the normal epidermis, peritumoural epidermis, tumour mass and tumour growth front between localised and recurrent/metastatic primary cSCC tumours. This comparative regional analysis was performed in order to define the region in which AMBRA1, cytoplasmic or nuclear p62 expression had the highest prognostic potential. Results however, revealed no significant difference in either AMBRA1 or cytoplasmic or nuclear p62 expression in any region between localised and recurrent/metastatic primary cSCCs (Appendix Figure A.1, A.8 and A.15). Comparative sub cohort analysis was thus repeated in well, moderately or poorly differentiated tumour subsets. Results again revealed no significant difference in AMBRA1 or p62 expression in any region between localised and recurrent/metastatic primary cSCC tumours (Appendix Figure A.5-A.7, A.12-A.14 and A.19-A.21). These results may have been

limited by the initial statistical approach. While data analysis was performed using both parametric and non-parametric one-way ANOVA tests, this statistical approach is not in fact best suited to determining the prognostic potential of a given protein (Mishra et al., 2019).

Digital quantification led biomarker discovery has been demonstrated to have several limitations and given the heavy reliance on this methodology in the present study, these may have prevented the identification of a region with prognostic potential in several discreet ways (Aeffner et al., 2019, Jahn et al., 2020). Firstly, several representative areas of AMBRA1 and p62 expression within a cSCC tumour were identified, with the aim to capturing the mean differential expression, but the resultant average H-score derived may not reflect the greatest loss of expression observed in some cSCC tumours. Given the well-documented subclonal expansion model of squamous cell carcinogenesis (Perez-Ordoñez et al., 2006, Shergill et al., 2018, Greaves and Maley, 2012), expression of either AMBRA1 or p62 in a specific region, defined by either clinical, histopathological or phenotypical markers may actually be better suited for biomarker discovery. Secondly, the software used for the quantification of AMBRA1 and p62 expression may also introduce several potential issues (as detailed in Section 2.14 and 3.2.3). Whilst the Aperio ImageScope Software allows for a certain level of optimisation of the quantifying algorithm for a specific tissue, they remained better suited for use in the analysis of highly phenotypically consistent cancers. The large variability of cSCC phenotype, driven by differing levels of differentiation within cells, produced the occasional misidentification of either whole cells, the cytoplasm boundaries or the actual nucleus within an annotated area. This would therefore have potentially reduced the accuracy of the derived H-scores. Finally, quantification of p62 was based on algorithm assessment of the colour produced by the fast red counterstain. Given the blue colour of haematoxylin and the purple colour of fast red counterstaining, it is possible that given their close positions on the colour spectrum, haematoxylin blue may have been incorrectly identified as fast red staining. However, it is noteworthy that other biomarker discovery methodologies rely solely on human judgement to assign staining levels into discreet categories and thus, even with these potential limitations, this digital led methodology therefore still seems appropriate for the discovery of new biomarkers.

The ideal biomarker for any disease should leave little to no interpretation by a histopathologist and as such, ROC curve analysis was undertaken to better assess the prognostic potential of either AMBRA1 or p62 expression in any defined cSCC tumour region

(Kamarudin et al., 2017). ROC curve analysis was conducted on all primary cSCC tumours regardless of differentiation status, to limit potential bias and misinterpretation by histopathologists of influencing factors such as tumour differentiation (Aronson and Ferner, 2017). However, ROC curve analysis was nevertheless performed in sub-cohorts of well moderately and poorly differentiated cSCCs to evaluate the potential of tumour differentiation status as a prognostic variable.

Results revealed loss of cytoplasmic AMBRA1 expression in the tumour growth front region and loss of cytoplasmic p62 in the peritumoural epidermis of region in all primary cSCC tumours had the highest level of prognostic potential, with an AUC of 0.5522 and 0.6352 respectively (Figure 3.8). These relatively low AUC values however typically indicate that the expression of these individual proteins in these region have little to no prognostic potential (Kamarudin et al., 2017) as confirmed by Kaplan-Meier survival analysis, showing both markers were unable individually predict disease recurrence or metastasis (Figure 3.9 and 3.10). Nevertheless, these data did allow for the definition of AMBRA1 expression in the tumour growth front as a better prognostic indicator than expression in the tumour mass.

This result contradicts a sizeable amount of previously published work demonstrating the upregulation of autophagy is vital for the initiation and survival of metastatic cancer cells. This increase in active autophagy has been implicated in the scavenging and reuse of vital cell nutrients, the process of epithelial-to-mesenchymal transition, resistance to anoikis, cell motility, immune detection avoidance and the rearrangement of focal adhesion complexes (Kenific et al., 2010, Li et al., 2013, Fung et al., 2008, Kadandale et al., 2010, Sharifi et al., 2016, Akalay et al., 2013), suggesting that the loss of the pro-autophagy protein AMBRA1 is illogical. Noteworthy, was the fact that a total loss of AMBRA1 expression was not observed in the tumour growth front of cSCC tumours suggesting the maintenance of some automatic activity. Given the recent suggestion that AMBRA1 is a critical regulator of keratinocyte differentiation (Cosgarea et al., 2021) (further discussed in chapter 5), this suggests loss of expression is therefore more representative of reduced cell differentiation capacity and the preservation of a more stem cell state, another vital component of cancer cell metastasis (Chaffer and Weinberg, 2011). Collectively the level of AMBRA1 expression likely demonstrates the retention of some autophagy capacity and a more stem like cancer cell state which together facilitate and promote cSCC metastasis.

Interestingly, and in contrast to all other studies which have explored the potential for p62 as a biomarker in cancer tumourigenesis or progression, the present study in cSCC suggests the prognostic potential for p62 expression is derived from its reduced expression in the peritumoural epidermis, and not the tumour itself. Supporting this notion, p62 has been implicated in multiple tumour microenvironment reprogramming events, such lipid redistribution and metabolic reprogramming of adipose cells and Nrf2 activation of cancer-associated fibroblasts, allowing cancer tumourigenesis through an altered ECM (Reina-Campos et al., 2018, Kang et al., 2021). Additionally, recent work has demonstrated a correlation between breast cancer cell motility and suppressed p62 expression (Tan et al., 2018), suggesting the observed reduction in peritumoural epidermal p62 expression may allow early cSCC cell invasion due to a reduction in epidermal integrity. However, studies examining the specific role of p62 in the epithelial of tumour microenvironments is currently lacking, making it difficult to define the precise underlying mechanism underpinning the observed prognostic potential.

Taken together data from the present study suggest that individually AMBRA1 and p62 are not viable prognostic biomarkers for cSCC recurrence/metastasis. However, the combination of AMBRA1 expression in the tumour growth front with the cytoplasmic expression of p62 in the peritumoural epidermis was able to significantly distinguish high and low risk tumour subsets at risk of disease recurrence/metastasis independently of tumour differentiation status (Figure 3.11, $P<0.05$, HR 4.421 (1.322 to 14.91).

Furthermore the prognostic potential of combined AMBRA1 expression in the tumour growth front and cytoplasmic expression of p62 in the peritumoural epidermis is further strengthened when removing recurrent primary tumours and stratifying for the risk of metastasis in metastasis in poorly-differentiated cSCC tumours (Figures 3.19, $P<0.01$, HR 20.52 (95% CI 1.197-351.70)) and shows potential for cSCC tumours that contain a poorly-differentiated compartment (Figure 3.20, HR 3.34 (95% CI 0.56-19.72)).

As mentioned previously, the 40-gene biomarker test produced by Castle Bioscience is the most extensively studied biomarker to date for cSCC (Wysong et al., 2020). Comparing hazard ratios with the combined use of AMBRA1 and p62 in moderately/poorly differentiated cSCCs, its is clear to see use of AMBRA1/p62 outperforms the 40-gene test at a two-fold rate, with a hazard ratios of 20.52 and 9.55 respectively. The positive predictive value (PPV) of 66.67% and the assay specificity of 92.86% for combined AMBRA/p62 expression are also significantly

higher than the PPV or assay specificity for the 40 gene test. Furthermore, the negative predictive value of 81.25% for combined AMBRA1/p62 expression as a prognostic biomarker for metastatic development is comparable to the value of 91% reported for the 40 gene test. Assay sensitivity for combined AMBRA1/p62 expression is also comparable to that of the Castle Biosciences 40 gene test, with a value of 40.00%, which outperforms the Class 2B classification of the test at 28.80%. Additionally, upon further validation, the use of AMBRA1/p62 as an IHC based prognostic marker will fit seamlessly into current diagnostic procedures for cSCC, not requiring additional tissue as it can be performed using a serial FFPE tissue section and will easily be able to be developed as a rapid digital machine learning based test in line with the move of pathology services to a more digital approach.

Overall, the combined AMBRA1 expression in the tumour growth front and cytoplasmic expression of p62 in the peritumoural epidermis thus defines a novel putative prognostic biomarker able to predict disease recurrence/metastasis of cSCCs regardless of differentiation status, and more accurately as a prognostic biomarker of disease metastasis in moderately/poorly differentiated cSCCs.

3.4. Summary

- **Data resulted in the characterisation and validation of a novel recombinant antibody to p62, applicable for use in the development of a novel commercial AMBRA1/p62 prognostic test for cSCC**
- **Loss of AMBRA1 expression occurs in primary cSCC tumours regardless of differentiation status or disease outcome.**
- **Cytoplasmic and nuclear p62 expression increases in primary cSCC tumourigenesis regardless of differentiation status or disease outcome.**
- **Loss of cytoplasmic AMBRA1 expression in the tumour growth front and cytoplasmic p62 expression in the peritumoural epidermis identifies high risk cSCC tumour subsets at risk of disease recurrence/metastasis independently of differentiation status**
- **Loss of cytoplasmic AMBRA1 expression in the tumour growth front and cytoplasmic p62 expression in the peritumoural epidermis identifies high-risk poorly differentiated cSCC tumour subsets at risk of metastasis.**

Chapter 4. Mechanisms mediating AMBRA1 loss in cSCC tumourigenesis and progression: Investigating the potential for Cullin E3 Ligase-mediated degradation or TGF-β signalling-induced downregulation

Table of Contents

4.1. Introduction

Results from the previous chapter underpinned the clear association between the loss of AMBRA1 expression and cSCC tumourigenesis *in vivo*. Given the well-established paradoxical role of autophagy in cancer, and the association of a loss or blockade in activity leading to increased mutagenesis, (Mathew and White, 2011, Tang et al., 2016, Levine and Kroemer, 2008), the observed loss of AMBRA1 likely reflects the key tumour suppressor role of this protein in cSCC. As such, the principle aim of the present chapter was to define the mechanism(s) leading to loss of AMBRA1 in cSCC tumourigenesis and the potential to define novel targets for therapeutic intervention.

Key reported mechanisms leading to AMBRA1 loss in tumorigenesis and progression are Ubiquitin E3 ligase-mediated degradation, the mechanism behind loss of AMBRA1 expression in HPV^{+ve} Oropharyngeal Squamous Cell Carcinoma (OPSCC) (Antonioli et al., 2021) and TGF β signalling-mediated transcriptional down regulation, recently shown to mediate AMBRA1 loss in the melanoma epidermal microenvironment (Cosgarea et al., 2021).

Specifically, Antonioli *et al* identified a novel mechanism by which the E3 ligases Cullins 4A and 4B limit autophagic activity via the ubiquitination and proteasomal degradation of AMBRA1 (Antonioli et al., 2016, Antonioli et al., 2017). These observations of Ubiquitin E3 ligase-mediated degradation of AMBRA1 in OPSCC (Antonioli et al., 2021) couple with recent evidence indicating Cullin4A as a potential oncogene associated with a UV carcinogenic signature (Liu et al., 2009b, Sharma and Nag, 2014), question the possibility that overexpression of Cullin 4A in cSCC may be a potential mechanism underpinning loss of AMBRA1 expression. Furthermore, given the recent generation of novel clinical inhibitors of Cullin activity (Liu and Mallampalli, 2016), defining the potential contribution of Cullin E3 ligases to loss of AMBRA1 in cSCC may also define a novel therapeutic target.

Bioinformatic data identifying TGF-β response elements in the *AMBRA1* promoter (Lovat et al. unpublished data), the contribution of TGF-β2 secretion by high risk melanomas to the downregulation of AMBRA1 in the epidermal microenvironment (Cosgarea et al 2021 in press) and studies showing deregulated TGF-β signalling drives cSCC tumourigenesis, (Oshimori et al., 2015, Glick, 2012), suggests loss of AMBRA1 expression in cSCC may be mediated by TGF-

β induced transcriptional downregulation. TGF-β signalling however is reported as a 'double edged' sword in carcinogenesis (Akhurst and Derynck, 2001). While TGF-β1 exerts a tumour suppressive role as shown in recent reports of recessive dystrophic epidermolysis bullosa (RDEB) associated cSCC, TGF-β2 and TGF-β3 have been shown to be tumour promoting (Akhurst and Derynck, 2001, Pietenpol et al., 1990, Reed et al., 1994, Van Belle et al., 1996). Since increased TGF-β signalling has been linked with a metastatic phenotype in other cutaneous malignancies (Busse and Keilholz, 2011, Ke and Wang, 2021), the present study also aimed at defining the potential contribution of TGF-β2 and TGF-β3 to loss of AMBRA1 expression in cSCC and their potential as novel therapeutic targets.

To investigate the potential contribution of Cullin E3 ligase activity or TGF-β2/3 signalling to AMBRA1 degradation/downregulation in cSCC tumourigenesis, the specific objectives/aims of the current chapter were thus to:

- **Confirm loss of AMBRA1 in cSCC tumorigenesis *in vitro* in isogenic cell lines.**
- **Test the hypothesis that increased expression of Cullin 4A leads to increased ubiquitin-mediated degradation of AMBRA1 expression in cSCC tumourigenesis *in vitro.***
- **Test the hypothesis that TGF-β signalling mediates AMBRA1 downregulation in cSCC tumourigenesis in vitro**
- **Evaluate the potential for chemical TGF-β receptor inhibitors to prevent AMBRA1 down regulation and reduce cSCC cell viability *in vitro***

4.2. Results

4.2.1. cSCC tumourigenesis in vitro is associated with loss of AMBRA1 expression

To confirm observations of AMBRA1 loss in cSCC tumourigenesis *in vivo* are also linked to cSCC tumourigenesis *in vitro*, AMBRA1 expression was evaluated in two series of cSCC isogenic cell lines; PM1 (normal/dysplastic keratinocytes), MET1 (primary cSCC cells) and MET4 (metastatic cSCC cells) or IC1 (primary cSCC cells) and IC1-MET (metastatic cSCC cells). Since the IC1 and IC1-MET isogenic cSCC cell lines lacked a normal/dysplastic cell line, differentiated and undifferentiated CCD1106 cells were used for comparison. Western blot analysis revealed a loss of AMBRA1 expression with tumourigenesis in PM1, MET1 and MET 4 cells with expression in MET 1 and MET 4 cells significantly reduced compared to expression in PM1 ($P<0.01$, for MET 1 and $P<0.001$ for MET 4 cells, Figure 4.1B). Whilst a significant loss of AMBRA1 expression was also observed between differentiated CCD1106 cells and the IC1 and IC1-MET cell lines ($P<0.01$, Figure 4.1D), no significant difference in expression however, was detected between undifferentiated CCD1106 and IC1 and IC1-MET cells. Taken together, data suggest loss of AMBRA1 expression is associated with cSCC tumourigenesis, in the PM1, MET1 and MET4 isogenic cell lines but not the IC1 and IC1-MET cell lines. Moreover, loss of AMBRA1 expression in MET 1 and MET 4 cells closely reflects observations of loss of AMBRA1 expression in cSCC tumourigenesis shown in *vivo*.

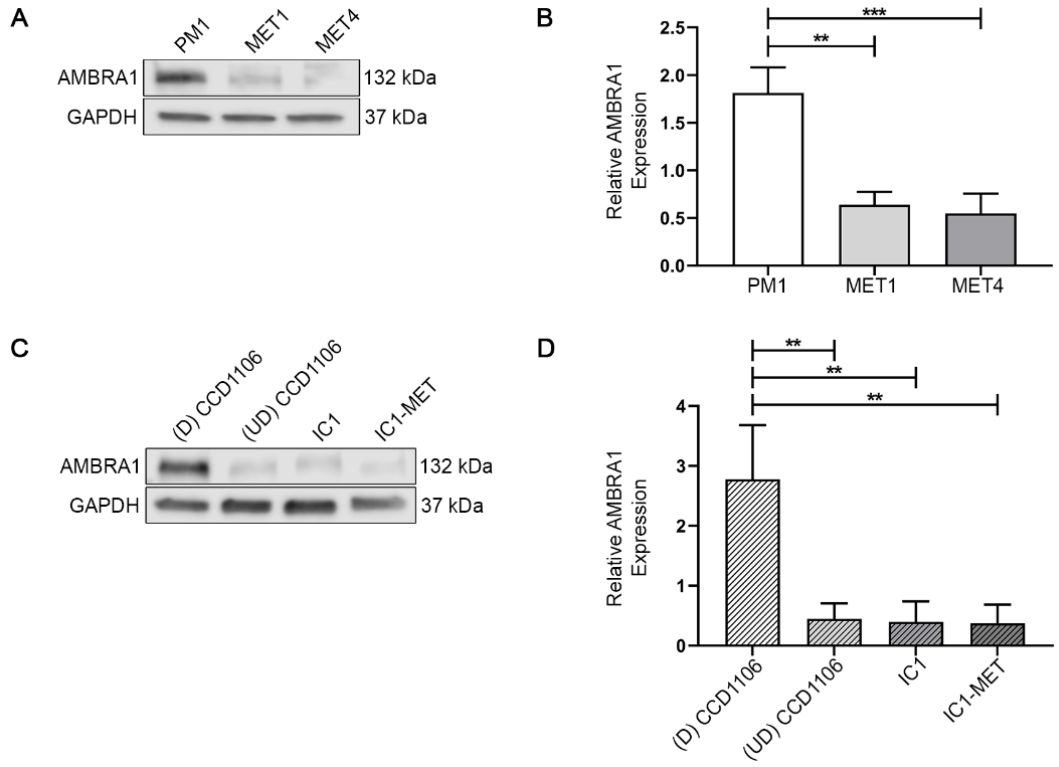

FIGURE 4. 1 AMBRA1 EXPRESSION IS LOST DURING CSCC PROGRESSION IN THE PM1, MET1 AND MET4 CELL LINES BUT NOT IN THE IC1 AND IC1-MET CELL LINES.

*(**A**) Representative western blot of AMBRA1 (132 kDa) and GAPDH (37 kDa, loading control) expression in the PM1, MET1 and MET4 cell lines. (**B**) Relative AMBRA1 expression in the PM1, MET1 and MET4 cell lines. Each bar represents three replicates of AMBRA1 band intensity, normalised against GAPDH band intensity for each cell line, and expressed relative to each individual experimental average (mean ± SD, N=3). Statistics acquired by one-way ANOVA with Tukey's post hoc correction (**P<0.01) (***P<0.001). (**C**) Representative western blot of AMBRA1 (132 kDa) and GAPDH (37 kDa, loading control) expression in differentiated (**D**) CCD1106, undifferentiated (UD) CCD1106, IC1 and IC1-MET cell lines. (**D**) Relative AMBRA1 expression in the differentiated (D) CCD1106, undifferentiated (UD) CCD1106, IC1 and IC1-MET cell lines. Each bar represents three replicates of AMBRA1 band intensity, normalised against GAPDH band intensity for each cell line, and expressed relative to each individual experimental average (mean ± SD, N=3). Statistics acquired by one-way ANOVA with Tukey's post hoc correction (**P<0.01).*

4.2.2 Cullin 4A overexpression is not associated with cSCC tumourigenesis in vitro

To evaluate the potential contribution of increased Cullin 4A expression to AMBRA1 degradation (Antonioli et al., 2016, Antonioli et al., 2021), Cullin 4A expression levels were evaluated and compared by Western blotting in PM1, MET1 and MET4 cells (Figure 4.2). Compared to GAPDH expression, results revealed however, no statistically significant change in Cullin 4A expression between these cell lines (Figure 4.2B), suggesting ubiquitin mediated degradation of AMBRA1 is unlikely responsible for the observed loss of AMBRA1 expression in cSCC tumourigenesis.

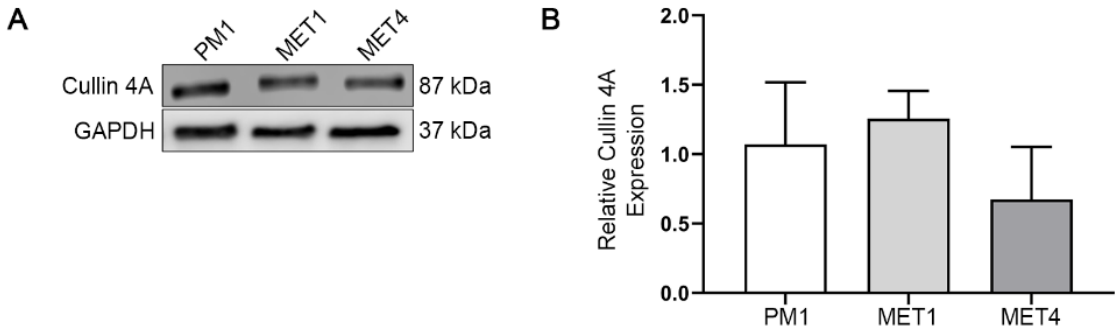

FIGURE 4. 2. CULLIN 4A EXPRESSION IS NOT SIGNIFICANTLY ALTERED DURING CSCC PROGRESSION IN VITRO.
*(**A**) Representative western blots of Cullin 4A (87 kDa) and GAPDH (37 kDa, loading control) expression in PM1, MET1 and MET4 cell lines. (**B**) Relative Cullin 4A expression in the PM1, MET1 and MET4 cell lines. Each bar represents three replicates of Cullin 4A band intensity, normalised against GAPDH band intensity for each cell line, and expressed relative to each individual experimental average (mean ± SD, N=3). Statistics acquired by one-way ANOVA with Tukey's post hoc correction.*

4.2.3. Increased TGFB2 secretion by the primary cSCC cell line, MET 1 results in canonical activation of the ALK5 receptor and is associated with loss of AMBRA1 expression.

To evaluate the potential contribution of pro oncogenic TGFβ signalling to loss of AMBRA1 expression in cSCC tumourigenesis in vitro, TGF-β2 and TGF-β3 expression levels were evaluated and compared by Western blotting in PM1, MET1 and MET4 cell lines as well as in IC1 and IC1-MET cell lines (Figure 4.3). Results revealed a significant increase in TGF-β2 expression between the PM1 and MET1 cell lines ($P<0.05$, Figure 4.3C) and between IC1-MET and IC1 cell lines ($P<0.05$, Figure 4.3D). No significant difference in TGF-β3 expression levels however, was detected between either PM1, MET1 and MET 4 or IC1 and IC1-MET cells (Figure 4.3E and F), suggesting TGF-β2 may contribute to the down regulation/loss of AMBRA1 observed during cSCC tumourigenesis *in vitro*.

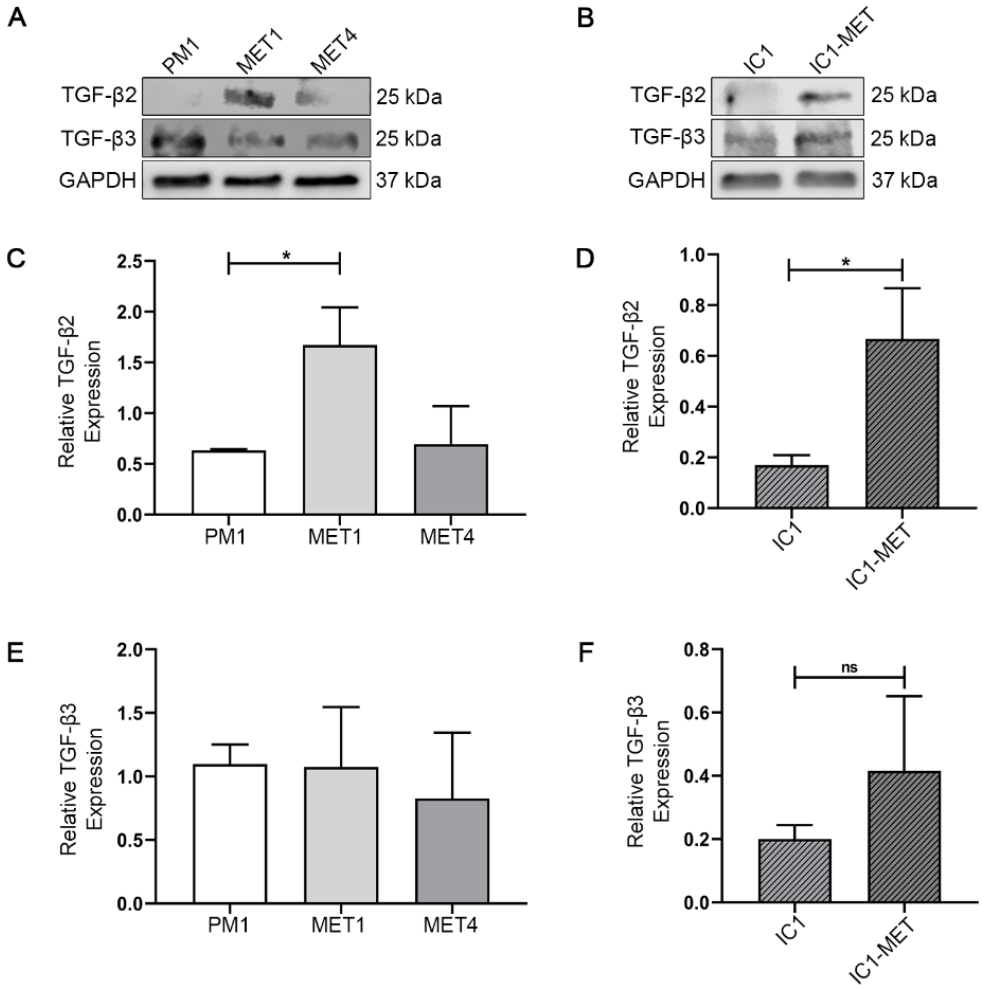

FIGURE 4. 3. INCREASED TGF-Β2 BUT NOT TGF-Β3 EXPRESSION IS ASSOCIATED WITH CSCC TUMOURIGENESIS IN VITRO.
*(**A**) Representative western blots of TGF-β2 (25 kDa), TGF-β3 (25 kDa) and GAPDH (37 kDa, loading control) expression in the PM1, MET1 and MET4 cell lines. (**B**) Representative western blots of TGF-β2 (25 kDa), TGF-β3 (25 kDa) and GAPDH (37 kDa, loading control) expression in the IC1 and IC1-MET cell lines. (**C**) Relative TGF-β2 expression in the PM1, MET1 and MET4 cell lines. Each bar represents three replicates of TGF-β2 band intensity, normalised against GAPDH band intensity for each cell line, and expressed relative to each individual experimental average (mean ± SD, N=3). Statistics acquired by one-way ANOVA with Tukey's post hoc correction (*P<0.05). (**D**) Relative TGF-β2 expression in the IC1 and IC1-MET cell lines. Each bar represents three replicates of TGF-β2 band intensity, normalised against GAPDH band intensity for each cell line, and expressed relative to each individual experimental average (mean ± SD, N=3). Statistics acquired by unpaired t-test (*P<0.05). (**E**) Relative TGF-β3 expression in the PM1, MET1 and MET4 cell lines. Each bar represents three replicates of TGF-β3 band intensity, normalised against GAPDH band intensity for each cell line, and expressed relative to each individual experimental average (mean ± SD, N=3). Statistics acquired by one-way ANOVA with Tukey's post hoc correction. (**F**) Relative TGF-β3 expression in the IC1 and IC1-MET cell lines. Each bar represents three replicates of TGF-β3 band intensity, normalised against GAPDH band intensity for each cell line, and expressed relative to each individual experimental average (mean ± SD, N=3). Statistics acquired by unpaired t-test.*

To confirm the observed increase in TGF-β2 expression in both MET1 and IC1-MET cell lines was reflective of an increase in TGF-β2 secretion, TGF-β2 as well as 3 secretion by PM1, MET1, MET4, IC1 and IC1-MET cells were assessed using commercially available ELISA assays (Figure 4.4). Results revealed significantly increased TGF-β2 secretion by MET1 cells compared to PM1 ($P<0.001$, Figure 4.4A) and MET4 cell lines ($P<0.01$, Figure 4.4A). IC1-MET1 cells also secreted significantly increased levels of The TGF-β2 compared to IC1 cells ($P<0.05$, Figure 4.4B). However, the only significant increase in TGF-β3 secretion observed was in MET4 cells as compared to secretion by PM1 cells ($P<0.05$, Figure 4.4C), which was surprising given TGF-β3 expression levels did not differ in these cells (Figure 4.3E). Collectively these data confirmed TGF-β2 expression levels observed in cSCC cell lines correlated with observed changes in secretory levels. This increase in TGF-β2 expression/secretion by MET1 cells also correlated with the observed decline in AMBRA1 expression.

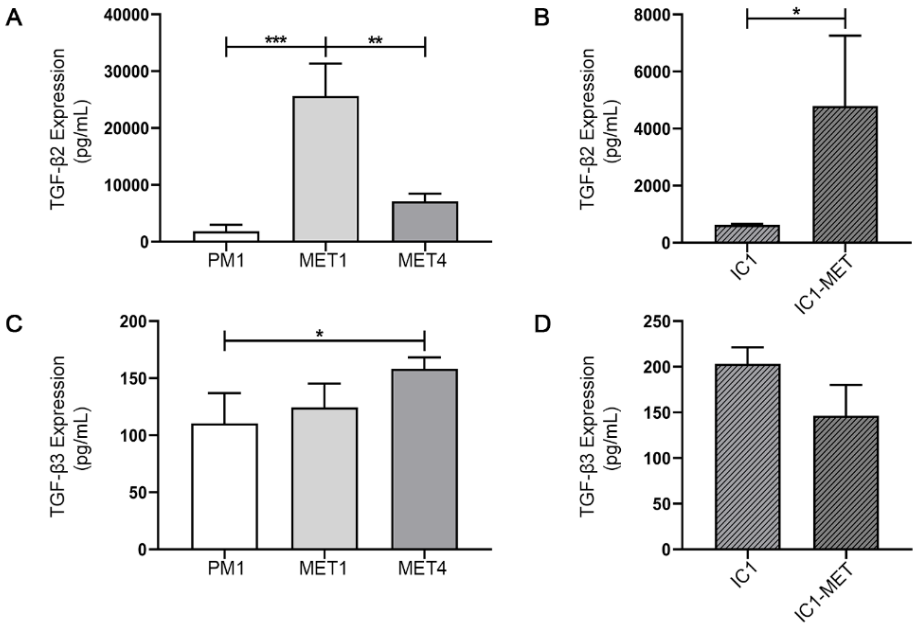

FIGURE 4. 4. TGF-B2 BUT NOT TGF-B3 EXPRESSION IS SECRETED BY THE MET1 AND IC1-MET CELL LINES.
*(**A**) TGF-β2 secretion (pg/mL) by PM1, MET1 and MET4 cells. Each bar is the mean ± SD of three independent experiments. Statistics acquired by one-way ANOVA with Tukey's post hoc correction (N=3) (*P<0.05) (****P<0.0001). (**B**) TGF-β2 secretion (pg/mL) by IC1 and IC1-MET cells. Bar is the mean ± SD of three independent experiments. Statistics acquired by unpaired t-test (N=3) (*P<0.05). (**C**) TGF-β3 secretion (pg/mL) by PM1, MET1 and MET4 cells. Bar is the mean ± SD of three independent experiments. Statistics acquired by one-way ANOVA with Tukey's post hoc correction (N=3) (P<0.05). (**D**) TGF-β3 secretion (pg/mL) in IC1 and IC1-MET cells. Bar is the mean ± SD of three independent experiments. Statistics acquired by unpaired t-test (N=3).*

Since previous studies have identified SMAD3 and SMAD5 response elements in the AMBRA1 promoter (Lovat et al unpublished data), the observed increase in TGF-β2 expression in MET 1 cells likely results in the activation of the TGF-β receptors ALK1 and ALK5 , and the downstream transduction of TGF-β signalling (Heldin et al., 1997). To investigate if ALK1 and/or ALK5 were activated by TGF-β2 secretion, total and phosphorylated levels of SMAD1, SMAD2, SMAD3, SMAD5 expression were evaluated in PM1, MET1 and MET 4 cells by Western blotting (Figure 4.5). Results revealed a significant increase in activated SMAD2 and SMAD3 expression in MET1 compared to PM1 ($P<0.05$, Figure 4.5C and $P<0.01$ respectively, Figure 4.5D) and MET4 cell lines ($P<0.05$, Figure 4.C and D). These data therefore suggest that TGF-β2 secretion by MET 1 cells results in canonical ALK5 receptor activation. Additionally, whilst no significant increase in SMAD1 activation was observed, a significant increase in SMAD5 activation was detected between the MET1 and PM1 ($P<0.01$, Figure 4.5E) and MET4 cells ($P<0.01$, Figure 4.5E). Given that SMAD5, but not SMAD1, was activated in the MET1 cell line, this suggests that ALK5 and not ALK1 is activated by TGF-β2 secretion, resulting in the activation of both canonical and non-canonical signalling.

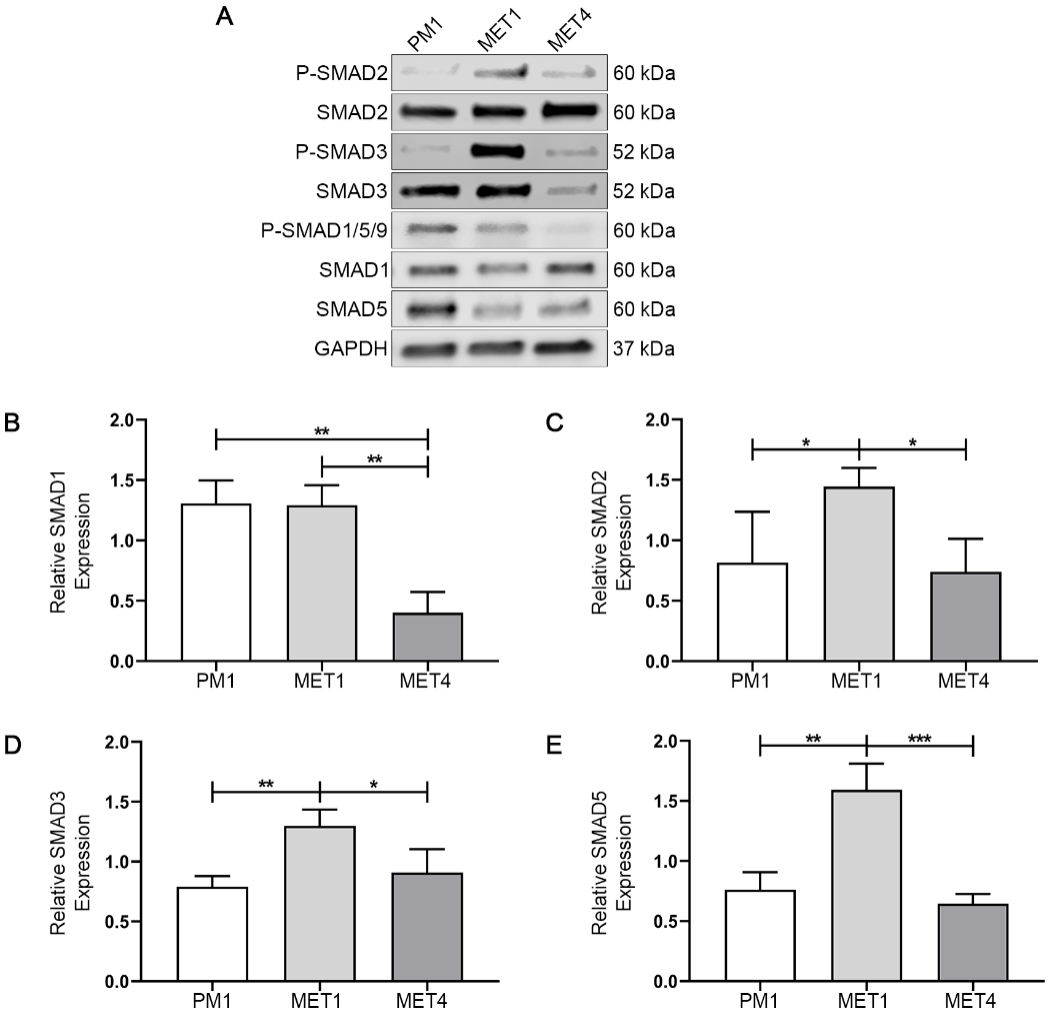

FIGURE 4. 5. SMAD2, SMAD3 AND SMAD5 ACTIVATION IS INCREASED IN MET 1 CSCC CELLS.
*(**A**) Representative western blot of P-Smad2 (60 kDa), Smad2 (60 kDa), P-Smad3 (52 kDa), Smad3 (52 kDa), P-SMAD1/5/9 (60 kDa), SMAD1 (60 kDa), SMAD5 (60 kDa) and GAPDH (37 kDa, loading control) expression in PM1, MET1 and MET4 cells. (Aii) P-Smad1/5/9 (60 kDa), Smad1 (60 kDa), Smad5 (60 kDa) and GAPDH (37 kDa, loading control) in the PM1, MET1 and MET4 cell lines. (**B**) Relative P-SMAD1 expression of PM1, MET1 and MET4 cells. Each bar represents three replicates of P-SMAD1/5/9 band intensity, normalised against SMAD1 band intensity for each cell line, and expressed relative to each individual experimental average (mean ± SD, N=3). Statistics acquired by one-way ANOVA with Tukey's post hoc correction (N=3) (**P<0.01). (**C**) Relative P-SMAD2 expression of the PM1, MET1 and MET4 cell lines. Each bar represents three replicates of P-SMAD2 band intensity, normalised against SMAD2 band intensity for each cell line, and expressed relative to each individual experimental average (mean ± SD, N=3). Statistics acquired by one-way ANOVA with Tukey's post hoc correction (N=3) (*P<0.05). (**D**) Relative P-SMAD3 expression of the PM1, MET1 and MET4 cell lines. Each bar represents three replicates of P-SMAD3 band intensity, normalised against SMAD2 band intensity for each cell line, and expressed relative to each individual experimental average (mean ± SD, N=3). Statistics acquired by one-way ANOVA with Tukey's post hoc correction (N=3) (*P<0.05) (**p<0.01). (**E**) Relative P-SMAD5 expression of PM1, MET1 and MET4 cells. Each bar represents three replicates of P-SMAD1/5/9 band intensity, normalised against SMAD5 band intensity for each cell line, and expressed relative to each individual experimental average (mean ± SD, N=3). Statistics acquired by one-way ANOVA with Tukey's post hoc correction (N=3) (**P<0.01) (***P<0.001).*

This observed activation of SMAD5 in response to increased TGF-β2 secretion by MET1 cells was difficult to distinguish since the antibody used to detect activation was a pan antibody to P-SMAD1/5/9. To test if activation of ALK5 caused the non-canonical activation of SMAD5, MET1 cells were cultured in the presence of the ALK5 chemical inhibitor ALX-270-445 prior to western blotting for P-SMAD1/5/9, SMAD5 and GAPDH (loading control) expression (Figure 4.6). Results however, revealed the chemical inhibition of ALK5 had no significant effect on the reduction of SMAD5 activation in MET1 cells (Figure 4.6B), suggesting the previously observed increase in activated SMAD5 was most likely an artefact and TGF-β2 secretion by MET1 cells leads to the canonical activation of the ALK5 receptor.

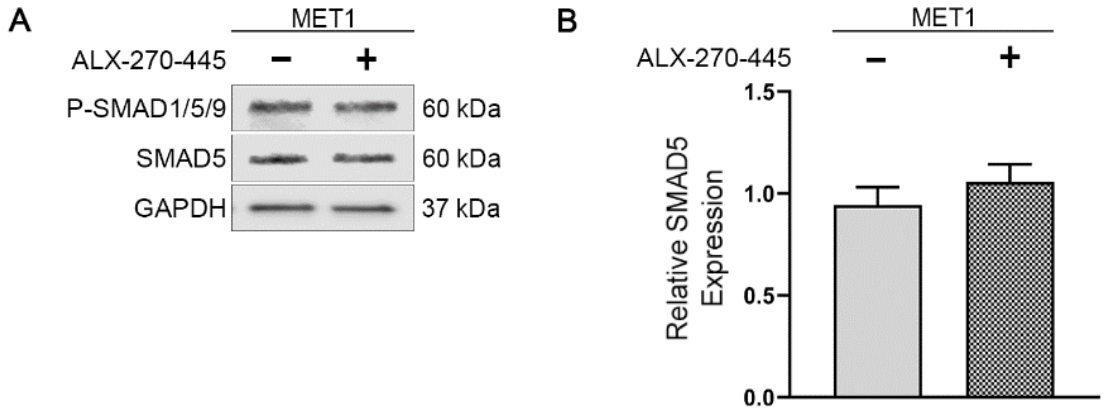

FIGURE 4. 6. INHIBITION OF ALK5 ACTIVATION DOES NOT REDUCE SMAD5 ACTIVATION IN THE MET1 CELL LINE.
*(**A**) Representative western blot P-SMAD1/5/9 (60 kDa), SMAD5 (60 kDa) and GAPDH (37 kDa, loading control) expression in the PM1, MET1 and MET4 cell line following 2-hour treatment with ALX-270-445 (50 nM) prior to lysis. (**B**) Relative P-SMAD5 expression in the MET1 cell line following 2-hour treatment with ALX-270-445 (50 nM) prior to lysis. Each bar represents three replicates of P-SMAD1/5/9 band intensity, normalised against SMAD5 band intensity for each cell line, and expressed relative to each individual experimental average (mean ± SD, N=3). Statistics acquired an unpaired t-test.*

4.2.4. Chemical inhibition of the ALK 5 receptor fails to rescue AMBRA1 loss but reduces cell viability of MET 1 cells.

Next to test if TGF-β2 secretion by MET 1 cells drives the downregulation of AMBRA1 expression, MET1 or PM1 cells for comparison, were cultured in the presence of the ALK5 chemical inhibitor ALX-270-445 for either 2 or 72 hours prior to western blotting for AMBRA1, P-SMAD2, SMAD2, P-SMAD3, SMAD3 and GAPDH (loading control) expression (Figure 4.7). Results revealed ALX-270-445 prevented ALK5 activation in MET1 cells with a concurrent significant decrease at either time point in expression levels of pSMAD2 ($P<0.01$, Figure 4.7C) and pSMAD3 ($P<0.05$-$P<-0.01$, Figure 4.7D), an effect not observed in PM1 cells (Figure 4.7C and D). However, the inhibition of ALK5 had no significant effect on AMBRA1 expression by MET1 cells (Figure 4.7B) ,collectively suggesting increased TGF-β2 in this cell line unlikely drives the loss of AMBRA1 expression.

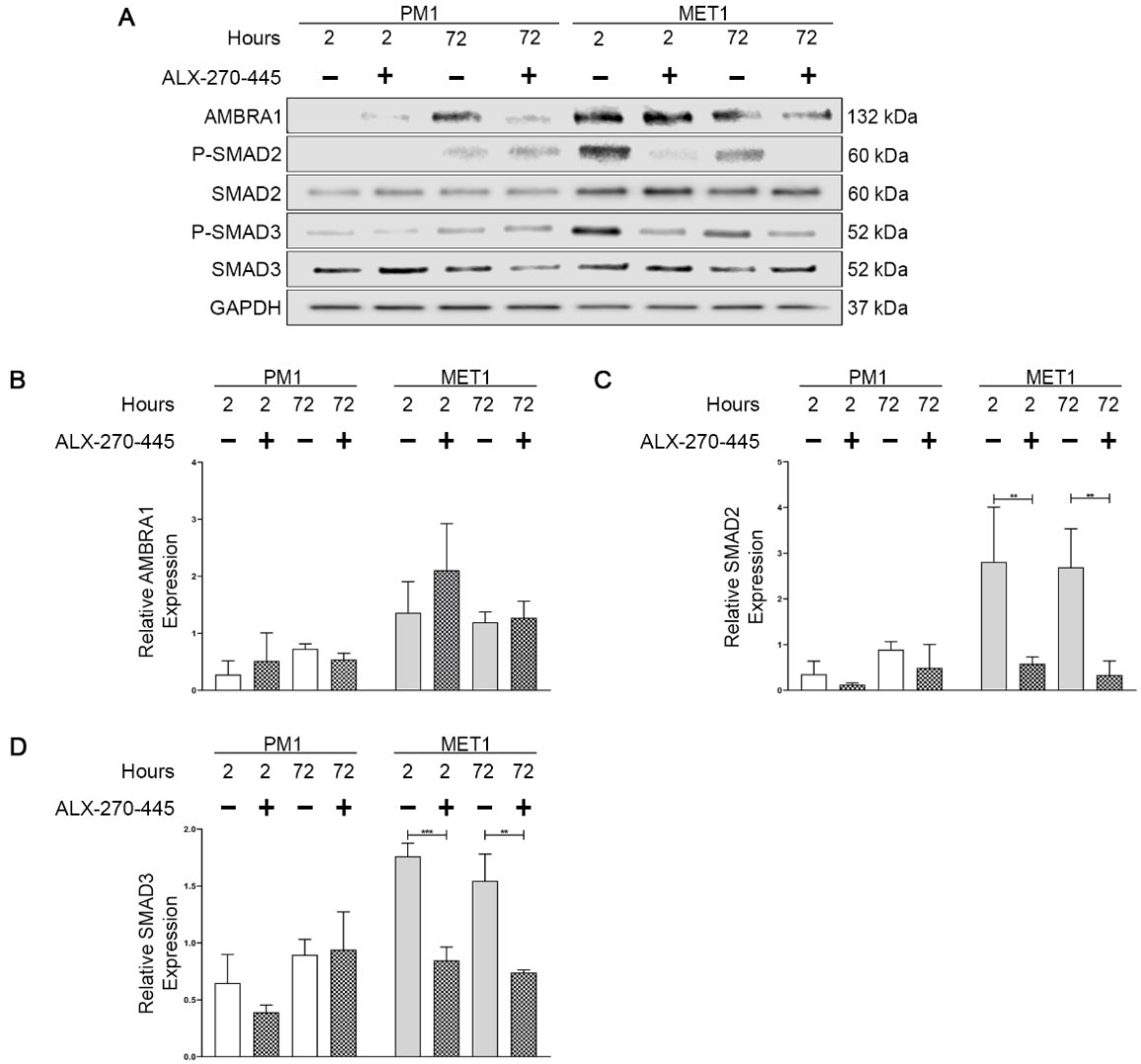

FIGURE 4. 7. ALK5 INHIBITION REDUCES SMAD2 AND SMAD3 ACTIVATION BUT DOES NOT RESCUE AMBRA1 LOSS IN MET1 CELLS.

*(**A**) Representative western blot of AMBRA1 (132 kDa), P-SMAD2 (60 kDa), SMAD2 (60 kDa), P-SMAD3 (52 kDa), SMADd3 (52 kDa) and GAPDH (37 kDa) expression in the PM1 and MET1 cell lines cultured in the presence or absence of ALX-270-445 (50 nM) for either 2-hours or 72-hours. (**B**) Relative AMBRA1 expression in the PM1 and MET1 cell lines cultured in the presence or absence of ALX-270-445 (50 nM) for either 2-hours or 72-hours. Each bar represents three replicates of AMBRA1 band intensity, normalised against GAPDH band intensity for each cell line, and expressed relative to each individual experimental average (mean ± SD, N=3). Statistics acquired by one-way ANOVA with Tukey's post hoc correction. (**C**) Relative P-SMAD2 expression in the PM1 and MET1 cell lines cultured in the presence or absence of ALX-270-445 (50 nM) for either 2-hours or 72-hours. Each bar represents three replicates of P-SMAD2 band intensity, normalised against SMAD2 band intensity for each cell line, and expressed relative to each individual experimental average (mean ± SD, N=3). Statistics acquired by one-way ANOVA with Tukey's post hoc correction (**P<0.01). (**D**) Relative P-SMAD3 expression in the PM1 and MET1 cell lines cultured in the presence or absence of ALX-270-445 (50 nM) for either 2-hours or 72-hours. Each bar represents three replicates of P-SMAD3 band intensity, normalised against SMAD3 band intensity for each cell line, and expressed relative to each individual experimental average (mean ± SD, N=3). Statistics acquired by one-way ANOVA with Tukey's post hoc correction (**P<0.01) (***P<0.001).*

Finally to evaluate if the observed increase in TGF-β2 secretion/expression by MET 1 cells contributes to their sustained /increased viability, cells were cultured in the presence or absence of ALX-270-445 for 24 hours prior to assessment of the effects on cell viability. Results revealed a small but significant decrease in MET 1 cell viability by ALK5 inhibition ($P<0.01$, Figure 4.8) suggesting that while TGF-β2 secretion supports MET1 cell viability, it more likely contributes to cellular mechanisms facilitating cSCC metastasis.

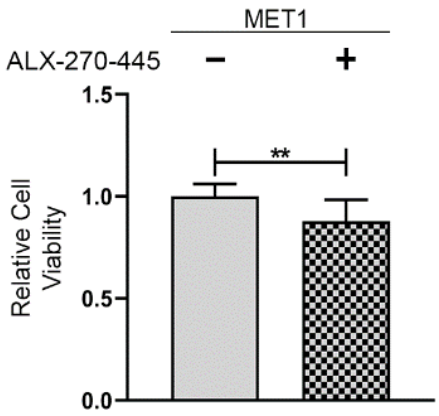

FIGURE 4. 8. ALK5 INHIBITION INHIBITS MET1 CELL VIABILITY.
*Relative cell viability of MET1 cells cultured in the presence or absence of ALX-270-445 (50 nM) for 24-hours. Each bar represents the mean ± SD of three independent experiments. Statistics acquired by an unpaired t-test (**P<0.01).*

4.3. Discussion

4.3.1. cSCC tumourigenesis in vitro is associated with loss of AMBRA1 expression

As shown in chapter 3, loss of AMBRA1 expression in the tumour mass of cSCCs is a consistent event in cSCC tumourigenesis. This effect was mirrored by studies of tumourigenesis in cSCC *in vitro* using the isogenic cell lines PM1, MET 1 and MET 4. Specifically results confirmed a decline in AMBRA1 expression in MET1 and MET4 cells compared to PM1 cells (Figure 4.1). Interestingly however, this decline in AMBRA1 expression was not observed in IC1 or IC1-MET cells compared to undifferentiated CCD1106 cells (Figure 4.1D). This was unexpected, and may have been confounded by the lack of an isogenic normal/dysplastic isogenic control cell line to allow for a more accurate comparison of AMBRA1 expression in IC1 or IC1- MET cells. Alternatively, the inconsistency in AMBRA1 loss between these two isogenic cell lines may reflect their origin from different stem cell initiators. Studies aimed at identifying the cell of origin for cSCC carcinogenesis have shown cSCC initiation may arise from multiple different resident stem cell pools in different anatomical locations of the skin (Page et al., 2013, Horsley et al., 2006, Jaks et al., 2008, Sánchez-Danés and Blanpain, 2018). Additionally, lineage tracing studies have demonstrated that stem cell pools in both the interfollicular epidermis and hair follicle may contribute to cSCC formation, thus suggesting the possibility that PM1-MET4 and IC1-IC1-MET arose from distinct and separate stem cell populations. Given mounting evidence for the role of AMBRA1 in keratinocyte differentiation (Cosgarea et al., 2021, Tang et al., 2016, Ellis et al., 2020), and a lack of evidence for its role in hair follicle differentiation (Rogers, 2004), this could suggest that the IC1-IC1-MET cell line may have originated from a hair follicle stem cell rather than an inter follicular epidermal stem cell.

Another possible explanation is that the difference in AMBRA1 expression between these cSCC isogenic cell lines is due to the fact they were isolated at different stages of differentiation. Rodríguez-Paredes et al. has shown that cSCC tumours can be stratified based on DNA keratin methylation profiles, that either resemble that of a keratinocyte or of a stem cell (Rodríguez-Paredes et al., 2018, Moran et al., 2016). If this is the case, the PM1-MET4 cell line series may have originated from a cell group with a more keratinocyte origin, having progressed through some initial differentiation processes, meaning the loss of AMBRA1 expression is more detectable. The production of these cell lines don't specify at what stratum the origin of these cells were isolated from and thus this remains a possibility (Proby et al., 2000, Watt et al., 2011).

Whilst fundamental differences in cell origin may provide an answer to the difference between the *in vivo* and *in vitro* observations of AMBRA1 expression, as stated above, the lack of an isogenic normal keratinocyte cell line for the IC1 and IC1-MET cell lines makes this difficult to access. Given CCD1106 keratinocytes display high differentiation capability, unlike PM1 cells (later discussed in chapter 5), undifferentiated CCD1106 cells may be a poor substitute. Collectively, this suggests AMBRA1 expression may have been lost during the tumourigenesis of IC1 cells but was undetectable given experimental limitations.

Taken together however, these data demonstrate that the PM1, MET1 and MET4 cSCC isogenic cell line series most closely aligns with the loss of AMBRA1 expression observed *in vivo* and thus, all future investigations into the underlying mechanism(s) mediating a reduction in expression were conducted with these cell lines.

4.3.2. Increased TGF-β2 expression and secretion, and not over expression of Cullin 4A, correlated with loss of AMBRA1 expression in the MET1 primary cSCC cell line

The ubiquitin E3 ligase Cullin 4A has been shown to act with the substrate adapter DDB1 to degrade AMBRA1 expression during extended periods of active autophagy and has also been implicated as an oncogene in liver, lung and bile duct cancers (Hung et al., 2016, Zhang et al., 2017b, Chen et al., 2018, Antonioli et al., 2014). However, results revealed no observable difference in Cullin 4A expression between PM1, MET1 and MET4 cells (Figure 4.2), suggesting an increase in Cullin 4A expression is not responsible for degrading AMBRA1 expression during cSCC tumourigenesis.

Noteworthy however, recent work has suggested that Cullin 4A is not a central regulator of AMBRA1 expression, with RNF being a more likely candidate (Cianfanelli et al., 2015d). RNF, like Cullin 4A, is an ubiquitin E3 ligase that has been shown to interact with WASP to mediate AMBRA1 degradation. Given this, future studies should also examine the role of RNF in cSCC tumourigenesis. Additionally, the expression level of Cullin 4A alone may not have been sufficient to access its potential contribution to the loss of AMBRA1 expression. Given the modularity of Cullin-RING complexes, their complex regulation by the CAND1/NEDD8 cycle and the requirement for substrate adaptors to interact with their target proteins, alterations to any of these components could have influenced the rate of AMBRA1 degradation without altering Cullin 4A expression directly (Petroski and Deshaies, 2005, Wu et al., 2000, Ohh et al.,

2002, Yu et al., 1998, Nikolaev et al., 2003). Additionally, and specifically in relation to AMBRA1, the mechanism connecting DDB1 to target substrates and to Cullin 4A is poorly understood and thus, separate regulation of DDB1 may also have influenced AMBRA1 degradation (Wertz et al., 2004, Shiyanov et al., 1999). As such, future work should also investigate potential alterations to these regulatory mechanisms of Cullin 4A activity and the subsequent effect on AMBRA1 expression.

Bioinformatic studies have also identified SMAD3 and SMAD5 responsive elements in the AMBRA1 promoter (Lovat et al. unpublished data), suggesting TGF-β signalling may impact on AMBRA1 expression. Coupled with observations of loss of AMBRA1 expression in the melanoma epidermal microenvironment, mediated by tumoural secretion of TGF-β2, these findings prompted analysis of TGF-β2 and TGF-β3 expression in cSCC isogenic cell lines. Results revealed increased expression of TGF-β2, but not TGF-β3, in both MET1 and IC1-MET cells (Figure 4.3). These observations were corroborated by studies of TGF-β secretion, which demonstrated significantly increased TGF-β2 secretion by both MET1 and IC1-MET cells (Figure 4.4). Collectively these data suggest that primary cSCC MET1 cells undergo autocrine/paracrine TGF-β2 signalling, which in turn mediates downregulation of AMBRA1 expression. Additionally, the fact that AMBRA1 loss and increased TGF-β signalling is only seen in MET1, and not in the IC1 cells, provides further evidence that these two cellular events may be interlinked.

The role of TGF-β signalling in cancer has been well studied but an exact understanding of its function is still poorly understood, with conflicting reports of certain signalling pathways being either tumour suppressive or promoting (Syed, 2016). The general consensus for epithelial malignancies however, is that whilst TGF-β signalling represses growth and promotes cellular differentiation of premalignant cells, it exerts a tumour promoting role upon the accumulation of more pro-oncogenic mutations. In terms of its tumour promoting action, TGF-β signalling has specifically been shown to facilitate epithelial-to-mesenchymal transition (EMT), angiogenesis, preventing cellular differentiation and immune suppression within the tumour microenvironment of certain cancers (Principe et al., 2014, Moustakas and Heldin, 2016, Komuro et al., 2009, Sakaki-Yumoto et al., 2013, Batlle and Massague, 2019). TGF-β signalling has also been studied specifically within the context of epithelial carcinogenesis. To date, considerable evidence has demonstrated the involvement of TGF-β signalling in promoting

cSCC to undergo EMT and invade into deeper tissue compartments, however studies disagree with whether the loss (Rose et al., 2018, Cammareri et al., 2016) or gain (Ju et al., 2019, Siljamäki et al., 2020) of activation causes this phenomenon. Additionally, work by Rose et al. has demonstrated that broad loss of TGF-β signalling drives cSCC formation from epidermal stem cells (Cammareri et al., 2016, Rose et al., 2017). However, these same studies did identify a smaller subset of cSCC tumours that had increased activation of TGF-β signalling and that is was associated with a poor prognostic outcome. This suggests that even within cSCC, TGF-β signalling is context specific and the mutation profile of any given tumour will influence if the TGF-β signalling is tumour promoting or suppressive.

These studies, combined with our results, suggest that TGF-β2 signalling is activated in the MET1 cell line and that it may have a tumour promoting effect, which may include the suppression of AMBRA1 expression, to prevent cellular differentiation and allow continued proliferation.

4.3.3. Activation of TGF-β2 secretion in MET1 cells activates canonical signalling of the ALK5 receptor

The present study has demonstrated increased expression and secretion of TGF-β2 by MET1 cells. Generally, TGF-β ligands interact with a dual receptor complex that is composed of a TGF-β type II receptor (TGFβRII) and a TGF-β type I receptor (TGFβRI), with multiple receptors belonging to each receptor family (Shi and Massagué, 2003, Tzavlaki and Moustakas, 2020). Numerous TGFβRI have been identified, with ALK5 being shown to have the broadest expressed across multiple cell types and activated by TGF-β2 ligand binding (Heldin and Moustakas, 2016). Another identified TGFβRI is ALK1, which is predominantly expressed by endothelial cells but is still activated by interaction with TGF-β2 (Goumans et al., 2003). Following ligand binding and allosteric conformational change, these receptor complexes lead to the phosphorylation and activation of specific substrates. ALK5 activation leads to phosphorylation of both SMAD2 and SMAD3 (Vander Ark et al., 2018), while activation of ALK1 leads to SMAD1, SMAD5 and SMAD8 activation (Roman and Hinck, 2017). As both receptors have the potential to respond to TGF-β2, the level of activation of SMAD1, SMAD2, SMAD3 and SMAD5 was assessed in the PM1, MET1 and MET4 isogenic cell line series (Figure 4.5). Results revealed that MET1 cells demonstrated a significant increase in the activation of both

SMAD2 and SMAD3, suggesting that increased TGF-β2 secretion by MET1 cells leads to canonical activation of ALK5 (Figure 4.5C and 4.5D). This observation is consistent with published data demonstrating increased SMAD2 and SMAD3 activation is involved in multiple cancers, including pancreatic, breast and ovarian cancer (An et al., 2021, Zhou et al., 2018, Wang et al., 2020a)

Results also revealed that only SMAD5, but not SMAD1, was also significantly activated in the MET1 cell line. As not all downstream elements were observed to be phosphorylated, this suggests that ALK1 is not directly activated by increased TGF-β2 secretion (van den Bosch et al., 2014). This concurs with recent published data showing primary keratinocytes (differentiated or undifferentiated) do not express the ALK1 receptor (Cosgarea et al., 2021). However, given the observed activation of SMAD5, this suggests that another route of phosphorylation may have been evoked. Previous studies have demonstrated that SMAD5 can be activated through the non-canonical activation of the ALK5 receptor. Liu et al has demonstrated that in breast cancer cells, the non-canonical activation of SMAD5 by ALK5, via its L45 loop motif, is linked with a switch of TGF-β2 response to a tumour promoting role, including the promotion of tumour cell migration, invasion and metastasis (Liu et al., 2009a). Given this switch in response is also critical in epithelial cancer progression, it is possible that this is a mechanism in cSCC tumourigenesis (Lamouille et al., 2014). Taken together, non-canonical activation of ALK5 is the most likely explanation for the observed phosphorylation of SMAD5.

Nevertheless, given the experimental limitation of using a combined P-SMAD1/5/9 and not a specific pSMAD5 antibody, it is possible that the observed statistical increase in SMAD5 phosphorylation may not reflect specific SMAD5 activation. To test this, the ALK5 inhibitor ALX-270-445 was used to prevent ALK5 activation as a selective ATP-competitive inhibitor (Gellibert et al., 2004). Results however, revealed no reduction in SMAD5 activation (Figure 4.6), suggesting TGF-β2 signalling only results in canonical activation of the ALK5 receptor.

4.3.4. ALK5 inhibition reduces cSCC cell viability in vitro but does not prevent loss of AMBRA1 expression

Studies to evaluate the potential for ALX-270-445 to prevent loss of AMBRA1 expression by MET 1 cells revealed inhibition of the ALK5 receptor did not prevent loss of AMBRA1 expression (Figure 4.7). These data suggest that whilst increased TGF-β2 expression, secretion and canonical ALK5 activation in MET1 cells correlated with AMBRA1 loss, this signalling event is not responsible for the down regulation of AMBRA1 expression. The link between AMBRA1 expression and TGF-β signalling is poorly understood but recent work has attempted to elucidate this relationship. Interestingly, AMBRA1 has shown to have a transcriptional regulatory role, being able to enter the nucleus through interacting with nuclear pore complexes. Once inside, AMBRA1 associates with scaffold, regulatory and chromatin remodelling proteins and together they act to induce the transcription of a variety of tumour promoting proteins, including TGF-β2 (Schoenherr et al., 2020). Additional studies have shown that AMBRA1, through an interaction with Cullin 4, is able to induce the polyubiquitination of SMAD4, increasing its transcriptional activity and leading to the induction and fine tuning of TGF-β signalling and the promotion of metastasis (Liu et al., 2021). These results disagree with the current study, which demonstrates that AMBRA1 loss is associated with an increase in TGF-β signalling. This highlights the current lack of understanding of the role of TGF-β in cancer more generally and the interplay between AMBRA1 and TGF-β2 in cSCC carcinogenesis specifically.

To further investigate a potential role of TGF-β2 signalling in cSCC progression, the effect of ALX-270-445 on the inhibition of MET1 cell viability was assessed (Figure 4.8). Results revealed a small but significant decrease in cell viability, suggesting that TGF-β2 signalling more likely contributes to its more classical tumour promoting roles, such as mediating EMT or surviving anoikis (Ahmadi et al., 2019, Fung et al., 2008).

Overall, these data demonstrate that whilst loss of AMBRA1 expression observed in MET1 cells is associated with an increase in TGF-β2 induced canonical signalling of the ALK5 receptor, these are two independent cellular events. The mechanisms underpinning AMBRA1 loss in cSCC tumorigenesis thus require further investigation.

Given the high mutational burden that occurs during cSCC development, including mutations in *p53, CDKN2A, NOTCH* and *RAS* (Corchado-Cobos et al., 2020, Ratushny et al., 2012, Ziegler

et al., 1994, South et al., 2014, Brown et al., 2004, Pierceall et al., 1991), and recent preliminary studies demonstrating missense genetic mutations in *AMBRA1* are associated with a poor outcome (Pickering et al., 2014), further studies of the potential contribution of *AMBRA1* mutations to cSCC development and any association with protein expression are also warranted.

4.4. Summary

- **The isogenic cell line series PM1, MET1 and MET4 most closely model loss of AMBRA1 expression observed during cSCC tumourigenesis *in vivo*.**
- **Increased TGF-β2 expression and secretion, and not an increase in Cullin 4A expression, is correlated with loss of AMBRA1 expression in the primary tumour cSCC cell line MET1.**
- **Increased TGF-β2 expression and secretion leads to the canonical activation of the ALK5 receptor in the MET1 cell line.**
- **The TGF-β2 induced canonical activation of ALK5 is not responsible for the observed loss of AMBRA1 expression in the MET1 cell line and the underlying mechanism remains undefined.**

Chapter 5. Defining the relationship between AMBRA1, autophagy and keratinocyte differentiation in cSCC

Table of Contents

5.1. Introduction

As discussed in Chapter 1, loss of AMBRA1 expression by primary cSCCs is clearly associated with tumourigenesis and disease progression. As a key autophagy regulatory protein, the loss of AMBRA1 in cSCC supports the paradoxical role of autophagy in cancer whereby autophagy blockade or deregulation leads to genotoxicity thereby promoting tumourigenesis (Russo and Russo, 2018). Studies have also shown the importance of AMBRA1 in keratinocyte differentiation, where expression in the epidermis increases from the basal layer to the stratum corneum and where by its knock down in leads to deregulated keratinocyte differentiation, in particular the loss of the terminal differentiation marker Loricrin, enhanced cytokeratin 14 expression (a marker of epidermal stem-like state, (Alam et al., 2011)) and uncontrolled proliferation (Ellis et al 2020).

One of the key signalling drivers responsible for keratinocyte differentiation is the presence of calcium. The presence of calcium causes the activation of the GPCR calcium sensing receptor (CaSR) and the ultimate activation of PKC, which in turn is responsible for activating a variety of gene responses that ultimately lead to terminal differentiation (Tu and Bikle, 2013). Calcium signalling however, also cooperates with another environmental pressure, increasing low nutrient stress, to induce the activation of autophagy (Mahanty et al., 2019). Differentiating keratinocytes employ autophagy to ensure complete removal of all cell organelles, to allow for morphological cell flattening, which is required for terminal differentiation (Akinduro et al., 2016). Calcium signalling is therefore key to both processes and any deregulation may lead to deregulated cell proliferation and differentiation.

It is therefore highly likely AMBRA1 functions as a gate-keeper of epidermal tumourigenesis through its intimate relationship with keratinocyte differentiation autophagy. Moreover, this potential dual role of AMBRA1 likely contributes to cSCC carcinogenesis whereby loss of expression or function may impact on both the process of autophagy and differentiation at once, i.e., causing both the potential blockade of autophagy resulting in tumourigenesis but also impairing keratinocyte differentiation and thereby promoting proliferation

To further define the relationship between AMBRA1, autophagy and differentiation in cSCC, the aim of the present chapter was to:

- ***Confirm the effect of calcium-induced differentiation and/or starvation-induced autophagy in keratinocytes using the keratinocyte cell line CCD1106 as a model on AMBRA1 expression, and the expression of markers of cellular differentiation and autophagy***
- ***Determine the impact of calcium-induced differentiation and nutrient deprivation-induced autophagy in cSCC and the impact of the deregulation of these processes on AMBRA1 expression and function using a series of isogenic cSCC cell lines that model progressing tumorigenesis in vitro***

5.2. Results

5.2.1. Calcium-induced differentiation and serum starvation-induced autophagy are required for AMBRA1 induction in CCD1106 keratinocyte differentiation, while expression is sustained by cellular differentiation alone

To confirm the role of AMBRA1 in both keratinocyte differentiation and autophagy, CCD1106 cells were subjected to calcium-induced differentiation for five days and/or serum starvation for an additional 24 hours, prior to determining the effect on AMBRA1, loricrin, p62, LC3B II and GAPDH expression by Western blotting (Figure 5.1 A).

Results revealed serum starvation of undifferentiated CCD1106 cells induced a small , but not significant increase in AMBRA1, LC3B-II and p62 expression (Figure 5.1 B, D and E). In addition there was no significant effect of serum starvation-induced autophagy on loricrin expression (Figure 5.1C).

Calcium-induced differentiation was also associated with a small non-significant induction of AMBRA1 (Figure 5.1 B), a reduction in p62 expression (Figure 5.1D) and a statistically significant increase in loricrin expression (*P<0.05, Figure 5.1C). A non-significant reduction in LC3B-II expression was also observed in response to calcium-induced differentiation. (Figure 5.1E).

Interestingly, serum starvation of calcium-induced differentiated CCD1106 cells resulted in a significant increase in AMBRA1 expression compared to undifferentiated cells subjected to serum starvation (*P<0.05, Figure 5.1B), as well as compared to control undifferentiated cells maintained in normal serum conditions (*P<0.05, Figure 5.1B). Serum starvation of differentiated CCD1106 cells also resulted in a statistically significant induction of loricrin expression, again compared to expression in control non-starved, undifferentiated cells or cells only subjected to serum starvation (*P<0.01, Figure 5.1C). However, there was no significant effect on the induction of loricrin beyond levels induced by calcium-induced differentiation alone (Figure 5.1C). Furthermore, although serum starvation of calcium-induced differentiated CCD1106 cells appeared to result in an increase in LC3B-II expression compared to cells singularly subjected to calcium-induced differentiation, levels of induction were not significantly different to those induced by serum starvation alone (Figure 5.1 A and E). Similarly, although p62 expression appeared to be reduced to a greater extent in serum

starved, calcium-induced differentiated CCD106 cells, this did not significantly differ to p62 expression levels in undifferentiated cells subjected to serum starvation (Figure 5.1A and D).

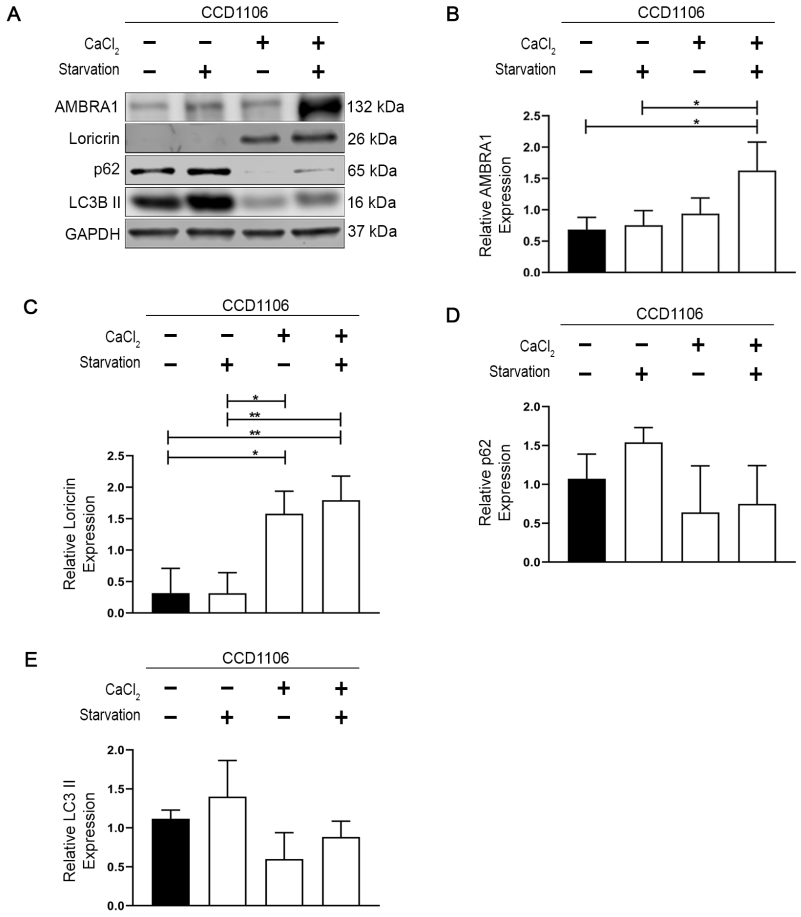

FIGURE 5. 1 CALCIUM-INDUCED DIFFERENTIATION AND STARVATION INDUCED AUTOPHAGY RESULTS IN INCREASED AMBRA1 EXPRESSION IN CCD1106 KERATINOCYTES.

(A) *Representative western blot of AMBRA1 (132 kDa), Loricrin (26 kDa), p62 (65 kDa), LC3B (16 kDa) and GAPDH (37 kDa, loading control) expression in CCD1106 cells in the presence or absence of calcium chloride ($CaCl_2$) (72 hours, 1.3 mM) and serum starvation (24 hours). Densitometric expression of* ***(B)*** *AMBRA1* ***(C)*** *Loricrin* ***(D)*** *p62 and* ***(E)*** *LC3B II expression. Each bar represents three replicates of the protein of interest expression, normalised against GAPDH expression, following the previously described treatments, and expressed relative to each individual experimental average (mean ± SD, N=3). Statistics acquired by one-way ANOVA with Tukey's post hoc correction (*P<0.05) (**P<0.01) (**P<0.01) (****P<0.0001).*

Collectively these data highlight an increase in AMBRA1 expression in CCD1106 cells in response to both calcium-induced differentiation and serum starvation induced autophagy, with a further likely additive effect on expression levels in calcium-induced differentiated cells subsequently subjected to serum starvation, suggesting AMBRA1 plays a role in both keratinocyte differentiation and autophagy.

Whilst this experiment suggested a correlation between AMBRA1 expression and keratinocyte differentiation in CCD1106 cells, it was unclear if the higher expression levels observed resulted outside the influence of autophagic signalling. The increase in AMBRA1 correlated with a trend wise reduction in LC3B-II expression (Figure 5.1E), suggesting that autophagic signalling was not responsible for the induced expression. However, since the relative expression of LC3B-II alone is not a sufficient marker of active autophagy, further experiments were undertaken in CD1106 cells to evaluate autophagic flux following prolonged exposure to serum starvation and in presence or absence of the lysosomal inhibitor chloroquine (CQ) which prevents autophagosome-lysosome fusion (Mauthe et al., 2018).

Specifically, CCD1106 cells were again subjected to calcium-induced differentiation for 72 hours and/or serum starvation for 72 hours in the presence or absence of treatment for the final 2 hours of incubation with CQ and the assessment of AMBRA1, loricrin, c-Myc , p62, LC3B II and GAPDH expression (Figure 5.2 A).

By inhibiting autophagosome- lysosomal fusion CQ prevents the cycle of LC3, resulting in accumulation of lipidated LC3-II. Additionally, CQ prevents the degradation of p62–by preventing its degradation in the completed autophagolysosome (Wu et al., 2020). As such, the accumulation of this protein, alongside the relative expression of LC3B-II, when compared to LC3B-I, is a marker of autophagic flux.

Results revealed, in a similar manor to the previous experiment, that subjecting calcium-induced differentiated CCD1106 cells to serum starvation resulted in significant increase in both AMBRA1 expression and loricrin expression (****P<0.0001, Figure 5.2 B and C). A significant increase in AMBRA1 expression (*P<0.05, Figure 5.2 B) was also observed when calcium-induced differentiated CCD1106 cells subjected to serum starvation were incubated in the presence of CQ, suggesting autophagy is responsible for some loss of AMBRA1 expression. Conversely, the significant loss in loricrin expression (****P<0.0001, Figure 5.2 C) by calcium-induced differentiated CCD1106 cells subjected to serum starvation in the

presence of CQ also suggests the inhibition of lysosomal fusion and pH disrupts inhibits loricrin expression. Interestingly, serum starvation, calcium-induced differentiation and calcium-induced differentiation together with serum starvation all caused a significant decrease in the level of c-Myc expression by CCD1106 cells (*P<0.05 - ***P<0.001, Figure 5.2 D), regardless of whether cells were co treated with CQ or not. Results also revealed serum starvation resulted in a significant accumulation of p62 expression, suggesting a blockade in autophagy flux (Figure 5.2 E). However, calcium-induced differentiation and calcium-induced differentiation together with serum starvation in the presence of chloroquine did not result in p62 accumulation (Figure 5.2E). Nevertheless whether or not CQ was present in cells subjected to calcium induced differentiated +/- serum starvation, a significant decrease in p62 expression was observed (***P<0.001-**** P<0.0001, Figure 5.2E).

Finally, evaluation of LC3B-II expression levels revealed the only significant changes observed in the presence or absence of CQ were in CD1106 cells subjected to calcium-induced differentiation, where a significant increase in expression was observed (**P<0.01, Figure 5.2 F). In addition regardless of the presence or absence of CQ, the greatest levels of LC3B expression were observed in CCD1106 cells subjected to serum starvation-induced autophagy.

Taken together, these data suggest AMBRA1 expression in CCD106 cells is induced maximally as a result of combined calcium-induced differentiation and serum starvation-induced autophagy. Further, these data suggest while autophagic signalling is required for AMBRA1 expression in keratinocytes, the process and completion of keratinocyte differentiation and cornification maintains AMBRA1 expression. This suggests AMBRA1 expression becomes decoupled from autophagy-mediated regulation when the cellular requirement for active autophagy falls, during the process of cellular differentiation.

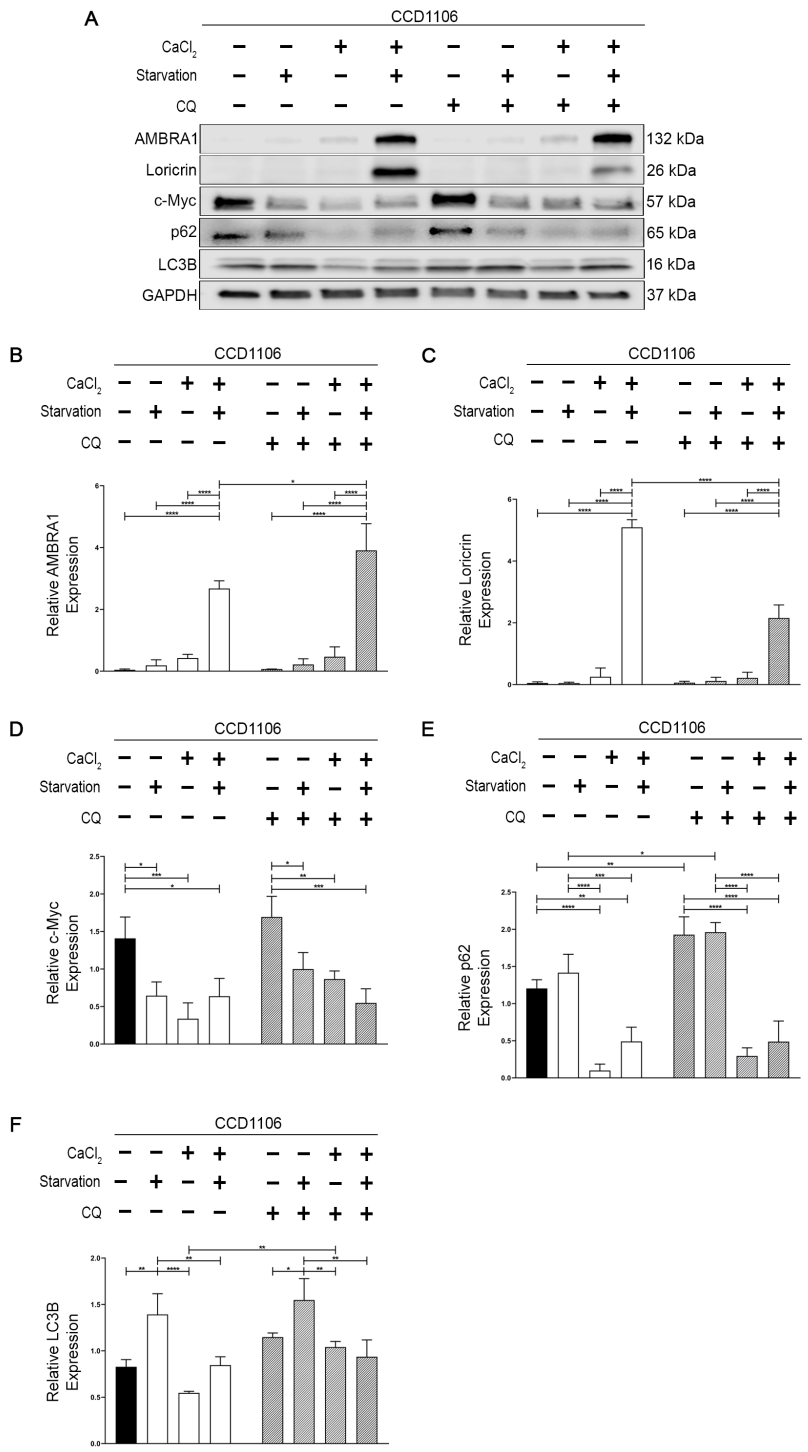

FIGURE 5. 2. INCREASED AMBRA1 EXPRESSION INDUCED BY THE PRESENCE OF CALCIUM AND STARVATION IS MAINTAINED BEYOND THE LOSS OF AUTOPHAGIC ACTIVITY IN CCD1106 KERATINOCYTES.

(A) *Representative western blot of AMBRA1 (132 kDa), Loricrin (26 kDa), c-Myc (57 kDa), p62 (65 kDa), LC3B (16 kDa) and GAPDH (37 kDa, loading control) expression in CCD1106 cells in the presence or absence of calcium chloride ($CaCl_2$) (72 hours, 1.3 mM), serum starvation (72 hours) and chloroquine treatment (10 µM). Densitometric expression of* ***(B)*** *AMBRA1* ***(C)*** *Loricrin* ***(D)*** *c-Myc* ***(E)*** *p62 and* ***(F)*** *LC3B expression. Each bar represents three replicates of the protein of interest expression, normalised against GAPDH expression, following the previously described treatments, and expressed relative to each individual experimental average (mean ± SD, N=3). Statistics acquired by one-way ANOVA with Tukey's post hoc correction (*P<0.05) (**P<0.01) (**P<0.01) (****P<0.0001).*

5.2.2. Calcium-induced differentiation is deregulated and autophagy is decoupled from keratinocyte differentiation in cSCC tumourigenesis in vitro.

To investigate the dynamics of AMBRA1 expression in response to calcium-induced differentiation and or serum starvation-induced autophagy in cSCC cells *in vitro* , PM1 cells were first subjected to calcium-induced differentiation for 72 hours and/or serum starvation for 72 hours in the presence or absence of CQ for the final 2hrs of incubation before evaluating the effects on AMBRA1, loricrin, c-Myc, p62, LC3B and GAPDH expression by Western blotting (Figure 5.3 A). Results revealed only calcium and serum starvation treatment in the presence of CQ had a significant effect on AMBRA1 induction (*P<0.05, Figure 5.3 B). Noteworthy however, was an observable trend for increased expression of AMBRA1 in PM1 cells subjected to treatment with high calcium and/or serum starvation in the presence of CQ (Figure 5.3 A and B).

Results also revealed neither treatment in high calcium or serum starvation in the presence or absence of CQ had any effect on Loricrin expression in PM1 cells (Figure 5.3A), while c-Myc expression was significantly decreased in cells subjected to serum starvation in the presence or absence of high calcium and/or in the presence of CQ (***P<0.001 - ****P<0.0001, Figure 5.3 C). Similarly to the effects of serum starvation on c-Myc expression by PM1 cells, serum starvation induced a reduction in p62 expression, both in the presence of high calcium and additional treatment with CQ, although this effect was only significant in cells treated in the presence of CQ (***P<0.001-****P<0.0001, Figure 5.3 D).

In contrast, there was a significant accumulation in LC3B-II expression in PM1 cells following serum starvation and /or high calcium in the presence of CQ (*P<0.05 - ****P<0.0001, Figure 5.3 E).

Collectively these data showing a trend wise increase in AMBRA1 and significant accumulation of LC3B-II in PM1 cells subjected to treatment in high calcium +/- serum starvation suggest these cells retain their ability to respond to calcium signalling as well as autophagy induction. However, the fact that there was no observable change in loricrin expression or c-Myc in PM1 cells subjected to high calcium alone suggest homeostatic differentiation is deregulated.

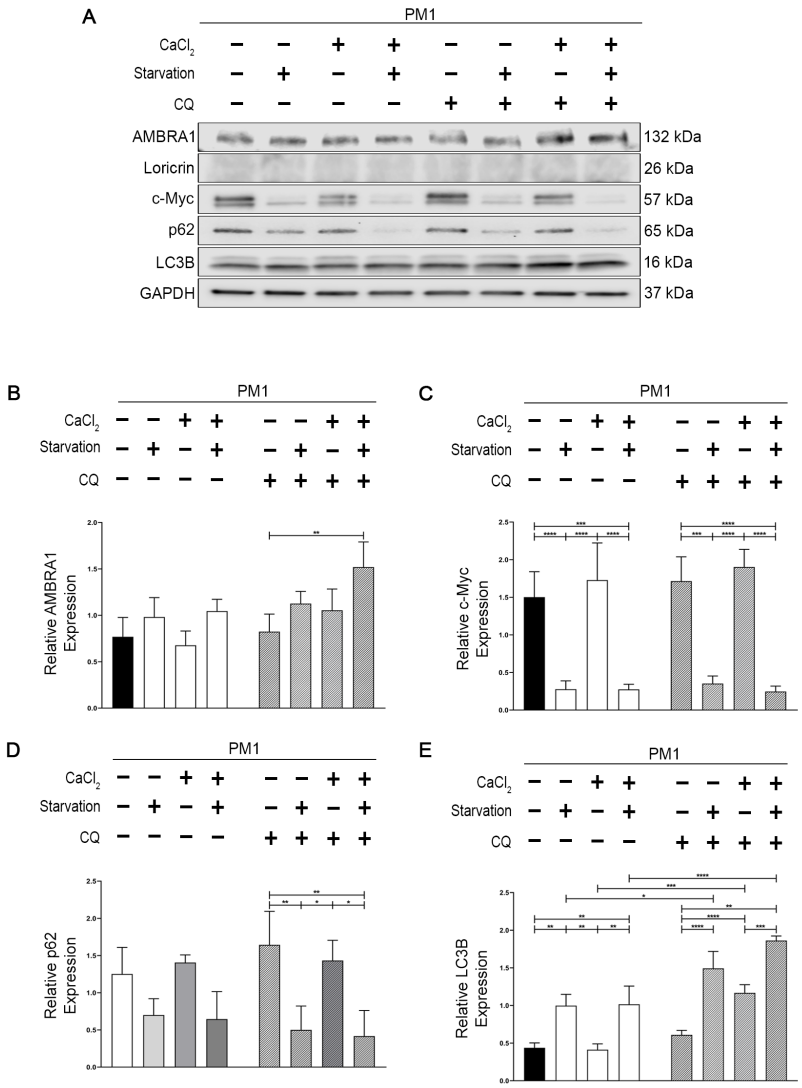

FIGURE 5. 3. AMBRA1 EXPRESSION IS STILL INFLUENCED BY THE PRESENCE OF CALCIUM IN PM1 CELLS.
(A)** Representative western blot of AMBRA1 (132 kDa), Loricrin (26 kDa), c-Myc (57 kDa), p62 (65 kDa), LC3B (16 kDa) and GAPDH (37 kDa, loading control) expression in PM1 cells in the presence or absence of calcium chloride ($CaCl_2$) (72 hours, 1.3 mM), serum starvation (72 hours) and chloroquine treatment (10 µM). Densitometric expression of **(B)** AMBRA1 **(C)** c-Myc **(D)** p62 and **(E)** LC3B expression. Each bar represents three replicates of the protein of interest expression, normalised against GAPDH expression, following the previously described treatments, and expressed relative to each individual experimental average (mean ± SD, N=3). Statistics acquired by one-way ANOVA with Tukey's post hoc correction (*P<0.05) (**P<0.01) (**P<0.01) (*P<0.0001).*

Next, cSCC MET1 cells were subjected to calcium-induced differentiation for 72 hours and/or serum starvation for 72 hours in the presence or absence of 2 hours final treatment with CQ , prior to evaluating AMBRA1, loricrin, c-Myc, p62, LC3B and GAPDH expression by western blotting (Figure 5.4 A). Unlike results observed in PM1 cells, results demonstrated a significant decrease in AMBRA1 expression in cells subjected to serum starvation in the presence or absence of high calcium or CQ (**P<0.01 - ***P<0.001, Figure 5.4 B).

Similar to results derived from studies of PM1 cells, neither serum starvation nor treatment in the presence or absence of high calcium and or CQ had any effect on loricrin expression (Figure 5.3A).

Again similarly to results observed in PM1 cells, subjecting MET 1 cells to serum starvation in the presence or absence of treatment in high calcium with CQ resulted in a significant decrease in c-Myc expression (**P<0.01 - *** P<0.001, Figure 5.4 C). In contrast to data derived from studies in PM1 cells, culture of MET 1 cells in high calcium in the absence of CQ resulted in a significant decrease in c-Myc expression (* P< 0.05, Figure 5.4C).

In terms of p62 expression, subjecting of MET 1 cells to serum starvation in the presence or absence of high calcium and/or CQ resulted in a significant down regulation of expression (***P< 0.001, Figure 5.4D). Culture of MET 1 cells in high calcium alone also resulted in significant reduction of p62 expression (* P< 0.05, Figure 5.4D), but this was not observed in cells cultured in high calcium in the presence of CQ.

While studies in PM1 Cells (Figure 5.3) demonstrated significant accumulation of LC3B-II following culture in high calcium and/or serum starvation in the presence of CQ, the culture of MET 1 cells in high calcium in the presence of CQ did not results in LC3B-II accumulation (Figure 5.4E). However, serum starvation in the presence of absence of high calcium and in the presence of CQ did result in a significant accumulation of LC3B-II (*** P<0.001 - ****P<0.0001, Figure 5.4E).

Taken together, these data suggest calcium signalling and autophagy in MET1 cells is deregulated or uncoupled. Furthermore, the inability of MET 1 cells to respond to calcium signalling likely sustains their de-differentiated phenotype thereby promoting carcinogenesis.

.

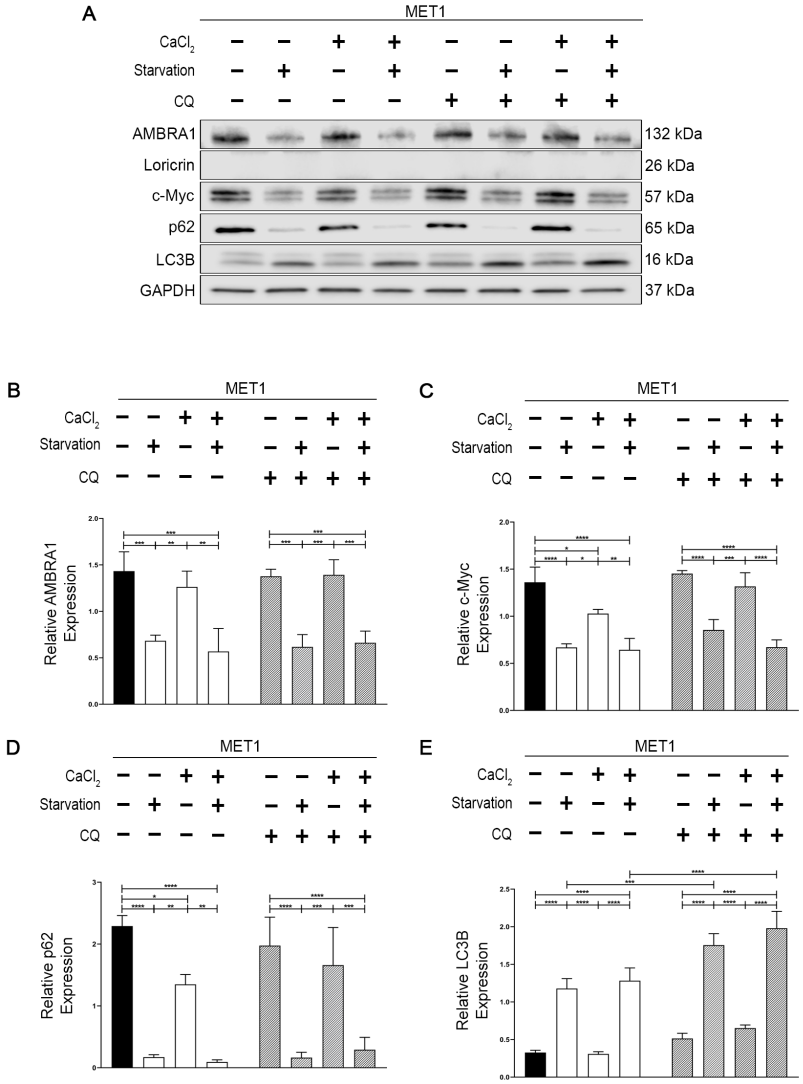

FIGURE 5. 4. AUTOPHAGY INDUCTION IS RESPONSIBLE FOR ALL ALTERATIONS TO AMBRA1 EXPRESSION IN MET1 CELLS. ***(A)*** *Representative western blot of AMBRA1 (132 kDa), Loricrin (26 kDa), c-Myc (57 kDa), p62 (65 kDa), LC3B (16 kDa) and GAPDH (37 kDa, loading control) expression in MET1 cells in the presence or absence of calcium chloride ($CaCl_2$) (72 hours, 1.3 mM), serum starvation (72 hours) and chloroquine treatment (10 µM). Densitometric expression of* ***(B)*** *AMBRA1* ***(C)*** *c-Myc* ***(D)*** *p62 and* ***(E)*** *LC3B expression. Each bar represents three replicates of the protein of interest expression, normalised against GAPDH expression, following the previously described treatments, and expressed relative to each individual experimental average (mean ± SD, N=3). Statistics acquired by one-way ANOVA with Tukey's post hoc correction (*P<0.05) (**P<0.01) (**P<0.01) (****P<0.0001).*

Finally, the metastatic cSCC MET4 cells were subjected to culture in high calcium and/or serum starvation for 72 hours, again in the presence or absence of CQ, and prior to western blotting for AMBRA1, loricrin, c-Myc, p62, LC3B and GAPDH expression (Figure 5.5 A).

Similarly to data derived from studies in PM1 cells (Figure 5.3), studies in MET 4 cells revealed only calcium and serum starvation treatment in the presence of CQ had a significant effect on AMBRA1 induction (*P<0.05, Figure 5.5 B). In addition, as again seen in PM1 cells, there was a non-significant observable trend for increased expression of AMBRA1 in MET4 cells subjected to treatment with high calcium and/or serum starvation in the presence of CQ (Figure 5.3 A and B).

As in PM1 and MET 1 cells, neither culture in high calcium nor serum starvation of MET 4 cells, in the presence or absence of CQ had any effect on Loricrin expression (Figure 5.5A).

Again as observed in both PM1 and MET 1 cells, the subjection of MET 4 cells to serum starvation alone and in combination with treatment in high calcium in the presence or absence of CQ resulted in a significant reduction in c-Myc expression (**P<0.01- ****P<0.0001, Figure 5.5 C). Interestingly, there was also a significant increase in c-Myc expression in MET 4 cells following treatment in high calcium in the absence of CQ (*P<0.05, Figure 5.5 C).

Similarly to observations in MET 1 cells, serum starvation in the presence or absence of culture in high calcium and/or CQ also resulted in the significant down regulation of p62 in MET4 cells (***P<0.001 - ****P<0.0001, Figure 5.5 D).

Interestingly, an accumulation of p62 in MET4 cells was observed in response to culture in the presence of high calcium and CQ (*P<0.05, Figure 5.5 D), suggesting calcium signalling induces active autophagy in MET 4 cells.

Finally, serum starvation, alone or in combination with culture in high calcium in the presence of CQ resulted in a significant induction of LC3B-II expression (*P<0.05 - ***P, 0.001, Figure 5.5 E). Unexpectedly, this accumulation of LC3B-II expression in response to culture in high calcium in the presence of CQ, also observed in PM1 cells (figure 5.3E), was not observed in MET 1 cells (Figures 5.4E).

Taken together these data suggest the relationship between calcium signalling, autophagy induction and the dynamics of AMBRA1 expression in MET 4 cells more closely align observation is PM1 cells compared to MET 1 cells.

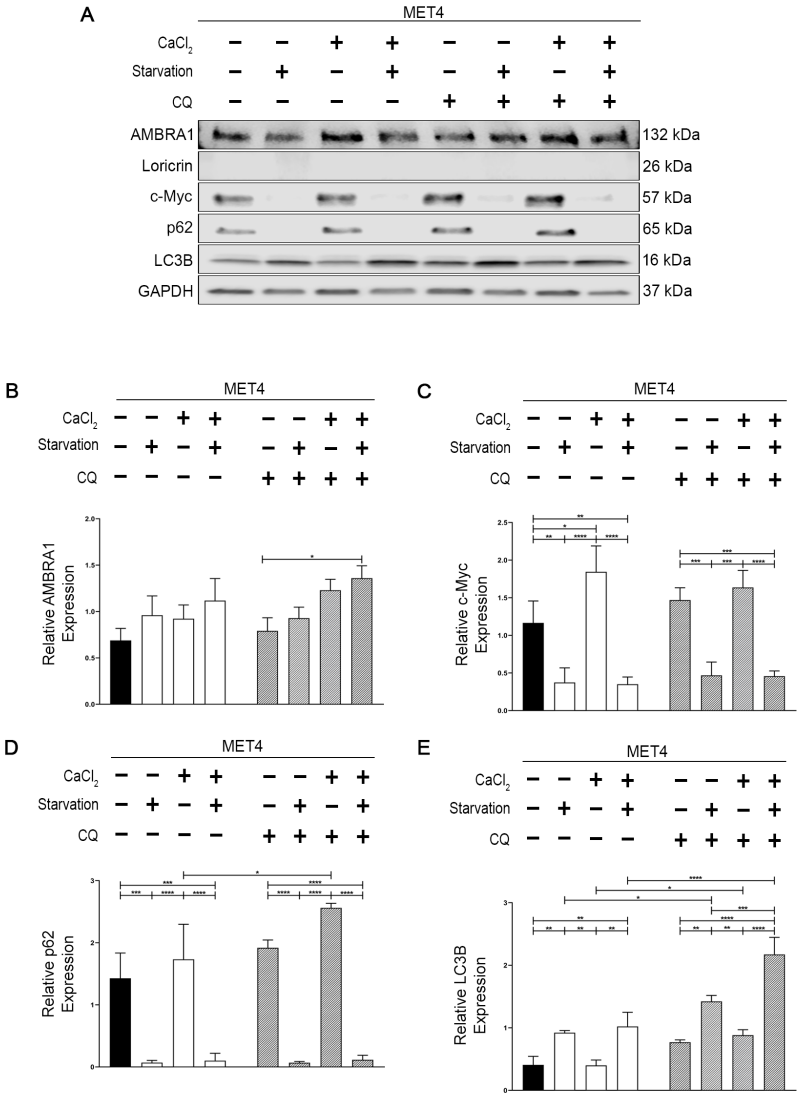

FIGURE 5. 5. AMBRA1 EXPRESSION REGAINS ITS SENSITIVITY TO THE PRESENCE OF CALCIUM IN MET4 CELLS.
(A) *Representative western blot of AMBRA1 (132 kDa), Loricrin (26 kDa), c-Myc (57 kDa), p62 (65 kDa), LC3B (16 kDa) and GAPDH (37 kDa, loading control) expression in MET4 cells in the presence or absence of calcium chloride ($CaCl_2$) (72 hours, 1.3 mM), serum starvation (72 hours) and chloroquine treatment (10 µM). Densitometric expression of* ***(B)*** *AMBRA1* ***(C)*** *c-Myc* ***(D)*** *p62 and* ***(E)*** *LC3B expression. Each bar represents three replicates of the protein of interest expression, normalised against GAPDH expression, following the previously described treatments, and expressed relative to each individual experimental average (mean ± SD, N=3). Statistics acquired by one-way ANOVA with Tukey's post hoc correction (*P<0.05) (**P<0.01) (**P<0.01) (****P<0.0001).*

5.3 Discussion

5.3.1. AMBRA1 promotes keratinocyte differentiation in the presence of calcium and nutrient starvation

To model the process of keratinocyte differentiation and the effects of autophagy on this process and the dynamics of AMBRA1 expression in normal keratinocytes, CCD1106 cells were subjected to both calcium-induced differentiation and serum starvation-induced autophagy (Figure 5.1). These environmental pressures closely model those present in the epidermis as keratinocytes migrate to the stratum corneum (Mahanty et al., 2019). Consistent with previous observations results showed calcium-induced differentiation increased both AMBRA1 and Loricrin expression (Figure 5.1 B and C) (Tang et al., 2016), also supporting recent observations of the critical role AMBRA1 plays in epidermal differentiation (Cosgarea et al., 2021). Interestingly, AMBRA1 expression levels in CCD1106 cells were further induced by combined calcium-induced differentiation and serum starvation, compared to expression levels induced by single agent treatment. However, this high level of AMBRA1 expression resulting from dual calcium-induced differentiation and serum starvation did not correlate with a significant increase in LC3B-II expression (Figure 5.1 E). This was surprising as AMBRA1 expression levels would normally closely reflect the level of active autophagy with a cell (Fimia et al., 2007). Also surprisingly, treatment of CCD1106 cells with single agent, high dose calcium over 72 hours resulted in a trend wise reduction in LC3B-II expression, suggesting that the presence of calcium is unable to induce autophagic activity, a well-known component of keratinocyte differentiation (Hohl et al., 1993, Bikle et al., 2012). Nevertheless, the relative expression of LC3B-II to the loading control protein GAPDH is not a sufficient marker to analyse the level of active autophagic flux within a cell and thus further experiments were under taken in the presence of the lysosomal inhibitor chloroquine (CQ), to block autophagic flux and the accumulation LC3B-II and p62 (Klionsky et al., 2012). In addition, to allow for persistent autophagic stress and more complete organelle clearance and thus differentiation (Mahanty et al., 2019), CCD1106 cells were also subsequently subjected to extended serum-starvation (Figure 5.2).

Similarly to initial experiments, prolonged exposure of CCD1106 cells to calcium-induced differentiation and serum starvation-induced autophagy resulted in the greatest increase in AMBRA1 expression (Figure 5.2 B). However, unlike initial experiments (Figure 5.1C) the greatest increase in loricrin expression was observed following calcium-induced

differentiation in combination with serum-induced autophagy (Figure 5.2 C). It is possible that the extended period of starvation allowed for more complete differentiation to occur in the presence of high calcium, however, cell seeding density was also optimised to ensure cell contact signalling to encourage full differentiation (Charest et al., 2009).

This significant increase in loricrin expression when CCD1106 cells were subjected to both calcium-induced differentiation and serum-starvation induced autophagy (Figure 5.2 C) highlights the importance of considering the *in vivo* conditions in a model system when studying keratinocyte differentiation. Many studies utilise a calcium only approach to induce differentiation, which may be insufficient (Wilson, 2014, Mahanty et al., 2019, Richardson et al., 2020). Additional evidence to support this possibility were the observations that whilst a significant accumulation of LC3B-II was demonstrated in CCD1106 cells subjected to calcium-induced differentiation in the presence of chloroquine, suggesting active autophagy, this was not observed in cells subjected to calcium-induced differentiation in combination with serum-starvation-induced autophagy (Figure 5.2 F). This suggests that cell clearance has already been completed in the cells exposed to both treatments, allowing further and more complete differentiation. However, further investigation is required to compare the genomic and proteomic profile of the two modelling approaches and to evaluate if the presence of a nutrient deprived environment results in any significant changes to cell phenotype or genotype. There is also still a need for a standardised approach to modelling keratinocyte differentiation *in vitro* in dermatological research.

The ability of calcium-induced differentiation and serum starvation-induced autophagy to induce the greatest levels of AMBRA1 expression in CCD1106 cells, in the absence of high levels of autophagic flux, was surprising (Figure 5.2 B). Coupled, with observations that AMBRA1 induction by dual exposure to high calcium and serum starvation was greater than expression levels induced by either condition alone suggests that both conditions are needed in parallel to produce a fully differentiated keratinocyte.

As such, it is most likely that a nutrient deprived environment in the presence of calcium signalling allows for the largest sustained expression of AMBRA1. Importantly these data suggest AMBRA1 expression in keratinocyte differentiation becomes uncoupled from its normal autophagy-regulated degradation. Moreover, these data suggest the process of keratinocyte differentiation and cornification actively sustains AMBRA1 expression.

The question however, still remains as to how AMBRA1 expression becomes decoupled from autophagic regulation at later stages of keratinocyte differentiation and before terminal differentiation occurs. One possibility is that AMBRA1 expression is able to escape the normal ubiquitin mediated degradation that acts as a limiting factor in autophagy to prevent cell death (Antonioli et al., 2014). This may result from post translational modifications leading to structural alterations that cause the obscuring of either the E3 ligase binding site or the ubiquitin target sites directly (Duan and Walther, 2015). The ability of AMBRA1 to be post-translationally modified has been extensively studied, with key phosphorylation and ubiquitin sites identified, mostly relating to autophagy regulation (Cianfanelli et al., 2015d, Nazio et al., 2013). These specific binding and target sites that lead to AMBRA1- mediated degradation are still however, poorly understood. Two possible candidates have been identified, the first of which is the CULLIN4–DDB1–complex (Antonioli et al., 2014), which binds to the WD40 sequence present in amino acid region 111-126, however, the target ubiquitin residue is currently unknown (Cianfanelli et al., 2015b, Cianfanelli et al., 2015d, He et al., 2006). The second possibility is the protein RNF (Xia et al., 2014), which has a currently unknown binding site, is able to induce K48-ubiquitination at lys45 (Cianfanelli et al., 2015d). Nevertheless, the current lack of understanding of protein interaction makes speculating on the possible mechanisms of masking either E3 ligase binding site or ubiquitination target residue difficult. Such understanding would however, provide a novel insight into AMBRA1 regulation, as current literature has only profiled post-translational modifications altering autophagy regulation.

Since the cross talk between calcium signalling and autophagy regulation has been well documented in the context of cellular stress and cancer (Dubois et al., 2016, Høyer-Hansen and Jäättelä, 2007, Kania et al., 2015), it is possible that calcium signalling can directly impact AMBRA1 regulation (Kania et al., 2015, Settembre et al., 2012). However, to date there have been no reports of calcium signalling and autophagy cross talk in the context of cellular differentiation.

An alternative mechanism potentially influencing the genetic regulation of AMBRA1 in CCD1106 cells is the possibility that calcium signalling is able to induce AMBRA1 transcription. Possible connections between AMBRA1 and calcium signalling have only been suggested in

the context of autophagy activation (Bootman et al., 2018, Patergnani et al., 2020, Medina et al., 2015). However, there are currently no published data to suggest AMBRA1 expression can be induced by calcium outside of this context, thereby suggesting that calcium specific transcriptional activation of AMBRA1 expression is unlikely. Another potential is for AMBRA1 to be incorporated into multi-protein complexes and as such, evade detection by potential degradation pathways, a possibility given the large scale cellular alterations that occur during differentiation, including the formation of the cornified envelope and alterations to protein compositions at tight junctional complexes (Bikle et al., 2012). Autophagy has already been studied and been shown to be involved in protein arrangements at tight junctional complexes (Nighot and Ma, 2016). Additionally, AMBRA1 has been directly implicated in this alteration through its association with FAK (Schoenherr et al., 2017).

AMBRA1 is also a highly intrinsically disordered protein. Given their high degree of structural flexibility, intrinsically disordered proteins have been implicated as core components of multi-protein signalling complexes (Wright and Dyson, 2015), suggesting AMBRA1 may be readily incorporated into a wide variety of protein complexes that give rise to a differentiated cellular phenotype. Given the high degree of changes and multiple protein interlinking that occurs during keratinocyte differentiation this seems the most likely explanation for the maintained levels of AMBRA1 expression observed in CCD1106 cells following calcium-induced differentiation in combination with serum starvation.

In agreement with previous published studies, the subjection of CCD1106 cells to both calcium-induced differentiation and serum starvation-induced autophagy resulted in a significant decrease in the level of c-Myc expression (Figure 5.2 D) (Cianfanelli et al., 2015c). Furthermore supporting the present study in the context of keratinocyte differentiation, Cianfanelli et al. demonstrated that AMBRA1 is able to induce PP2A phosphatase to inactive c-Myc and reduce the rate of cell proliferation (Cianfanelli et al., 2015c). Moreover, also supporting the current studies and the observed reduction in c-Myc expression following both calcium-induced differentiation and serum starvation-induced autophagy, previous studies have also demonstrated that whilst the transient amplification of keratinocytes relies on c-Myc (Kolly et al., 2005, Arnold and Watt, 2001), a low level of c-Myc is required to ensure complete differentiation (Gandarillas and Watt, 1997, Pelengaris et al., 1999, Waikel et al., 1999).

One possible mechanism for loss of c-Myc transcriptional activity is through calcium-dependant, and thus differentiation related, calpain mediated cleavage (Small et al., 2002), which in certain tissues has been shown to promote differentiation (Conacci-Sorrell and Eisenman, 2011). Another option is loss of c-Myc in the more common ubiquitin-mediated autophagy/proteasome manor, which has also been highly implicated in keratinocyte differentiation and suggests a level of redundancy (Dikic, 2017, Farrell and Sears, 2014, Mahanty et al., 2019).

Given the well-established role of p62 as a cargo adaptor protein delivering ubiquitinated proteins to autophagosomes (Lamark et al., 2017), results derived from studies of p62 expression in CCD1106 cells subjected to calcium-induced differentiation and serum-starvation-induced autophagy were surprising. Given the high level of autophagy that occurs during keratinocyte differentiation it was hypothesised that treatment of CCD1106 cells pre exposed to high dose calcium (either in the presence or absence of serum starvation) with chloroquine would result in p62 accumulation. In contrast results showed no such accumulation of p62 (Figure 5.2 E). It is possible that two hours treatment with CQ may not have been sufficient to allow for p62 accumulation, perhaps additionally impaired by a low level of active autophagy. Alternatively, treatment of cells with high calcium alone wasn't enough to sufficiently replenish p62 through genetic transcription causing a lag in the production and translation of new proteins. p62, as a cargo delivery protein, is degraded during the stage of autophagosome-lysosomal fusion, which is prevented by chloroquine. Whilst calcium has previously been shown to be able to induce pro-autophagy elements through a TFEB dependent mechanism (Medina and Ballabio, 2015), it is possible that calcium signalling alone can't sufficiently induce enough expression of p62 to replace that lost by autophagic degradation, thus preventing an observable accumulation. However, there was also no observable accumulation of p62 in CCD1106 cells in response to both calcium-induced differentiation and serum starvation-induced autophagy (Figure 5.2E). This was unexpected since nutrient deprivation is a well-known inducer of autophagy related gene expression (Russell et al., 2014, Settembre et al., 2012, Martina et al., 2012). It is therefore likely that cells subjected to both calcium-induced differentiation and serum starvation-induced autophagy have undergone terminal differentiation and therefore lost autophagic capacity as well as the ability to induce *de novo* genetic expression.

Comparative studies of the effects of calcium-induced differentiation and/or serum starvation-induced autophagy in CCD1106 cells on LC3B-II expression in the presence or absence of chloroquine demonstrated that only culture in high calcium in the presence of chloroquine resulted in the significant accumulation of LC3B-II (Figure 5.2 F).

These observations were in conflict to the observed effects on p62 accumulation under the same treatment conditions (Figure 5.2 E), which suggested an absence of active autophagy. These conflicting results could be explained by the alternative mechanism of action of chloroquine on p62 and LC3B expression. Unlike p62, LC3B is not degraded by the process of autophagy and as such does not require genetic transcription to replenish its expression (Klionsky et al., 2016). As LC3B cycles between a non-lipidated and a lipidated form to expand the autophagophore, an action that is prevented by chloroquine (Tanida et al., 2008, Klionsky et al., 2016), an accumulation of lipidated LC3 would therefore be more readily detected, thereby suggesting results derived from calcium-induced LC3B expression in CCD 1106 cells are a more representative indicator of active autophagy than p62 expression.

Surprisingly, CQ treatment of CCD1106 cells in a nutrient deprived and high calcium environment did not result in LC3B accumulation (Figure 5.2F). This suggests that whole cell clearance by autophagy was completed and as such, the autophagy machinery was degraded preventing LC3B accumulation. Linked to this conclusion, the high levels of loricrin expression observed in cells subjected to calcium-induced differentiation in combination with serum starvation-induced autophagy further supports the likely hood that terminal differentiation has occurred, and consistent with levels of loricrin observed in the stratum granulosum, pre-cornification (Steinert and Marekov, 1999).

Unexpectedly CCD1106 cells subjected to serum starvation with chloroquine did not result in a block in LC3B flux (figure 5.2F). However, exposing keratinocytes cells to 72 hours of complete serum starvation is not representative of an environment cells would be exposed to *in vivo*, and although a model of nutrient deprivation *in vitro,* this is a non-typical environmental pressure. Current published literature focuses on the temporal regulation of starvation-induced autophagy in a short-term time frame (0-8 hrs) and no long term study to date has analysed the temporal regulation of autophagy at substantially longer time points (Sahani et al., 2014, Antonioli et al., 2016). However, given the negative regulation of AMBRA1 through ubiquitin-mediated degradation during periods of prolonged stress, this suggests that

severe extended autophagy may cause higher levels of self-regulated degradation of this and other pro-autophagy regulators (Antonioli et al., 2014), completely ablating the ability of the cell to undergo active autophagy. It also possible that degradation of pro-autophagy proteins such as seen here indicates a switch to cell death fate and the population of cells analysed in this experiment were likely at the point of undergoing cell death (Antonioli et al., 2014, Pagliarini et al., 2012, Fimia et al., 2013). Further studies however, are required to determine if primary keratinocytes would be as resistant to such a switch in cell fate as appears to be observed in transformed CCD1106 keratinocytes.

In conclusion, the present studies in CCD1106 cells suggest keratinocytes require the cooperation of both calcium-induced differentiation and autophagy induction to ensure complete terminal differentiation and that this differentiation is associated with significantly increased AMBRA1 expression which is decoupled from its standard regulation as a pro-autophagy protein.

5.3.2. AMBRA1 loses calcium signalling-induced regulation during cSCC tumourigenesis in vitro

To understand if calcium signalling, autophagy induction and the dynamics of AMBRA1 expression are altered in cSCC cells compared to CCD1106 cells, the isogenic series of cSCC cell lines, PM1, MET 1 and MET 4 representing dysplastic skin, primary and metastatic cSCC (Proby et al., 2000) were also subjected to culture in high calcium and/or serum starvation-induced autophagy.

The paradoxical role of autophagy in cancer has been extensively reported and is widely accepted as a major component of tumourigenesis as well as a target for treatment (Huang et al., 2018). AMBRA1 as a pro-autophagy protein has been implicated in several cancers (Li et al., 2016, Sun et al., 2018, Liu et al., 2019), with specific interest in its role in cutaneous malignancies (Ellis et al., 2020, Ellis et al., 2014, Tang et al., 2016). Calcium and its downstream signalling has also been implicated in cancer through a variety of different mechanisms impacting on gene and protein expression, tumour microenvironment remodelling and treatment resistance (Monteith et al., 2017). Calcium signalling in this context is of particular relevance in keratinocyte carcinomas, as evidenced by the established relationship between calcium signalling and keratinocyte differentiation (Bikle et al., 2012). The uncoupling of this relationship therefore likely leads to the resistance of keratinocytes to cell death, their

sustained proliferative signalling, and the maintenance of a dedifferentiated cell state, all classical hallmarks of cancer (Hanahan and Weinberg, 2000, Hanahan and Weinberg, 2011) .

Studies in the dysplastic/pre-lesional keratinocyte cell line PM1 (Figure 5.3) demonstrated these cells retained their capacity to respond to both calcium signalling and autophagy induction, and in this context the induction of AMBRA1, in a similar manner to CCD1106 keratinocytes. Collectively these data therefore suggest that even though dysplastic, the relationship between calcium signalling and AMBRA1 expression is maintained in PM1 cells. Nevertheless, in contrast to calcium signalling and the induction of Loricrin in CCD1106 cells and primary epidermal keratinocytes (Cosgarea et al 2021 in press), there was no effect of culturing PM1 cells in high calcium on Loricrin expression, suggesting some alteration of calcium signalling in these dysplastic keratinocytes prevents their ability to terminally differentiate, even though their culture in high calcium still induces AMBRA1 expression.

Further alterations to calcium signalling in PM1 cells as compared with CCD1106 cells was evident in the context of the resulting effect on c-Myc expression. While serum starvation in both cell types resulted in a significant reduction in c-Myc expression, unlike in CCD1106 cells, culture of PM1 cells in high dose calcium had no impact on the reduction of c-Myc expression (Figure 5.3 C). This is likely explained by the dysplastic nature of PM1 cells where deregulated proliferation is an already characterised component of this atypia (Azazmeh and Ben-Porath, 2020). Furthermore, the loss of c-Myc regulation has also been characterised as a key molecular event in early cSCC tumourigenesis (Zheng et al., 2014). However, given that expression of c-Myc in PM1 cells exposed to high calcium returned to control levels (ie levels observed in cells cultured under normal/lower calcium concentrations), rather than increasing, this suggests PM1 cells lose a tumour suppressive mechanism rather than gaining a pro oncogenic transformation.

Studies of LC3B-II expression in PM1 cells revealed, as expected, that serum starvation induced autophagy, but that subjecting cells to high calcium in the presence of chloroquine also resulted in the accumulation of LC3B-II (Figure 5.3E). This provides further evidence for the preservation of calcium signalling responses in this dysplastic/pre-lesional skin cell line. Furthermore it is likely that PM1 cells therefore hijack the ability of the calcium-induced differentiation machinery to activate autophagy, allowing for increased cell survival in the early stage of tumourigenesis, without losing their proliferative capacity. This hypothesis

however, is complexed by results showing culture of PM1 cells in high calcium in the presence of chloroquine did not result in accumulation of p62. It is possible that two hours of chloroquine treatment may not have been sufficient for p62 accumulation. Alternatively, the level of active autophagy (although demonstrable by the trend wise increase in AMBRA1 expression and the accumulation of LC3B-II) was not high enough to be detected following only two hours of chloroquine treatment.

Taken together, these data suggest that PM1 cells retain the ability to respond to calcium signals but the downstream elements have been altered to a level that sustains pro-survival mechanisms such as active autophagy and proliferation. Nevertheless and critical to cSCC tumourigenesis PM1 cells have lost their ability to undergo terminal differentiation thereby sustaining a de differentiated cell phenotype.

In contrast to the effects of culture in high calcium and serum starvation-induced autophagy in PM1 cells, the effects of these treatments on AMBRA1 expression in the primary cSCC cell line MET1 differed dramatically. Results revealed AMBRA1 expression in MET 1 cells decreased in the presence of serum starvation for 72 hrs (Figure 5.4 B). However, as discussed previously, prolonged serum starvation for 72 hours is not a typical environmental pressure *in vivo,* and it is therefore unclear how such exposure impacts on autophagy regulatory protein expression. It is likely therefore that serum starvation for 72 hours *in vitro* leads to increased temporal downregulation and degradation of autophagy regulatory proteins, such as AMBRA1. However, since culture of MET1 cells in high dose calcium did not result in an increase in AMBRA1 expression, as observed in PM1 and CCD1106 cells, this suggests that the ability of calcium signalling in MET 1 cells to induce active autophagy has been lost. It is therefore possible that whilst the preservation of the ability for calcium signalling to induce autophagy is vital in early dysplastic/pre-lesional cells to ensure cell survival, by the time the cells have formed large scale tumour growth, this activity is detrimental to further cSCC progression.

Studies in MET 1 cells also revealed, in line with observations in PM1 cells that there was no detectable change in loricrin expression in response to culture in high calcium in the presence or absence of serum starvation and/or chloroquine suggesting loss of calcium-induced terminal differentiation is also a maintained feature in cSCC tumourigenesis.

Interestingly, unlike the expression of c-Myc observed in PM1 cells, culture of MET1 cells in the presence of high calcium in the absence of chloroquine resulted in a significant decrease in the level of c-Myc expression (Figure 5.4 C). This decrease was prevented by treatment with chloroquine, suggesting loss of c-Myc results from general autophagic recycling rather than targeted degradation. The fact that c-Myc is retained in the presence of high calcium therefore suggests that primary MET 1 cells retain increased proliferative capacity as initially observed in the PM1, dysplastic/pre-lesional cell line.

Similar to results from studies in PM1 cells, the subjection of MET1 cells to culture in high calcium and/or serum starvation in the presence of chloroquine did not result in p62 accumulation. As previously discussed this is likely due to 2 hrs chloroquine treatment not being sufficient enough to allow for p62 accumulation. Interestingly, the culture of MET 1 cells in high calcium in the presence of chloroquine also did not result in LC3B-II accumulation (Figure 5.4 E). These data suggest that while CCD1106 cells and PM1 cells retain their sensitivity to calcium-induced autophagy, MET1 cells have lost this ability. The fact that calcium signalling is diminished in MET1 cells also likely leads to an overall reduction in autophagic activity, thus facilitating further mutagenesis and ultimately tumour progression (Amaravadi et al., 2016).

The pattern of changes in protein expression in MET4 cells exposed to high calcium and or serum starvation in the presence or absence of chloroquine was near identical to that observed in PM1 cells (Figures 5.3 and 5.5). Specifically and most critically AMBRA1 expression displayed a trend wise increase in response to serum starvation, culture in high calcium and both high calcium and serum starvation (Figure 5.5 B). In contrast in MET1 cells, calcium signalling was unable to increase AMBRA1 expression, suggesting MET4 cells regain their ability to respond to calcium signalling and calcium-induced AMBRA1 expression. In addition these data suggest that the loss of calcium-induced AMBRA1 expression in primary cSCC cells is temporary, and most likely arises from a mechanistic alteration rather than a mutational mediated loss of response to calcium signalling.

Data demonstrating MET4 cells cultured in high calcium in the presence of chloroquine resulted in increased AMBRA1 expression coupled with an accumulation in LC3B-II (Figure 5.5), suggesting that MET4 cells regain their capacity for calcium-induced autophagy, and supports the notion that metastatic cSCC cells have a higher capacity for and more readily

inducible autophagy, likely supporting their survival following metastasis (Mowers et al., 2017). Further supporting metastatic cSCC survival, observations in MET4 cells also showed culture in high calcium in the absence of chloroquine resulted in a significant increase in c-Myc expression. This not only suggests that cSCC cells will be highly proliferative in their metastatic environment but also suggests that a pro-oncogenic mutation has occurred that leads to increased c-Myc expression further driving tumour proliferation (Waitzberg et al., 2004, Ba et al., 2020).

Taken together, these data demonstrate pre-lesional/dysplastic skin cells and metastatic cSCC cells *in vitro* respond to calcium signalling, allowing for the induction of pro-survival autophagy but resisting terminal differentiation thereby allowing for continued cell proliferation. This pro survival autophagy response to calcium signalling is lost however in primary cSCC cells, resulting in reduced autophagic capacity, thereby allowing increased mutagenic stress, driving cSCC progression.

Overall these studies demonstrate that AMBRA1 expression is key to terminal keratinocyte differentiation and is reliant on both calcium signalling and autophagy induction. In cSCC tumourigenesis however, the dynamics of AMBRA 1 expression are uncoupled through the deregulation and hijacking of calcium signalling to facility pro-autophagy survival and the maintenance of a proliferative and de differentiated cell phenotype.

5.4 Summary

- ***Calcium signalling and autophagy initiation are required for full AMBRA1 induction, which is required for terminal keratinocyte differentiation in vitro.***
- ***While AMBRA1 expression in keratinocyte differentiation relies on both calcium signalling and autophagy induction, its expression is decoupled from homeostatic autophagy regulation***
- ***In cSCC tumourigenesis and progression, the dynamics of AMBRA 1 expression are uncoupled through the deregulation and hijacking of calcium signalling to facility pro-autophagy survival and the maintenance of a proliferative and de differentiated cell phenotype.***

Chapter 6. Final Discussion and Concluding Remarks

Cutaneous Squamous Cell Carcinoma (cSCC) poses a significant burden to health care systems and has a growing worldwide incidence (Lomas et al., 2012, Venables et al., 2019a). Whilst largely treatable, some patients do go onto develop disease reoccurrence and/or metastasis (Weinberg et al., 2007, Tokez et al., 2021) and highlighting the current lack of reliable biomarkers or ability of clinical guidelines to identify high-risk patient subsets. Whilst several biomarkers have been proposed, all lack consistency, reliability, accuracy and/or feasibility (Kreppel et al., 2013, Campos et al., 2019, Shapanis et al., 2021), further emphasising the unmet need for both novel prognostic biomarkers, as well as improved understanding of the underlying mechanisms that promote cSCC tumourigenesis and progression.

Autophagy has been shown to be essential to both cellular homeostasis and keratinocyte differentiation, with the deregulation of these processes being associated with cSCC initiation (Ravanan et al., 2017, Akinduro et al., 2016). Given AMBRA1 is a key regulatory protein in autophagy induction, coupled with mounting evidence for its involvement in keratinocyte differentiation, the aim of the current study was to define crosstalk between AMBRA1 and the deregulation of these processes in cSCC development and progression as well as its potential as a prognostic biomarker (Cianfanelli et al., 2015a, Cosgarea et al., 2021).

Data from the present study in a retrospective cohort of primary cSCC tumours, which either remained localised or subsequently progressed (reoccurred/metastasised), revealed loss of AMBRA1 expression occurs during cSCC tumourigenesis regardless of differentiation status or disease outcome. Given SQSTM1 (p62) is a selective autophagy receptor protein, analysis of its expression in primary cSCC tumours was undertaken to investigate its potential either alone or in combination with AMBRA1 (Katsuragi et al., 2015). Results demonstrated both cytoplasmic and nuclear p62 expression increased in primary cSCC tumourigenesis, regardless of tumour differentiation status or disease outcome, similarly to AMBRA1 expression. Since cSCC cells in the tumour mass or tumour growth front likely represent cells at different levels of cancerous progression and invasive capacity, the expression of both AMBRA1 and p62 was defined in these regions of primary cSCC tumour, along with their expression in the normal and peritumoural epidermis. Given that manual H-score quantification of any given protein revealed by immunohistochemical expression is subjective and inconsistent, a digital approach was therefore used to quantify AMBRA1 and p62 expression. Subsequent regional ROC curve analysis identified loss of cytoplasmic AMBRA1 expression in the tumour growth front and loss of cytoplasmic p62 expression in the peritumoural epidermis as the regions of

primary cSCC tumour with greatest prognostic potential for stratifying patients based on disease outcome. Survival curve analysis then revealed that loss of AMBRA1 tumour growth front and peritumoural epidermal p62 expression identified high-risk cSCC tumour subsets at increased risk of disease recurrence/metastasis, independently of tumour differentiation status.

Further sub-cohort analysis of poorly differentiated primary cSCC tumours, which either remained localised or developed metastasis, revealed loss of cytoplasmic AMBRA1 expression in the tumour growth front and loss of cytoplasmic p62 expression in the peritumoural epidermis identified high-risk tumour subsets with a significant propensity for metastasis. Notably, with a significant separation of low-risk and high-risk subsets, a hazard ratio of 30.070, an assay specificity of 97% and a positive predictive value (PPV) of 86%. As such, the combined immunohistochemical loss of tumour growth front expression of AMBRA1, in combination with loss of peritumoural epidermal p62 expression in FFPE cSCC sections, outperforms the currently most well studied prognostic 40 gene test for poorly-differentiated tumours (Wysong et al., 2020). Additionally, given this test can be performed on the original excision biopsy tissue, it will fit seamlessly into current clinical diagnostic and histopathology pathways. Nevertheless, further retrospective and perspective validation studies are warranted, to include the validation of the novel recombinant antibody to p62 prevalidated in the present study. Since we are entering a new generation of digital pathology with the use of AI to interpret immunohistochemical biomarker expression (Bera et al., 2019), the present study also provides a platform through which to inform the development of a novel machine learning driven biomarker test for cSCC.

The loss of AMBRA1 expression, in the context of its potential as prognostic biomarker for cSCC, has been linked to the secretion of TGF-β2 by high-risk melanomas that result in transcriptional down regulation of AMBRA1 within its epidermal environment (Cosgarea et al., 2021), while in HPV driven OPSCC, AMBRA1 loss is driven by HPV-induced calpain-mediated ubiquitin-dependent degradation (Antonioli et al., 2021). Studies of these two potential mechanisms of AMBRA1 loss in cSCC *in vitro* however revealed only increased TGF-β2 expression and secretion, and not an increase in Cullin 4A expression, correlated with loss of AMBRA1 expression. Further studies of TGF-β signalling revealed increased TGF-β2 expression and secretion resulted in canonical activation of the TGF-β receptor ALK5 and downstream activation of SMAD2 and SMAD3. However, although successful in inhibiting cSCC cell viability

in vitro, chemical inhibition of the TGF-β2 evoked ALK5 canonical signalling pathway did not prevent the loss of AMBRA1 expression, suggesting this pathway is unlikely responsible for the observed loss of AMBRA1 seen in cSCC tumourigenesis *in vivo*. Several alternative mechanisms may drive the loss of AMBRA1 in cSCC tumourigenesis and one that warrants further investigation is the potential role of the ubiquitin E3 ligase RNF, also identified as a potential regulator of AMBRA1 expression, and whose overexpression may also lead to deregulated autophagy, tumorigenesis and ultimately cSCC progression (Xia et al., 2014).

As well as its importance in autophagy, AMBRA1 has been shown to contribute to epidermal differentiation (Cosgarea et al., 2021). Given the well-documented importance of the maintenance of a dedifferentiated or stem-like cell state for carcinogenesis (Hanahan and Weinberg, 2000, Hanahan and Weinberg, 2011), the involvement of AMBRA1 in keratinocyte differentiation and autophagy was explored, in order to determine how loss of AMBRA1 expression and the subsequent deregulation of these processes contribute to cSCC tumourigenesis. Studies of immortalised keratinocytes demonstrated AMBRA1 expression is initially reliant upon autophagy activation, but is later maintained through calcium-mediated epidermal differentiation signalling, suggesting AMBRA1 expression completely dissociates from autophagic regulation during keratinocyte differentiation. Nevertheless, to confirm the specific role of AMBRA1 in keratinocyte differentiation, further studies should include an investigation into whether its expression also contributes to the structural formation of the cornified envelope and/or cell junctional complexes of higher-level epidermal strata. Furthermore, given the role of AMBRA1 in membrane nucleation through phospholipid production (Axe et al., 2008), studies should also explore its potential role in lamellar body formation. In addition to confirming the initial reliance of AMBRA1 expression on autophagy activation, further studies are also required to understand if AMBRA1 expression is subject to a regulatory switch to calcium signalling-mediated differentiation only or if structural integration into required differentiation related machinery prevents standard targeted degradation pathways from reducing its expression.

Additional studies of cSCC *in vitro* also revealed that calcium-signalling mediated regulation of AMBRA1 expression is lost during tumourigenesis, likely resulting in the maintenance of a dedifferentiated cell phenotype and facilitating sustained tumour cell proliferation. This further highlights that loss of AMBRA1 expression as a key event in the uncoupling of

autophagy and keratinocyte differentiation in cSCC development. Given the observations of AMBRA1 loss in cSCC *in vivo* and the suggested regulation by calcium signalling, this highlights the potential for perturbed or hijacked calcium signalling, which may result in severely reduced AMBRA1 expression.

Collectively these data highlight the tumour suppressive role of AMBRA1 in cSCC and its loss of expression in the tumour growth front in combination with the loss of peritumoural epidermal p62 expression as a novel prognostic biomarker.

Chapter 7. References

AEFFNER, F., ZARELLA, M. D., BUCHBINDER, N., BUI, M. M., GOODMAN, M. R., HARTMAN, D. J., LUJAN, G. M., MOLANI, M. A., PARWANI, A. V., LILLARD, K., TURNER, O. C., VEMURI, V. N. P., YUIL-VALDES, A. G. & BOWMAN, D. 2019. Introduction to Digital Image Analysis in Whole-slide Imaging: A White Paper from the Digital Pathology Association. *J Pathol Inform,* 10**,** 9.

AHMADI, A., NAJAFI, M., FARHOOD, B. & MORTEZAEE, K. 2019. Transforming growth factor-beta signaling: Tumorigenesis and targeting for cancer therapy. *J Cell Physiol,* 234**,** 12173-12187.

AITA, V. M., LIANG, X. H., MURTY, V. V., PINCUS, D. L., YU, W., CAYANIS, E., KALACHIKOV, S., GILLIAM, T. C. & LEVINE, B. 1999. Cloning and genomic organization of beclin 1, a candidate tumor suppressor gene on chromosome 17q21. *Genomics,* 59**,** 59-65.

AKALAY, I., JANJI, B., HASMIM, M., NOMAN, M. Z., ANDRÉ, F., DE CREMOUX, P., BERTHEAU, P., BADOUAL, C., VIELH, P., LARSEN, A. K., SABBAH, M., TAN, T. Z., KEIRA, J. H., HUNG, N. T., THIERY, J. P., MAMI-CHOUAIB, F. & CHOUAIB, S. 2013. Epithelial-to-mesenchymal transition and autophagy induction in breast carcinoma promote escape from T-cell-mediated lysis. *Cancer Res,* 73**,** 2418-27.

AKHURST, R. J. & DERYNCK, R. 2001. TGF-beta signaling in cancer--a double-edged sword. *Trends Cell Biol,* 11**,** S44-51.

AKINDURO, O., SULLY, K., PATEL, A., ROBINSON, D. J., CHIKH, A., MCPHAIL, G., BRAUN, K. M., PHILPOTT, M. P., HARWOOD, C. A., BYRNE, C., O'SHAUGHNESSY, R. F. L. & BERGAMASCHI, D. 2016. Constitutive Autophagy and Nucleophagy during Epidermal Differentiation. *J Invest Dermatol,* 136**,** 1460-1470.

ALAM, H., SEHGAL, L., KUNDU, S. T., DALAL, S. N. & VAIDYA, M. M. 2011. Novel function of keratins 5 and 14 in proliferation and differentiation of stratified epithelial cells. *Mol Biol Cell,* 22**,** 4068-78.

AMARAVADI, R., KIMMELMAN, A. C. & WHITE, E. 2016. Recent insights into the function of autophagy in cancer. *Genes Dev,* 30**,** 1913-30.

AN, Q., LIU, T., WANG, M. Y., YANG, Y. J., ZHANG, Z. D., LIU, Z. J. & YANG, B. 2021. KRT7 promotes epithelial-mesenchymal transition in ovarian cancer via the TGF-β/Smad2/3 signaling pathway. *Oncol Rep,* 45**,** 481-492.

ANDERSSON, E. M., PAOLI, J. & WASTENSSON, G. 2011. Incidence of cutaneous squamous cell carcinoma in coastal and inland areas of Western Sweden. *Cancer Epidemiol,* 35**,** e69-74.

ANTONIOLI, M., ALBIERO, F., NAZIO, F., VESCOVO, T., PERDOMO, A. B., CORAZZARI, M., MARSELLA, C., PISELLI, P., GRETZMEIER, C., DENGJEL, J., CECCONI, F., PIACENTINI, M. & FIMIA, G. M. 2014. AMBRA1 interplay with cullin E3 ubiquitin ligases regulates autophagy dynamics. *Dev Cell,* 31**,** 734-46.

ANTONIOLI, M., ALBIERO, F., PIACENTINI, M. & FIMIA, G. M. 2016. Temporal regulation of autophagy response by the CULLIN 4-AMBRA1-CULLIN 5 axis. *Mol Cell Oncol,* 3**,** e1008304.

ANTONIOLI, M., DI RIENZO, M., PIACENTINI, M. & FIMIA, G. M. 2017. Emerging Mechanisms in Initiating and Terminating Autophagy. *Trends Biochem Sci,* 42**,** 28-41.

ANTONIOLI, M., PAGNI, B., VESCOVO, T., ELLIS, R., COSWAY, B., ROLLO, F., BORDONI, V., AGRATI, C., LABUS, M., COVELLO, R., BENEVOLO, M., IPPOLITO, G., ROBINSON, M., PIACENTINI, M., LOVAT, P. & FIMIA, G. M. 2021. HPV sensitizes OPSCC cells to cisplatin-induced apoptosis by inhibiting autophagy through E7-mediated degradation of AMBRA1. *Autophagy,* 17**,** 2842-2855.

ARDA, O., GOKSUGUR, N. & TUZUN, Y. 2014. Basic histological structure and functions of facial skin. *Clin Dermatol,* 32**,** 3-13.

ARMSTRONG, J. L., HILL, D. S., MCKEE, C. S., HERNANDEZ-TIEDRA, S., LORENTE, M., LOPEZ-VALERO, I., ELENI ANAGNOSTOU, M., BABATUNDE, F., CORAZZARI, M., REDFERN, C. P. F., VELASCO, G. & LOVAT, P. E. 2015. Exploiting cannabinoid-induced cytotoxic autophagy to drive melanoma cell death. *J Invest Dermatol,* 135**,** 1629-1637.

ARNOLD, I. & WATT, F. M. 2001. c-Myc activation in transgenic mouse epidermis results in mobilization of stem cells and differentiation of their progeny. *Current Biology,* 11**,** 558-568.

ARONSON, J. K. & FERNER, R. E. 2017. Biomarkers-A General Review. *Curr Protoc Pharmacol,* 76**,** 9.23.1-9.23.17.

ASASHIMA, M., NAKANO, H., SHIMADA, K., KINOSHITA, K., ISHII, K., SHIBAI, H. & UENO, N. 1990. Mesodermal induction in early amphibian embryos by activin A (erythroid differentiation factor). *Rouxs Arch Dev Biol,* 198**,** 330-335.

AXE, E. L., WALKER, S. A., MANIFAVA, M., CHANDRA, P., RODERICK, H. L., HABERMANN, A., GRIFFITHS, G. & KTISTAKIS, N. T. 2008. Autophagosome formation from membrane compartments enriched in phosphatidylinositol 3-phosphate and dynamically connected to the endoplasmic reticulum. *J Cell Biol,* 182**,** 685-701.

AZAZMEH, N. & BEN-PORATH, I. 2020. Stimulation of epidermal hyperplasia and tumorigenesis by resident p16(INK4a)-expressing cells. *Mol Cell Oncol,* 7**,** 1819752.

AZIMI, A., LO, K., KIM, J. & FERNANDEZ-PENAS, P. 2020a. Investigating proteome changes between primary and metastatic cutaneous squamous cell carcinoma using SWATH mass spectrometry. *J Dermatol Sci,* 99**,** 119-127.

AZIMI, A., YANG, P., ALI, M., HOWARD, V., MANN, G. J., KAUFMAN, K. L. & FERNANDEZ-PENAS, P. 2020b. Data Independent Acquisition Proteomic Analysis Can Discriminate between Actinic Keratosis, Bowen's Disease, and Cutaneous Squamous Cell Carcinoma. *J Invest Dermatol,* 140**,** 212-222.e11.

BA, Y., LIU, Y., LI, C., ZHU, Y. & XING, W. 2020. HIPK3 Promotes Growth and Metastasis of Esophageal Squamous Cell Carcinoma via Regulation of miR-599/c-MYC Axis. *Onco Targets Ther,* 13**,** 1967-1978.

BAKIN, A. V., TOMLINSON, A. K., BHOWMICK, N. A., MOSES, H. L. & ARTEAGA, C. L. 2000. Phosphatidylinositol 3-kinase function is required for transforming growth factor beta-mediated epithelial to mesenchymal transition and cell migration. *J Biol Chem,* 275**,** 36803-10.

BARBARA, N. P., WRANA, J. L. & LETARTE, M. 1999. Endoglin is an accessory protein that interacts with the signaling receptor complex of multiple members of the transforming growth factor-beta superfamily. *J Biol Chem,* 274**,** 584-94.

BARONI, A., BUOMMINO, E., DE GREGORIO, V., RUOCCO, E., RUOCCO, V. & WOLF, R. 2012. Structure and function of the epidermis related to barrier properties. *Clin Dermatol,* 30**,** 257-62.

BASLER, K., BERGMANN, S., HEISIG, M., NAEGEL, A., ZORN-KRUPPA, M. & BRANDNER, J. M. 2016. The role of tight junctions in skin barrier function and dermal absorption. *J Control Release,* 242**,** 105-118.

BATLLE, E. & MASSAGUE, J. 2019. Transforming Growth Factor-beta Signaling in Immunity and Cancer. *Immunity,* 50**,** 924-940.

BERA, K., SCHALPER, K. A., RIMM, D. L., VELCHETI, V. & MADABHUSHI, A. 2019. Artificial intelligence in digital pathology - new tools for diagnosis and precision oncology. *Nat Rev Clin Oncol,* 16**,** 703-715.

BI, S., LI, L., GU, H., LI, M., XU, S., BU, W., ZHANG, M., ZHOU, Z. & CHEN, X. 2019. Lycopene upregulates ZO-1 and downregulates claudin-1 through autophagy inhibition in the human cutaneous squamous cell carcinoma cell line COLO-16. *J Cancer,* 10**,** 510-521.

BIKLE, D. D., XIE, Z. & TU, C. L. 2012. Calcium regulation of keratinocyte differentiation. *Expert Rev Endocrinol Metab,* 7**,** 461-472.

BLANK, U. & KARLSSON, S. 2015. TGF-β signaling in the control of hematopoietic stem cells. *Blood,* 125**,** 3542-50.

BLANPAIN, C. & FUCHS, E. 2014. Stem cell plasticity. Plasticity of epithelial stem cells in tissue regeneration. *Science,* 344**,** 1242281.

BLAZQUEZ, C., CARRACEDO, A., BARRADO, L., REAL, P. J., FERNANDEZ-LUNA, J. L., VELASCO, G., MALUMBRES, M. & GUZMAN, M. 2006. Cannabinoid receptors as novel targets for the treatment of melanoma. *Faseb j,* 20**,** 2633-5.

BLUM, V., MULLER, B., HOFER, S., PARDO, E., ZEIDLER, K., DIEBOLD, J., STROBEL, K., BRAND, C., AEBI, S. & GAUTSCHI, O. 2018. Nivolumab for recurrent cutaneous squamous cell carcinoma: three cases. *Eur J Dermatol,* 28**,** 78-81.

BONERANDI, J. J., BEAUVILLAIN, C., CAQUANT, L., CHASSAGNE, J. F., CHAUSSADE, V., CLAVERE, P., DESOUCHES, C., GARNIER, F., GROLLEAU, J. L., GROSSIN, M., JOURDAIN, A., LEMONNIER, J. Y., MAILLARD, H., ORTONNE, N., RIO, E., SIMON, E., SEI, J. F., GROB, J. J. & MARTIN, L. 2011. Guidelines for the diagnosis and treatment of cutaneous squamous cell carcinoma and precursor lesions. *J Eur Acad Dermatol Venereol,* 25 Suppl 5**,** 1-51.

BOOTMAN, M. D., CHEHAB, T., BULTYNCK, G., PARYS, J. B. & RIETDORF, K. 2018. The regulation of autophagy by calcium signals: Do we have a consensus? *Cell Calcium,* 70**,** 32-46.

BORTNIK, S. & GORSKI, S. M. 2017. Clinical Applications of Autophagy Proteins in Cancer: From Potential Targets to Biomarkers. *Int J Mol Sci,* 18.

BOUWSTRA, J. A. & HONEYWELL-NGUYEN, P. L. 2002. Skin structure and mode of action of vesicles. *Adv Drug Deliv Rev,* 54 Suppl 1**,** S41-55.

BRANTSCH, K. D., MEISNER, C., SCHONFISCH, B., TRILLING, B., WEHNER-CAROLI, J., ROCKEN, M. & BREUNINGER, H. 2008. Analysis of risk factors determining prognosis of cutaneous squamous-cell carcinoma: a prospective study. *Lancet Oncol,* 9**,** 713-20.

BREUNINGER, H., EIGENTLER, T., BOOTZ, F., HAUSCHILD, A., KORTMANN, R. D., WOLFF, K., STOCKFLETH, E., SZEIMIES, R. M., ROMPEL, R., GARBE, C. & GRABBE, S. 2013. Brief S2k guidelines--Cutaneous squamous cell carcinoma. *J Dtsch Dermatol Ges,* 11 Suppl 3**,** 37-45, 39-47.

BRODLAND, D. G. & ZITELLI, J. A. 1992. Surgical margins for excision of primary cutaneous squamous cell carcinoma. *J Am Acad Dermatol,* 27**,** 241-8.

BROWN, V. L., HARWOOD, C. A., CROOK, T., CRONIN, J. G., KELSELL, D. P. & PROBY, C. M. 2004. p16INK4a and p14ARF tumor suppressor genes are commonly inactivated in cutaneous squamous cell carcinoma. *J Invest Dermatol,* 122**,** 1284-92.

BUSSE, A. & KEILHOLZ, U. 2011. Role of TGF-β in melanoma. *Curr Pharm Biotechnol,* 12**,** 2165-75.

CALIFANO, J. A. L., W.M.; NEHAL, K.S.; O'SULLIVAN, B.; SCHMULTS, C.; SEETHALA, R.R.; WEBER, R.S.; SHAH, J.P. 2017. Chapter 15: Cutaneous Squamous Cell Carcinoma of the Head and Neck AJCC Cancer Staging Manual. *Springer, New York, NY, USA,* 8th ed**,** 10.

CAMMARERI, P., ROSE, A. M., VINCENT, D. F., WANG, J., NAGANO, A., LIBERTINI, S., RIDGWAY, R. A., ATHINEOS, D., COATES, P. J., MCHUGH, A., POURREYRON, C., DAYAL, J. H., LARSSON, J., WEIDLICH, S., SPENDER, L. C., SAPKOTA, G. P., PURDIE, K. J., PROBY, C. M., HARWOOD, C. A., LEIGH, I. M., CLEVERS, H., BARKER, N., KARLSSON, S., PRITCHARD, C., MARAIS, R., CHELALA, C., SOUTH, A. P., SANSOM, O. J. & INMAN, G. J. 2016. Inactivation of TGFbeta receptors in stem cells drives cutaneous squamous cell carcinoma. *Nat Commun,* 7**,** 12493.

CAMPOS, M. A., MACEDO, S., FERNANDES, M., PESTANA, A., PARDAL, J., BATISTA, R., VINAGRE, J., SANCHES, A., BAPTISTA, A., LOPES, J. M. & SOARES, P. 2019. TERT promoter mutations are associated with poor prognosis in cutaneous squamous cell carcinoma. *J Am Acad Dermatol,* 80**,** 660-669.e6.

CAÑUETO, J., CARDEÑOSO-ÁLVAREZ, E., COSANO-QUERO, A., SANTOS-BRIZ, Á., FERNÁNDEZ-LÓPEZ, E., PÉREZ-LOSADA, J. & ROMÁN-CURTO, C. 2017a. The expression of podoplanin is associated with poor outcome in cutaneous squamous cell carcinoma. *J Cutan Pathol,* 44**,** 144-151.

CAÑUETO, J., CARDEÑOSO-ÁLVAREZ, E., GARCÍA-HERNÁNDEZ, J. L., GALINDO-VILLARDÓN, P., VICENTE-GALINDO, P., VICENTE-VILLARDÓN, J. L., ALONSO-LÓPEZ, D., DE LAS RIVAS, J., VALERO, J., MOYANO-SANZ, E., FERNÁNDEZ-LÓPEZ, E., MAO, J. H., CASTELLANOS-MARTÍN, A., ROMÁN-CURTO, C. & PÉREZ-LOSADA, J. 2017b. MicroRNA (miR)-203 and miR-205 expression patterns

identify subgroups of prognosis in cutaneous squamous cell carcinoma. *Br J Dermatol,* 177**,** 168-178.
CAÑUETO, J., CARDEÑOSO, E., GARCÍA, J. L., SANTOS-BRIZ, Á., CASTELLANOS-MARTÍN, A., FERNÁNDEZ-LÓPEZ, E., BLANCO GÓMEZ, A., PÉREZ-LOSADA, J. & ROMÁN-CURTO, C. 2017c. Epidermal growth factor receptor expression is associated with poor outcome in cutaneous squamous cell carcinoma. *Br J Dermatol,* 176**,** 1279-1287.
CARLSSON, S. R. & SIMONSEN, A. 2015. Membrane dynamics in autophagosome biogenesis. *J Cell Sci,* 128**,** 193-205.
CARTER, J. B., JOHNSON, M. M., CHUA, T. L., KARIA, P. S. & SCHMULTS, C. D. 2013. Outcomes of primary cutaneous squamous cell carcinoma with perineural invasion: an 11-year cohort study. *JAMA Dermatol,* 149**,** 35-41.
CAVALLARO, U. & CHRISTOFORI, G. 2000. Molecular mechanisms of tumor angiogenesis and tumor progression. *J Neurooncol,* 50**,** 63-70.
CELLI, A., SANCHEZ, S., BEHNE, M., HAZLETT, T., GRATTON, E. & MAURO, T. 2010. The epidermal Ca(2+) gradient: Measurement using the phasor representation of fluorescent lifetime imaging. *Biophys J,* 98**,** 911-21.
CHACKO, B. M., QIN, B. Y., TIWARI, A., SHI, G., LAM, S., HAYWARD, L. J., DE CAESTECKER, M. & LIN, K. 2004. Structural basis of heteromeric smad protein assembly in TGF-beta signaling. *Mol Cell,* 15**,** 813-23.
CHAFFER, C. L. & WEINBERG, R. A. 2011. A perspective on cancer cell metastasis. *Science,* 331**,** 1559-64.
CHAREST, J. L., JENNINGS, J. M., KING, W. P., KOWALCZYK, A. P. & GARCÍA, A. J. 2009. Cadherin-mediated cell-cell contact regulates keratinocyte differentiation. *J Invest Dermatol,* 129**,** 564-72.
CHEN, G., ZHAO, X., TAN, Z., WANG, D., LUO, D., ZHANG, P., CAO, J., WANG, F., LIU, Q. & LI, L. 2018. Investigation of the role of cullin 4A overexpression in human liver cancer. *Mol Med Rep,* 18**,** 2531-2540.
CHEN, M. K., CAI, M. Y., LUO, R. Z., TIAN, X., LIAO, Q. M., ZHANG, X. Y. & HAN, J. D. 2015. Overexpression of p300 correlates with poor prognosis in patients with cutaneous squamous cell carcinoma. *Br J Dermatol,* 172**,** 111-9.
CHOI, A. M., RYTER, S. W. & LEVINE, B. 2013. Autophagy in human health and disease. *N Engl J Med,* 368**,** 651-62.
CIANFANELLI, V., D'ORAZIO, M. & CECCONI, F. 2015a. AMBRA1 and BECLIN 1 interplay in the crosstalk between autophagy and cell proliferation. *Cell Cycle,* 14**,** 959-63.
CIANFANELLI, V., DE ZIO, D., DI BARTOLOMEO, S., NAZIO, F., STRAPPAZZON, F. & CECCONI, F. 2015b. Ambra1 at a glance. *J Cell Sci,* 128**,** 2003-8.
CIANFANELLI, V., FUOCO, C., LORENTE, M., SALAZAR, M., QUONDAMATTEO, F., GHERARDINI, P. F., DE ZIO, D., NAZIO, F., ANTONIOLI, M., D'ORAZIO, M., SKOBO, T., BORDI, M., ROHDE, M., DALLA VALLE, L., HELMER-CITTERICH, M., GRETZMEIER, C., DENGJEL, J., FIMIA, G. M., PIACENTINI, M., DI BARTOLOMEO, S., VELASCO, G. & CECCONI, F. 2015c. AMBRA1 links autophagy to cell proliferation and tumorigenesis by promoting c-Myc dephosphorylation and degradation. *Nat Cell Biol,* 17**,** 706.
CIANFANELLI, V., NAZIO, F. & CECCONI, F. 2015d. Connecting autophagy: AMBRA1 and its network of regulation. *Mol Cell Oncol,* 2**,** e970059.
CLAERHOUT, S., VERSCHOOTEN, L., VAN KELST, S., DE VOS, R., PROBY, C., AGOSTINIS, P. & GARMYN, M. 2010. Concomitant inhibition of AKT and autophagy is required for efficient cisplatin-induced apoptosis of metastatic skin carcinoma. *Int J Cancer,* 127**,** 2790-803.
CONACCI-SORRELL, M. & EISENMAN, R. N. 2011. Post-translational control of Myc function during differentiation. *Cell Cycle,* 10**,** 604-10.
CORCHADO-COBOS, R., GARCÍA-SANCHA, N., GONZÁLEZ-SARMIENTO, R., PÉREZ-LOSADA, J. & CAÑUETO, J. 2020. Cutaneous Squamous Cell Carcinoma: From Biology to Therapy. *Int J Mol Sci,* 21.
COSGAREA, I., MCCONNELL, A. T., EWEN, T., TANG, D., HILL, D. S., ANAGNOSTOU, M., ELIAS, M., ELLIS, R. A., MURRAY, A., SPENDER, L. C., GIGLIO, P., GAGLIARDI,

M., GREENWOOD, A., PIACENTINI, M., INMAN, G. J., FIMIA, G., CORAZZARI, M., ARMSTRONG, J. L. & LOVAT, P. E. 2021. Melanoma secretion of TGFβ-2 leads to loss of epidermal AMBRA1 threatening epidermal integrity and facilitating tumour ulceration. *Br J Dermatol*. Available at: 10.1111/bjd.20889

CUI, C. Y. & SCHLESSINGER, D. 2015. Eccrine sweat gland development and sweat secretion. *Exp Dermatol,* 24**,** 644-50.

CUI, W., FOWLIS, D. J., BRYSON, S., DUFFIE, E., IRELAND, H., BALMAIN, A. & AKHURST, R. J. 1996. TGFβ1 Inhibits the Formation of Benign Skin Tumors, but Enhances Progression to Invasive Spindle Carcinomas in Transgenic Mice. *Cell,* 86**,** 531-542.

CUI, W., FOWLIS, D. J., COUSINS, F. M., DUFFIE, E., BRYSON, S., BALMAIN, A. & AKHURST, R. J. 1995. Concerted action of TGF-beta 1 and its type II receptor in control of epidermal homeostasis in transgenic mice. *Genes Dev,* 9**,** 945-55.

CUMSKY, H. J. L., COSTELLO, C. M., ZHANG, N., BUTTERFIELD, R., BURAS, M. R., SCHMIDT, J. E., DRENNER, K., NELSON, S. A., OCHOA, S. A., BAUM, C. L., PITTELKOW, M. R., DICAUDO, D. J., SEKULIC, A. & MANGOLD, A. R. 2019. The prognostic value of inositol polyphosphate 5-phosphatase in cutaneous squamous cell carcinoma. *J Am Acad Dermatol,* 80**,** 626-632.e1.

CUST, A. E. 2017. Estimating the future health service burden of keratinocyte cancers in the U.K. *Br J Dermatol,* 176**,** 1107-1108.

D'ERRICO, M., CALCAGNILE, A., CANZONA, F., DIDONA, B., POSTERARO, P., CAVALIERI, R., CORONA, R., VORECHOVSKY, I., NARDO, T., STEFANINI, M. & DOGLIOTTI, E. 2000. UV mutation signature in tumor suppressor genes involved in skin carcinogenesis in xeroderma pigmentosum patients. *Oncogene,* 19**,** 463-7.

DAHL, M. V. 2012. Stem cells and the skin. *J Cosmet Dermatol,* 11**,** 297-306.

DALLAGLIO, K., PETRACHI, T., MARCONI, A., TRUZZI, F., LOTTI, R., SALTARI, A., MORANDI, P., PUVIANI, M., MAIORANA, A., ROOP, D. R. & PINCELLI, C. 2013. Isolation and characterization of squamous cell carcinoma-derived stem-like cells: role in tumor formation. *Int J Mol Sci,* 14**,** 19540-55.

DELVA, E., TUCKER, D. K. & KOWALCZYK, A. P. 2009. The desmosome. *Cold Spring Harb Perspect Biol,* 1**,** a002543.

DENK, H., STUMPTNER, C., ABUJA, P. M. & ZATLOUKAL, K. 2019. Sequestosome 1/p62-related pathways as therapeutic targets in hepatocellular carcinoma. *Expert Opin Ther Targets,* 23**,** 393-406.

DERYNCK, R. & BUDI, E. H. 2019. Specificity, versatility, and control of TGF-β family signaling. *Sci Signal,* 12.

DERYNCK, R. & ZHANG, Y. E. 2003. Smad-dependent and Smad-independent pathways in TGF-β family signalling. *Nature,* 425**,** 577-584.

DIKIC, I. 2017. Proteasomal and Autophagic Degradation Systems. *Annu Rev Biochem,* 86**,** 193-224.

DING, Y. & CHOI, M. E. 2014. Regulation of autophagy by TGF-β: emerging role in kidney fibrosis. *Semin Nephrol,* 34**,** 62-71.

DING, Y., KIM, J. K., KIM, S. I., NA, H. J., JUN, S. Y., LEE, S. J. & CHOI, M. E. 2010. TGF-{beta}1 protects against mesangial cell apoptosis via induction of autophagy. *J Biol Chem,* 285**,** 37909-19.

DONG, X., ZHAO, B., IACOB, R. E., ZHU, J., KOKSAL, A. C., LU, C., ENGEN, J. R. & SPRINGER, T. A. 2017. Force interacts with macromolecular structure in activation of TGF-β. *Nature,* 542**,** 55-59.

DOOLEY, H. C., RAZI, M., POLSON, H. E., GIRARDIN, S. E., WILSON, M. I. & TOOZE, S. A. 2014. WIPI2 links LC3 conjugation with PI3P, autophagosome formation, and pathogen clearance by recruiting Atg12-5-16L1. *Mol Cell,* 55**,** 238-52.

DOTTO, G. P. & RUSTGI, A. K. 2016. Squamous Cell Cancers: A Unified Perspective on Biology and Genetics. *Cancer Cell,* 29**,** 622-637.

DOUKI, T., REYNAUD-ANGELIN, A., CADET, J. & SAGE, E. 2003. Bipyrimidine photoproducts rather than oxidative lesions are the main type of DNA damage involved in the genotoxic effect of solar UVA radiation. *Biochemistry,* 42 30**,** 9221-6.

DRISKELL, R. R., LICHTENBERGER, B. M., HOSTE, E., KRETZSCHMAR, K., SIMONS, B. D., CHARALAMBOUS, M., FERRON, S. R., HERAULT, Y., PAVLOVIC, G., FERGUSON-SMITH, A. C. & WATT, F. M. 2013. Distinct fibroblast lineages determine dermal architecture in skin development and repair. *Nature,* 504**,** 277-281.

DUAN, G. & WALTHER, D. 2015. The roles of post-translational modifications in the context of protein interaction networks. *PLoS Comput Biol,* 11**,** e1004049.

DUBOIS, C., PREVARSKAYA, N. & VANDEN ABEELE, F. 2016. The calcium-signaling toolkit: Updates needed. *Biochim Biophys Acta,* 1863**,** 1337-43.

DYCZYNSKI, M., YU, Y., OTROCKA, M., PARPAL, S., BRAGA, T., HENLEY, A. B., ZAZZI, H., LERNER, M., WENNERBERG, K., VIKLUND, J., MARTINSSON, J., GRANDER, D., DE MILITO, A. & POKROVSKAJA TAMM, K. 2018. Targeting autophagy by small molecule inhibitors of vacuolar protein sorting 34 (Vps34) improves the sensitivity of breast cancer cells to Sunitinib. *Cancer Lett,* 435**,** 32-43.

ECKHART, L., LIPPENS, S., TSCHACHLER, E. & DECLERCQ, W. 2013. Cell death by cornification. *Biochim Biophys Acta,* 1833**,** 3471-3480.

ELIAS, P. M. 2005. Stratum corneum defensive functions: an integrated view. *J Invest Dermatol,* 125**,** 183-200.

ELIAS, P. M., CULLANDER, C., MAURO, T., RASSNER, U., KOMUVES, L., BROWN, B. E. & MENON, G. K. 1998. The secretory granular cell: the outermost granular cell as a specialized secretory cell. *J Investig Dermatol Symp Proc,* 3**,** 87-100.

ELLIS, R., TANG, D., NASR, B., GREENWOOD, A., MCCONNELL, A., ANAGNOSTOU, M. E., ELIAS, M., VERYKIOU, S., BAJWA, D., EWEN, T., REYNOLDS, N. J., BARRETT, P., CARLING, E., WATSON, G., ARMSTRONG, J., ALLEN, A. J., HORSWELL, S., LABUS, M. & LOVAT, P. E. 2020. Epidermal AMBRA1 and Loricrin; a paradigm shift in the prognostication and stratification of AJCC stage I melanomas. *Br J Dermatol,* 182(1)**,** 156-165.

ELLIS, R. A., HORSWELL, S., NESS, T., LUMSDON, J., TOOZE, S. A., KIRKHAM, N., ARMSTRONG, J. L. & LOVAT, P. E. 2014. Prognostic impact of p62 expression in cutaneous malignant melanoma. *J Invest Dermatol,* 134**,** 1476-1478.

ELSHOLZ, F., HARTENECK, C., MULLER, W. & FRIEDLAND, K. 2014. Calcium--a central regulator of keratinocyte differentiation in health and disease. *Eur J Dermatol,* 24**,** 650-61.

ENDRIZZI, B., AHMED, R. L., RAY, T., DUDEK, A. & LEE, P. 2013. Capecitabine to reduce nonmelanoma skin carcinoma burden in solid organ transplant recipients. *Dermatol Surg,* 39**,** 634-45.

FARRELL, A. S. & SEARS, R. C. 2014. MYC degradation. *Cold Spring Harb Perspect Med,* 4.

FENG, Y., HE, D., YAO, Z. & KLIONSKY, D. J. 2014. The machinery of macroautophagy. *Cell Res,* 24**,** 24-41.

FIMIA, G. M., CORAZZARI, M., ANTONIOLI, M. & PIACENTINI, M. 2013. Ambra1 at the crossroad between autophagy and cell death. *Oncogene,* 32**,** 3311-8.

FIMIA, G. M., STOYKOVA, A., ROMAGNOLI, A., GIUNTA, L., DI BARTOLOMEO, S., NARDACCI, R., CORAZZARI, M., FUOCO, C., UCAR, A., SCHWARTZ, P., GRUSS, P., PIACENTINI, M., CHOWDHURY, K. & CECCONI, F. 2007. Ambra1 regulates autophagy and development of the nervous system. *Nature,* 447**,** 1121-5.

FRIEDMAN, H. I., COOPER, P. H. & WANEBO, H. J. 1985. Prognostic and therapeutic use of microstaging of cutaneous squamous cell carcinoma of the trunk and extremities. *Cancer,* 56**,** 1099-105.

FUNG, C., LOCK, R., GAO, S., SALAS, E. & DEBNATH, J. 2008. Induction of autophagy during extracellular matrix detachment promotes cell survival. *Mol Biol Cell,* 19**,** 797-806.

GANDARILLAS, A. & WATT, F. M. 1997. c-Myc promotes differentiation of human epidermal stem cells. *Genes Dev,* 11**,** 2869-82.

GE, G. & GREENSPAN, D. S. 2006a. BMP1 controls TGFbeta1 activation via cleavage of latent TGFbeta-binding protein. *J Cell Biol,* 175**,** 111-20.

GE, G. & GREENSPAN, D. S. 2006b. Developmental roles of the BMP1/TLD metalloproteinases. *Birth Defects Res C Embryo Today,* 78**,** 47-68.

GELLIBERT, F., WOOLVEN, J., FOUCHET, M. H., MATHEWS, N., GOODLAND, H., LOVEGROVE, V., LAROZE, A., NGUYEN, V. L., SAUTET, S., WANG, R., JANSON, C., SMITH, W., KRYSA, G., BOULLAY, V., DE GOUVILLE, A. C., HUET, S. & HARTLEY, D. 2004. Identification of 1,5-naphthyridine derivatives as a novel series of potent and selective TGF-beta type I receptor inhibitors. *J Med Chem,* 47**,** 4494-506.

GHADIALLY, R. 2012. 25 years of epidermal stem cell research. *J Invest Dermatol,* 132**,** 797-810.

GHAVAMI, S., YEGANEH, B., ZEKI, A. A., SHOJAEI, S., KENYON, N. J., OTT, S., SAMALI, A., PATTERSON, J., ALIZADEH, J., MOGHADAM, A. R., DIXON, I. M. C., UNRUH, H., KNIGHT, D. A., POST, M., KLONISCH, T. & HALAYKO, A. J. 2018. Autophagy and the unfolded protein response promote profibrotic effects of TGF-β(1) in human lung fibroblasts. *Am J Physiol Lung Cell Mol Physiol,* 314**,** L493-l504.

GIATROMANOLAKI, A., KOUKOURAKIS, M. I., HARRIS, A. L., POLYCHRONIDIS, A., GATTER, K. C. & SIVRIDIS, E. 2010. Prognostic relevance of light chain 3 (LC3A) autophagy patterns in colorectal adenocarcinomas. *J Clin Pathol,* 63**,** 867-72.

GLICK, A. B. 2012. The Role of TGFβ Signaling in Squamous Cell Cancer: Lessons from Mouse Models. *J Skin Cancer,* 2012**,** 249063.

GOON, P. K. C., GREENBERG, D. C., IGALI, L. & LEVELL, N. J. 2017. Predicted cases of U.K. skin squamous cell carcinoma and basal cell carcinoma in 2020 and 2025: horizon planning for National Health Service dermatology and dermatopathology. *Br J Dermatol,* 176**,** 1351-1353.

GOUMANS, M. J., VALDIMARSDOTTIR, G., ITOH, S., LEBRIN, F., LARSSON, J., MUMMERY, C., KARLSSON, S. & TEN DIJKE, P. 2003. Activin receptor-like kinase (ALK)1 is an antagonistic mediator of lateral TGFbeta/ALK5 signaling. *Mol Cell,* 12**,** 817-28.

GREAVES, M. & MALEY, C. C. 2012. Clonal evolution in cancer. *Nature,* 481**,** 306-13.

GREEN, A. 2021. The Prognostic Impact of Autophagy Biomarkers for Skin Cancer. *MPhil Thesis, Newcaslte University, Newcastle upon Tyne*.

GROPPE, J., HINCK, C. S., SAMAVARCHI-TEHRANI, P., ZUBIETA, C., SCHUERMANN, J. P., TAYLOR, A. B., SCHWARZ, P. M., WRANA, J. L. & HINCK, A. P. 2008. Cooperative assembly of TGF-beta superfamily signaling complexes is mediated by two disparate mechanisms and distinct modes of receptor binding. *Mol Cell,* 29**,** 157-68.

GUDJONSSON, T., VILLADSEN, R., NIELSEN, H. L., RØNNOV-JESSEN, L., BISSELL, M. J. & PETERSEN, O. W. 2002. Isolation, immortalization, and characterization of a human breast epithelial cell line with stem cell properties. *Genes Dev,* 16**,** 693-706.

GWINN, D. M., SHACKELFORD, D. B., EGAN, D. F., MIHAYLOVA, M. M., MERY, A., VASQUEZ, D. S., TURK, B. E. & SHAW, R. J. 2008. AMPK phosphorylation of raptor mediates a metabolic checkpoint. *Mol Cell,* 30**,** 214-26.

HANAHAN, D. & WEINBERG, R. A. 2000. The hallmarks of cancer. *Cell,* 100**,** 57-70.

HANAHAN, D. & WEINBERG, R. A. 2011. Hallmarks of cancer: the next generation. *Cell,* 144**,** 646-74.

HARDIE, D. G. 2011. AMP-activated protein kinase: an energy sensor that regulates all aspects of cell function. *Genes Dev,* 25**,** 1895-908.

HARRIS, B. N., BAYOUMI, A., RAO, S., MOORE, M. G., FARWELL, D. G. & BEWLEY, A. F. 2017. Factors Associated with Recurrence and Regional Adenopathy for Head and Neck Cutaneous Squamous Cell Carcinoma. *Otolaryngol Head Neck Surg,* 156**,** 863-869.

HARTEVELT, M. M., BAVINCK, J. N., KOOTTE, A. M., VERMEER, B. J. & VANDENBROUCKE, J. P. 1990. Incidence of skin cancer after renal transplantation in The Netherlands. *Transplantation,* 49**,** 506-9.

HARUNA, K., SUGA, Y., MURAMATSU, S., TANEDA, K., MIZUNO, Y., IKEDA, S., UENO, T., KOMINAMI, E., TANIDA, I., TANIDA, I. & HANADA, K. 2008. Differentiation-specific expression and localization of an autophagosomal marker protein (LC3) in human epidermal keratinocytes. *J Dermatol Sci,* 52**,** 213-5.

HE, Y. J., MCCALL, C. M., HU, J., ZENG, Y. & XIONG, Y. 2006. DDB1 functions as a linker to recruit receptor WD40 proteins to CUL4-ROC1 ubiquitin ligases. *Genes Dev,* 20**,** 2949-54.

HELDIN, C. H., MIYAZONO, K. & TEN DIJKE, P. 1997. TGF-beta signalling from cell membrane to nucleus through SMAD proteins. *Nature,* 390**,** 465-71.

HELDIN, C. H. & MOUSTAKAS, A. 2016. Signaling Receptors for TGF-β Family Members. *Cold Spring Harb Perspect Biol,* 8.

HEMMATI-BRIVANLOU, A., KELLY, O. G. & MELTON, D. A. 1994. Follistatin, an antagonist of activin, is expressed in the Spemann organizer and displays direct neuralizing activity. *Cell,* 77**,** 283-95.

HINCK, A. P., MUELLER, T. D. & SPRINGER, T. A. 2016. Structural Biology and Evolution of the TGF-β Family. *Cold Spring Harb Perspect Biol,* 8.

HOHL, D., RUF OLANO, B., DE VIRAGH, P. A., HUBER, M., DETRISAC, C. J., SCHNYDER, U. W. & ROOP, D. R. 1993. Expression patterns of loricrin in various species and tissues. *Differentiation,* 54**,** 25-34.

HOOVER, E. & KRISHNAMURTHY, K. 2019. Physiology, Sebaceous Glands. *StatPearls.* Treasure Island (FL): StatPearls Publishing

StatPearls Publishing LLC.

HORSLEY, V., O'CARROLL, D., TOOZE, R., OHINATA, Y., SAITOU, M., OBUKHANYCH, T., NUSSENZWEIG, M., TARAKHOVSKY, A. & FUCHS, E. 2006. Blimp1 defines a progenitor population that governs cellular input to the sebaceous gland. *Cell,* 126**,** 597-609.

HØYER-HANSEN, M. & JÄÄTTELÄ, M. 2007. Connecting endoplasmic reticulum stress to autophagy by unfolded protein response and calcium. *Cell Death Differ,* 14**,** 1576-82.

HUANG, T., SONG, X., YANG, Y., WAN, X., ALVAREZ, A. A., SASTRY, N., FENG, H., HU, B. & CHENG, S. Y. 2018. Autophagy and Hallmarks of Cancer. *Crit Rev Oncog,* 23**,** 247-267.

HUNG, M. S., CHEN, I. C., YOU, L., JABLONS, D. M., LI, Y. C., MAO, J. H., XU, Z., LUNG, J. H., YANG, C. T. & LIU, S. T. 2016. Knockdown of cullin 4A inhibits growth and increases chemosensitivity in lung cancer cells. *J Cell Mol Med,* 20**,** 1295-306.

INMAN, G. J., WANG, J., NAGANO, A., ALEXANDROV, L. B., PURDIE, K. J., TAYLOR, R. G., SHERWOOD, V., THOMSON, J., HOGAN, S., SPENDER, L. C., SOUTH, A. P., STRATTON, M., CHELALA, C., HARWOOD, C. A., PROBY, C. M. & LEIGH, I. M. 2018. The genomic landscape of cutaneous SCC reveals drivers and a novel azathioprine associated mutational signature. *Nature Communications,* 9**,** 3667.

JAHN, S. W., PLASS, M. & MOINFAR, F. 2020. Digital Pathology: Advantages, Limitations and Emerging Perspectives. *J Clin Med,* 9.

JAIN, A., LAMARK, T., SJØTTEM, E., LARSEN, K. B., AWUH, J. A., ØVERVATN, A., MCMAHON, M., HAYES, J. D. & JOHANSEN, T. 2010. p62/SQSTM1 is a target gene for transcription factor NRF2 and creates a positive feedback loop by inducing antioxidant response element-driven gene transcription. *J Biol Chem,* 285**,** 22576-91.

JAKS, V., BARKER, N., KASPER, M., VAN ES, J. H., SNIPPERT, H. J., CLEVERS, H. & TOFTGÅRD, R. 2008. Lgr5 marks cycling, yet long-lived, hair follicle stem cells. *Nat Genet,* 40**,** 1291-9.

JAVELAUD, D. & MAUVIEL, A. 2005. Crosstalk mechanisms between the mitogen-activated protein kinase pathways and Smad signaling downstream of TGF-beta: implications for carcinogenesis. *Oncogene,* 24**,** 5742-50.

JENSEN, P., MOLLER, B. & HANSEN, S. 2000. Skin cancer in kidney and heart transplant recipients and different long-term immunosuppressive therapy regimens. *J Am Acad Dermatol,* 42**,** 307.

JI, A. L., RUBIN, A. J., THRANE, K., JIANG, S., REYNOLDS, D. L., MEYERS, R. M., GUO, M. G., GEORGE, B. M., MOLLBRINK, A., BERGENSTRÅHLE, J., LARSSON, L., BAI, Y., ZHU, B., BHADURI, A., MEYERS, J. M., ROVIRA-CLAVÉ, X., HOLLMIG, S. T., AASI, S. Z., NOLAN, G. P., LUNDEBERG, J. & KHAVARI, P. A. 2020. Multimodal Analysis of Composition and Spatial Architecture in Human Squamous Cell Carcinoma. *Cell,* 182**,** 497-514.e22.

JOHNSON, C. E. & TEE, A. R. 2017. Exploiting cancer vulnerabilities: mTOR, autophagy, and homeostatic imbalance. *Essays Biochem,* 61**,** 699-710.

JU, W., LUO, X. & ZHANG, N. 2019. LncRNA NEF inhibits migration and invasion of HPV-negative cervical squamous cell carcinoma by inhibiting TGF-β pathway. *Biosci Rep,* 39 (4): BSR20180878.

KADANDALE, P., STENDER, J. D., GLASS, C. K. & KIGER, A. A. 2010. Conserved role for autophagy in Rho1-mediated cortical remodeling and blood cell recruitment. *Proc Natl Acad Sci U S A,* 107**,** 10502-7.

KAMARUDIN, A. N., COX, T. & KOLAMUNNAGE-DONA, R. 2017. Time-dependent ROC curve analysis in medical research: current methods and applications. *BMC Med Res Methodol,* 17**,** 53.

KANAYAMA, M., INOUE, M., DANZAKI, K., HAMMER, G., HE, Y. W. & SHINOHARA, M. L. 2015. Autophagy enhances NFκB activity in specific tissue macrophages by sequestering A20 to boost antifungal immunity. *Nat Commun,* 6**,** 5779.

KANG, J. I., KIM, D. H., SUNG, K. W., SHIM, S. M., CHA-MOLSTAD, H., SOUNG, N. K., LEE, K. H., HWANG, J., LEE, H. G., KWON, Y. T. & KIM, B. Y. 2021. p62-Induced Cancer-Associated Fibroblast Activation via the Nrf2-ATF6 Pathway Promotes Lung Tumorigenesis. *Cancers (Basel),* 13(4)**,** 864.

KANIA, E., PAJĄK, B. & ORZECHOWSKI, A. 2015. Calcium homeostasis and ER stress in control of autophagy in cancer cells. *Biomed Res Int,* 2015**,** 352794.

KARANASIOS, E., STAPLETON, E., MANIFAVA, M., KAIZUKA, T., MIZUSHIMA, N., WALKER, S. A. & KTISTAKIS, N. T. 2013. Dynamic association of the ULK1 complex with omegasomes during autophagy induction. *J Cell Sci,* 126**,** 5224-38.

KARIA, P. S., JAMBUSARIA-PAHLAJANI, A., HARRINGTON, D. P., MURPHY, G. F., QURESHI, A. A. & SCHMULTS, C. D. 2014. Evaluation of American Joint Committee on Cancer, International Union Against Cancer, and Brigham and Women's Hospital tumor staging for cutaneous squamous cell carcinoma. *J Clin Oncol,* 32**,** 327-34.

KATSURAGI, Y., ICHIMURA, Y. & KOMATSU, M. 2015. p62/SQSTM1 functions as a signaling hub and an autophagy adaptor. *Febs j,* 282**,** 4672-8.

KAUSHIK, S. & CUERVO, A. M. 2018. The coming of age of chaperone-mediated autophagy. *Nat Rev Mol Cell Biol,* 19**,** 365-381.

KE, Y. & WANG, X. J. 2021. TGFβ Signaling in Photoaging and UV-Induced Skin Cancer. *J Invest Dermatol,* 141**,** 1104-1110.

KENIFIC, C. M., THORBURN, A. & DEBNATH, J. 2010. Autophagy and metastasis: another double-edged sword. *Curr Opin Cell Biol,* 22**,** 241-5.

KHANSUR, T. & KENNEDY, A. 1991. Cisplatin and 5-fluorouracil for advanced locoregional and metastatic squamous cell carcinoma of the skin. *Cancer,* 67**,** 2030-2.

KIM, D. J., LEE, M. H., LIU, K., LIM, D. Y., ROH, E., CHEN, H., KIM, S. H., SHIM, J. H., KIM, M. O., LI, W., MA, F., FREDIMOSES, M., BODE, A. M. & DONG, Z. 2017. Herbacetin suppresses cutaneous squamous cell carcinoma and melanoma cell growth by targeting AKT and ODC. *Carcinogenesis,* 38**,** 1136-1146.

KIM, J., KIM, Y. C., FANG, C., RUSSELL, R. C., KIM, J. H., FAN, W., LIU, R., ZHONG, Q. & GUAN, K. L. 2013a. Differential regulation of distinct Vps34 complexes by AMPK in nutrient stress and autophagy. *Cell,* 152**,** 290-303.

KIM, J., KUNDU, M., VIOLLET, B. & GUAN, K. L. 2011. AMPK and mTOR regulate autophagy through direct phosphorylation of Ulk1. *Nat Cell Biol,* 13**,** 132-41.

KIM, J. S., BAE, G. E., KIM, K. H., LEE, S. I., CHUNG, C., LEE, D., LEE, T. H., KWON, I. S. & YEO, M. K. 2019. Prognostic Significance of LC3B and p62/SQSTM1 Expression in Gastric Adenocarcinoma. *Anticancer Res,* 39**,** 6711-6722.

KIM, K. H. & LEE, M. S. 2014. Autophagy--a key player in cellular and body metabolism. *Nat Rev Endocrinol,* 10**,** 322-37.

KIM, K. W., PAUL, P., QIAO, J., LEE, S. & CHUNG, D. H. 2013b. Enhanced autophagy blocks angiogenesis via degradation of gastrin-releasing peptide in neuroblastoma cells. *Autophagy,* 9**,** 1579-90.

KIMURA, T., TAKABATAKE, Y., TAKAHASHI, A. & ISAKA, Y. 2013. Chloroquine in cancer therapy: a double-edged sword of autophagy. *Cancer Res,* 73**,** 3-7.

KIYONO, K., SUZUKI, H. I., MATSUYAMA, H., MORISHITA, Y., KOMURO, A., KANO, M. R., SUGIMOTO, K. & MIYAZONO, K. 2009. Autophagy is activated by TGF-beta and potentiates TGF-beta-mediated growth inhibition in human hepatocellular carcinoma cells. *Cancer Res,* 69**,** 8844-52.

KLIONSKY, D. J., ABDALLA, F. C., ABELIOVICH, H., ABRAHAM, R. T., ACEVEDO-AROZENA, A., ADELI, K., AGHOLME, L., AGNELLO, M., AGOSTINIS, P., AGUIRRE-GHISO, J. A., AHN, H. J., AIT-MOHAMED, O., AIT-SI-ALI, S., AKEMATSU, T., AKIRA, S., AL-YOUNES, H. M., AL-ZEER, M. A., ALBERT, M. L., ALBIN, R. L., ALEGRE-ABARRATEGUI, J., ALEO, M. F., ALIREZAEI, M., ALMASAN, A., ALMONTE-BECERRIL, M., AMANO, A., AMARAVADI, R., AMARNATH, S., AMER, A. O., ANDRIEU-ABADIE, N., ANANTHARAM, V., ANN, D. K., ANOOPKUMAR-DUKIE, S., AOKI, H., APOSTOLOVA, N., ARANCIA, G., ARIS, J. P., ASANUMA, K., ASARE, N. Y., ASHIDA, H., ASKANAS, V., ASKEW, D. S., AUBERGER, P., BABA, M., BACKUES, S. K., BAEHRECKE, E. H., BAHR, B. A., BAI, X. Y., BAILLY, Y., BAIOCCHI, R., BALDINI, G., BALDUINI, W., BALLABIO, A., BAMBER, B. A., BAMPTON, E. T., BÁNHEGYI, G., BARTHOLOMEW, C. R., BASSHAM, D. C., BAST, R. C., JR., BATOKO, H., BAY, B. H., BEAU, I., BÉCHET, D. M., BEGLEY, T. J., BEHL, C., BEHRENDS, C., BEKRI, S., BELLAIRE, B., BENDALL, L. J., BENETTI, L., BERLIOCCHI, L., BERNARDI, H., BERNASSOLA, F., BESTEIRO, S., BHATIA-KISSOVA, I., BI, X., BIARD-PIECHACZYK, M., BLUM, J. S., BOISE, L. H., BONALDO, P., BOONE, D. L., BORNHAUSER, B. C., BORTOLUCI, K. R., BOSSIS, I., BOST, F., BOURQUIN, J. P., BOYA, P., BOYER-GUITTAUT, M., BOZHKOV, P. V., BRADY, N. R., BRANCOLINI, C., BRECH, A., BRENMAN, J. E., BRENNAND, A., BRESNICK, E. H., BREST, P., BRIDGES, D., BRISTOL, M. L., BROOKES, P. S., BROWN, E. J., BRUMELL, J. H., et al. 2012. Guidelines for the use and interpretation of assays for monitoring autophagy. *Autophagy,* 8**,** 445-544.

KLIONSKY, D. J., ABDELMOHSEN, K., ABE, A., ABEDIN, M. J., ABELIOVICH, H., ACEVEDO AROZENA, A., ADACHI, H., ADAMS, C. M., ADAMS, P. D., ADELI, K., ADHIHETTY, P. J., ADLER, S. G., AGAM, G., AGARWAL, R., AGHI, M. K., AGNELLO, M., AGOSTINIS, P., AGUILAR, P. V., AGUIRRE-GHISO, J., AIROLDI, E. M., AIT-SI-ALI, S., AKEMATSU, T., AKPORIAYE, E. T., AL-RUBEAI, M., ALBAICETA, G. M., ALBANESE, C., ALBANI, D., ALBERT, M. L., ALDUDO, J., ALGUL, H., ALIREZAEI, M., ALLOZA, I., ALMASAN, A., ALMONTE-BECERIL, M., ALNEMRI, E. S., ALONSO, C., ALTAN-BONNET, N., ALTIERI, D. C., ALVAREZ, S., ALVAREZ-ERVITI, L., ALVES, S., AMADORO, G., AMANO, A., AMANTINI, C., AMBROSIO, S., AMELIO, I., AMER, A. O., AMESSOU, M., AMON, A., AN, Z., ANANIA, F. A., ANDERSEN, S. U., ANDLEY, U. P., ANDREADI, C. K., ANDRIEU-ABADIE, N., ANEL, A., ANN, D. K., ANOOPKUMAR-DUKIE, S., ANTONIOLI, M., AOKI, H., APOSTOLOVA, N., AQUILA, S., AQUILANO, K., ARAKI, K., ARAMA, E., ARANDA, A., ARAYA, J., ARCARO, A., ARIAS, E., ARIMOTO, H., ARIOSA, A. R., ARMSTRONG, J. L., ARNOULD, T., ARSOV, I., ASANUMA, K., ASKANAS, V., ASSELIN, E., ATARASHI, R., ATHERTON, S. S., ATKIN, J. D., ATTARDI, L. D., AUBERGER, P., AUBURGER, G., AURELIAN, L., AUTELLI, R., AVAGLIANO, L., AVANTAGGIATI, M. L., AVRAHAMI, L., AWALE, S., AZAD, N., BACHETTI, T., BACKER, J. M., BAE, D. H., BAE, J. S., BAE, O. N., BAE, S. H., BAEHRECKE, E. H., BAEK, S. H., BAGHDIGUIAN, S., BAGNIEWSKA-ZADWORNA, A., et al. 2016. Guidelines for the use and interpretation of assays for monitoring autophagy (3rd edition). *Autophagy,* 12**,** 1-222.

KNAEVELSRUD, H., SORENG, K., RAIBORG, C., HABERG, K., RASMUSON, F., BRECH, A., LIESTOL, K., RUSTEN, T. E., STENMARK, H., NEUFELD, T. P., CARLSSON, S. R. & SIMONSEN, A. 2013. Membrane remodeling by the PX-BAR protein SNX18 promotes autophagosome formation. *J Cell Biol,* 202**,** 331-49.

KOLLY, C., SUTER, M. M. & MÜLLER, E. J. 2005. Proliferation, Cell Cycle Exit, and Onset of Terminal Differentiation in Cultured Keratinocytes: Pre-Programmed Pathways in Control of C-Myc and Notch1 Prevail Over Extracellular Calcium Signals. *Journal of Investigative Dermatology,* 124**,** 1014-1025.

KOMURO, A., YASHIRO, M., IWATA, C., MORISHITA, Y., JOHANSSON, E., MATSUMOTO, Y., WATANABE, A., ABURATANI, H., MIYOSHI, H., KIYONO, K., SHIRAI, Y. T., SUZUKI, H. I., HIRAKAWA, K., KANO, M. R. & MIYAZONO, K. 2009. Diffuse-type gastric carcinoma: progression, angiogenesis, and transforming growth factor beta signaling. *J Natl Cancer Inst,* 101**,** 592-604.

KREPPEL, M., KRAKOWEZKI, A., KREPPEL, B., DREBBER, U., WEDEMEYER, I., MAUCH, C., ZÖLLER, J. E. & SCHEER, M. 2013. Podoplanin expression in cutaneous head and neck squamous cell carcinoma--prognostic value and clinicopathologic implications. *J Surg Oncol,* 107**,** 376-83.

KRETZSCHMAR, M., DOODY, J., TIMOKHINA, I. & MASSAGUE, J. 1999. A mechanism of repression of TGFbeta/ Smad signaling by oncogenic Ras. *Genes Dev,* 13**,** 804-16.

KRIEGLSTEIN, K., ZHENG, F., UNSICKER, K. & ALZHEIMER, C. 2011. More than being protective: functional roles for TGF-β/activin signaling pathways at central synapses. *Trends Neurosci,* 34**,** 421-9.

KULUNCSICS, Z., PERDIZ, D., BRULAY, E., MUEL, B. & SAGE, E. 1999. Wavelength dependence of ultraviolet-induced DNA damage distribution: involvement of direct or indirect mechanisms and possible artefacts. *J Photochem Photobiol B,* 49**,** 71-80.

KUNZ, J. B., SCHWARZ, H. & MAYER, A. 2004. Determination of four sequential stages during microautophagy in vitro. *J Biol Chem,* 279**,** 9987-96.

KYPRIOTOU, M., HUBER, M. & HOHL, D. 2012. The human epidermal differentiation complex: cornified envelope precursors, S100 proteins and the 'fused genes' family. *Exp Dermatol,* 21**,** 643-9.

LAI-CHEONG, J. E. & MCGRATH, J. A. 2009. Structure and function of skin, hair and nails. *Medicine,* 37**,** 3.

LAMARK, T., SVENNING, S. & JOHANSEN, T. 2017. Regulation of selective autophagy: the p62/SQSTM1 paradigm. *Essays Biochem,* 61**,** 609-624.

LAMOUILLE, S., XU, J. & DERYNCK, R. 2014. Molecular mechanisms of epithelial-mesenchymal transition. *Nat Rev Mol Cell Biol,* 15**,** 178-96.

LAPLANTE, M. & SABATINI, D. M. 2012. mTOR signaling in growth control and disease. *Cell,* 149**,** 274-93.

LAWRENCE F. EICHENFIELD, I. J. F., ERIN MATHES, ANDREA ZAENGLEIN, NANCY B. ESTERLY 2001. *Neonatal Dermatology*. 2nd edn. Philadelphia: Saunders.

LAZOVA, R., CAMP, R. L., KLUMP, V., SIDDIQUI, S. F., AMARAVADI, R. K. & PAWELEK, J. M. 2012. Punctate LC3B expression is a common feature of solid tumors and associated with proliferation, metastasis, and poor outcome. *Clin Cancer Res,* 18**,** 370-9.

LEE, M. K., PARDOUX, C., HALL, M. C., LEE, P. S., WARBURTON, D., QING, J., SMITH, S. M. & DERYNCK, R. 2007. TGF-beta activates Erk MAP kinase signalling through direct phosphorylation of ShcA. *Embo j,* 26**,** 3957-67.

LEI, C., ZHAO, B., LIU, L., ZENG, X., YU, Z. & WANG, X. 2020. Expression and clinical significance of p62 protein in colon cancer. *Medicine (Baltimore),* 99**,** e18791.

LEVINE, B. & KROEMER, G. 2008. Autophagy in the pathogenesis of disease. *Cell,* 132**,** 27-42.

LEVY, J. M. M., TOWERS, C. G. & THORBURN, A. 2017. Targeting autophagy in cancer. *Nat Rev Cancer,* 17**,** 528-542.

LEWIS, C. M., GLISSON, B. S., FENG, L., WAN, F., TANG, X., WISTUBA, II, EL-NAGGAR, A. K., ROSENTHAL, D. I., CHAMBERS, M. S., LUSTIG, R. A. & WEBER, R. S. 2012. A phase II study of gefitinib for aggressive cutaneous squamous cell carcinoma of the head and neck. *Clin Cancer Res,* 18**,** 1435-46.

LEWIS, K. G., LEWIS, M. D., ROBINSON-BOSTOM, L. & PAN, T. D. 2004. Inflammation of actinic keratoses during capecitabine therapy. *Arch Dermatol,* 140**,** 367-8.

LI, D., HE, C., YE, F., YE, E., HE, H., CHEN, G. & ZHANG, J. 2021. p62 Overexpression Promotes Bone Metastasis of Lung Adenocarcinoma out of LC3-Dependent Autophagy. *Front Oncol,* 11**,** 609548.

LI, J., YANG, B., ZHOU, Q., WU, Y., SHANG, D., GUO, Y., SONG, Z., ZHENG, Q. & XIONG, J. 2013. Autophagy promotes hepatocellular carcinoma cell invasion through activation of epithelial-mesenchymal transition. *Carcinogenesis,* 34**,** 1343-51.

LI, M. O. & FLAVELL, R. A. 2008. TGF-beta: a master of all T cell trades. *Cell,* 134**,** 392-404.
LI, W., NIE, T., XU, H., YANG, J., YANG, Q. & MAO, Z. 2019. Chaperone-mediated autophagy: Advances from bench to bedside. *Neurobiol Dis,* 122**,** 41-48.
LI, W. W., LI, J. & BAO, J. K. 2012. Microautophagy: lesser-known self-eating. *Cell Mol Life Sci,* 69**,** 1125-36.
LI, X., ZHANG, L., YU, L., WEI, W., LIN, X., HOU, X. & TIAN, Y. 2016. shRNA-mediated AMBRA1 knockdown reduces the cisplatin-induced autophagy and sensitizes ovarian cancer cells to cisplatin. *J Toxicol Sci,* 41**,** 45-53.
LIANG, X. H., JACKSON, S., SEAMAN, M., BROWN, K., KEMPKES, B., HIBSHOOSH, H. & LEVINE, B. 1999. Induction of autophagy and inhibition of tumorigenesis by beclin 1. *Nature,* 402**,** 672-6.
LINARES, J. F., DURAN, A., REINA-CAMPOS, M., AZA-BLANC, P., CAMPOS, A., MOSCAT, J. & DIAZ-MECO, M. T. 2015. Amino Acid Activation of mTORC1 by a PB1-Domain-Driven Kinase Complex Cascade. *Cell Rep,* 12**,** 1339-52.
LINARES, J. F., DURAN, A., YAJIMA, T., PASPARAKIS, M., MOSCAT, J. & DIAZ-MECO, M. T. 2013. K63 polyubiquitination and activation of mTOR by the p62-TRAF6 complex in nutrient-activated cells. *Mol Cell,* 51**,** 283-96.
LIU-SMITH, F., JIA, J. & ZHENG, Y. 2017. UV-Induced Molecular Signaling Differences in Melanoma and Non-melanoma Skin Cancer. *Adv Exp Med Biol,* 996**,** 27-40.
LIU, I. M., SCHILLING, S. H., KNOUSE, K. A., CHOY, L., DERYNCK, R. & WANG, X. F. 2009a. TGFbeta-stimulated Smad1/5 phosphorylation requires the ALK5 L45 loop and mediates the pro-migratory TGFbeta switch. *Embo j,* 28**,** 88-98.
LIU, J., CHEN, Z., GUO, J., WANG, L. & LIU, X. 2019. Ambra1 induces autophagy and desensitizes human prostate cancer cells to cisplatin. *Biosci Rep,* 39.
LIU, J., YUAN, B., CAO, J., LUO, H., GU, S., ZHANG, M., DING, R., ZHANG, L., ZHOU, F., HUNG, M. C., XU, P., LIN, X., JIN, J. & FENG, X. H. 2021. AMBRA1 Promotes TGFβ Signaling via Nonproteolytic Polyubiquitylation of Smad4. *Cancer Res,* 81**,** 5007-5020.
LIU, J. L., CHEN, F. F., LUNG, J., LO, C. H., LEE, F. H., LU, Y. C. & HUNG, C. H. 2014. Prognostic significance of p62/SQSTM1 subcellular localization and LC3B in oral squamous cell carcinoma. *Br J Cancer,* 111**,** 944-54.
LIU, L., LEE, S., ZHANG, J., PETERS, S. B., HANNAH, J., ZHANG, Y., YIN, Y., KOFF, A., MA, L. & ZHOU, P. 2009b. CUL4A abrogation augments DNA damage response and protection against skin carcinogenesis. *Mol Cell,* 34**,** 451-60.
LIU, Y. & MALLAMPALLI, R. K. 2016. Small molecule therapeutics targeting F-box proteins in cancer. *Semin Cancer Biol,* 36**,** 105-19.
LOCHHEAD, P., CHAN, A. T., NISHIHARA, R., FUCHS, C. S., BECK, A. H., GIOVANNUCCI, E. & OGINO, S. 2015. Etiologic field effect: reappraisal of the field effect concept in cancer predisposition and progression. *Mod Pathol,* 28**,** 14-29.
LOMAS, A., LEONARDI-BEE, J. & BATH-HEXTALL, F. 2012. A systematic review of worldwide incidence of nonmelanoma skin cancer. *Br J Dermatol,* 166**,** 1069-80.
LÓPEZ-CASILLAS, F., PAYNE, H. M., ANDRES, J. L. & MASSAGUÉ, J. 1994. Betaglycan can act as a dual modulator of TGF-beta access to signaling receptors: mapping of ligand binding and GAG attachment sites. *J Cell Biol,* 124**,** 557-68.
LUCARELLI, P., SCHILLING, M., KREUTZ, C., VLASOV, A., BOEHM, M. E., IWAMOTO, N., STEIERT, B., LATTERMANN, S., WÄSCH, M., STEPATH, M., MATTER, M. S., HEIKENWÄLDER, M., HOFFMANN, K., DEHARDE, D., DAMM, G., SEEHOFER, D., MUCIEK, M., GRETZ, N., LEHMANN, W. D., TIMMER, J. & KLINGMÜLLER, U. 2018. Resolving the Combinatorial Complexity of Smad Protein Complex Formation and Its Link to Gene Expression. *Cell Syst,* 6**,** 75-89.e11.
MAHANTY, S., DAKAPPA, S. S., SHARIFF, R., PATEL, S., SWAMY, M. M., MAJUMDAR, A. & SETTY, S. R. G. 2019. Keratinocyte differentiation promotes ER stress-dependent lysosome biogenesis. *Cell Death Dis,* 10**,** 269.
MAJESKI, A. E. & DICE, J. F. 2004. Mechanisms of chaperone-mediated autophagy. *Int J Biochem Cell Biol,* 36**,** 2435-44.
MALY, C. J., CUMSKY, H. J. L., COSTELLO, C. M., SCHMIDT, J. E., BUTTERFIELD, R. J., ZHANG, N., DICAUDO, D. J., NELSON, S. A., SMITH, M. L., OCHOA, S. A., BAUM,

C. L., NAGEL, T. H., PITTELKOW, M. R., SEKULIC, A. & MANGOLD, A. R. 2020. Prognostic value of inositol polyphosphate-5-phosphatase expression in recurrent and metastatic cutaneous squamous cell carcinoma. *J Am Acad Dermatol,* 82**,** 846-853.

MAO, Y., DENG, S. J., SU, Y. J., DIAO, C., PENG, Y., MA, J. F. & CHENG, R. C. 2021. The role of P62 in the development of human thyroid cancer and its possible mechanism. *Cancer Genet,* 256-257**,** 5-16.

MARINKOVIC, M., SPRUNG, M., BULJUBASIC, M. & NOVAK, I. 2018. Autophagy Modulation in Cancer: Current Knowledge on Action and Therapy. *Oxid Med Cell Longev,* 2018**,** 8023821.

MARKOWITZ, S., WANG, J., MYEROFF, L., PARSONS, R., SUN, L., LUTTERBAUGH, J., FAN, R. S., ZBOROWSKA, E., KINZLER, K. W., VOGELSTEIN, B. & ET AL. 1995. Inactivation of the type II TGF-beta receptor in colon cancer cells with microsatellite instability. *Science,* 268**,** 1336-8.

MARTINA, J. A., CHEN, Y., GUCEK, M. & PUERTOLLANO, R. 2012. MTORC1 functions as a transcriptional regulator of autophagy by preventing nuclear transport of TFEB. *Autophagy,* 8**,** 903-14.

MARTINEZ, J. C., OTLEY, C. C., STASKO, T., EUVRARD, S., BROWN, C., SCHANBACHER, C. F. & WEAVER, A. L. 2003. Defining the clinical course of metastatic skin cancer in organ transplant recipients: a multicenter collaborative study. *Arch Dermatol,* 139**,** 301-6.

MASSAGUÉ, J., BLAIN, S. W. & LO, R. S. 2000. TGFbeta signaling in growth control, cancer, and heritable disorders. *Cell,* 103**,** 295-309.

MATHEW, R. & WHITE, E. 2011. Autophagy in tumorigenesis and energy metabolism: friend by day, foe by night. *Curr Opin Genet Dev,* 21**,** 113-9.

MATSUI, M. S., PELLE, E., DONG, K. & PERNODET, N. 2016. Biological Rhythms in the Skin. *Int J Mol Sci,* 17(6)**,** 801.

MATSUI, T. & AMAGAI, M. 2015. Dissecting the formation, structure and barrier function of the stratum corneum. *Int Immunol,* 27**,** 269-80.

MAUBEC, E., PETROW, P., SCHEER-SENYARICH, I., DUVILLARD, P., LACROIX, L., GELLY, J., CERTAIN, A., DUVAL, X., CRICKX, B., BUFFARD, V., BASSET-SEGUIN, N., SAEZ, P., DUVAL-MODESTE, A. B., ADAMSKI, H., MANSARD, S., GRANGE, F., DOMPMARTIN, A., FAIVRE, S., MENTRE, F. & AVRIL, M. F. 2011. Phase II study of cetuximab as first-line single-drug therapy in patients with unresectable squamous cell carcinoma of the skin. *J Clin Oncol,* 29**,** 3419-26.

MAUTHE, M., ORHON, I., ROCCHI, C., ZHOU, X., LUHR, M., HIJLKEMA, K. J., COPPES, R. P., ENGEDAL, N., MARI, M. & REGGIORI, F. 2018. Chloroquine inhibits autophagic flux by decreasing autophagosome-lysosome fusion. *Autophagy,* 14**,** 1435-1455.

MEDINA, D. L. & BALLABIO, A. 2015. Lysosomal calcium regulates autophagy. *Autophagy,* 11**,** 970-1.

MEDINA, D. L., DI PAOLA, S., PELUSO, I., ARMANI, A., DE STEFANI, D., VENDITTI, R., MONTEFUSCO, S., SCOTTO-ROSATO, A., PREZIOSO, C., FORRESTER, A., SETTEMBRE, C., WANG, W., GAO, Q., XU, H., SANDRI, M., RIZZUTO, R., DE MATTEIS, M. A. & BALLABIO, A. 2015. Lysosomal calcium signalling regulates autophagy through calcineurin and TFEB. *Nat Cell Biol,* 17**,** 288-99.

MEHRANY, K., WEENIG, R. H., PITTELKOW, M. R., ROENIGK, R. K. & OTLEY, C. C. 2005. High recurrence rates of squamous cell carcinoma after Mohs' surgery in patients with chronic lymphocytic leukemia. *Dermatol Surg,* 31**,** 38-42; discussion 42.

MENON, G. K. 2002. New insights into skin structure: scratching the surface. *Adv Drug Deliv Rev,* 54 Suppl 1**,** S3-17.

MENON, G. K., CLEARY, G. W. & LANE, M. E. 2012. The structure and function of the stratum corneum. *Int J Pharm,* 435**,** 3-9.

MIJALJICA, D., PRESCOTT, M. & DEVENISH, R. J. 2011. Microautophagy in mammalian cells: revisiting a 40-year-old conundrum. *Autophagy,* 7**,** 673-82.

MINA N LE, E. L. A. B. S. 2017. The Evolution of Staging of Cutaneous Squamous Cell Carcinoma: A Structured Review *International Journal of Head and Neck Surgery,* 8**,** 6.

MISHRA, P., SINGH, U., PANDEY, C. M., MISHRA, P. & PANDEY, G. 2019. Application of student's t-test, analysis of variance, and covariance. *Ann Card Anaesth,* 22**,** 407-411.

MISSERO, C. & ANTONINI, D. 2014. Crosstalk among p53 family members in cutaneous carcinoma. *Exp Dermatol,* 23**,** 143-6.

MIYAZONO, K. & HELDIN, C. H. 1989. Role for carbohydrate structures in TGF-beta 1 latency. *Nature,* 338**,** 158-60.

MONTEITH, G. R., PREVARSKAYA, N. & ROBERTS-THOMSON, S. J. 2017. The calcium-cancer signalling nexus. *Nat Rev Cancer,* 17**,** 367-380.

MORAN, S., MARTÍNEZ-CARDÚS, A., SAYOLS, S., MUSULÉN, E., BALAÑÁ, C., ESTIVAL-GONZALEZ, A., MOUTINHO, C., HEYN, H., DIAZ-LAGARES, A., DE MOURA, M. C., STELLA, G. M., COMOGLIO, P. M., RUIZ-MIRÓ, M., MATIAS-GUIU, X., PAZO-CID, R., ANTÓN, A., LOPEZ-LOPEZ, R., SOLER, G., LONGO, F., GUERRA, I., FERNANDEZ, S., ASSENOV, Y., PLASS, C., MORALES, R., CARLES, J., BOWTELL, D., MILESHKIN, L., SIA, D., TOTHILL, R., TABERNERO, J., LLOVET, J. M. & ESTELLER, M. 2016. Epigenetic profiling to classify cancer of unknown primary: a multicentre, retrospective analysis. *Lancet Oncol,* 17**,** 1386-1395.

MORIKAWA, M., DERYNCK, R. & MIYAZONO, K. 2016. TGF-β and the TGF-β Family: Context-Dependent Roles in Cell and Tissue Physiology. *Cold Spring Harb Perspect Biol,* 8.

MOUSTAKAS, A. & HELDIN, C. H. 2016. Mechanisms of TGFbeta-Induced Epithelial-Mesenchymal Transition. *J Clin Med,* 5(7)**,** 63.

MOWERS, E. E., SHARIFI, M. N. & MACLEOD, K. F. 2017. Autophagy in cancer metastasis. *Oncogene,* 36**,** 1619-1630.

MULLEN, A. C., ORLANDO, D. A., NEWMAN, J. J., LOVÉN, J., KUMAR, R. M., BILODEAU, S., REDDY, J., GUENTHER, M. G., DEKOTER, R. P. & YOUNG, R. A. 2011. Master transcription factors determine cell-type-specific responses to TGF-β signaling. *Cell,* 147**,** 565-76.

MURPHREY, M. B. & VAIDYA, T. 2019. Histology, Apocrine Gland. *StatPearls.* Treasure Island (FL): StatPearls Publishing

StatPearls Publishing LLC.

NAZIO, F. & CECCONI, F. 2017. Autophagy up and down by outsmarting the incredible ULK. *Autophagy,* 13**,** 967-968.

NAZIO, F., STRAPPAZZON, F., ANTONIOLI, M., BIELLI, P., CIANFANELLI, V., BORDI, M., GRETZMEIER, C., DENGJEL, J., PIACENTINI, M., FIMIA, G. M. & CECCONI, F. 2013. mTOR inhibits autophagy by controlling ULK1 ubiquitylation, self-association and function through AMBRA1 and TRAF6. *Nat Cell Biol,* 15**,** 406-16.

NEVILLE, J. A., WELCH, E. & LEFFELL, D. J. 2007. Management of nonmelanoma skin cancer in 2007. *Nat Clin Pract Oncol,* 4**,** 462-9.

NGUYEN, T. H. & HO, D. Q. 2002. Nonmelanoma skin cancer. *Curr Treat Options Oncol,* 3**,** 193-203.

NIGHOT, P. & MA, T. 2016. Role of autophagy in the regulation of epithelial cell junctions. *Tissue Barriers,* 4**,** e1171284.

NIKOLAEV, A. Y., LI, M., PUSKAS, N., QIN, J. & GU, W. 2003. Parc: a cytoplasmic anchor for p53. *Cell,* 112**,** 29-40.

O'HARA, J., FERLITO, A., TAKES, R. P., RINALDO, A., STROJAN, P., SHAHA, A. R., RODRIGO, J. P. & PALERI, V. 2011. Cutaneous squamous cell carcinoma of the head and neck metastasizing to the parotid gland--a review of current recommendations. *Head Neck,* 33**,** 1789-95.

OGATA, D. & TSUCHIDA, T. 2019. Systemic Immunotherapy for Advanced Cutaneous Squamous Cell Carcinoma. *Curr Treat Options Oncol,* 20**,** 30.

OHH, M., KIM, W. Y., MOSLEHI, J. J., CHEN, Y., CHAU, V., READ, M. A. & KAELIN, W. G., JR. 2002. An intact NEDD8 pathway is required for Cullin-dependent ubiquitylation in mammalian cells. *EMBO Rep,* 3**,** 177-82.

OLIVEIRA, S. C., MONIZ, C. M., RIECHELMANN, R., ALEX, A. K., BRAGHIROLLI, M. I., BARIANI, G., NAHAS, C. & HOFF, P. M. 2016. Phase II Study of Capecitabine in Substitution of 5-FU in the Chemoradiotherapy Regimen for Patients with Localized Squamous Cell Carcinoma of the Anal Canal. *J Gastrointest Cancer,* 47**,** 75-81.

OMLAND, S. H., GNIADECKI, R., HAEDERSDAL, M., HELWEG-LARSEN, J. & OMLAND, L. H. 2016. Skin Cancer Risk in Hematopoietic Stem-Cell Transplant Recipients Compared With Background Population and Renal Transplant Recipients: A Population-Based Cohort Study. *JAMA Dermatol,* 152**,** 177-83.

OSHIMORI, N., ORISTIAN, D. & FUCHS, E. 2015. TGF-beta promotes heterogeneity and drug resistance in squamous cell carcinoma. *Cell,* 160**,** 963-976.

OWENS, D. M. & LUMPKIN, E. A. 2014. Diversification and specialization of touch receptors in skin. *Cold Spring Harb Perspect Med,* 4(6):a013656.

PAGE, M. E., LOMBARD, P., NG, F., GÖTTGENS, B. & JENSEN, K. B. 2013. The epidermis comprises autonomous compartments maintained by distinct stem cell populations. *Cell Stem Cell,* 13**,** 471-82.

PAGLIARINI, V., WIRAWAN, E., ROMAGNOLI, A., CICCOSANTI, F., LISI, G., LIPPENS, S., CECCONI, F., FIMIA, G. M., VANDENABEELE, P., CORAZZARI, M. & PIACENTINI, M. 2012. Proteolysis of Ambra1 during apoptosis has a role in the inhibition of the autophagic pro-survival response. *Cell Death Differ,* 19**,** 1495-504.

PAN, H. Y., ALAMRI, A. H. & VALAPALA, M. 2019. Nutrient deprivation and lysosomal stress induce activation of TFEB in retinal pigment epithelial cells. *Cell Mol Biol Lett,* 24**,** 33.

PANKIV, S., CLAUSEN, T. H., LAMARK, T., BRECH, A., BRUUN, J. A., OUTZEN, H., OVERVATN, A., BJORKOY, G. & JOHANSEN, T. 2007. p62/SQSTM1 binds directly to Atg8/LC3 to facilitate degradation of ubiquitinated protein aggregates by autophagy. *J Biol Chem,* 282**,** 24131-45.

PAPPAS, A. 2015. *Lipids and Skin Health*, Springer.

PATERGNANI, S., DANESE, A., BOUHAMIDA, E., AGUIARI, G., PREVIATI, M., PINTON, P. & GIORGI, C. 2020. Various Aspects of Calcium Signaling in the Regulation of Apoptosis, Autophagy, Cell Proliferation, and Cancer. *Int J Mol Sci,* 21(21):8323.

PELENGARIS, S., LITTLEWOOD, T., KHAN, M., ELIA, G. & EVAN, G. 1999. Reversible activation of c-Myc in skin: induction of a complex neoplastic phenotype by a single oncogenic lesion. *Mol Cell,* 3**,** 565-77.

PEREZ-ORDOÑEZ, B., BEAUCHEMIN, M. & JORDAN, R. C. 2006. Molecular biology of squamous cell carcinoma of the head and neck. *J Clin Pathol,* 59**,** 445-53.

PETROSKI, M. D. & DESHAIES, R. J. 2005. Function and regulation of cullin-RING ubiquitin ligases. *Nat Rev Mol Cell Biol,* 6**,** 9-20.

PICKERING, C. R., ZHOU, J. H., LEE, J. J., DRUMMOND, J. A., PENG, S. A., SAADE, R. E., TSAI, K. Y., CURRY, J. L., TETZLAFF, M. T., LAI, S. Y., YU, J., MUZNY, D. M., DODDAPANENI, H., SHINBROT, E., COVINGTON, K. R., ZHANG, J., SETH, S., CAULIN, C., CLAYMAN, G. L., EL-NAGGAR, A. K., GIBBS, R. A., WEBER, R. S., MYERS, J. N., WHEELER, D. A. & FREDERICK, M. J. 2014. Mutational landscape of aggressive cutaneous squamous cell carcinoma. *Clin Cancer Res,* 20**,** 6582-92.

PIERCEALL, W. E., GOLDBERG, L. H., TAINSKY, M. A., MUKHOPADHYAY, T. & ANANTHASWAMY, H. N. 1991. Ras gene mutation and amplification in human nonmelanoma skin cancers. *Mol Carcinog,* 4**,** 196-202.

PIETENPOL, J. A., HOLT, J. T., STEIN, R. W. & MOSES, H. L. 1990. Transforming growth factor beta 1 suppression of c-myc gene transcription: role in inhibition of keratinocyte proliferation. *Proc Natl Acad Sci U S A,* 87**,** 3758-62.

POTENZA, C., BERNARDINI, N., BALDUZZI, V., LOSCO, L., MAMBRIN, A., MARCHESIELLO, A., TOLINO, E., ZUBER, S., SKROZA, N. & PROIETTI, I. 2018. A Review of the Literature of Surgical and Nonsurgical Treatments of Invasive Squamous Cells Carcinoma. *Biomed Res Int,* 2018**,** 9489163.

PRINCIPE, D. R., DOLL, J. A., BAUER, J., JUNG, B., MUNSHI, H. G., BARTHOLIN, L., PASCHE, B., LEE, C. & GRIPPO, P. J. 2014. TGF-β: duality of function between tumor prevention and carcinogenesis. *J Natl Cancer Inst,* 106**,** djt369.

PROBY, C. M., PURDIE, K. J., SEXTON, C. J., PURKIS, P., NAVSARIA, H. A., STABLES, J. N. & LEIGH, I. M. 2000. Spontaneous keratinocyte cell lines representing early and advanced stages of malignant transformation of the epidermis. *Exp Dermatol,* 9**,** 104-17.

QU, X., YU, J., BHAGAT, G., FURUYA, N., HIBSHOOSH, H., TROXEL, A., ROSEN, J., ESKELINEN, E. L., MIZUSHIMA, N., OHSUMI, Y., CATTORETTI, G. & LEVINE, B. 2003. Promotion of tumorigenesis by heterozygous disruption of the beclin 1 autophagy gene. *J Clin Invest,* 112**,** 1809-20.

QUE, S. K. T., ZWALD, F. O. & SCHMULTS, C. D. 2018. Cutaneous squamous cell carcinoma: Incidence, risk factors, diagnosis, and staging. *J Am Acad Dermatol,* 78**,** 237-247.

RACANELLI, A. C., KIKKERS, S. A., CHOI, A. M. K. & CLOONAN, S. M. 2018. Autophagy and inflammation in chronic respiratory disease. *Autophagy,* 14**,** 221-232.

RATUSHNY, V., GOBER, M. D., HICK, R., RIDKY, T. W. & SEYKORA, J. T. 2012. From keratinocyte to cancer: the pathogenesis and modeling of cutaneous squamous cell carcinoma. *J Clin Invest,* 122**,** 464-72.

RAVANAN, P., SRIKUMAR, I. F. & TALWAR, P. 2017. Autophagy: The spotlight for cellular stress responses. *Life Sci,* 188**,** 53-67.

REED, J. A., MCNUTT, N. S., PRIETO, V. G. & ALBINO, A. P. 1994. Expression of transforming growth factor-beta 2 in malignant melanoma correlates with the depth of tumor invasion. Implications for tumor progression. *Am J Pathol,* 145**,** 97-104.

REICHRATH, J., SATERNUS, R. & VOGT, T. 2017. Endocrine actions of vitamin D in skin: Relevance for photocarcinogenesis of non-melanoma skin cancer, and beyond. *Mol Cell Endocrinol,* 453**,** 96-102.

REINA-CAMPOS, M., SHELTON, P. M., DIAZ-MECO, M. T. & MOSCAT, J. 2018. Metabolic reprogramming of the tumor microenvironment by p62 and its partners. *Biochim Biophys Acta Rev Cancer,* 1870**,** 88-95.

RICHARDSON, A., POWELL, A. K., SEXTON, D. W., PARSONS, J. L., REYNOLDS, N. J. & ROSS, K. 2020. microRNA-184 is induced by store-operated calcium entry and regulates early keratinocyte differentiation. *Journal of Cellular Physiology,* 235**,** 6854-6861.

ROBERTSON, E. J. 2014. Dose-dependent Nodal/Smad signals pattern the early mouse embryo. *Semin Cell Dev Biol,* 32**,** 73-9.

ROBERTSON, I. B. & RIFKIN, D. B. 2016. Regulation of the Bioavailability of TGF-β and TGF-β-Related Proteins. *Cold Spring Harb Perspect Biol,* 8(6):a021907.

RODRÍGUEZ-PAREDES, M., BORMANN, F., RADDATZ, G., GUTEKUNST, J., LUCENA-PORCEL, C., KÖHLER, F., WURZER, E., SCHMIDT, K., GALLINAT, S., WENCK, H., RÖWERT-HUBER, J., DENISOVA, E., FEUERBACH, L., PARK, J., BRORS, B., HERPEL, E., NINDL, I., HOFMANN, T. G., WINNEFELD, M. & LYKO, F. 2018. Methylation profiling identifies two subclasses of squamous cell carcinoma related to distinct cells of origin. *Nat Commun,* 9**,** 577.

RODRIGUEZ, M., BEAL, B. T., MANMOHAN, M., SIMMONS, E., VARRA, V., XIONG, D., EVERSMAN, A., BRISKIN, I. N., KNACKSTEDT, T. & VIDIMOS, A. T. 2021. Risk factors and timing of subsequent cutaneous squamous cell carcinoma in patients with cutaneous squamous cell carcinoma: A retrospective cohort study. *J Am Acad Dermatol,* 84**,** 719-724.

ROGERS, G. E. 2004. Hair follicle differentiation and regulation. *Int J Dev Biol,* 48**,** 163-70.

ROGERS, H. W., WEINSTOCK, M. A., FELDMAN, S. R. & COLDIRON, B. M. 2015. Incidence Estimate of Nonmelanoma Skin Cancer (Keratinocyte Carcinomas) in the U.S. Population, 2012. *JAMA Dermatol,* 151**,** 1081-6.

ROMAN, B. L. & HINCK, A. P. 2017. ALK1 signaling in development and disease: new paradigms. *Cell Mol Life Sci,* 74**,** 4539-4560.

ROSE, A. M., SANSOM, O. J. & INMAN, G. J. 2017. Loss of TGF-beta signaling drives cSCC from skin stem cells - More evidence. *Cell Cycle,* 16**,** 386-387.

ROSE, A. M., SPENDER, L. C., STEPHEN, C., MITCHELL, A., RICKABY, W., BRAY, S., EVANS, A. T., DAYAL, J., PURDIE, K. J., HARWOOD, C. A., PROBY, C. M., LEIGH, I. M., COATES, P. J. & INMAN, G. J. 2018. Reduced SMAD2/3 activation independently predicts increased depth of human cutaneous squamous cell carcinoma. *Oncotarget,* 9**,** 14552-14566.

ROSENFELDT, M. T. & RYAN, K. M. 2011. The multiple roles of autophagy in cancer. *Carcinogenesis,* 32**,** 955-63.

ROSSITER, H., KONIG, U., BARRESI, C., BUCHBERGER, M., GHANNADAN, M., ZHANG, C. F., MLITZ, V., GMEINER, R., SUKSEREE, S., FODINGER, D., ECKHART, L. & TSCHACHLER, E. 2013. Epidermal keratinocytes form a functional skin barrier in the absence of Atg7 dependent autophagy. *J Dermatol Sci,* 71**,** 67-75.

RUIZ, E. S., KARIA, P. S., BESAW, R. & SCHMULTS, C. D. 2019. Performance of the American Joint Committee on Cancer Staging Manual, 8th Edition vs the Brigham and Women's Hospital Tumor Classification System for Cutaneous Squamous Cell Carcinoma. *JAMA Dermatol,* 155(7)**,** 819-825.

RUSSELL, R. C., YUAN, H. X. & GUAN, K. L. 2014. Autophagy regulation by nutrient signaling. *Cell Res,* 24**,** 42-57.

RUSSO, M. & RUSSO, G. L. 2018. Autophagy inducers in cancer. *Biochem Pharmacol,* 153**,** 51-61.

SAHANI, M. H., ITAKURA, E. & MIZUSHIMA, N. 2014. Expression of the autophagy substrate SQSTM1/p62 is restored during prolonged starvation depending on transcriptional upregulation and autophagy-derived amino acids. *Autophagy,* 10**,** 431-441.

SAKAKI-YUMOTO, M., KATSUNO, Y. & DERYNCK, R. 2013. TGF-β family signaling in stem cells. *Biochim Biophys Acta,* 1830**,** 2280-96.

SAMARASINGHE, V., MADAN, V. & LEAR, J. T. 2011. Management of high-risk squamous cell carcinoma of the skin. *Expert Rev Anticancer Ther,* 11**,** 763-9.

SÁNCHEZ-DANÉS, A. & BLANPAIN, C. 2018. Deciphering the cells of origin of squamous cell carcinomas. *Nat Rev Cancer,* 18**,** 549-561.

SCHEMPP, C., EMDE, M. & WOLFLE, U. 2009. Dermatology in the Darwin anniversary. Part 1: Evolution of the integument. *J Dtsch Dermatol Ges,* 7**,** 750-7.

SCHMULTS, C. D., KARIA, P. S., CARTER, J. B., HAN, J. & QURESHI, A. A. 2013. Factors Predictive of Recurrence and Death From Cutaneous Squamous Cell Carcinoma: A 10-Year, Single-Institution Cohort Study. *JAMA Dermatology,* 149**,** 541-547.

SCHOENHERR, C., BYRON, A., GRIFFITH, B., LOFTUS, A., WILLS, J. C., MUNRO, A. F., VON KRIEGSHEIM, A. & FRAME, M. C. 2020. The autophagy protein Ambra1 regulates gene expression by supporting novel transcriptional complexes. *J Biol Chem,* 295**,** 12045-12057.

SCHOENHERR, C., BYRON, A., SANDILANDS, E., PALIASHVILI, K., BAILLIE, G. S., GARCIA-MUNOZ, A., VALACCA, C., CECCONI, F., SERRELS, B. & FRAME, M. C. 2017. Ambra1 spatially regulates Src activity and Src/FAK-mediated cancer cell invasion via trafficking networks. *Elife,* 6:e23172.

SEGRE, J. 2003. Complex redundancy to build a simple epidermal permeability barrier. *Curr Opin Cell Biol,* 15**,** 776-82.

SEKULIC, A., KIM, S. Y., HOSTETTER, G., SAVAGE, S., EINSPAHR, J. G., PRASAD, A., SAGERMAN, P., CURIEL-LEWANDROWSKI, C., KROUSE, R., BOWDEN, G. T., WARNEKE, J., ALBERTS, D. S., PITTELKOW, M. R., DICAUDO, D., NICKOLOFF, B. J., TRENT, J. M. & BITTNER, M. 2010. Loss of inositol polyphosphate 5-phosphatase is an early event in development of cutaneous squamous cell carcinoma. *Cancer Prev Res (Phila),* 3**,** 1277-83.

SELLHEYER, K., BICKENBACH, J. R., ROTHNAGEL, J. A., BUNDMAN, D., LONGLEY, M. A., KRIEG, T., ROCHE, N. S., ROBERTS, A. B. & ROOP, D. R. 1993. Inhibition of skin development by overexpression of transforming growth factor beta 1 in the epidermis of transgenic mice. *Proc Natl Acad Sci U S A,* 90**,** 5237-41.

SEO, E.-Y., NAMKUNG, J.-H., LEE, K.-M., LEE, W.-H., IM, M., KEE, S.-H., TAE PARK, G., YANG, J.-M., SEO, Y.-J., PARK, J.-K., DEOK KIM, C. & LEE, J.-H. 2005. Analysis of

calcium-inducible genes in keratinocytes using suppression subtractive hybridization and cDNA microarray. *Genomics,* 86**,** 528-538.
SETTEMBRE, C., ZONCU, R., MEDINA, D. L., VETRINI, F., ERDIN, S., ERDIN, S., HUYNH, T., FERRON, M., KARSENTY, G., VELLARD, M. C., FACCHINETTI, V., SABATINI, D. M. & BALLABIO, A. 2012. A lysosome-to-nucleus signalling mechanism senses and regulates the lysosome via mTOR and TFEB. *Embo j,* 31**,** 1095-108.
SHAPANIS, A., LAI, C., SMITH, S., COLTART, G., SOMMERLAD, M., SCHOFIELD, J., PARKINSON, E., SKIPP, P. & HEALY, E. 2021. Identification of proteins associated with development of metastasis from cutaneous squamous cell carcinomas (cSCCs) via proteomic analysis of primary cSCCs. *Br J Dermatol,* 184**,** 709-721.
SHARIFI, M. N., MOWERS, E. E., DRAKE, L. E., COLLIER, C., CHEN, H., ZAMORA, M., MUI, S. & MACLEOD, K. F. 2016. Autophagy Promotes Focal Adhesion Disassembly and Cell Motility of Metastatic Tumor Cells through the Direct Interaction of Paxillin with LC3. *Cell Rep,* 15**,** 1660-72.
SHARMA, P. & NAG, A. 2014. CUL4A ubiquitin ligase: a promising drug target for cancer and other human diseases. *Open Biol,* 4**,** 130217.
SHERGILL, K., SEN, A. & PILLAI, H. J. 2018. Role of E-cadherin and cyclin D1 as predictive markers of aggression and clonal expansion in head and neck squamous cell carcinoma. *J Korean Assoc Oral Maxillofac Surg,* 44**,** 182-190.
SHI, Y. & MASSAGUÉ, J. 2003. Mechanisms of TGF-beta signaling from cell membrane to the nucleus. *Cell,* 113**,** 685-700.
SHIYANOV, P., NAG, A. & RAYCHAUDHURI, P. 1999. Cullin 4A associates with the UV-damaged DNA-binding protein DDB. *J Biol Chem,* 274**,** 35309-12.
SILJAMÄKI, E., RAPPU, P., RIIHILÄ, P., NISSINEN, L., KÄHÄRI, V. M. & HEINO, J. 2020. H-Ras activation and fibroblast-induced TGF-β signaling promote laminin-332 accumulation and invasion in cutaneous squamous cell carcinoma. *Matrix Biol,* 87**,** 26-47.
SIMONACCI, F., BERTOZZI, N., GRIECO, M. P., GRIGNAFFINI, E. & RAPOSIO, E. 2018. Surgical therapy of cutaneous squamous cell carcinoma: our experience. *Acta Biomed,* 89**,** 242-248.
SINGH, S. S., VATS, S., CHIA, A. Y., TAN, T. Z., DENG, S., ONG, M. S., ARFUSO, F., YAP, C. T., GOH, B. C., SETHI, G., HUANG, R. Y., SHEN, H. M., MANJITHAYA, R. & KUMAR, A. P. 2018. Dual role of autophagy in hallmarks of cancer. *Oncogene,* 37**,** 1142-1158.
SMALL, G. W., CHOU, T. Y., DANG, C. V. & ORLOWSKI, R. Z. 2002. Evidence for involvement of calpain in c-Myc proteolysis in vivo. *Arch Biochem Biophys,* 400**,** 151-61.
SOENGAS, M. S. & LOWE, S. W. 2003. Apoptosis and melanoma chemoresistance. *Oncogene,* 22**,** 3138-51.
SOUCHELNYTSKYI, S., TAMAKI, K., ENGSTRÖM, U., WERNSTEDT, C., TEN DIJKE, P. & HELDIN, C. H. 1997. Phosphorylation of Ser465 and Ser467 in the C terminus of Smad2 mediates interaction with Smad4 and is required for transforming growth factor-beta signaling. *J Biol Chem,* 272**,** 28107-15.
SOUTH, A. P., PURDIE, K. J., WATT, S. A., HALDENBY, S., DEN BREEMS, N., DIMON, M., ARRON, S. T., KLUK, M. J., ASTER, J. C., MCHUGH, A., XUE, D. J., DAYAL, J. H., ROBINSON, K. S., RIZVI, S. H., PROBY, C. M., HARWOOD, C. A. & LEIGH, I. M. 2014. NOTCH1 mutations occur early during cutaneous squamous cell carcinogenesis. *J Invest Dermatol,* 134**,** 2630-2638.
STAPLES, M. P., ELWOOD, M., BURTON, R. C., WILLIAMS, J. L., MARKS, R. & GILES, G. G. 2006. Non-melanoma skin cancer in Australia: the 2002 national survey and trends since 1985. *Med J Aust,* 184**,** 6-10.
STEINERT, P. M. & MAREKOV, L. N. 1999. Initiation of assembly of the cell envelope barrier structure of stratified squamous epithelia. *Mol Biol Cell,* 10**,** 4247-61.
STEINERT, Z. N. A. P. M. 1999. Bricks and mortar of the epidermal barrier. *EXPERIMENTAL and MOLECULAR MEDICINE,* 31**,** 14.

SUN, K., DENG, W., ZHANG, S., CAI, N., JIAO, S., SONG, J. & WEI, L. 2013. Paradoxical roles of autophagy in different stages of tumorigenesis: protector for normal or cancer cells. *Cell Biosci,* 3**,** 35.

SUN, W. L., WANG, L., LUO, J., ZHU, H. W. & CAI, Z. W. 2018. Ambra1 modulates the sensitivity of breast cancer cells to epirubicin by regulating autophagy via ATG12. *Cancer Sci,* 109**,** 3129-3138.

SUN, X., OU, Z., CHEN, R., NIU, X., CHEN, D., KANG, R. & TANG, D. 2016. Activation of the p62-Keap1-NRF2 pathway protects against ferroptosis in hepatocellular carcinoma cells. *Hepatology,* 63**,** 173-84.

SYED, V. 2016. TGF-β Signaling in Cancer. *Journal of Cellular Biochemistry,* 117**,** 1279-1287.

TAKAHASHI, Y., HE, H., TANG, Z., HATTORI, T., LIU, Y., YOUNG, M. M., SERFASS, J. M., CHEN, L., GEBRU, M., CHEN, C., WILLS, C. A., ATKINSON, J. M., CHEN, H., ABRAHAM, T. & WANG, H. G. 2018. An autophagy assay reveals the ESCRT-III component CHMP2A as a regulator of phagophore closure. *Nat Commun,* 9**,** 2855.

TAN, P., YE, Y., HE, L., XIE, J., JING, J., MA, G., PAN, H., HAN, L., HAN, W. & ZHOU, Y. 2018. TRIM59 promotes breast cancer motility by suppressing p62-selective autophagic degradation of PDCD10. *PLoS Biol,* 16**,** e3000051.

TANG, D. Y., ELLIS, R. A. & LOVAT, P. E. 2016. Prognostic Impact of Autophagy Biomarkers for Cutaneous Melanoma. *Front Oncol,* 6**,** 236.

TANIDA, I., UENO, T. & KOMINAMI, E. 2008. LC3 and Autophagy. *Methods Mol Biol,* 445**,** 77-88.

THOMPSON, A. K., KELLEY, B. F., PROKOP, L. J., MURAD, M. H. & BAUM, C. L. 2016. Risk Factors for Cutaneous Squamous Cell Carcinoma Recurrence, Metastasis, and Disease-Specific Death: A Systematic Review and Meta-analysis. *JAMA Dermatol,* 152**,** 419-28.

TOKEZ, S., WAKKEE, M., KAN, W., VENABLES, Z. C., MOOYAART, A. L., LOUWMAN, M., NIJSTEN, T. & HOLLESTEIN, L. M. 2021. Cumulative incidence and disease-specific survival of metastatic cutaneous squamous cell carcinoma: A nationwide cancer registry study. *Journal of the American Academy of Dermatology,* 86(2)**,** 331-338.

TU, C. L. & BIKLE, D. D. 2013. Role of the calcium-sensing receptor in calcium regulation of epidermal differentiation and function. *Best Pract Res Clin Endocrinol Metab,* 27**,** 415-27.

TZAVLAKI, K. & MOUSTAKAS, A. 2020. TGF-β Signaling. *Biomolecules,* 10(3)**,** 487.

VAN BELLE, P., RODECK, U., NUAMAH, I., HALPERN, A. C. & ELDER, D. E. 1996. Melanoma-associated expression of transforming growth factor-beta isoforms. *Am J Pathol,* 148**,** 1887-94.

VAN DEN BOSCH, M. H., BLOM, A. B., VAN LENT, P. L., VAN BEUNINGEN, H. M., BLANEY DAVIDSON, E. N., VAN DER KRAAN, P. M. & VAN DEN BERG, W. B. 2014. Canonical Wnt signaling skews TGF-β signaling in chondrocytes towards signaling via ALK1 and Smad 1/5/8. *Cell Signal,* 26**,** 951-8.

VAN LEE, C. B., ROORDA, B. M., WAKKEE, M., VOORHAM, Q., MOOYAART, A. L., DE VIJLDER, H. C., NIJSTEN, T. & VAN DEN BOS, R. R. 2019. Recurrence rates of cutaneous squamous cell carcinoma of the head and neck after Mohs micrographic surgery vs. standard excision: a retrospective cohort study. *Br J Dermatol,* 181**,** 338-343.

VANDER ARK, A., CAO, J. & LI, X. 2018. TGF-beta receptors: In and beyond TGF-beta signaling. *Cell Signal,* 52**,** 112-120.

VELEZ, N. F., KARIA, P. S., VARTANOV, A. R., DAVIDS, M. S., BROWN, J. R. & SCHMULTS, C. D. 2014. Association of advanced leukemic stage and skin cancer tumor stage with poor skin cancer outcomes in patients with chronic lymphocytic leukemia. *JAMA Dermatol,* 150**,** 280-7.

VENABLES, Z. C., AUTIER, P., NIJSTEN, T., WONG, K. F., LANGAN, S. M., ROUS, B., BROGGIO, J., HARWOOD, C., HENSON, K., PROBY, C. M., RASHBASS, J. & LEIGH, I. M. 2019a. Nationwide Incidence of Metastatic Cutaneous Squamous Cell Carcinoma in England. *JAMA Dermatol,* 155**,** 298-306.

VENABLES, Z. C., NIJSTEN, T., WONG, K. F., AUTIER, P., BROGGIO, J., DEAS, A., HARWOOD, C. A., HOLLESTEIN, L. M., LANGAN, S. M., MORGAN, E., PROBY, C. M., RASHBASS, J. & LEIGH, I. M. 2019b. Epidemiology of basal and cutaneous squamous cell carcinoma in the U.K. 2013-15: a cohort study. *Br J Dermatol,* 181(3)**,** 474-482.

VERYKIOU, S., ALEXANDER, M., EDWARDS, N., PLUMMER, R., CHAUDHRY, B., LOVAT, P. E. & HILL, D. S. 2019. Harnessing autophagy to overcome mitogen-activated protein kinase kinase inhibitor-induced resistance in metastatic melanoma. *Br J Dermatol,* 180**,** 346-356.

WAIKEL, R. L., WANG, X. J. & ROOP, D. R. 1999. Targeted expression of c-Myc in the epidermis alters normal proliferation, differentiation and UV-B induced apoptosis. *Oncogene,* 18**,** 4870-8.

WAITZBERG, A. F., NONOGAKI, S., NISHIMOTO, I. N., KOWALSKI, L. P., MIGUEL, R. E., BRENTANI, R. R. & BRENTANI, M. M. 2004. Clinical significance of c-myc and p53 expression in head and neck squamous cell carcinomas. *Cancer Detect Prev,* 28**,** 178-86.

WANG, N., WENG, J., XIA, J., ZHU, Y., CHEN, Q., HU, D., ZHANG, X., SUN, R., FENG, J., MINATO, N., GONG, Y. & SU, L. 2020a. SIPA1 enhances SMAD2/3 expression to maintain stem cell features in breast cancer cells. *Stem Cell Res,* 49**,** 102099.

WANG, Z., ZHANG, J., LI, M., KONG, L. & YU, J. 2020b. The expression of p-p62 and nuclear Nrf2 in esophageal squamous cell carcinoma and association with radioresistance. *Thorac Cancer,* 11**,** 130-139.

WATT, S. A., POURREYRON, C., PURDIE, K., HOGAN, C., COLE, C. L., FOSTER, N., PRATT, N., BOURDON, J. C., APPLEYARD, V., MURRAY, K., THOMPSON, A. M., MAO, X., MEIN, C., BRUCKNER-TUDERMAN, L., EVANS, A., MCGRATH, J. A., PROBY, C. M., FOERSTER, J., LEIGH, I. M. & SOUTH, A. P. 2011. Integrative mRNA profiling comparing cultured primary cells with clinical samples reveals PLK1 and C20orf20 as therapeutic targets in cutaneous squamous cell carcinoma. *Oncogene,* 30**,** 4666-77.

WEI, W., CHEN, Y., XU, J., ZHOU, Y., BAI, X., YANG, M. & ZHU, J. 2018. Identification of Biomarker for Cutaneous Squamous Cell Carcinoma Using Microarray Data Analysis. *J Cancer,* 9**,** 400-406.

WEINBERG, A. S., OGLE, C. A. & SHIM, E. K. 2007. Metastatic cutaneous squamous cell carcinoma: an update. *Dermatol Surg,* 33**,** 885-99.

WERTZ, I. E., O'ROURKE, K. M., ZHANG, Z., DORNAN, D., ARNOTT, D., DESHAIES, R. J. & DIXIT, V. M. 2004. Human De-etiolated-1 regulates c-Jun by assembling a CUL4A ubiquitin ligase. *Science,* 303**,** 1371-4.

WHITE, E., MEHNERT, J. M. & CHAN, C. S. 2015. Autophagy, Metabolism, and Cancer. *Clin Cancer Res,* 21**,** 5037-46.

WILSON, V. G. 2014. Growth and Differentiation of HaCaT Keratinocytes. *In:* TURKSEN, K. (ed.) *Epidermal Cells: Methods and Protocols.* New York, NY: Springer New York.

WONG, R., GEYER, S., WENINGER, W., GUIMBERTEAU, J. C. & WONG, J. K. 2016. The dynamic anatomy and patterning of skin. *Exp Dermatol,* 25**,** 92-8.

WRANA, J. L. & ATTISANO, L. 2000. The Smad pathway. *Cytokine & growth factor reviews,* 11**,** 5-13.

WRANA, J. L., ATTISANO, L., WIESER, R., VENTURA, F. & MASSAGUÉ, J. 1994. Mechanism of activation of the TGF-beta receptor. *Nature,* 370**,** 341-7.

WRIGHT, P. E. & DYSON, H. J. 2015. Intrinsically disordered proteins in cellular signalling and regulation. *Nat Rev Mol Cell Biol,* 16**,** 18-29.

WRIGHT, T. J., MCKEE, C., BIRCH-MACHIN, M. A., ELLIS, R., ARMSTRONG, J. L. & LOVAT, P. E. 2013. Increasing the therapeutic efficacy of docetaxel for cutaneous squamous cell carcinoma through the combined inhibition of phosphatidylinositol 3-kinase/AKT signalling and autophagy. *Clin Exp Dermatol,* 38**,** 421-3.

WU, K., CHEN, A. & PAN, Z. Q. 2000. Conjugation of Nedd8 to CUL1 enhances the ability of the ROC1-CUL1 complex to promote ubiquitin polymerization. *J Biol Chem,* 275**,** 32317-24.

WU, Y., JIN, Y., SUN, T., ZHU, P., LI, J., ZHANG, Q., WANG, X., JIANG, J., CHEN, G. & ZHAO, X. 2020. p62/SQSTM1 accumulation due to degradation inhibition and transcriptional activation plays a critical role in silica nanoparticle-induced airway inflammation via NF-κB activation. *Journal of Nanobiotechnology,* 18**,** 77.

WYSONG, A., NEWMAN, J. G., COVINGTON, K. R., KURLEY, S. J., IBRAHIM, S. F., FARBERG, A. S., BAR, A., CLEAVER, N. J., SOMANI, A. K., PANTHER, D., BRODLAND, D. G., ZITELLI, J., TOYOHARA, J., MAHER, I. A., XIA, Y., BIBEE, K., GRIEGO, R., RIGEL, D. S., MELDI PLASSERAUD, K., ESTRADA, S., SHOLL, L. M., JOHNSON, C., COOK, R. W., SCHMULTS, C. D. & ARRON, S. T. 2020. Validation of a 40-gene expression profile test to predict metastatic risk in localized high-risk cutaneous squamous cell carcinoma. *J Am Acad Dermatol,* 84(2)**,** 361-369.

XIA, P., WANG, S., HUANG, G., DU, Y., ZHU, P., LI, M. & FAN, Z. 2014. RNF2 is recruited by WASH to ubiquitinate AMBRA1 leading to downregulation of autophagy. *Cell Res,* 24**,** 943-58.

XIANG, F., LUCAS, R., HALES, S. & NEALE, R. 2014. Incidence of nonmelanoma skin cancer in relation to ambient UV radiation in white populations, 1978-2012: empirical relationships. *JAMA Dermatol,* 150**,** 1063-71.

XIE, Z., NAIR, U. & KLIONSKY, D. J. 2008. Atg8 controls phagophore expansion during autophagosome formation. *Mol Biol Cell,* 19**,** 3290-8.

XU, R., CAI, M. Y., LUO, R. Z., TIAN, X., HAN, J. D. & CHEN, M. K. 2016. The Expression Status and Prognostic Value of Cancer Stem Cell Biomarker CD133 in Cutaneous Squamous Cell Carcinoma. *JAMA Dermatol,* 152**,** 305-11.

YAN, X. Y., ZHONG, X. R., YU, S. H., ZHANG, L. C., LIU, Y. N., ZHANG, Y., SUN, L. K. & SU, J. 2019. p62 aggregates mediated Caspase 8 activation is responsible for progression of ovarian cancer. *J Cell Mol Med,* 23**,** 4030-4042.

YAN, Y. T., LIU, J. J., LUO, Y., E, C., HALTIWANGER, R. S., ABATE-SHEN, C. & SHEN, M. M. 2002. Dual roles of Cripto as a ligand and coreceptor in the nodal signaling pathway. *Mol Cell Biol,* 22**,** 4439-49.

YAO, M., SHANG, Y. Y., ZHOU, Z. W., YANG, Y. X., WU, Y. S., GUAN, L. F., WANG, X. Y., ZHOU, S. F. & WEI, X. 2017. The research on lapatinib in autophagy, cell cycle arrest and epithelial to mesenchymal transition via Wnt/ErK/PI3K-AKT signaling pathway in human cutaneous squamous cell carcinoma. *J Cancer,* 8**,** 220-226.

YEH, Y. Y., SHAH, K. H., CHOU, C. C., HSIAO, H. H., WRASMAN, K. M., STEPHAN, J. S., STAMATAKOS, D., KHOO, K. H. & HERMAN, P. K. 2011. The identification and analysis of phosphorylation sites on the Atg1 protein kinase. *Autophagy,* 7**,** 716-26.

YOSHIHARA, N., TAKAGI, A., UENO, T. & IKEDA, S. 2014. Inverse correlation between microtubule-associated protein 1A/1B-light chain 3 and p62/sequestosome-1 expression in the progression of cutaneous squamous cell carcinoma. *J Dermatol,* 41**,** 311-5.

YOSHIHARA, N., UENO, T., TAKAGI, A., OLIVA TREJO, J. A., HARUNA, K., SUGA, Y., KOMATSU, M., TANAKA, K. & IKEDA, S. 2015. The significant role of autophagy in the granular layer in normal skin differentiation and hair growth. *Arch Dermatol Res,* 307**,** 159-69.

YU, H., PETERS, J. M., KING, R. W., PAGE, A. M., HIETER, P. & KIRSCHNER, M. W. 1998. Identification of a cullin homology region in a subunit of the anaphase-promoting complex. *Science,* 279**,** 1219-22.

YU, L., CHEN, Y. & TOOZE, S. A. 2018. Autophagy pathway: Cellular and molecular mechanisms. *Autophagy,* 14**,** 207-215.

YUN, C. W. & LEE, S. H. 2018. The Roles of Autophagy in Cancer. *Int J Mol Sci,* 19.

ZHANG, C., ZHANG, X., XU, R., HUANG, B., CHEN, A. J., LI, C., WANG, J. & LI, X. G. 2017a. TGF-β2 initiates autophagy via Smad and non-Smad pathway to promote glioma cells' invasion. *J Exp Clin Cancer Res,* 36**,** 162.

ZHANG, T., GUO, L., WANG, Y. & YANG, Y. 2018. Macroautophagy Regulates Nuclear NOTCH1 Activity Through Multiple p62 Binding Sites. *IUBMB Life,* 70**,** 985-994.

ZHANG, T. J., XUE, D., ZHANG, C. D., ZHANG, Z. D., LIU, Q. R. & WANG, J. Q. 2017b. Cullin 4A is associated with epithelial to mesenchymal transition and poor prognosis in perihilar cholangiocarcinoma. *World J Gastroenterol,* 23**,** 2318-2329.

ZHAO, M., MISHRA, L. & DENG, C. X. 2018. The role of TGF-beta/SMAD4 signaling in cancer. *Int J Biol Sci,* 14**,** 111-123.

ZHAO, Y. G. & ZHANG, H. 2019. Autophagosome maturation: An epic journey from the ER to lysosomes. *J Cell Biol,* 218**,** 757-770.

ZHENG, Y., WANG, G. R., JIA, J. J., LUO, S. J., WANG, H. & XIAO, S. X. 2014. Expressions of oncogenes c-fos and c-myc in skin lesion of cutaneous squamous cell carcinoma. *Asian Pac J Trop Med,* 7**,** 761-4.

ZHOU, B., GUO, W., SUN, C., ZHANG, B. & ZHENG, F. 2018. Linc00462 promotes pancreatic cancer invasiveness through the miR-665/TGFBR1-TGFBR2/SMAD2/3 pathway. *Cell Death Dis,* 9**,** 706.

ZHOU, W., ZHANG, S., LI, J., LI, Z., WANG, Y. & LI, X. 2019. lncRNA TINCR participates in ALA-PDT-induced apoptosis and autophagy in cutaneous squamous cell carcinoma. *J Cell Biochem,* 120(8)**,** 13893-13902.

ZIEGLER, A., JONASON, A. S., LEFFELL, D. J., SIMON, J. A., SHARMA, H. W., KIMMELMAN, J., REMINGTON, L., JACKS, T. & BRASH, D. E. 1994. Sunburn and p53 in the onset of skin cancer. *Nature,* 372**,** 773-6.

ZOTTI, T., SCUDIERO, I., SETTEMBRE, P., FERRAVANTE, A., MAZZONE, P., D'ANDREA, L., REALE, C., VITO, P. & STILO, R. 2014. TRAF6-mediated ubiquitination of NEMO requires p62/sequestosome-1. *Mol Immunol,* 58**,** 27-31.

Chapter 8. Appendix

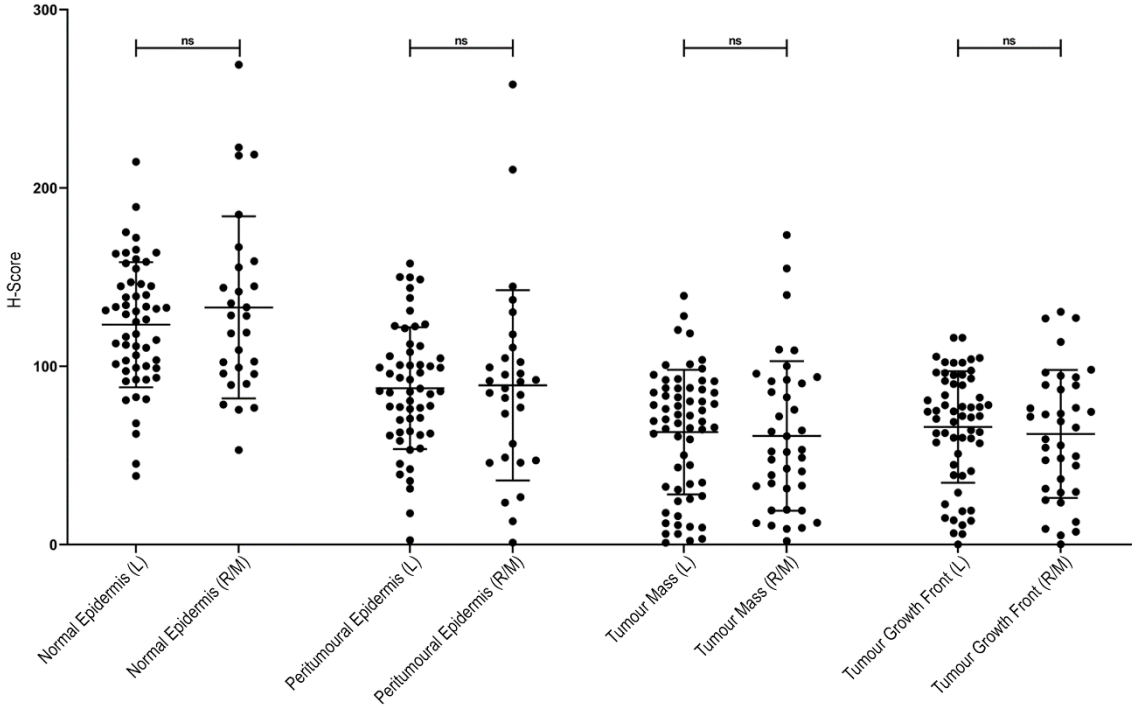

FIGURE A. 1. CYTOPLASMIC AMBRA1 EXPRESSION IN THE NORMAL EPIDERMIS, PERITUMOURAL EPIDERMIS, TUMOUR MASS OR GROWTH FRONT DOES NOT DIFFER BETWEEN LOCALISED AND RECURRENT/METASTATIC PRIMARY CSCC TUMOURS.
Scatter graph comparing the cytoplasmic AMBRA1 H-scores in the normal epidermis, peritumoural epidermis, tumour mass and tumour growth front regions in localised primary cSCC tumours (L) (n=62) or recurrent/metastatic primary cSCC tumours (R/M) (n=39). Horizontal bars represent the mean ± SD H-score for each group. Statistics acquired by Kruskal-Wallis test with Dunn's post hoc correction (ns = non-significant).

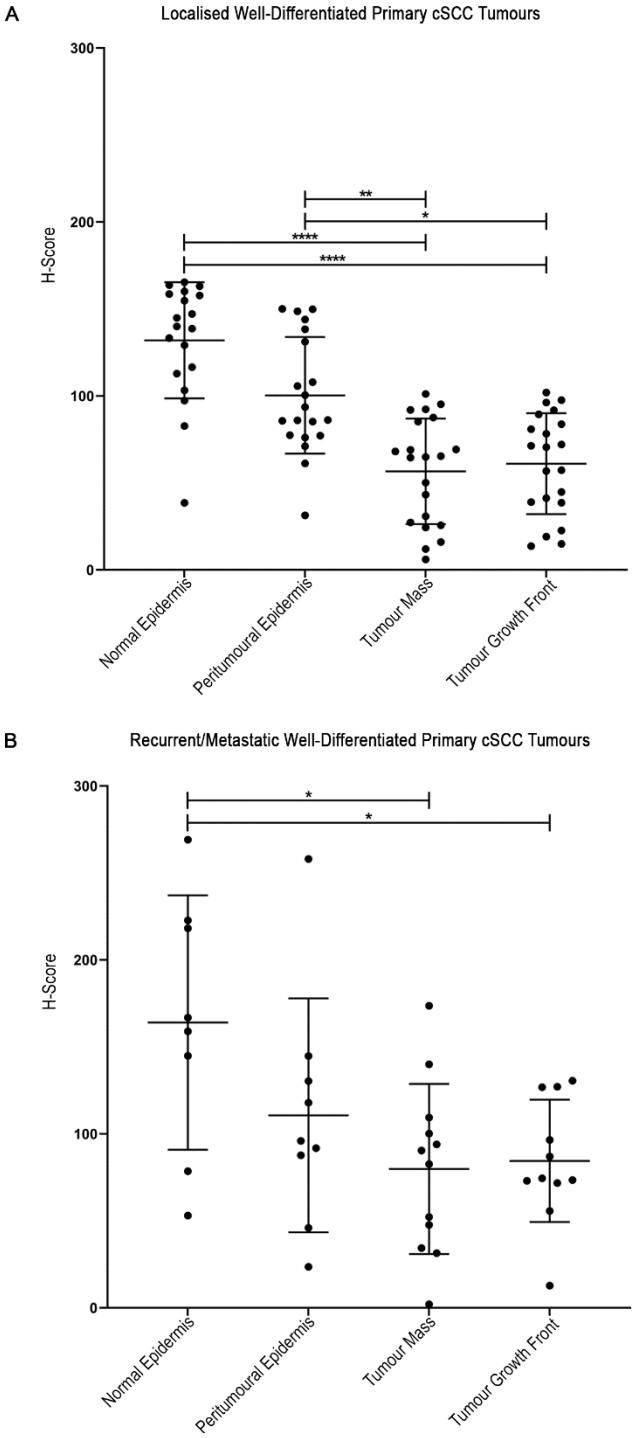

FIGURE A. 2. CYTOPLASMIC AMBRA1 EXPRESSION DECREASES IN THE PERITUMOURAL EPIDERMIS, TUMOUR MASS AND GROWTH FRONT OF LOCALISED AND RECURRENT/METASTATIC WELL-DIFFERENTIATED PRIMARY CSCC TUMOURS.
*(**A**) Scatter graph representing the cytoplasmic AMBRA1 H-scores in the normal epidermis (n=19), peritumoural epidermis (n=20), tumour mass (n=21) and tumour growth front regions (n=21) of 21 localised well-differentiated primary cSCC tumours. Horizontal bars represent the mean ± SD H-score for each group. Statistics acquired by Kruskal-Wallis test with Dunn's post hoc correction (*P<0.05) (**P<0.01) (****P<0.0001). (**B**) Scatter graph representing the cytoplasmic AMBRA1 H-scores in the normal epidermis (n=8), peritumoural epidermis (n=9), tumour mass (n=12) and tumour growth front regions (n=11) of 12 recurrent/metastatic well-differentiated primary cSCC tumours. Horizontal bars represent the mean ± SD H-score for each group. Statistics acquired by ordinary one-way ANOVA test with Tukey's post hoc correction (*P<0.05).*

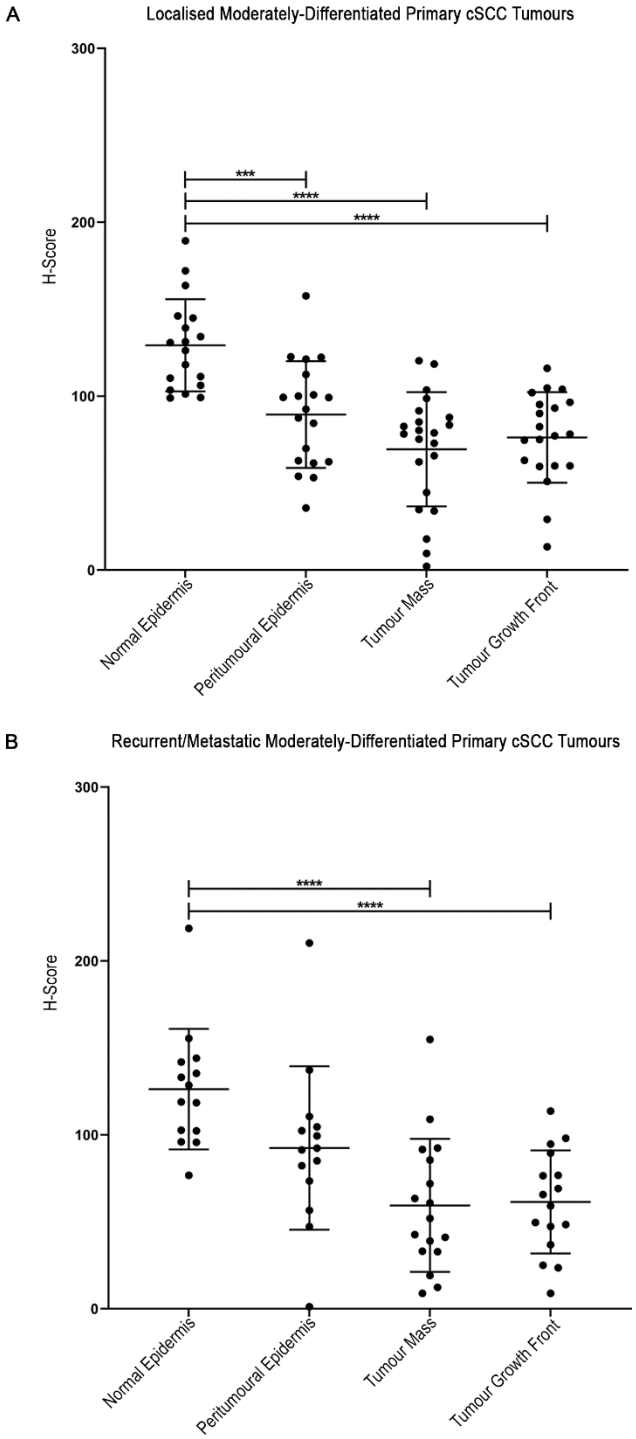

FIGURE A. 3. CYTOPLASMIC AMBRA1 EXPRESSION DECREASES IN THE TUMOUR MASS AND GROWTH FRONT OF LOCALISED AND RECURRENT/METASTATIC MODERATELY WELL-DIFFERENTIATED PRIMARY CSCC TUMOURS.

*(**A**) Scatter graph representing the cytoplasmic AMBRA1 H-scores in the normal epidermis (n=18), peritumoural epidermis (n=19), tumour mass (n=22) and tumour growth front regions (n=20) of 22 localised moderately-differentiated primary cSCC tumours. Horizontal bars represent the mean ± SD H-score for each group. Statistics acquired by ordinary one-way ANOVA test with Tukey's post hoc correction (***P<0.001) (****P<0.0001). (**B**) Scatter graph representing the cytoplasmic AMBRA1 H-scores in the normal epidermis (n=14), peritumoural epidermis (n=14), tumour mass (n=17) and tumour growth front regions (n=16) of 17 recurrent/metastatic moderately-differentiated primary cSCC tumours. Horizontal bars represent the mean ± SD H-score for each group. Statistics acquired by ordinary one-way ANOVA test with Tukey's post hoc correction (****P<0.0001).*

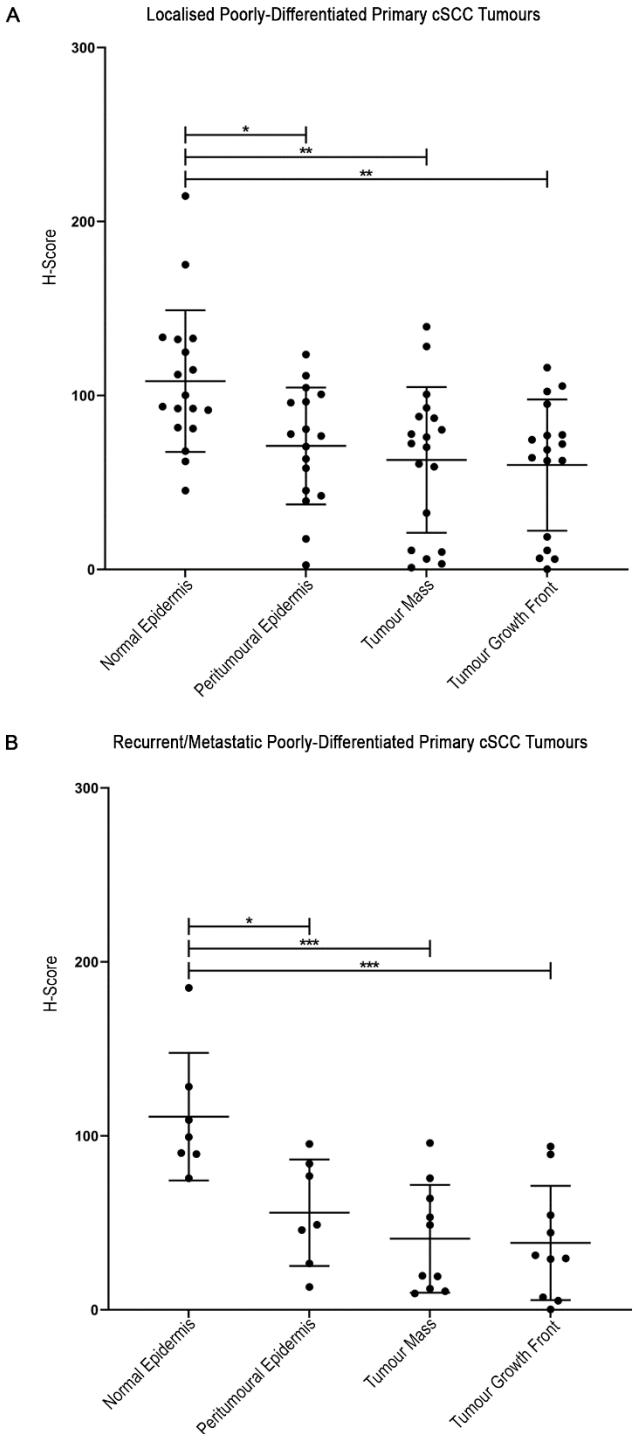

FIGURE A. 4. CYTOPLASMIC AMBRA1 EXPRESSION DECREASES IN THE PERITUMOURAL EPIDERMIS, TUMOUR MASS AND GROWTH FRONT OF LOCALISED AND RECURRENT/METASTATIC POORLY-DIFFERENTIATED PRIMARY CSCC TUMOURS.

*(**A**) Scatter graph representing the cytoplasmic AMBRA1 H-scores in the normal epidermis (n=18), peritumoural epidermis (n=17), tumour mass (n=19) and tumour growth front regions (n=17) of 19 localised poorly-differentiated primary cSCC tumours. Horizontal bars represent the mean ± SD H-score for each group. Statistics acquired by ordinary one-way ANOVA test with Tukey's post hoc correction (*P<0.05) (**P<0.01). (**B**) Scatter graph representing the cytoplasmic AMBRA1 H-scores in the normal epidermis (n=7), peritumoural epidermis (n=7), tumour mass (n=10) and tumour growth front regions (n=10) of 10 recurrent/metastatic poorly-differentiated primary cSCC tumours. Horizontal bars represent the mean ± SD H-score for each group. Statistics acquired by ordinary one-way ANOVA test with Tukey's post hoc correction (*P<0.05) (***P<0.001).*

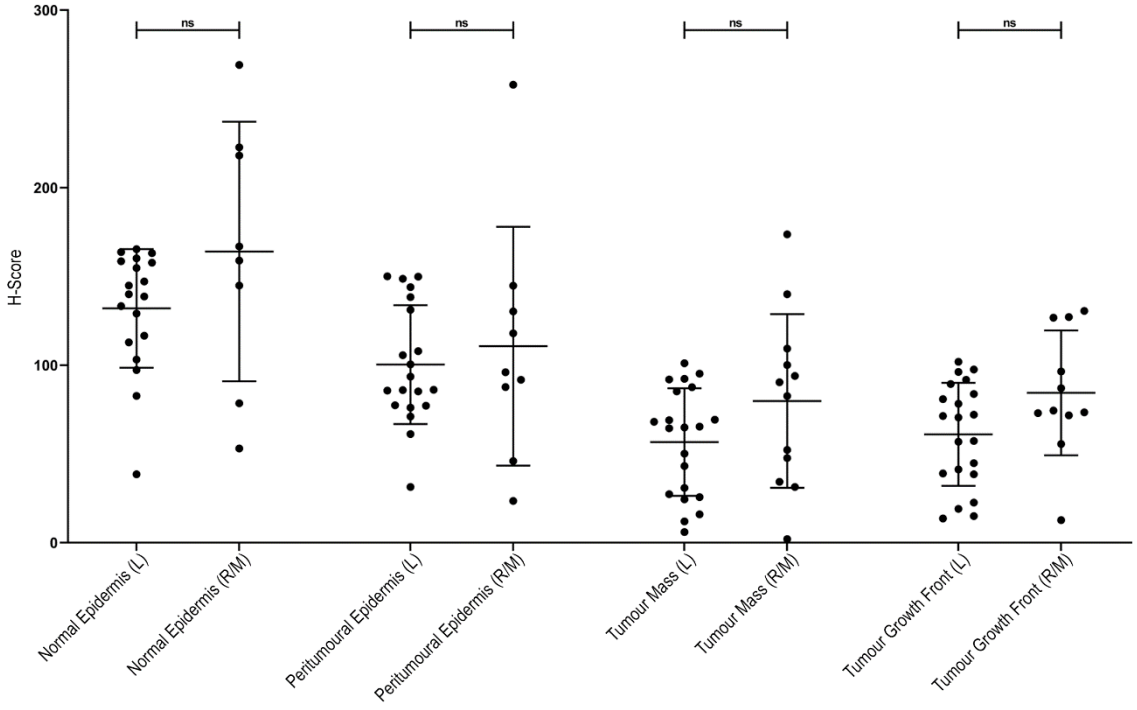

FIGURE A. 5. CYTOPLASMIC AMBR1 EXPRESSION IN THE NORMAL EPIDERMIS, PERITUMOURAL EPIDERMIS, TUMOUR MASS OR GROWTH FRONT DOES NOT DIFFER BETWEEN WELL-DIFFERENTIATED LOCALISED AND RECURRENT/METASTATIC PRIMARY CSCC.

Scatter graph comparing the cytoplasmic AMBRA1 H-scores in the normal epidermis, peritumoural epidermis, tumour mass and tumour growth front regions in well-differentiated localised primary cSCC tumours (L) (n=21) or well-differentiated recurrent/metastatic primary cSCC tumours (R/M) (n=12). Horizontal bars represent the mean ± SD H-score for each group. Statistics acquired by Kruskal-Wallis test with Dunn's post hoc correction (ns = nonsignificant).

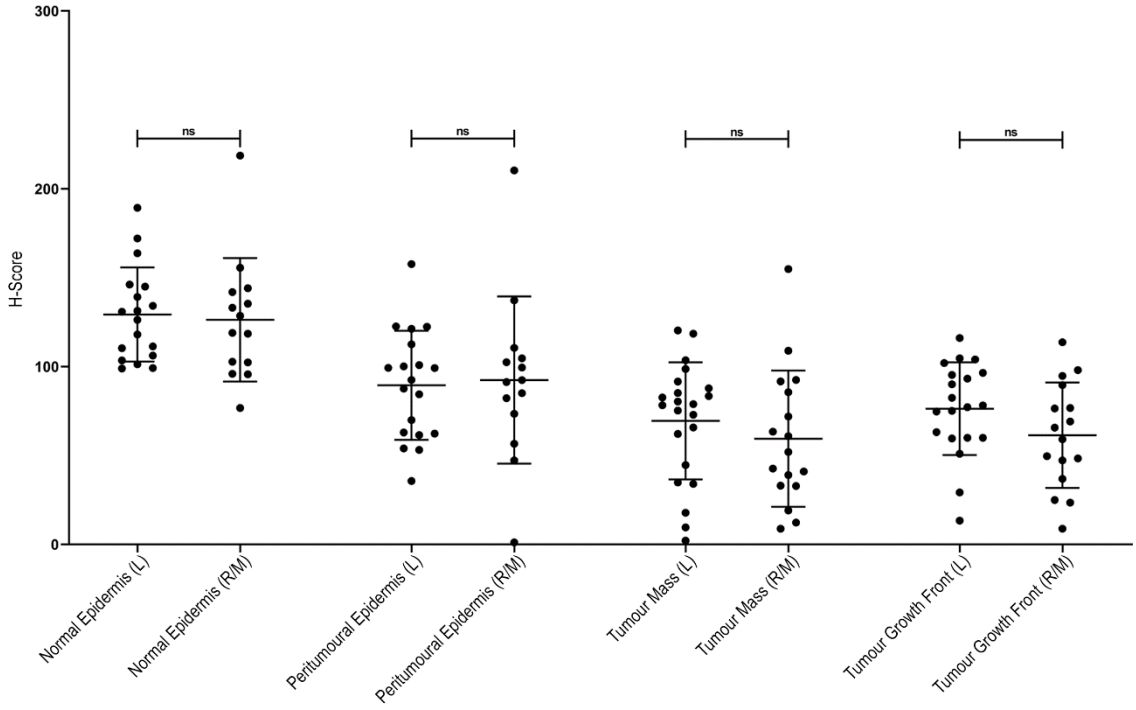

FIGURE A. 6. CYTOPLASMIC AMBR1 EXPRESSION IN THE NORMAL EPIDERMIS, PERITUMOURAL EPIDERMIS, TUMOUR MASS OR GROWTH FRONT DOES NOT DIFFER BETWEEN MODERATELY DIFFERENTIATED LOCALISED AND RECURRENT/METASTATIC PRIMARY CSCC.

Scatter graph comparing the cytoplasmic AMBRA1 H-scores in the normal epidermis, peritumoural epidermis, tumour mass and tumour growth front regions in moderately-differentiated localised primary cSCC tumours (L) (n=22) or moderately-differentiated recurrent/metastatic primary cSCC tumours (R/M) (n=17). Horizontal bars represent the mean ± SD H-score for each group. Statistics acquired by ordinary one-way ANOVA test with Tukey's post hoc correction (ns = non- significant).

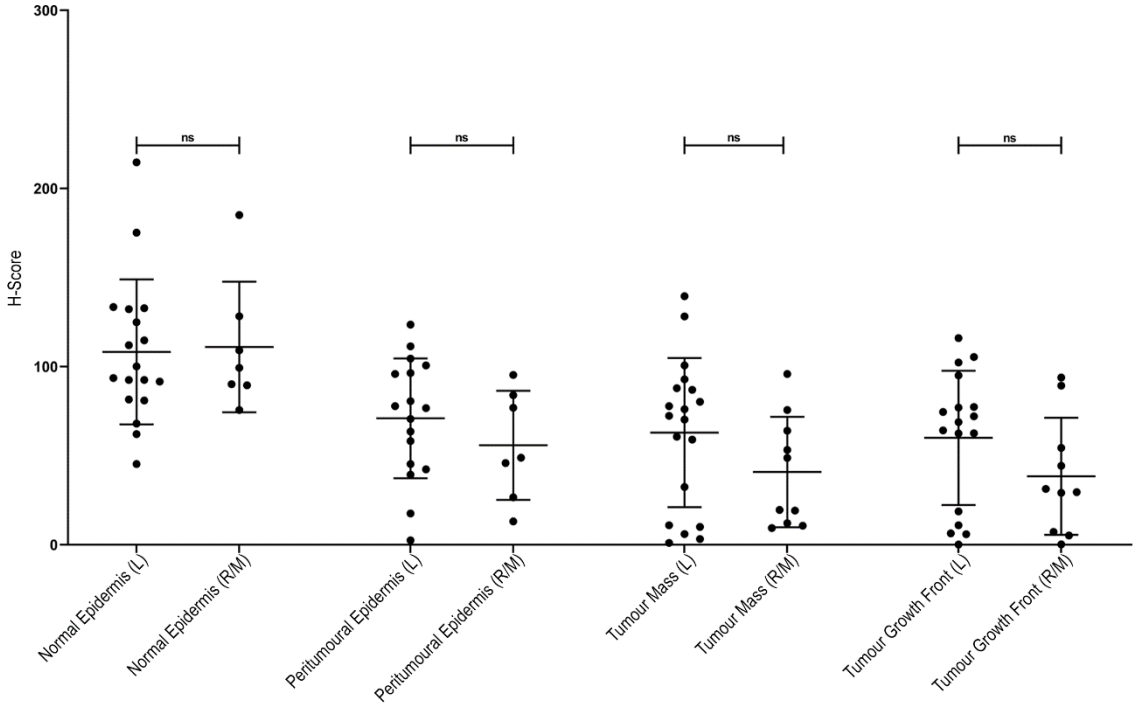

FIGURE A. 7. CYTOPLASMIC AMBR1 EXPRESSION IN THE NORMAL EPIDERMIS, PERITUMOURAL EPIDERMIS, TUMOUR MASS OR GROWTH FRONT DOES NOT DIFFER BETWEEN POORLY-DIFFERENTIATED LOCALISED AND RECURRENT/METASTATIC PRIMARY CSCC.

Scatter graph comparing the cytoplasmic AMBRA1 H-scores in the normal epidermis, peritumoural epidermis, tumour mass and tumour growth front regions in poorly-differentiated localised primary cSCC tumours (L) (n=19) or poorly-differentiated recurrent/metastatic primary cSCC tumours (R/M) (n=10). Horizontal bars represent the mean ± SD H-score for each group. Statistics acquired by ordinary one-way ANOVA test with Tukey's post hoc correction (ns = non-significant).

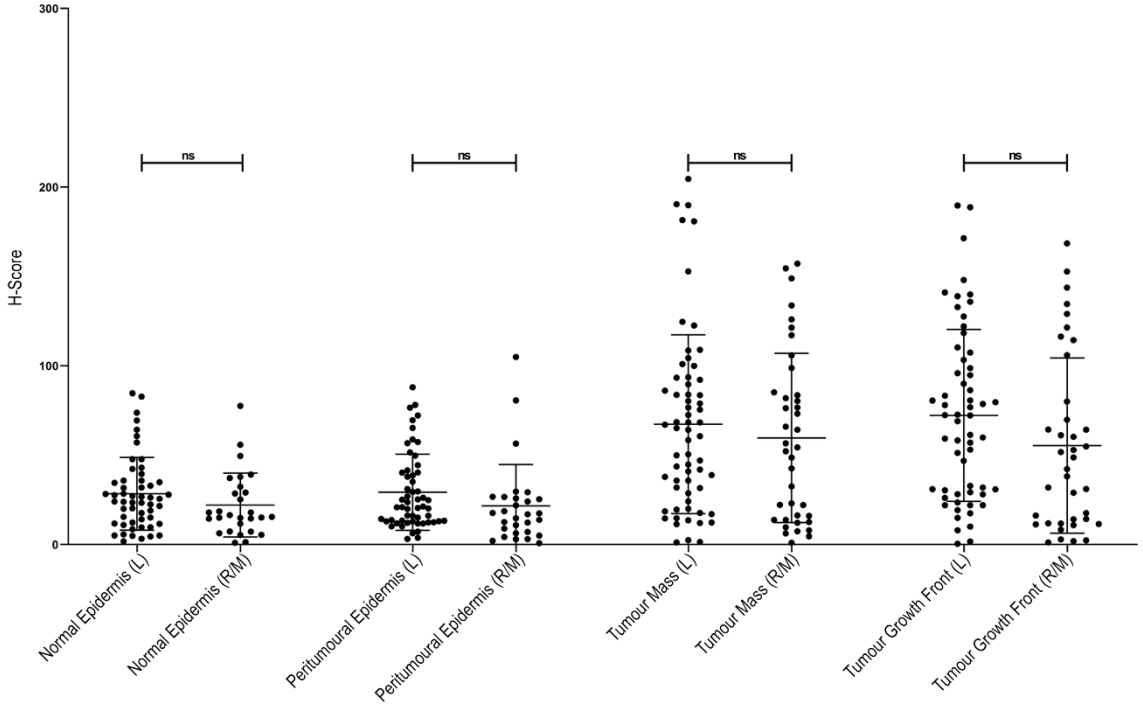

FIGURE A. 8. CYTOPLASMIC P62 EXPRESSION IN THE NORMAL OR PERITUMOURAL EPIDERMIS OR THE TUMOUR MASS OR GROWTH FRONT OF PRIMARY CSCCS DOES NOT DIFFER BETWEEN LOCALISED AND RECURRENT/METASTATIC TUMOURS.
Scatter graph comparing the cytoplasmic AMBRA1 H-scores in the normal epidermis, peritumoural epidermis, tumour mass and tumour growth front regions localised primary cSCC tumours (L) (n=63) or recurrent/metastatic primary cSCC tumours (R/M) (n=39). Horizontal bars represent the mean ± SD H-score for each group. Statistics acquired by Kruskal-Wallis test with Dunn's post hoc correction (ns = nonsignificant).

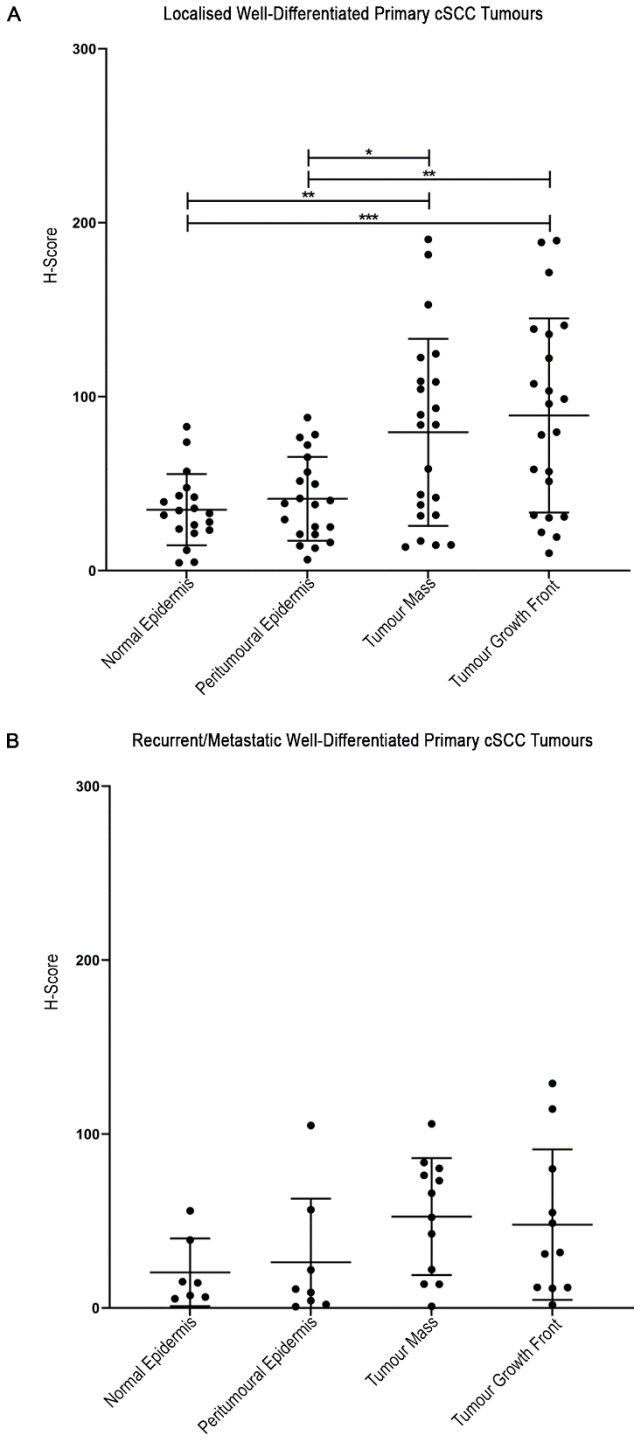

FIGURE A. 9. CYTOPLASMIC EXPRESSION OF P62 IN WELL-DIFFERENTIATED LOCALISED OR RECURRENT IN PRIMARY CSCC TUMOURS.

*(**A**) Scatter graph representing the cytoplasmic p62 H-scores in the normal epidermis (n=19), peritumoural epidermis (n=21), tumour mass (n=22) and tumour growth front regions (n=22) of 22 localised well-differentiated primary cSCC tumours. Horizontal bars represent the mean ± SD H-score for each group. Statistics acquired by ordinary one-way ANOVA test with Tukey's post hoc correction (*P<0.05) (**P<0.01) (***P<0.001). (**B**) Scatter graph representing the cytoplasmic p62 H-scores in the normal epidermis (n=7), peritumoural epidermis (n=8), tumour mass (n=12) and tumour growth front regions (n=11) of 12 recurrent/metastatic well-differentiated primary cSCC tumours. Horizontal bars represent the mean ± SD H-score for each group. Statistics acquired by Kruskal-Wallis test with Dunn's post hoc correction.*

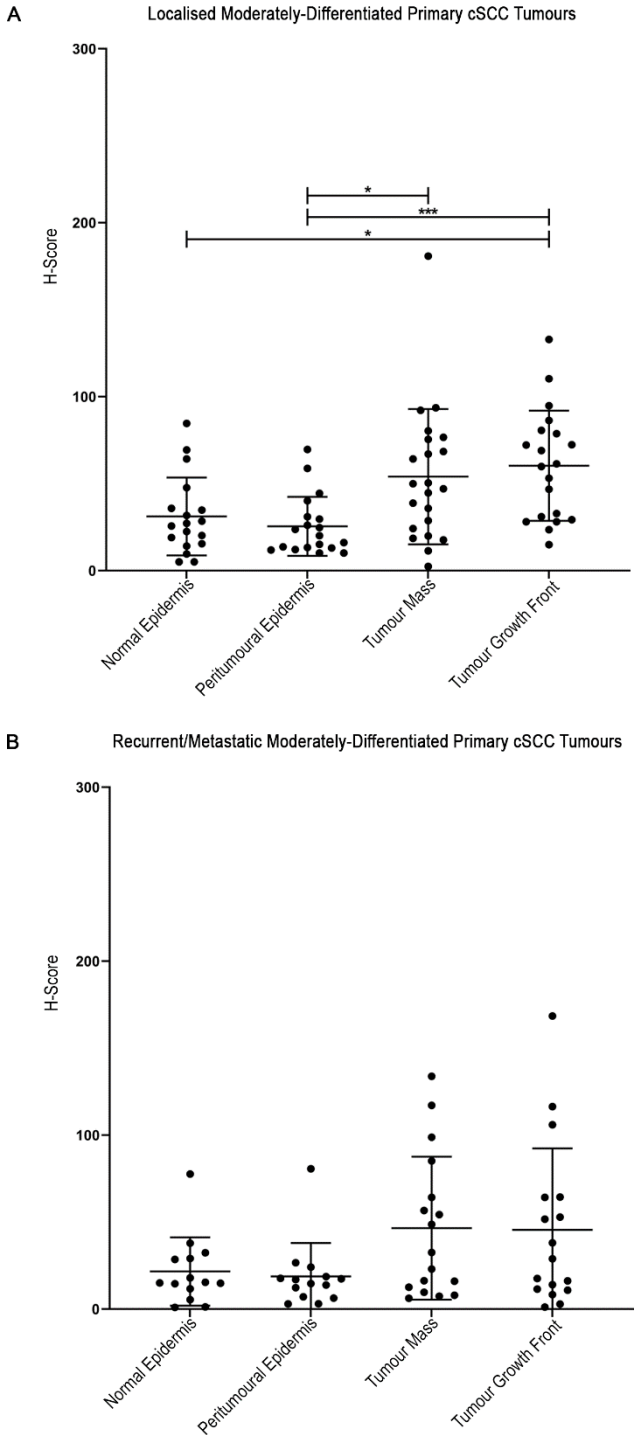

FIGURE A. 10. CYTOPLASMIC EXPRESSION OF P62 IN MODERATELY-DIFFERENTIATED LOCALISED OR RECURRENT/METASTATIC PRIMARY CSCC TUMOURS.

*(**A**) Scatter graph representing the cytoplasmic p62 H-scores in the normal epidermis (n=18), peritumoural epidermis (n=19), tumour mass (n=22) and tumour growth front regions (n=20) of 22 localised moderately-differentiated primary cSCC tumours. Horizontal bars represent the mean ± SD H-score for each group. Statistics acquired by Kruskal-Wallis test with Dunn's post hoc correction (*P<0.05) (***P<0.001). (**B**) Scatter graph representing the cytoplasmic p62 H-scores in the normal epidermis (n=14), peritumoural epidermis (n=14), tumour mass (n=17) and tumour growth front regions (n=17) of 17 recurrent/metastatic moderately-differentiated primary cSCC tumours. Horizontal bars represent the mean ± SD H-score for each group. Statistics acquired by Kruskal-Wallis test with Dunn's post hoc correction.*

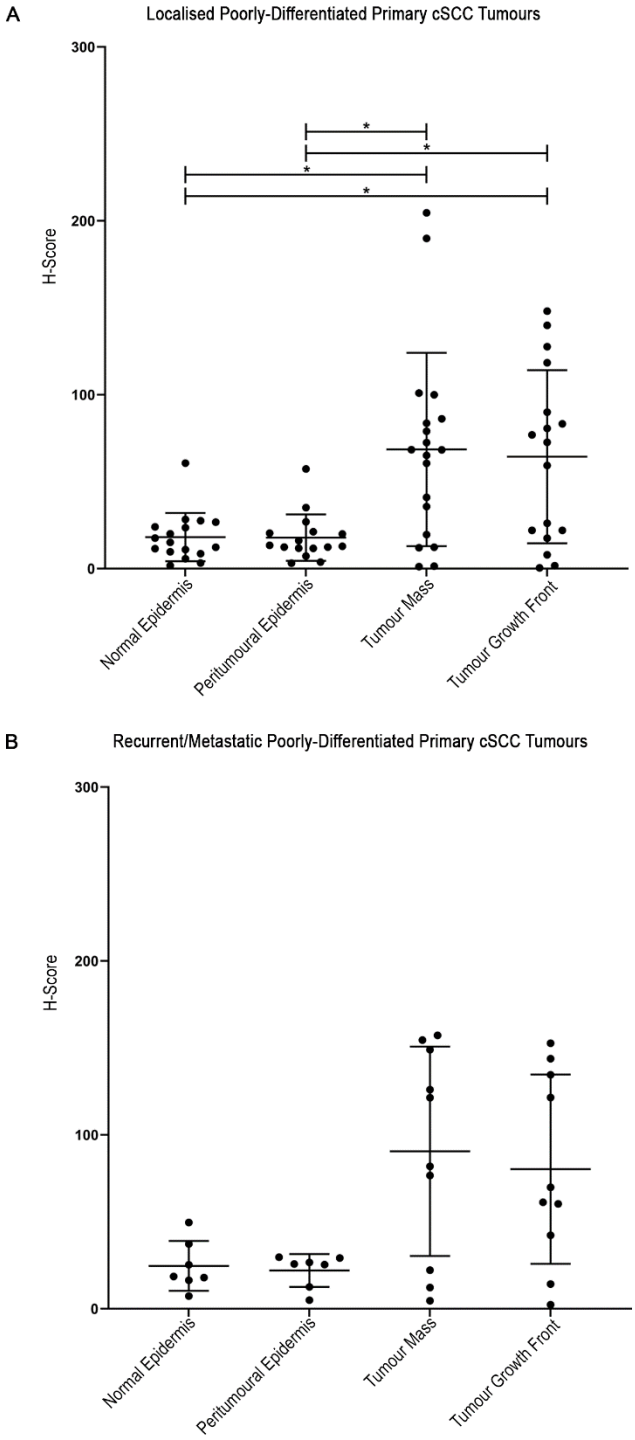

FIGURE A. 11. CYTOPLASMIC EXPRESSION OF P62 IN POORLY DIFFERENTIATED LOCALISED OR RECURRENT/METASTATIC CSCCS.

*(**A**) Scatter graph representing the cytoplasmic p62 H-scores in the normal epidermis (n=17), peritumoural epidermis (n=16), tumour mass (n=19) and tumour growth front regions (n=17) of 19 localised moderately-differentiated primary cSCC tumours. Horizontal bars represent the mean ± SD H-score for each group. Statistics acquired by Kruskal-Wallis test with Dunn's post hoc correction (*P<0.05). (**B**) Scatter graph representing the mean cytoplasmic p62 H-score in the normal epidermis (n=7), peritumoural epidermis (n=7), tumour mass (n=10) and tumour growth front regions (n=10) of 10 recurrent/metastatic moderately-differentiated primary cSCC tumours. Horizontal bars represent the mean ± SD H-score for each group. Statistics acquired by Kruskal-Wallis test with Dunn's post hoc correction.*

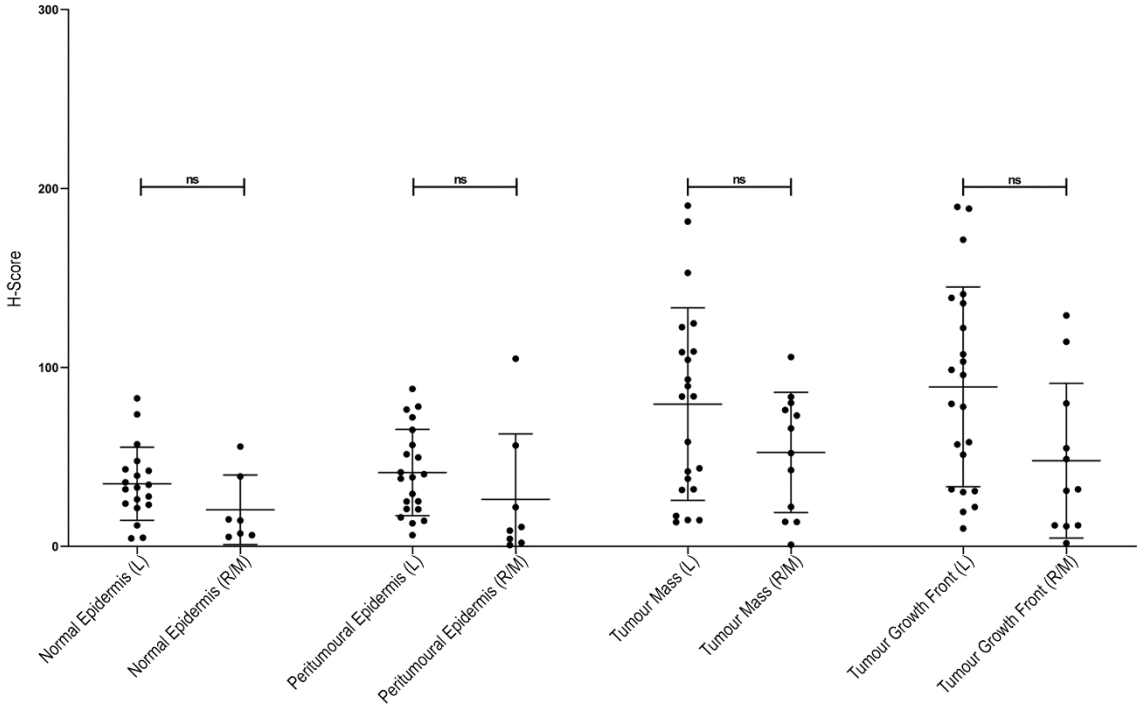

FIGURE A. 12. CYTOPLASMIC P62 EXPRESSION IN THE NORMAL OR PERITUMOURAL OR TUMOUR MASS OR GROWTH FRONT OF WELL-DIFFERENTIATED CSCCS DOES NOT DIFFER BETWEEN LOCALISED AND RECURRENT/METASTATIC TUMOURS.

Scatter graph comparing the cytoplasmic p62 H-scores in the normal epidermis, peritumoural epidermis, tumour mass and tumour growth front regions of well-differentiated localised primary cSCC tumours (L) (n=22) or-differentiated recurrent/metastatic primary cSCC tumours (R/M) (n=12). Horizontal bars represent the mean ± SD H-score for each group. Statistics acquired by Kruskal-Wallis test with Dunn's post hoc correction (ns = non-significant).

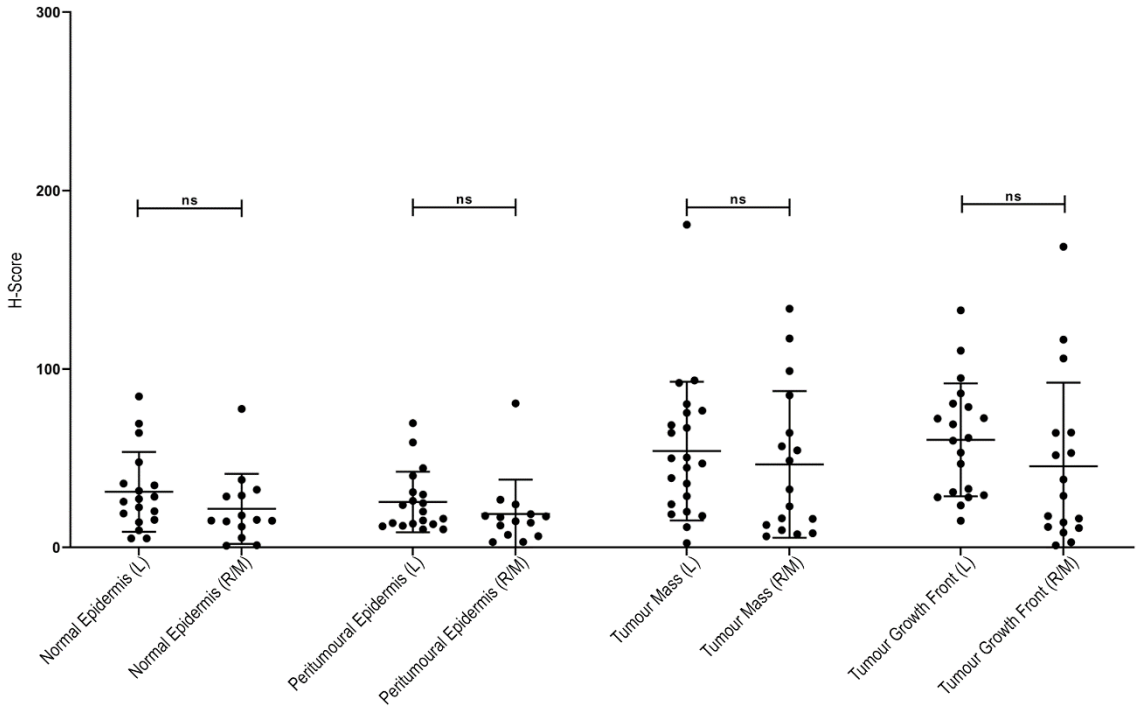

FIGURE A. 13. CYTOPLASMIC P62 EXPRESSION IN THE NORMAL OR PERITUMOURAL OR TUMOUR MASS OR GROWTH FRONT OF MODERATELY WELL-DIFFERENTIATED CSCCS DOES NOT DIFFER BETWEEN LOCALISED AND RECURRENT/METASTATIC TUMOURS.

Scatter graph comparing the cytoplasmic p62 H-scores in the normal epidermis, peritumoural epidermis, tumour mass and tumour growth front regions in moderately-differentiated localised primary cSCC tumours (L) (n=22) or moderately-differentiated recurrent/metastatic primary cSCC tumours (R/M) (n=17). Horizontal bars represent the mean ± SD H-score for each group. Statistics acquired by Kruskal-Wallis test with Dunn's post hoc correction (ns = non-significant).

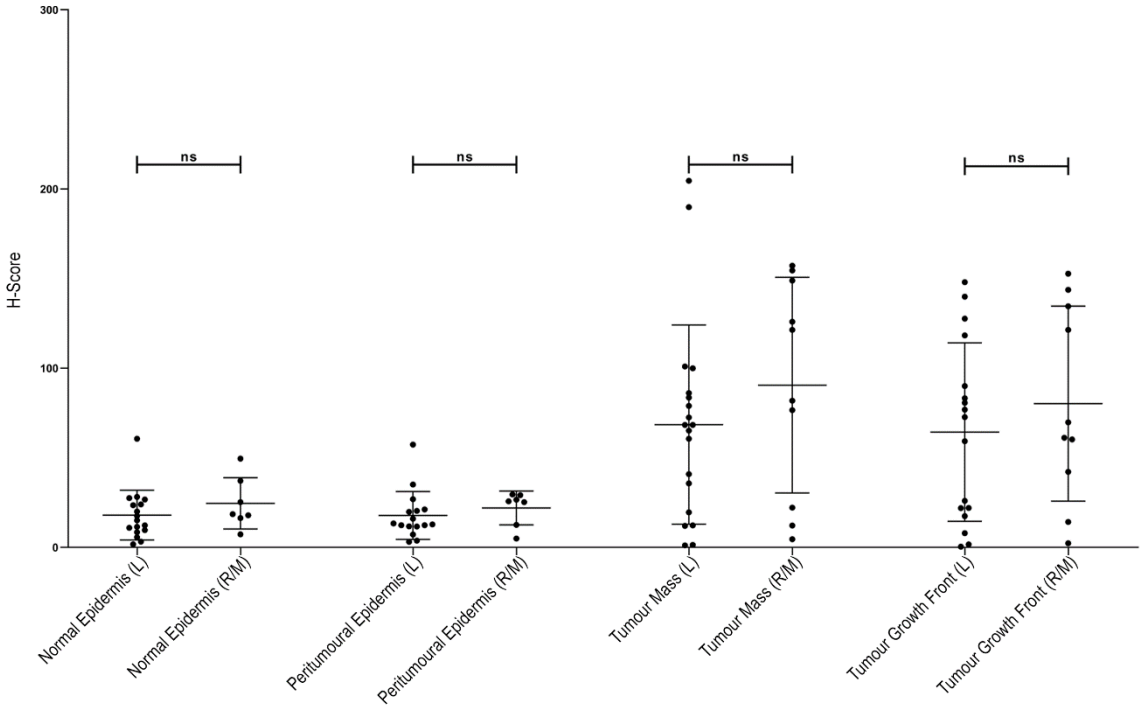

FIGURE A. 14. CYTOPLASMIC P62 EXPRESSION IN THE NORMAL OR PERITUMOURAL OR TUMOUR MASS OR GROWTH FRONT OF POORLY-DIFFERENTIATED CSCCS DOES NOT DIFFER BETWEEN LOCALISED AND RECURRENT/METASTATIC TUMOURS.
Scatter graph comparing the cytoplasmic p62 H-scores in the normal epidermis, peritumoural epidermis, tumour mass and tumour growth front regions in poorly-differentiated localised primary cSCC tumours (L) (n=19) recurrent/metastatic poorly-differentiated primary cSCC tumours (R/M) (n=10). Horizontal bars represent the mean ± SD H-score for each group. Statistics acquired by Kruskal-Wallis test with Dunn's post hoc correction (ns = non-significant).

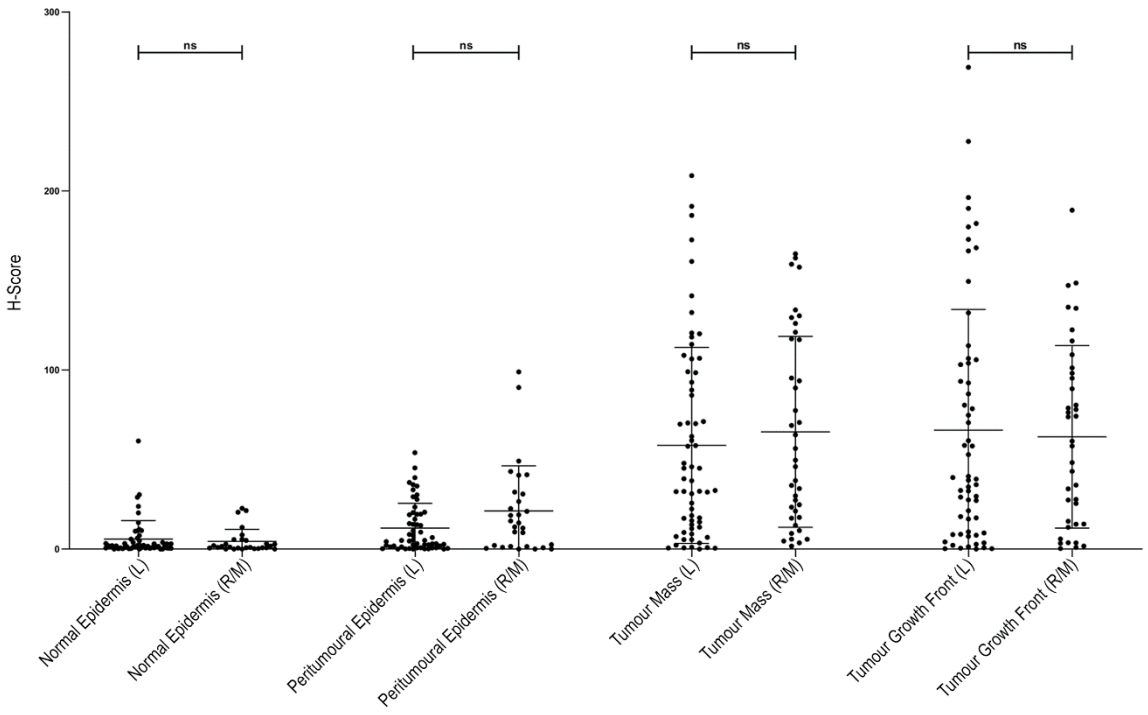

FIGURE A. 15. NUCLEAR P62 EXPRESSION IN THE NORMAL OR PERITUMOURAL EPIDERMIS OR THE TUMOUR MASS OR GROWTH FRONT DOES NOT DIFFER BETWEEN LOCALISED AND RECURRENT/METASTATIC PRIMARY CSCC TUMOURS.
Scatter graph comparing the nuclear p62 H-scores in the normal epidermis, peritumoural epidermis, tumour mass and tumour growth front regions of localised primary cSCC tumours (L) (n=63) to those in recurrent/metastatic primary cSCC tumours (R/M) (n=39). Horizontal bars represent the mean ± SD H-score for each group. Statistics acquired by Kruskal-Wallis test with Dunn's post hoc correction (ns = non-significant).

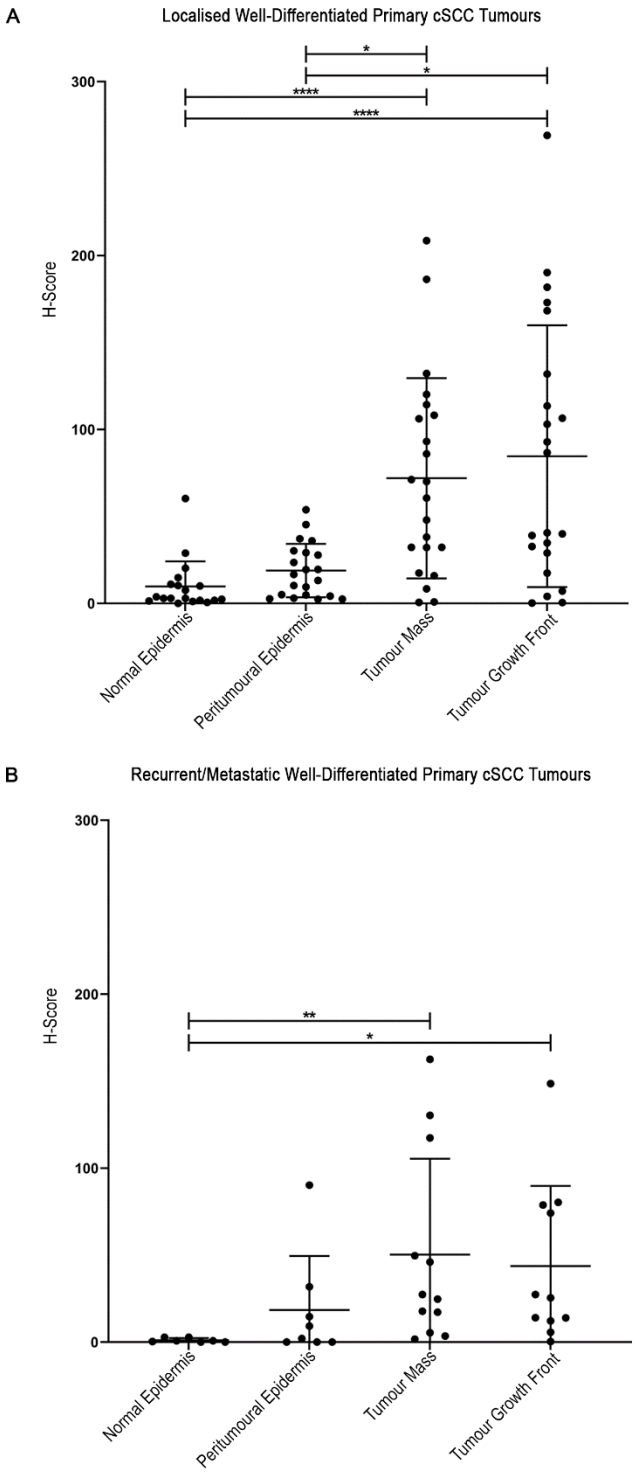

FIGURE A. 16. NUCLEAR P62 EXPRESSION INCREASES WITH CSCC PROGRESSION IN ALL WELL-DIFFERENTIATED CSCC TUMOURS REGARDLESS OF RECURRENT/METASTATIC OUTCOME.

*(**A**) Scatter graph representing the nuclear p62 H-scores in the normal epidermis (n=19), peritumoural epidermis (n=21), tumour mass (n=22) and tumour growth front regions (n=22) in 22 well-differentiated localised primary cSCC tumours. Horizontal bars represent the mean ± SD H-score for each group. Statistics acquired by Kruskal-Wallis test with Dunn's post hoc correction (*P<0.05) (****P<0.0001). (**B**) Scatter graph representing the mean nuclear p62 H-scores in the normal epidermis (n=7), peritumoural epidermis (n=8), tumour mass (n=12) and tumour growth front regions (n=11) of 12 well-differentiated recurrent/metastatic primary cSCC tumours. Horizontal bars represent the mean ± SD H-score for each group. Statistics acquired by Kruskal-Wallis test with Dunn's post hoc correction (*P<0.05) (**P<0.01).*

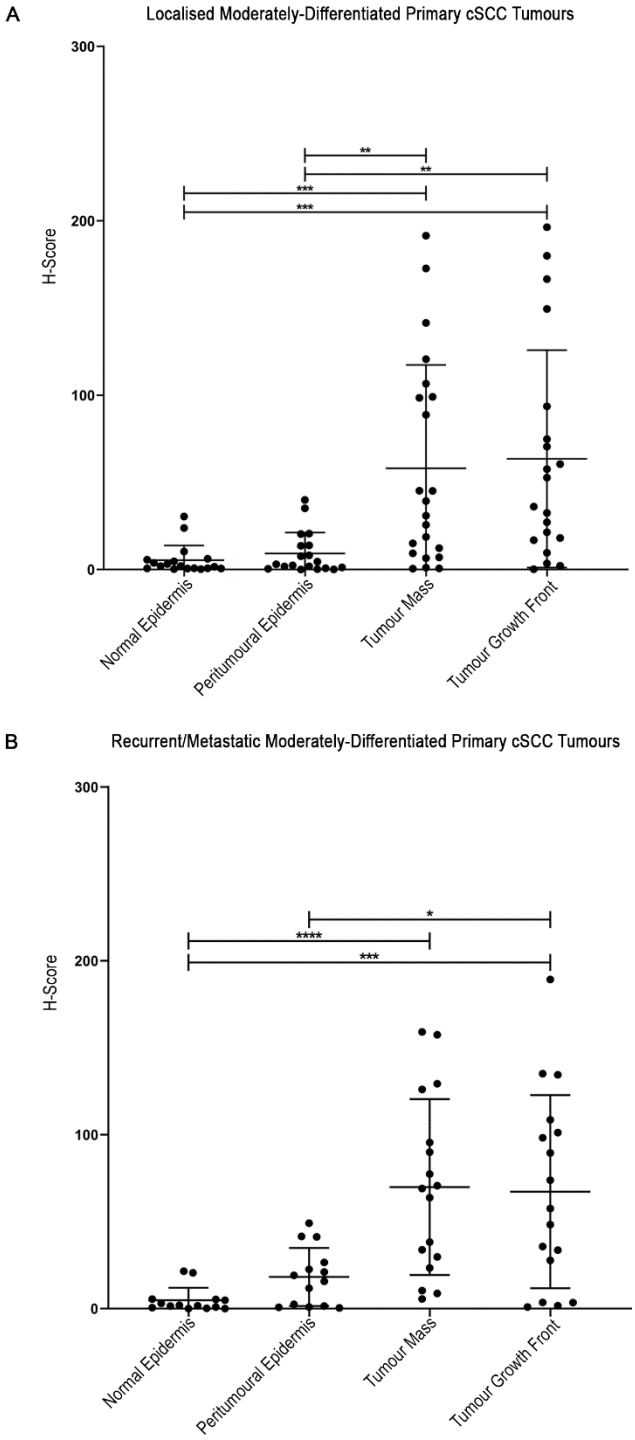

FIGURE A. 17. NUCLEAR P62 EXPRESSION INCREASES WITH CSCC PROGRESSION IN ALL MODERATELY-DIFFERENTIATED CSCC TUMOURS REGARDLESS OF DISEASE OUTCOME.

*(**A**) Scatter graph representing the nuclear p62 H-scores in the normal epidermis (n=18), peritumoural epidermis (n=19), tumour mass (n=22) and tumour growth front regions (n=20) in 22 moderately-differentiated localised primary cSCC tumours. Horizontal bars represent the mean ± SD H-score for each group. Statistics acquired by Kruskal-Wallis test with Dunn's post hoc correction (**P<0.01) (***P<0.001). (**B**) Scatter graph representing the nuclear p62 H-scores in the normal epidermis (n=14), peritumoural epidermis (n=14), tumour mass (n=17) and tumour growth front regions (n=17) in 17 moderately-differentiated recurrent/metastatic primary cSCC tumours. Horizontal bars represent the mean ± SD H-score for each group. Statistics acquired by Kruskal-Wallis test with Dunn's post hoc correction (*P<0.05) (***P<0.001) (****P<0.0001).*

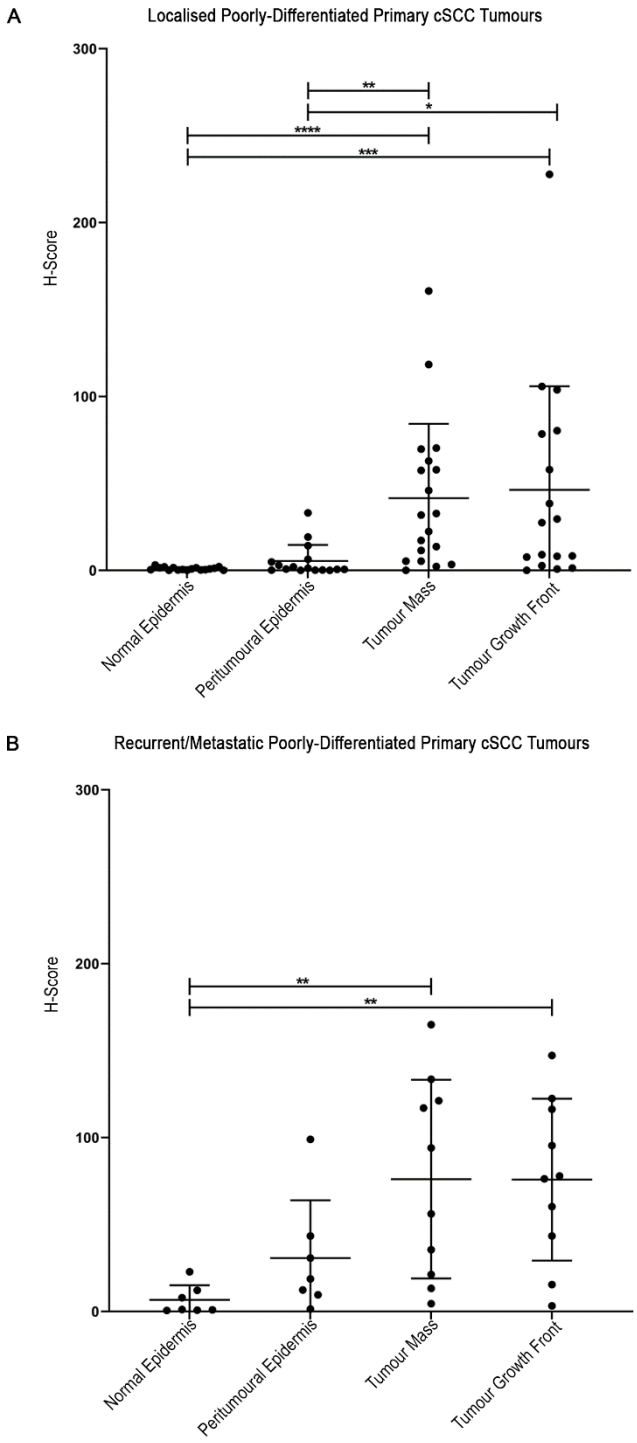

FIGURE A. 18. NUCLEAR P62 EXPRESSION INCREASES WITH CSCC PROGRESSION IN ALL POORLY-DIFFERENTIATED CSCC TUMOURS REGARDLESS OF DISEASE OUTCOME.

*(**A**) Scatter graph representing the nuclear p62 H-scores in the normal epidermis (n=17), peritumoural epidermis (n=16), tumour mass (n=19) and tumour growth front regions (n=17) in 19 poorly-differentiated localised primary cSCC tumours. Horizontal bars represent the mean ± SD H-score for each group. Statistics acquired by Kruskal-Wallis test with Dunn's post hoc correction (*P<0.05) (**P<0.01) (***P<0.001) (****P<0.0001). (**B**) Scatter graph representing the nuclear p62 H-scores in the normal epidermis (n=7), peritumoural epidermis (n=7), tumour mass (n=10) and tumour growth front regions (n=10) in 10 poorly-differentiated recurrent/metastatic primary cSCC tumours. Horizontal bars represent the mean ± SD H-score for each group. Statistics acquired by Kruskal-Wallis test with Dunn's post hoc correction (**P<0.01)*

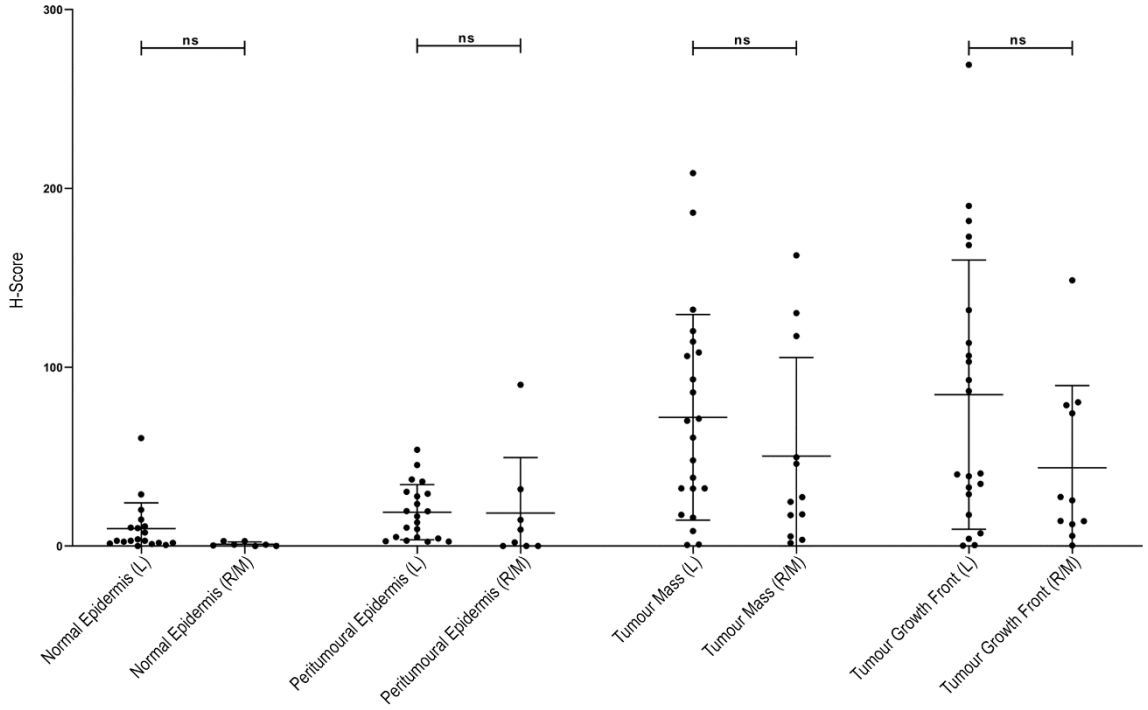

FIGURE A. 19. NUCLEAR P62 EXPRESSION IN THE NORMAL OR PERITUMOURAL EPIDERMIS OR THE TUMOUR MASS OR GROWTH FRONT DOES NOT DIFFER BETWEEN WELL-DIFFERENTIATED LOCALISED OR RECURRENT/METASTATIC CSCCS.
Scatter graph comparing the nuclear p62 H-scores in the normal epidermis, peritumoural epidermis, tumour mass and tumour growth front regions in well-differentiated localised primary cSCC tumours (L) (n=22) or well-differentiated recurrent/metastatic primary cSCC tumours (R/M) (n=39). Horizontal bars represent the mean ± SD H-score for each group. Statistics acquired by Kruskal-Wallis test with Dunn's post hoc correction (ns = non-significant).

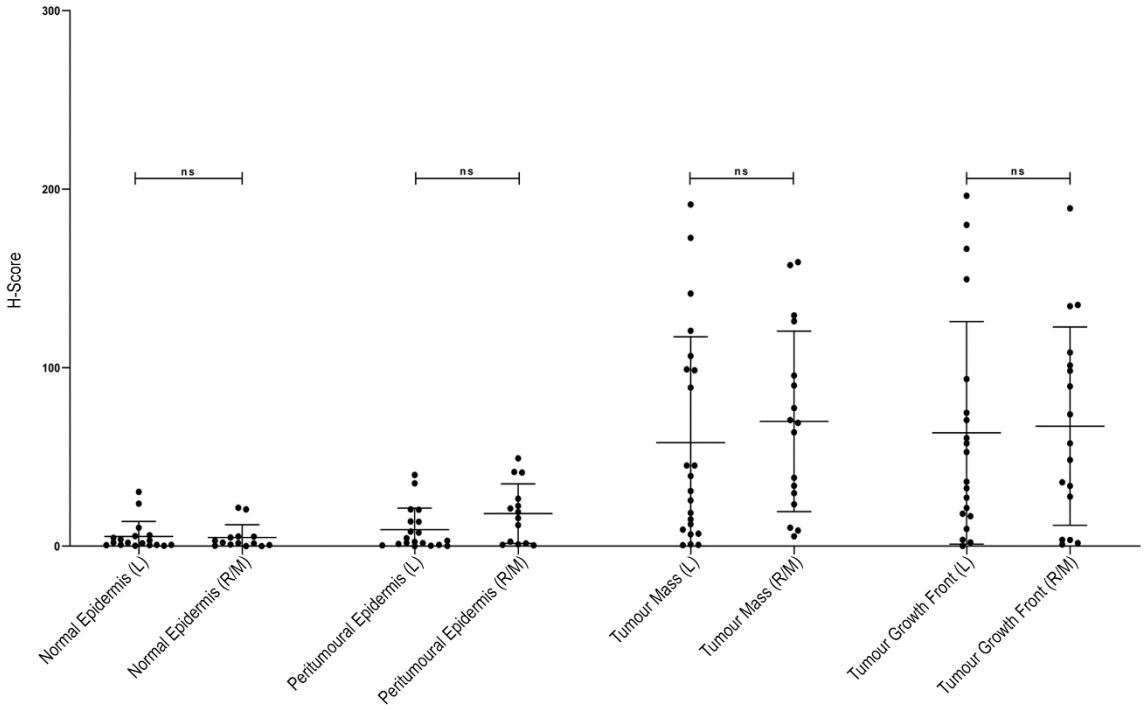

FIGURE A. 20. NUCLEAR P62 EXPRESSION IN THE NORMAL OR PERITUMOURAL EPIDERMIS OR THE TUMOUR MASS OR GROWTH FRONT DOES NOT DIFFER BETWEEN MODERATELY WELL-DIFFERENTIATED LOCALISED OR RECURRENT/METASTATIC CSCCS.

Scatter graph of nuclear p62 H-scores in the normal epidermis, peritumoural epidermis, tumour mass and tumour growth front regions of moderately-differentiated localised primary cSCC tumours (L) (n=22) or moderately-differentiated recurrent/metastatic moderately-differentiated primary cSCC tumours (R/M) (n=17). Horizontal bars represent the mean ± SD H-score for each group. Statistics acquired by Kruskal-Wallis test with Dunn's post hoc correction (ns = non-significant).

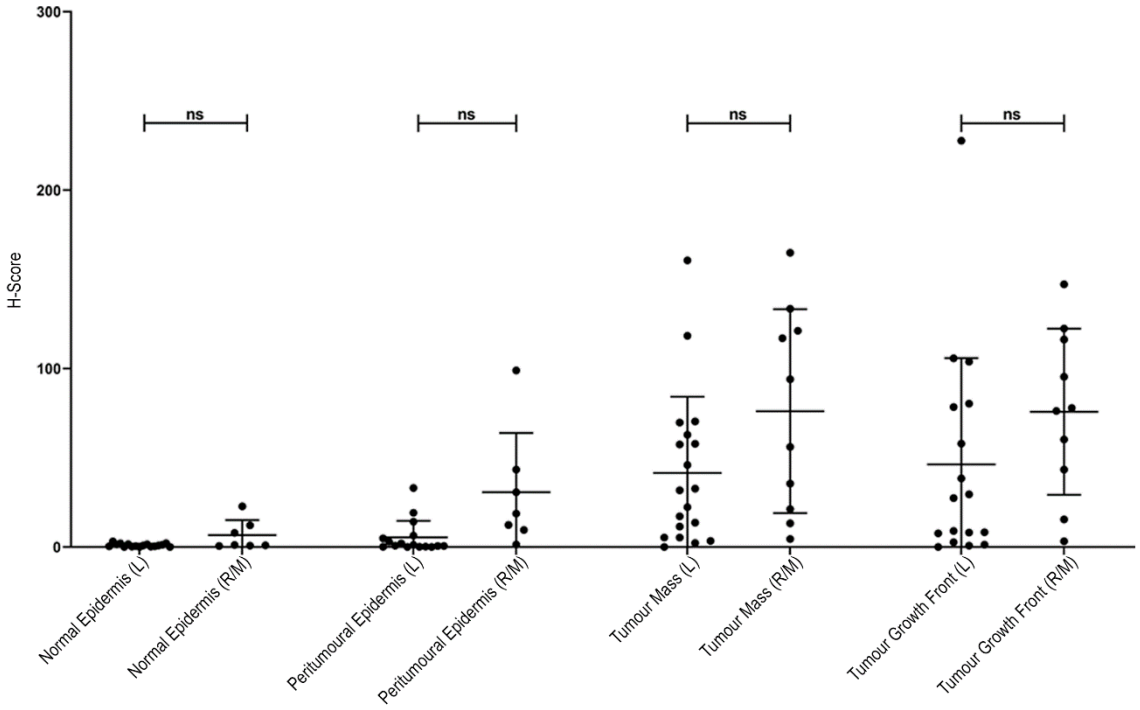

FIGURE A. 21. NUCLEAR P62 EXPRESSION IN THE NORMAL OR PERITUMOURAL EPIDERMIS OR THE TUMOUR MASS OR GROWTH FRONT DOES NOT DIFFER BETWEEN POORLY-DIFFERENTIATED LOCALISED OR RECURRENT/METASTATIC CSCCS.
Scatter graph of nuclear p62 H-scores of the normal epidermis, peritumoural epidermis, tumour mass and tumour growth front regions of poorly-differentiated localised primary cSCC tumours (L) (n=22) or poorly-differentiated recurrent/metastatic primary cSCC tumours (R/M) (n=17). Horizontal bars represent the mean ± SD H-score for each group. Statistics acquired by Kruskal-Wallis test with Dunn's post hoc correction (ns = non-significant).

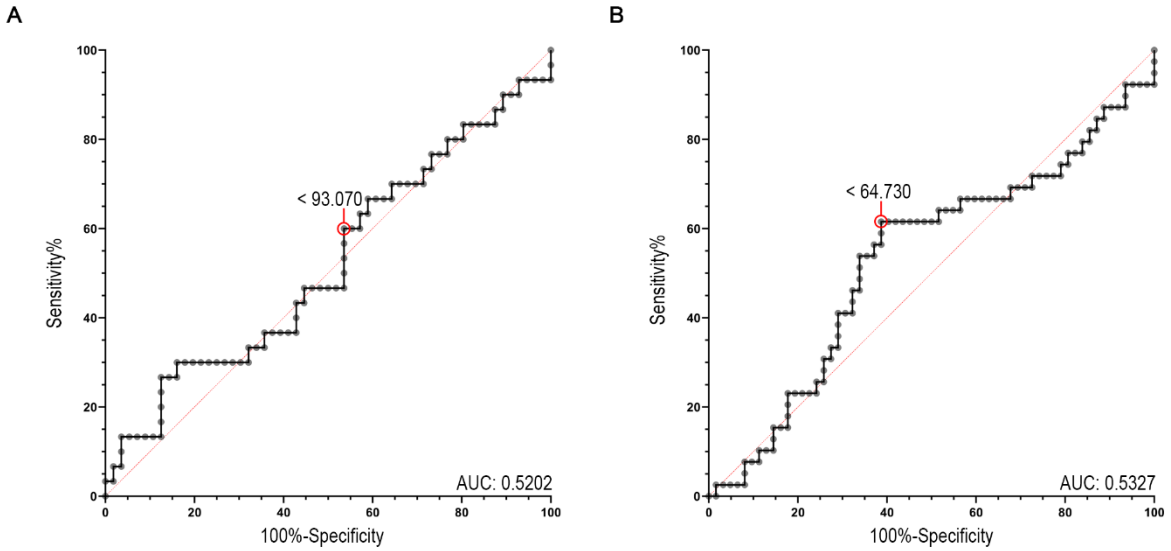

FIGURE A. 22. CYTOPLASMIC AMBRA1 EXPRESSION IN THE PERITUMOURAL EPIDERMIS OR THE TUMOUR MASS REGION DOES NOT PREDICT CSCC PROGRESSION OF PRIMARY CSCC TUMOURS AS WELL AS EXPRESSION IN THE TUMOUR GROWTH FRONT. *(**A**) Receiver operating characteristic (ROC) curve for prediction of a cSCC event (recurrence/metastasis) based on the cytoplasmic AMBRA1 H-score in the peritumoural epidermis of all primary cSCC tumours (n=86). The AMBRA1 H-score with the highest specificity and sensitivity is highlighted by a red circle. AUC = area under the curve. (**B**) Receiver operating characteristic (ROC) curve for prediction of prediction of a cSCC event (recurrence/metastasis) based on the cytoplasmic AMBRA1 H-score in the tumour mass of all primary cSCC tumours (n=101). The AMBRA1 H-score with the highest specificity and sensitivity is highlighted by a red circle. AUC = area under the curve.*

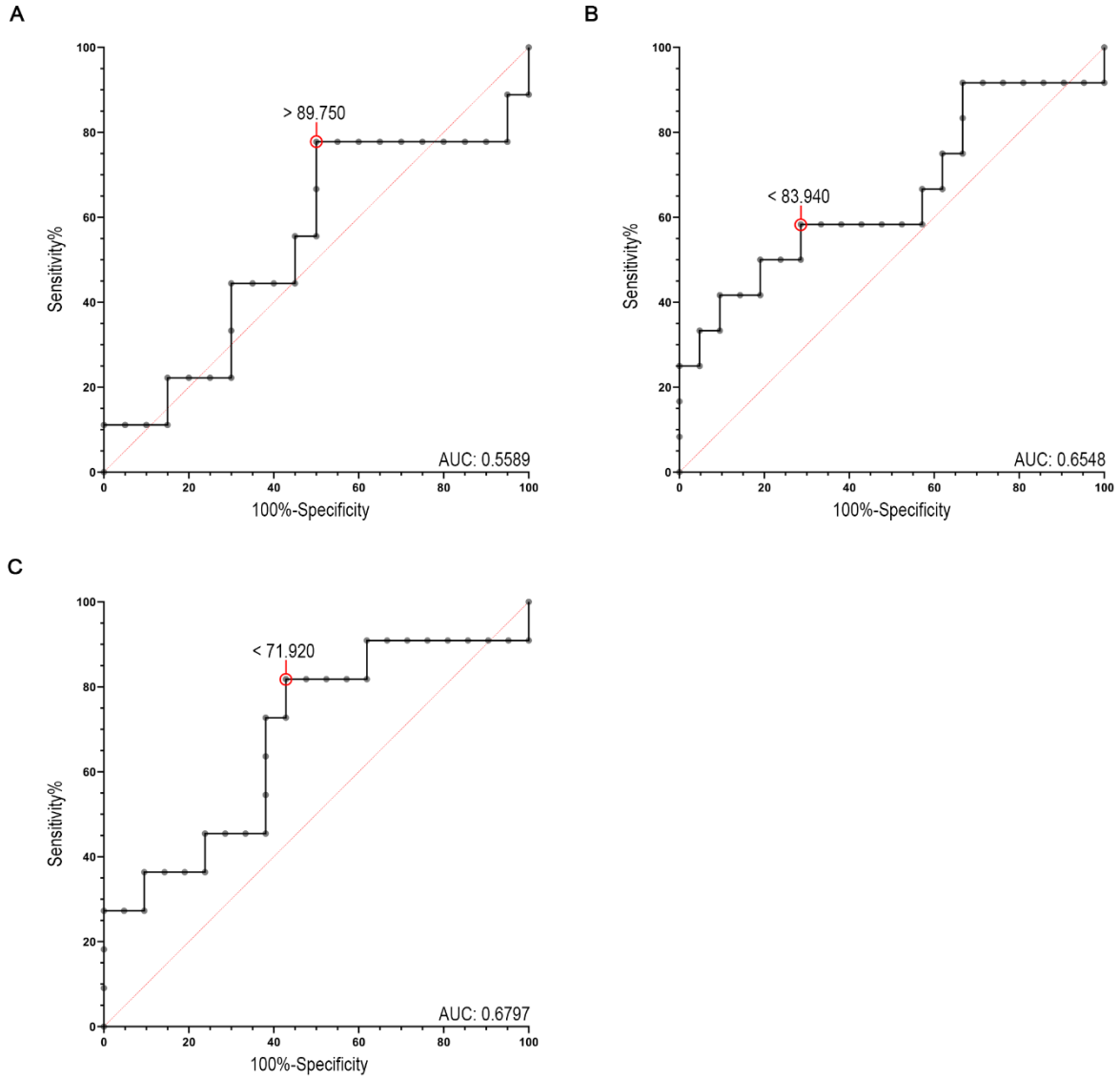

FIGURE A. 23. *CYTOPLASMIC AMBRA1 EXPRESSION IN THE TUMOUR GROWTH FRONT BEST PREDICTS A CSCC DISEASE EVENT IN WELL-DIFFERENTIATED PRIMARY CSCC TUMOURS.*

*(**A**) Receiver operating characteristic (ROC) curve for prediction of a cSCC event (reoccurrence/metastasis) based on the cytoplasmic AMBRA1 H-score in the peritumoural epidermis of well-differentiated primary cSCC tumours (n=29). The AMBRA1 H-score with the highest specificity and sensitivity is highlighted by a red circle. AUC = area under the curve. (**B**) Receiver operating characteristic (ROC) curve for prediction of a cSCC event (recurrence/metastasis) metastasis based on the cytoplasmic AMBRA1 H-score in the tumour mass of well-differentiated primary cSCC tumours (n=33). The AMBRA1 H-score with the highest specificity and sensitivity is highlighted by a red circle. AUC = area under the curve. (**C**) Receiver operating characteristic (ROC) curve for prediction of a cSCC event (recurrence/metastasis) based on the cytoplasmic AMBRA1 H-score in the tumour growth front of well-differentiated primary cSCC tumours (n=32). The AMBRA1 H-score with the highest specificity and sensitivity is highlighted by a red circle. AUC = area under the curve.*

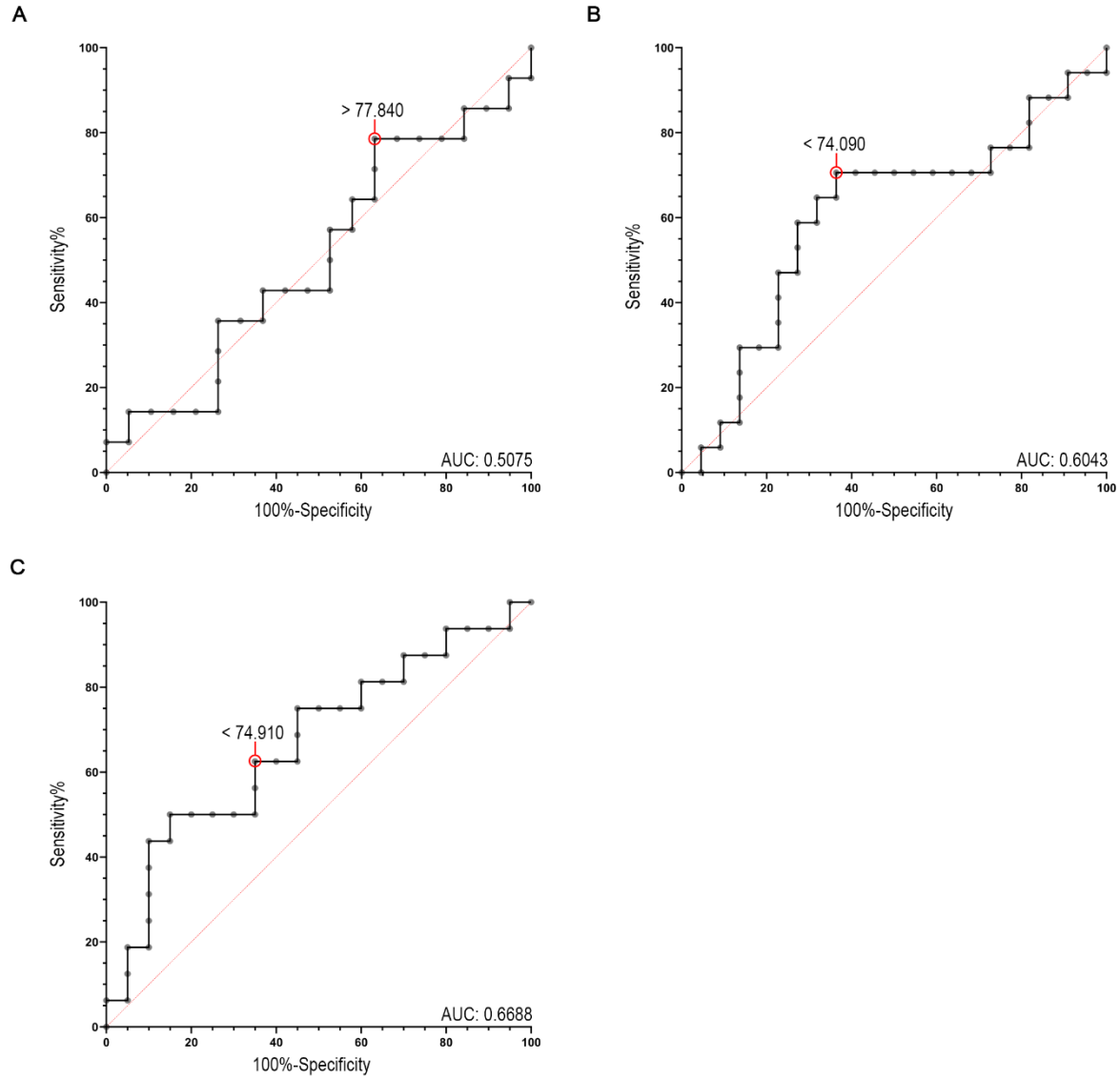

FIGURE A. 24. CYTOPLASMIC AMBRA1 EXPRESSION IN THE TUMOUR GROWTH FRONT BEST PREDICTS A CSCC DISEASE EVENT IN MODERATELY-DIFFERENTIATED PRIMARY CSCC TUMOURS.

*(**A**) Receiver operating characteristic (ROC) curve for prediction of a cSCC event (reoccurrence/metastasis) based on the cytoplasmic AMBRA1 H-score in the peritumoural epidermis of moderately-differentiated primary cSCC tumours (n=33). The AMBRA1 H-score with the highest specificity and sensitivity is highlighted by a red circle. AUC = area under the curve. (**B**) Receiver operating characteristic (ROC) curve for prediction of a cSCC event (recurrence/metastasis) based on the cytoplasmic AMBRA1 H-score in the tumour mass of moderately-differentiated primary cSCC tumours (n=39). The AMBRA1 H-score with the highest specificity and sensitivity is highlighted by a red circle. AUC = area under the curve. (**C**) Receiver operating characteristic (ROC) curve for prediction of a cSCC event (recurrence/metastasis) based on the cytoplasmic AMBRA1 H-score in the tumour growth front of moderately-differentiated cSCC tumours (n=36). The AMBRA1 H-score with the highest specificity and sensitivity is highlighted by a red circle. AUC = area under the curve.*

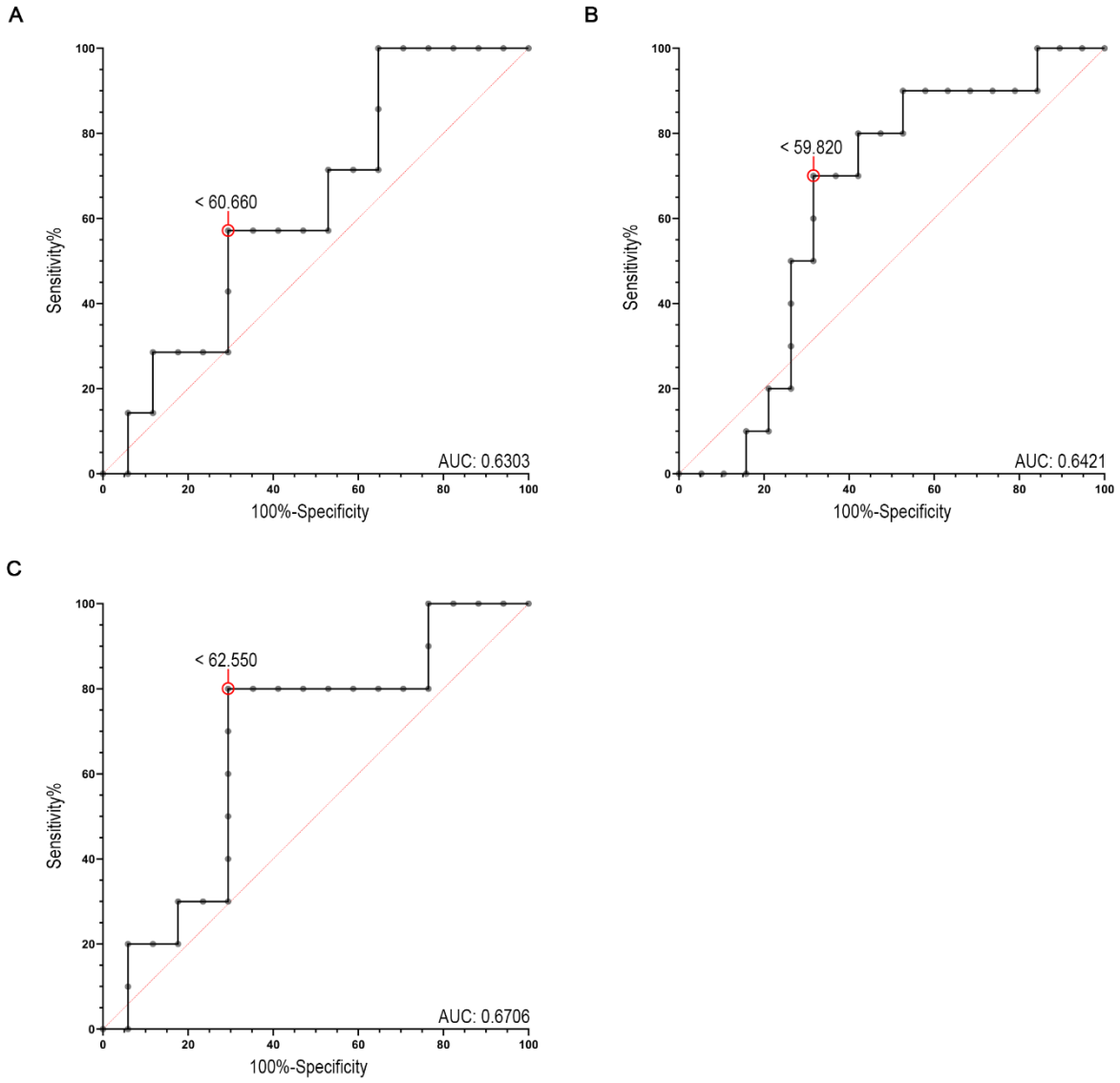

FIGURE A. 25. CYTOPLASMIC AMBRA1 EXPRESSION IN THE TUMOUR GROWTH FRONT BEST PREDICTS A CSCC EVENT OCCURRING IN POORLY-DIFFERENTIATED PRIMARY CSCC TUMOURS.
*(**A**) Receiver operating characteristic (ROC) curve for prediction of a cSCC event (reoccurrence/metastasis) based on the cytoplasmic AMBRA1 H-score in the peritumoural epidermis of poorly-differentiated primary cSCC tumours (n=24). The AMBRA1 H-score with the highest specificity and sensitivity is highlighted by a red circle. AUC = area under the curve. (**B**) Receiver operating characteristic (ROC) curve for prediction of a cSCC event (recurrence/metastasis) based on the cytoplasmic AMBRA1 H-score in the tumour mass of poorly-differentiated primary cSCC tumours (n=29). The AMBRA1 H-score with the highest specificity and sensitivity is highlighted by a red circle. AUC = area under the curve. (**C**) Receiver operating characteristic (ROC) curve for prediction of a cSCC event (recurrence/metastasis) based on the cytoplasmic AMBRA1 H-score in the tumour growth front of poorly-differentiated cSCC tumours (n=27). The AMBRA1 H-score with the highest specificity and sensitivity is highlighted by a red circle. AUC = area under the curve.*

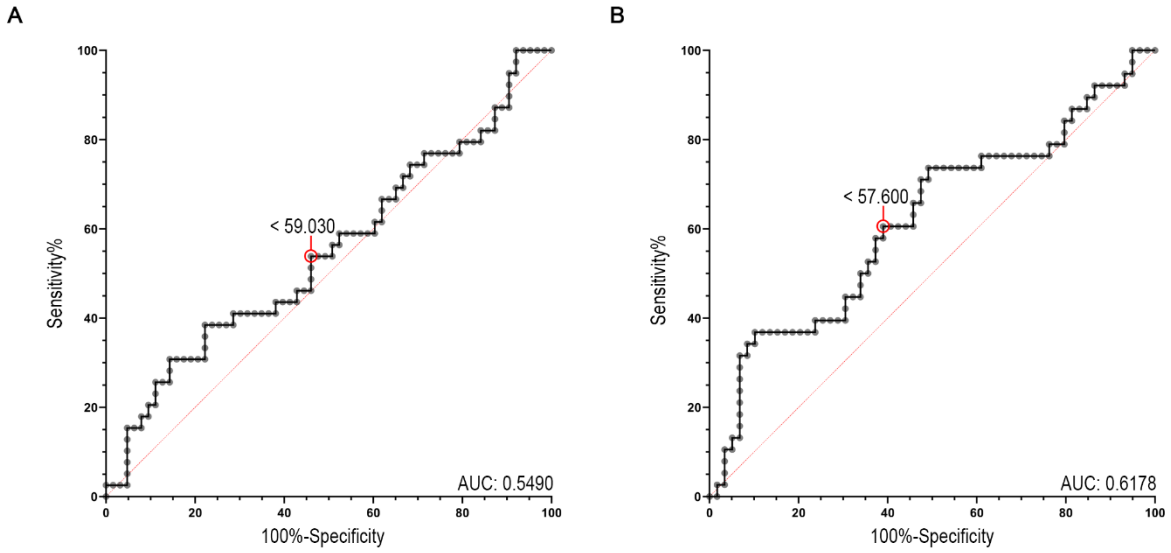

FIGURE A. 26. CYTOPLASMIC P62 EXPRESSION IN THE TUMOUR MASS OR GROWTH OF PRIMARY CSCCS DO NOT PREDICT DISEASE PROGRESSION AS WELL AS EXPRESSION IN THE PERI-TUMOURAL EPIDERMIS. TUMOUR GROWTH FRONT.

*(**A**) Receiver operating characteristic (ROC) curve for prediction of a cSCC event (recurrence/metastasis) based on the cytoplasmic p62 H-score in the tumour mass of all primary cSCC tumours (n=102). The p62 H-score with the highest specificity and sensitivity is highlighted by a red circle. AUC = area under the curve. (**B**) Receiver operating characteristic (ROC) curve for prediction of a cSCC event (recurrence/metastasis) based on the cytoplasmic p62 H-score in the tumour growth front of all primary cSCC tumours (n=97). The p62 H-score with the highest specificity and sensitivity is highlighted by a red circle. AUC = area under the curve*

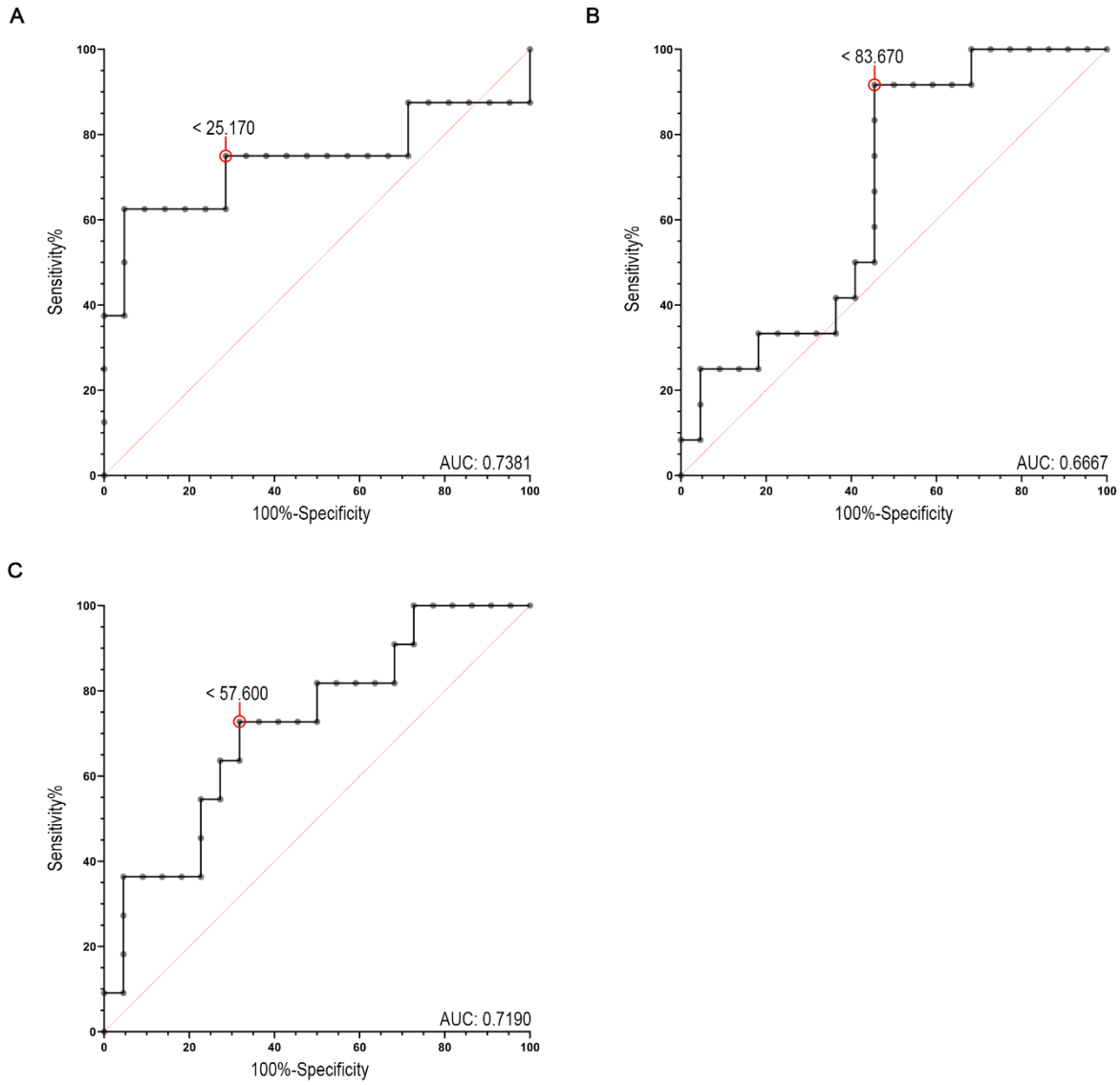

FIGURE A. 27. CYTOPLASMIC P62 EXPRESSION IN THE PERITUMOURAL EPIDERMIS BEST PREDICTS A CSCC EVENT OCCURRING IN WELL-DIFFERENTIATED PRIMARY CSCC TUMOURS.

*(**A**) Receiver operating characteristic (ROC) curve for prediction of a cSCC event (reoccurrence/metastasis) based on the cytoplasmic p62 H-score in the peritumoural epidermis of well-differentiated primary cSCC tumours (n=29). The p62 H-score with the highest specificity and sensitivity is highlighted by a red circle. AUC = area under the curve. (**B**) Receiver operating characteristic (ROC) curve for prediction of a cSCC event (recurrence/metastasis) based on the cytoplasmic p62 H-score in the tumour mass of well-differentiated primary cSCC tumours (n=34). The p62 H-score with the highest specificity and sensitivity is highlighted by a red circle. AUC = area under the curve. (**C**) Receiver operating characteristic (ROC) curve for prediction of a cSCC event (recurrence/metastasis) based on the cytoplasmic p62 H-score in the tumour growth front of well-differentiated primary cSCC tumours (n=33). The p62 H-score with the highest specificity and sensitivity is highlighted by a red circle. AUC = area under the curve.*

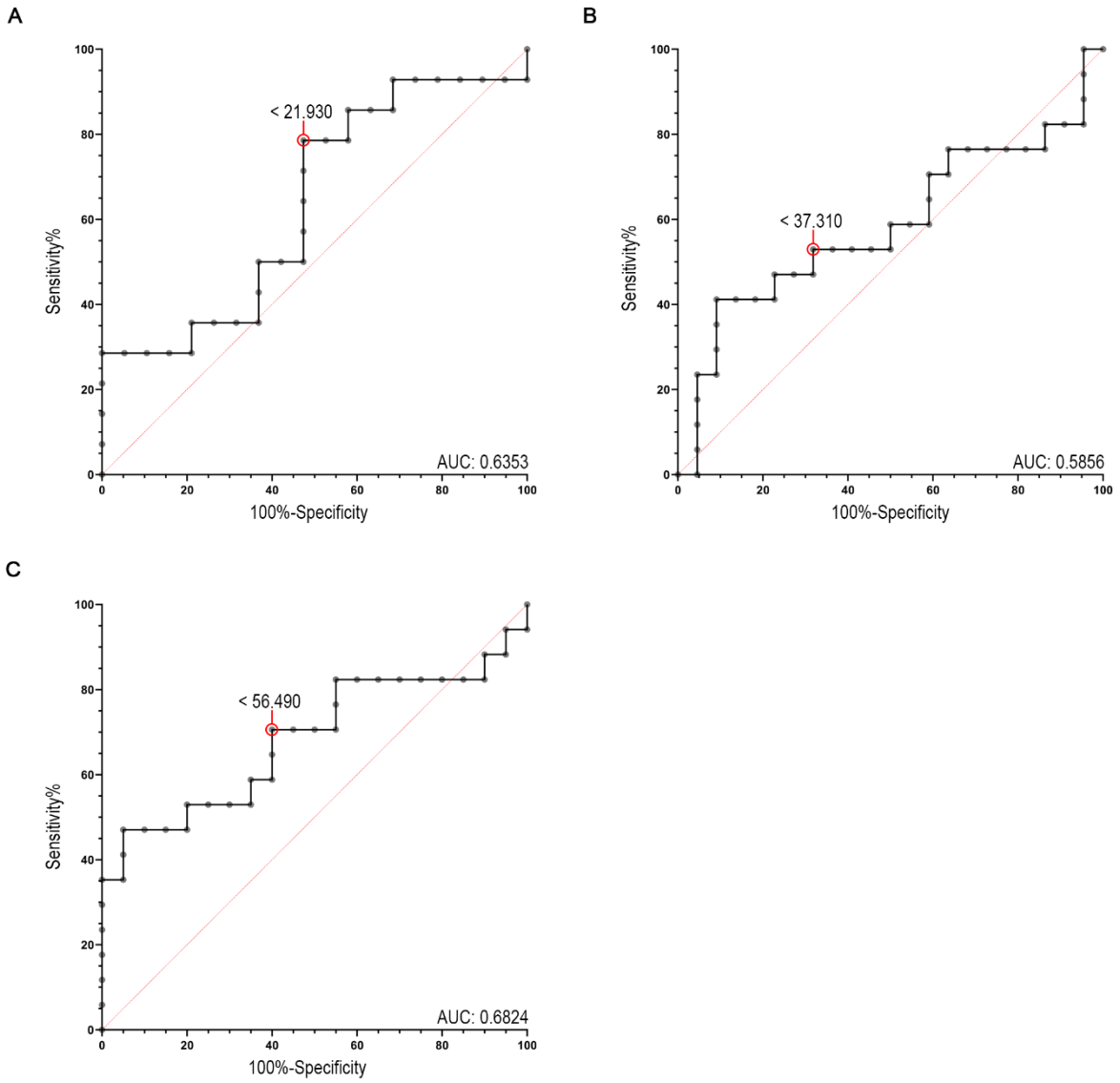

FIGURE A. 28. CYTOPLASMIC P62 EXPRESSION IN THE TUMOUR GROWTH FRONT BEST PREDICTS A CSCC EVENT OCCURRING IN MODERATELY-DIFFERENTIATED PRIMARY CSCC TUMOURS.

*(**A**) Receiver operating characteristic (ROC) curve for prediction of a cSCC event (reoccurrence/metastasis) based on the cytoplasmic p62 H-score in the peritumoural epidermis of moderately-differentiated primary cSCC tumours (n=23). The p62 H-score with the highest specificity and sensitivity is highlighted by a red circle. AUC = area under the curve. (**B**) Receiver operating characteristic (ROC) curve for prediction of a cSCC event (recurrence/metastasis) based on the cytoplasmic p62 H-score in the tumour mass of moderately-differentiated primary cSCC tumours (n=39). The p62 H-score with the highest specificity and sensitivity is highlighted by a red circle. AUC = area under the curve. (**C**) Receiver operating characteristic (ROC) curve for prediction of a cSCC event (recurrence/metastasis) based on the cytoplasmic p62 H-score in the tumour growth front of moderately-differentiated primary cSCC tumours (n=37). The p62 H-score with the highest specificity and sensitivity is highlighted by a red circle. AUC = area under the curve.*

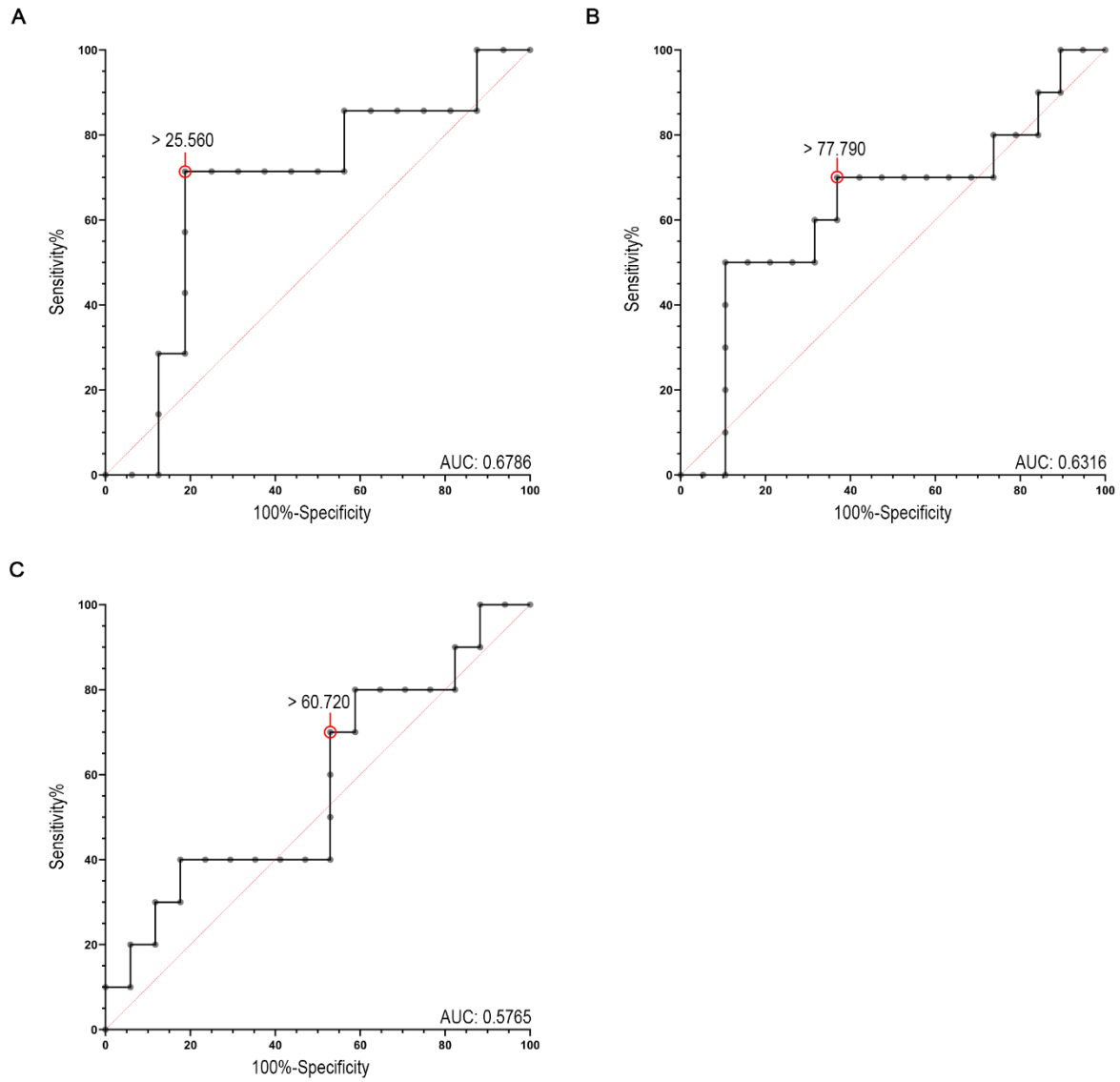

FIGURE A. 29. CYTOPLASMIC P62 EXPRESSION IN THE PERITUMOURAL EPIDERMIS BEST PREDICTS A CSCC EVENT OCCURRING IN POORLY-DIFFERENTIATED PRIMARY CSCC TUMOURS.

*(**A**) Receiver operating characteristic (ROC) curve for prediction of a cSCC event (reoccurrence/metastasis) based on the cytoplasmic p62 H-score in the peritumoural epidermis of poorly-differentiated primary cSCC tumours (n=23). The p62 H-score with the highest specificity and sensitivity is highlighted by a red circle. AUC = area under the curve. (**B**) Receiver operating characteristic (ROC) curve for prediction of a cSCC event (recurrence/metastasis) based on the cytoplasmic p62 H-score in the tumour mass of poorly-differentiated primary cSCC tumours (n=29). The p62 H-score with the highest specificity and sensitivity is highlighted by a red circle. AUC = area under the curve. (**C**) Receiver operating characteristic (ROC) curve for prediction of a cSCC event (recurrence/metastasis) based on the cytoplasmic p62 H-score in the tumour growth front of poorly-differentiated primary cSCC tumours (n=27). The p62 H-score with the highest specificity and sensitivity is highlighted by a red circle. AUC = area under the curve.*

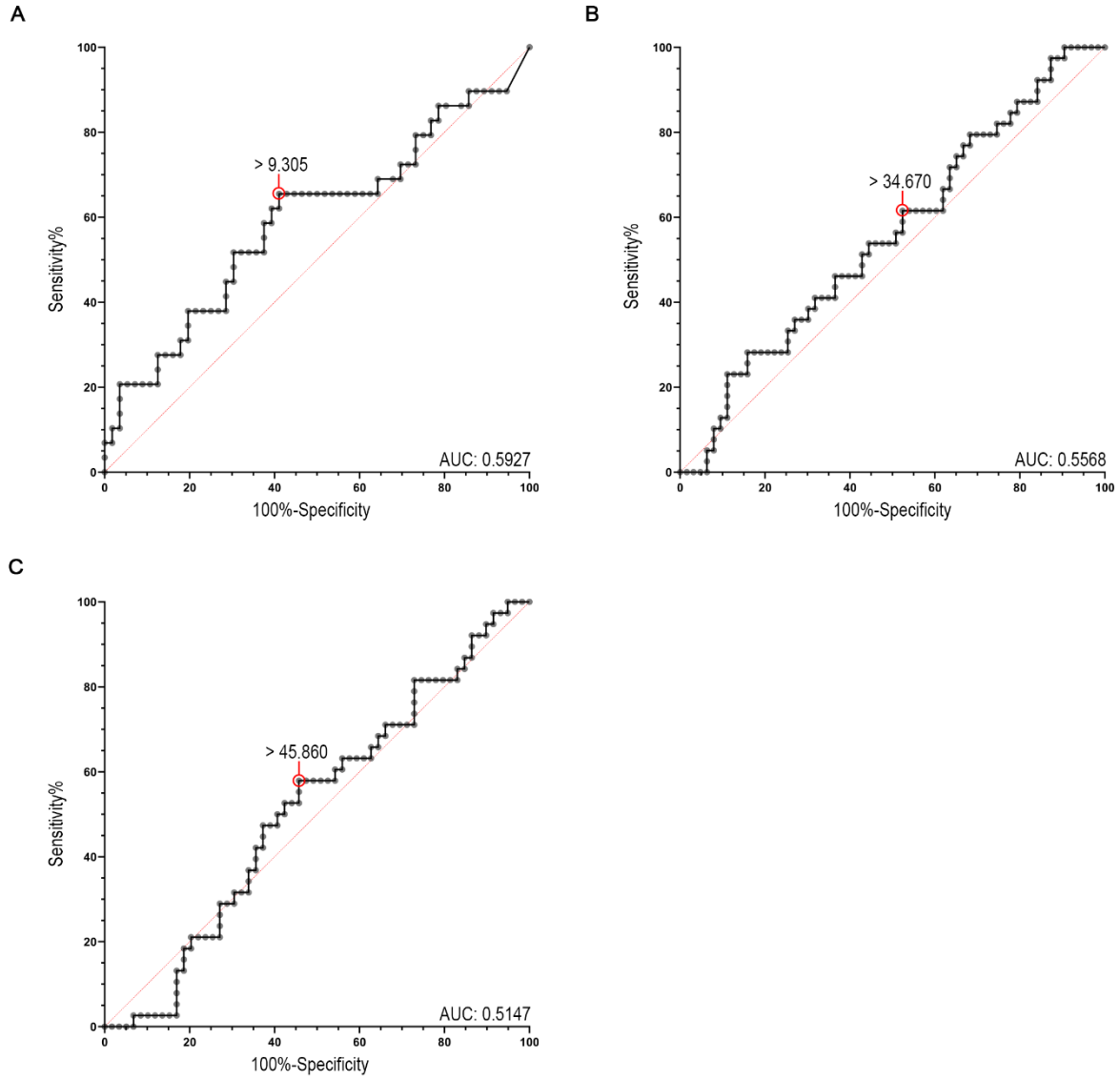

FIGURE A. 30. EXPRESSION OF NUCLEAR P62 IN PERITUMOURAL EPIDERMIS, TUMOUR MASS OR GROWTH FRONT DOES NOT PREDICT DISEASE PROGRESSION AS WELL AS CYTOPLASMIC EXPRESSION IN THE PERITUMOURAL EPIDERMIS.

*(**A**) Receiver operating characteristic (ROC) curve for prediction of a cSCC event (reoccurrence/metastasis) based on the nuclear p62 H-score in the peritumoural epidermis of all primary cSCC tumours (n=85). The p62 H-score with the highest specificity and sensitivity is highlighted by a red circle. AUC = area under the curve. (**B**) Receiver operating characteristic (ROC) curve for prediction of a cSCC event (recurrence/metastasis) based on the nuclear p62 H-score in the tumour mass of all primary cSCC tumours (n=102). The p62 H-score with the highest specificity and sensitivity is highlighted by a red circle. AUC = area under the curve. (**C**) Receiver operating characteristic (ROC) curve for prediction of a cSCC event (recurrence/metastasis) based on the nuclear p62 H-score in the tumour growth front of all primary cSCC tumours (n=97). The p62 H-score with the highest specificity and sensitivity is highlighted by a red circle. AUC = area under the curve.*

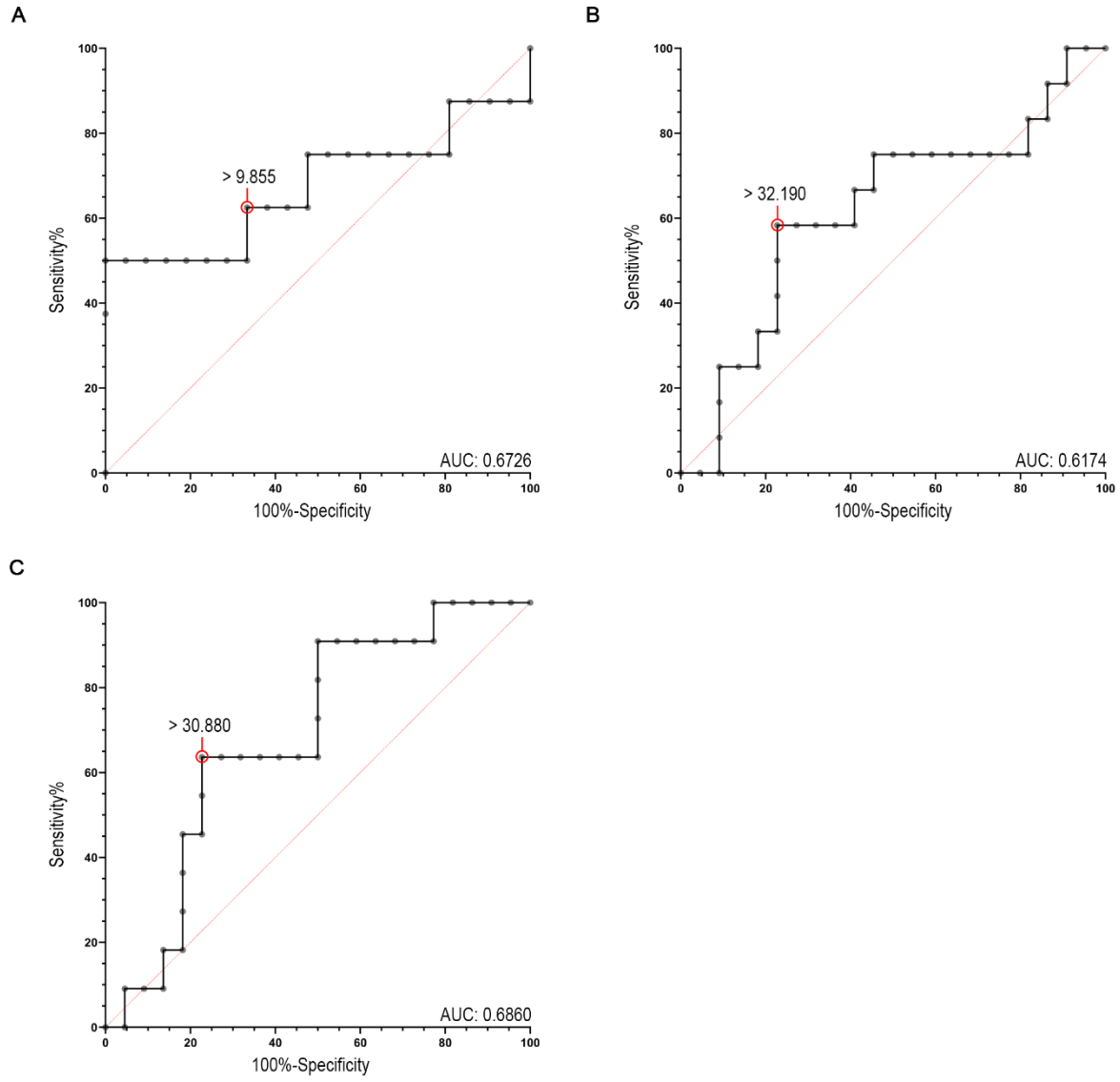

FIGURE A. 31. NUCLEAR P62 EXPRESSION IN THE TUMOUR GROWTH FRONT BEST PREDICTS A CSCC EVENT OCCURRING IN WELL-DIFFERENTIATED PRIMARY CSCC TUMOURS.

*(**A**) Receiver operating characteristic (ROC) curve for prediction of a cSCC event (reoccurrence/metastasis) based on the nuclear p62 H-score in the peritumoural epidermis of well-differentiated primary cSCC tumours (n=29). The p62 H-score with the highest specificity and sensitivity is highlighted by a red circle. AUC = area under the curve. (**B**) Receiver operating characteristic (ROC) curve for prediction of a cSCC event (recurrence/metastasis) s based on the nuclear p62 H-score in the tumour mass of well-differentiated primary cSCC tumours (n=34). The p62 H-score with the highest specificity and sensitivity is highlighted by a red circle. AUC = area under the curve. (**C**) Receiver operating characteristic (ROC) curve for prediction of a cSCC event (recurrence/metastasis) based on the nuclear p62 H-score in the tumour growth front of well-differentiated primary cSCC tumours (n=33). The p62 H-score with the highest specificity and sensitivity is highlighted by a red circle. AUC = area under the curve.*

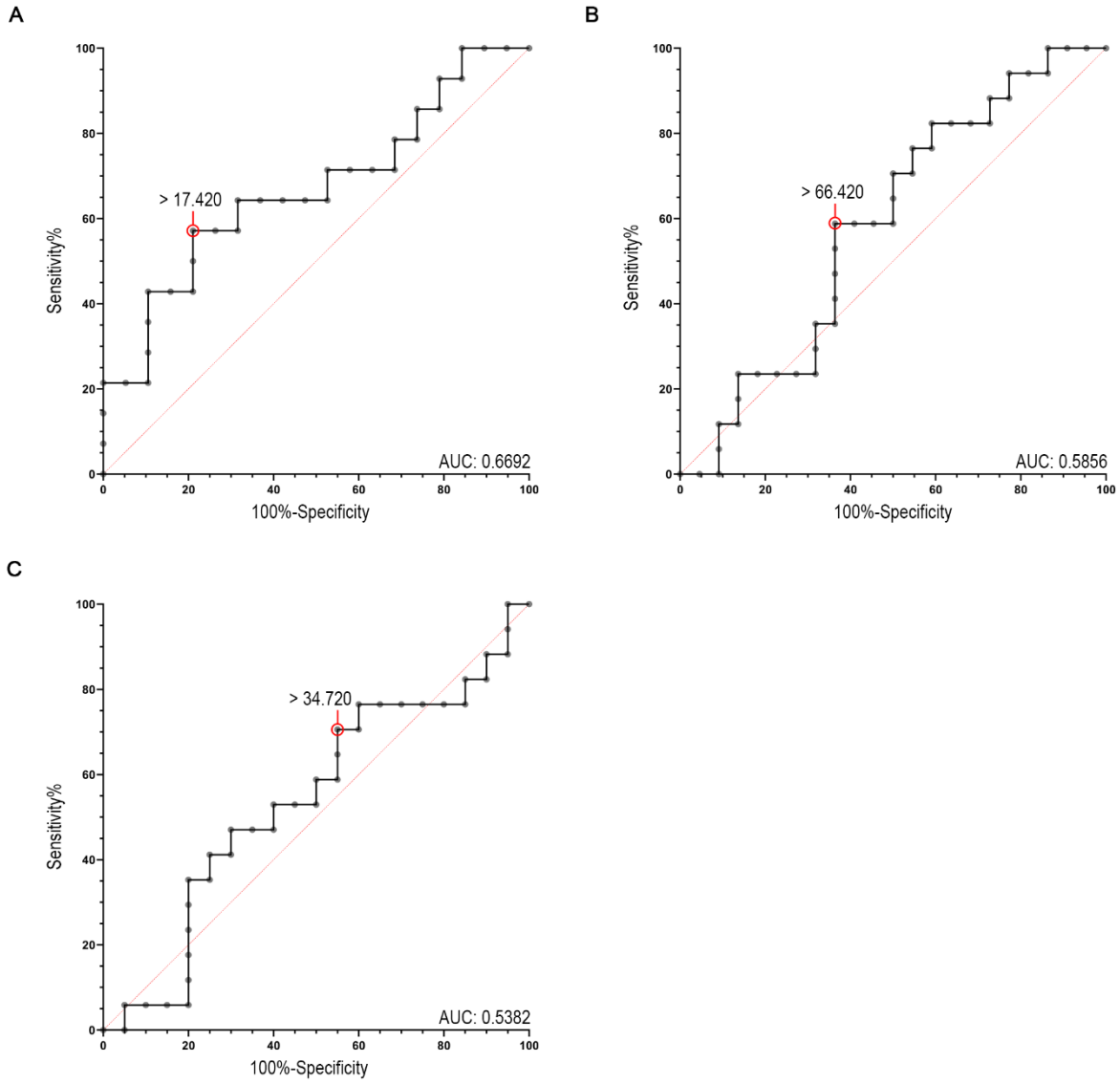

FIGURE A. 32. NUCLEAR P62 EXPRESSION IN THE PERITUMOURAL EPIDERMIS BEST PREDICTS A CSCC EVENT OCCURRING IN MODERATELY-DIFFERENTIATED PRIMARY CSCC TUMOURS.

*(**A**) Receiver operating characteristic (ROC) curve for prediction of a cSCC event (reoccurrence/metastasis) based on the nuclear p62 H-score in the peritumoural epidermis of moderately-differentiated primary cSCC tumours (n=33). The p62 H-score with the highest specificity and sensitivity is highlighted by a red circle. AUC = area under the curve. (**B**) Receiver operating characteristic (ROC) curve for prediction of a cSCC event (recurrence/metastasis) based on the nuclear p62 H-score in the tumour mass of moderately-differentiated primary cSCC tumours (n=39). The p62 H-score with the highest specificity and sensitivity is highlighted by a red circle. AUC = area under the curve. (**C**) Receiver operating characteristic (ROC) curve for prediction of a cSCC event (recurrence/metastasis) based on the nuclear p62 H-score in the tumour growth front of moderately-differentiated primary cSCC tumours (n=37). The p62 H-score with the highest specificity and sensitivity is highlighted by a red circle. AUC = area under the curve.*

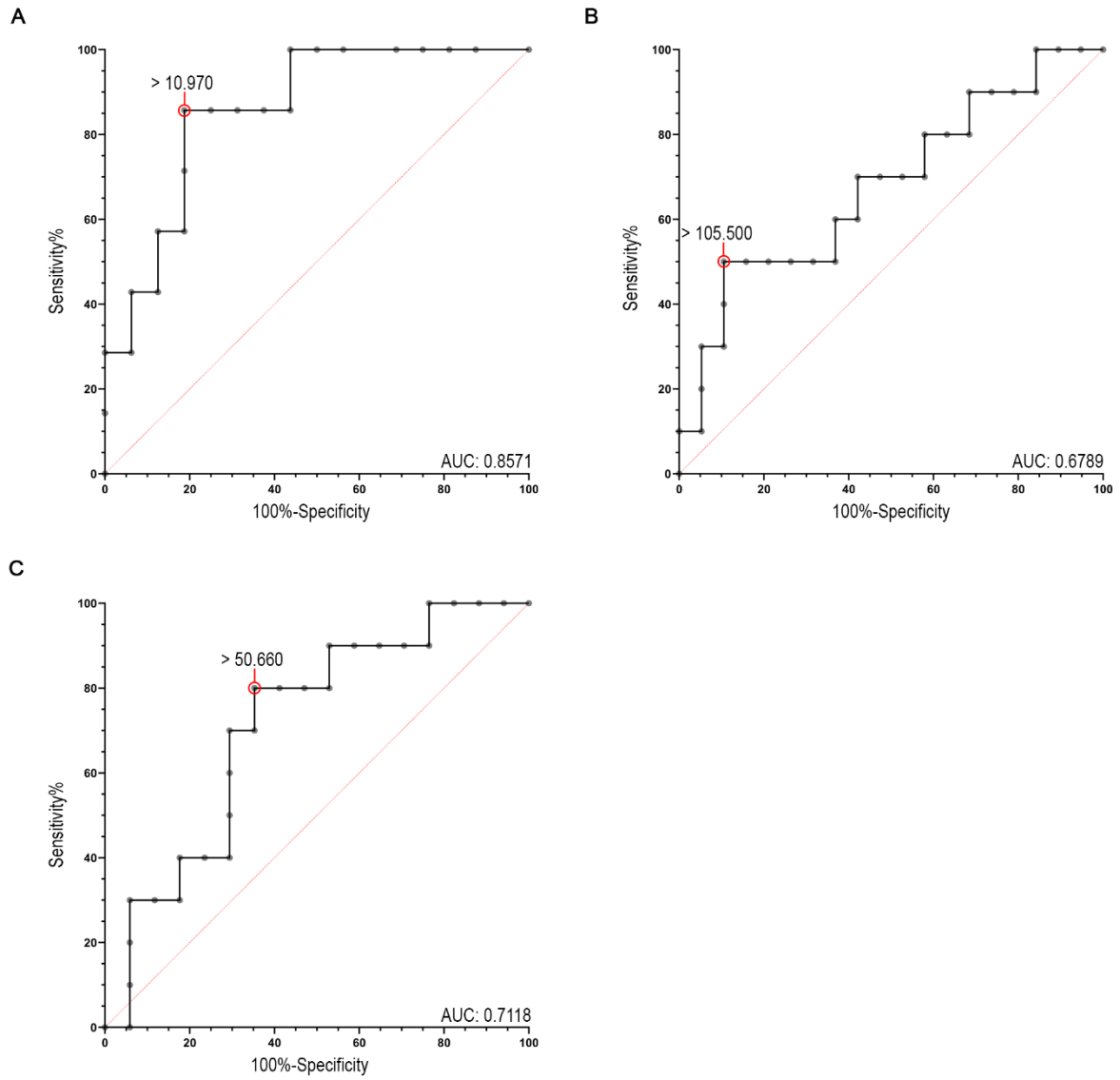

FIGURE A. 33. NUCLEAR P62 EXPRESSION IN THE PERITUMOURAL EPIDERMIS BEST PREDICTS A CSCC EVENT OCCURRING IN POORLY-DIFFERENTIATED PRIMARY CSCC TUMOURS.

*(**A**) Receiver operating characteristic (ROC) curve for prediction of a cSCC event (reoccurrence/metastasis) based on the nuclear p62 H-score in the peritumoural epidermis of poorly-differentiated primary cSCC tumours (n=23). The p62 H-score with the highest specificity and sensitivity is highlighted by a red circle. AUC = area under the curve. (**B**) Receiver operating characteristic (ROC) curve for prediction of a cSCC event (recurrence/metastasis) based on the nuclear p62 H-score in the tumour mass of poorly-differentiated primary cSCC tumours (n=29). The p62 H-score with the highest specificity and sensitivity is highlighted by a red circle. AUC = area under the curve. (**C**) Receiver operating characteristic (ROC) curve for prediction of a cSCC event (recurrence/metastasis) based on the nuclear p62 H-score in the tumour growth front of poorly-differentiated primary cSCC tumours (n=27). The p62 H-score with the highest specificity and sensitivity is highlighted by a red circle. AUC = area under the curve.*

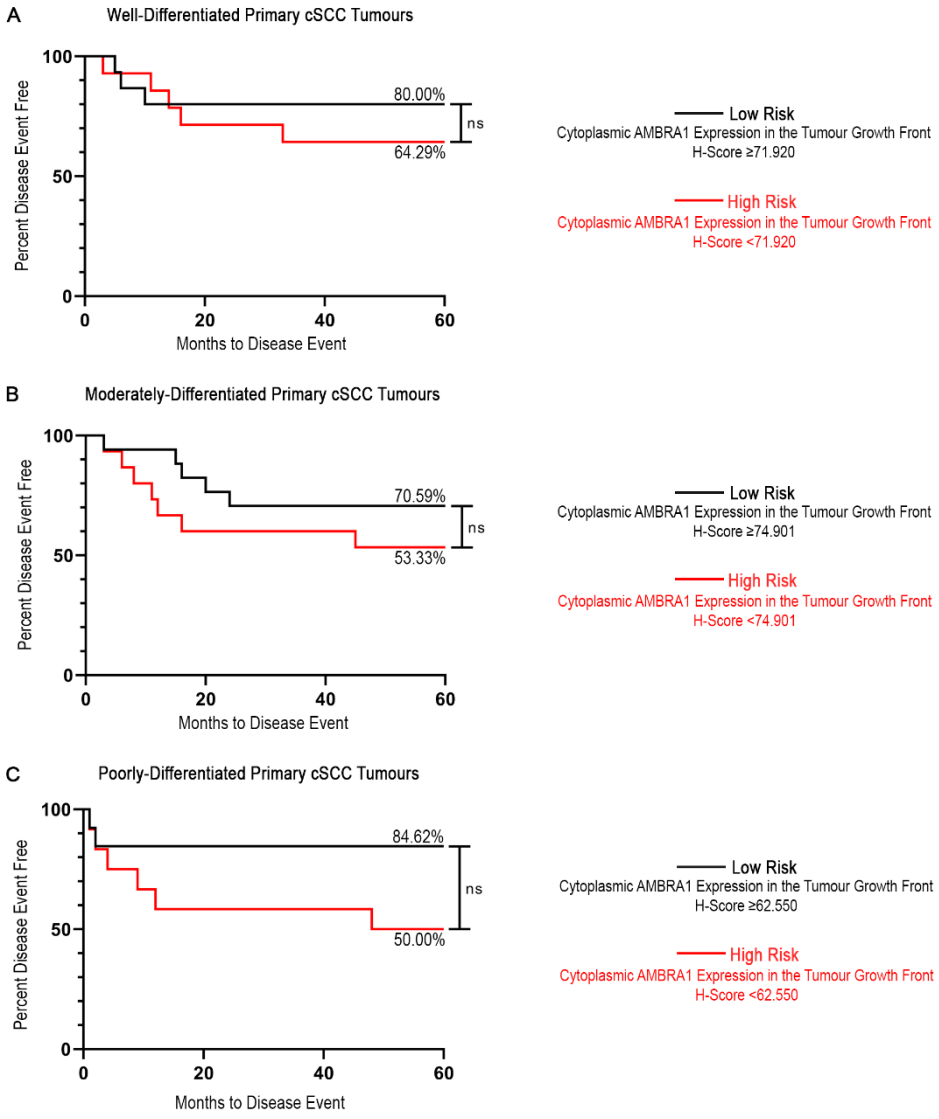

FIGURE A. 34. CYTOPLASMIC AMBRA1 EXPRESSION IN THE TUMOUR GROWTH FRONT ALONE IS UNABLE TO IDENTIFY HIGH RISK WELL, MODERATELY OR POORLY DIFFERENTIATED CSCC TUMOUR SUBSETS.

*(**A**) Kaplan-Meier survival analysis representing 60-month disease event free rate in 29 primary cSCC tumours stratified as low risk (n=15) and high risk (n=14) groups based on cytoplasmic AMBRA1 expression in the tumour growth front region. (**B**) Kaplan-Meier survival analysis representing 60-month disease event free rate in 32 primary cSCC tumours stratified as low risk (n=17) and high risk (n=15) groups based on cytoplasmic AMBRA1 expression in the tumour growth front region. (**C**) Kaplan-Meier survival analysis representing 60-month disease event free rate in 25 primary cSCC tumours stratified as low risk (n=13) and high risk (n=12) groups based on cytoplasmic AMBRA1 expression in the tumour growth front region. Statistics acquired by Mantel-Cox log-rank test and Mantel-Haenszel test (ns=non-significant).*

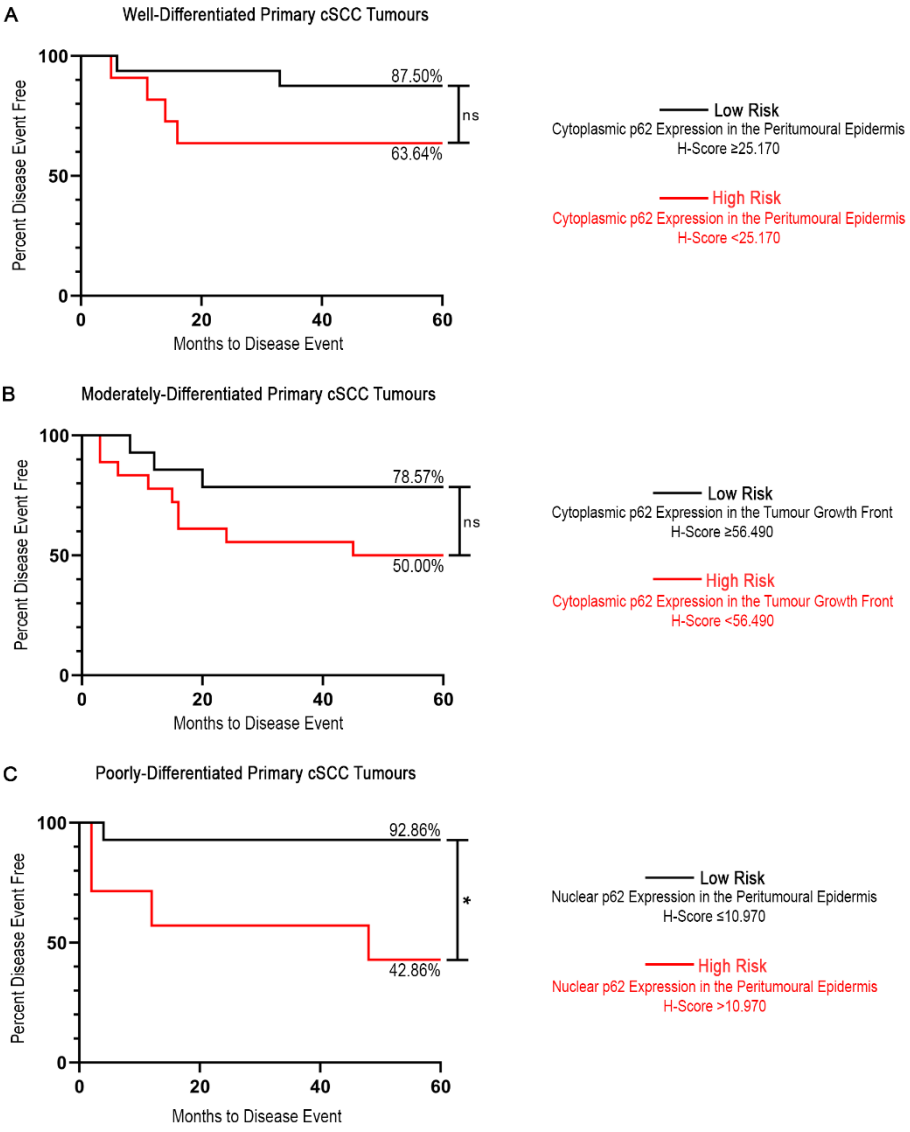

FIGURE A. 35. ONLY NUCLEAR P62 EXPRESSION IN POORLY-DIFFERENTIATED CSCC TUMOURS IS ABLE TO STRATIFY CSCC PATIENTS BASED ON DISEASE OUTCOME.

*(**A**) Kaplan-Meier survival analysis representing 60-month disease event free rate in 27 primary cSCC tumours stratified as low risk (n=16) and high risk (n=11) groups based on cytoplasmic p62 expression in the peritumoural epidermis. (**B**) Kaplan-Meier survival analysis representing 60-month disease event free rate in 32 primary cSCC tumours stratified as low risk (n=14) and high risk (n=18) groups based on cytoplasmic p62 expression in the tumour growth front region. (**C**) Kaplan-Meier survival analysis representing 60-month disease event free rate in 21 primary cSCC tumours stratified as low risk (n=14) and high risk (n=7) groups based on nuclear p62 expression in the peritumoural epidermis. Statistics acquired by Mantel-Cox log-rank test and Mantel-Haenszel test (ns=non-significant) (*P<0.05).*

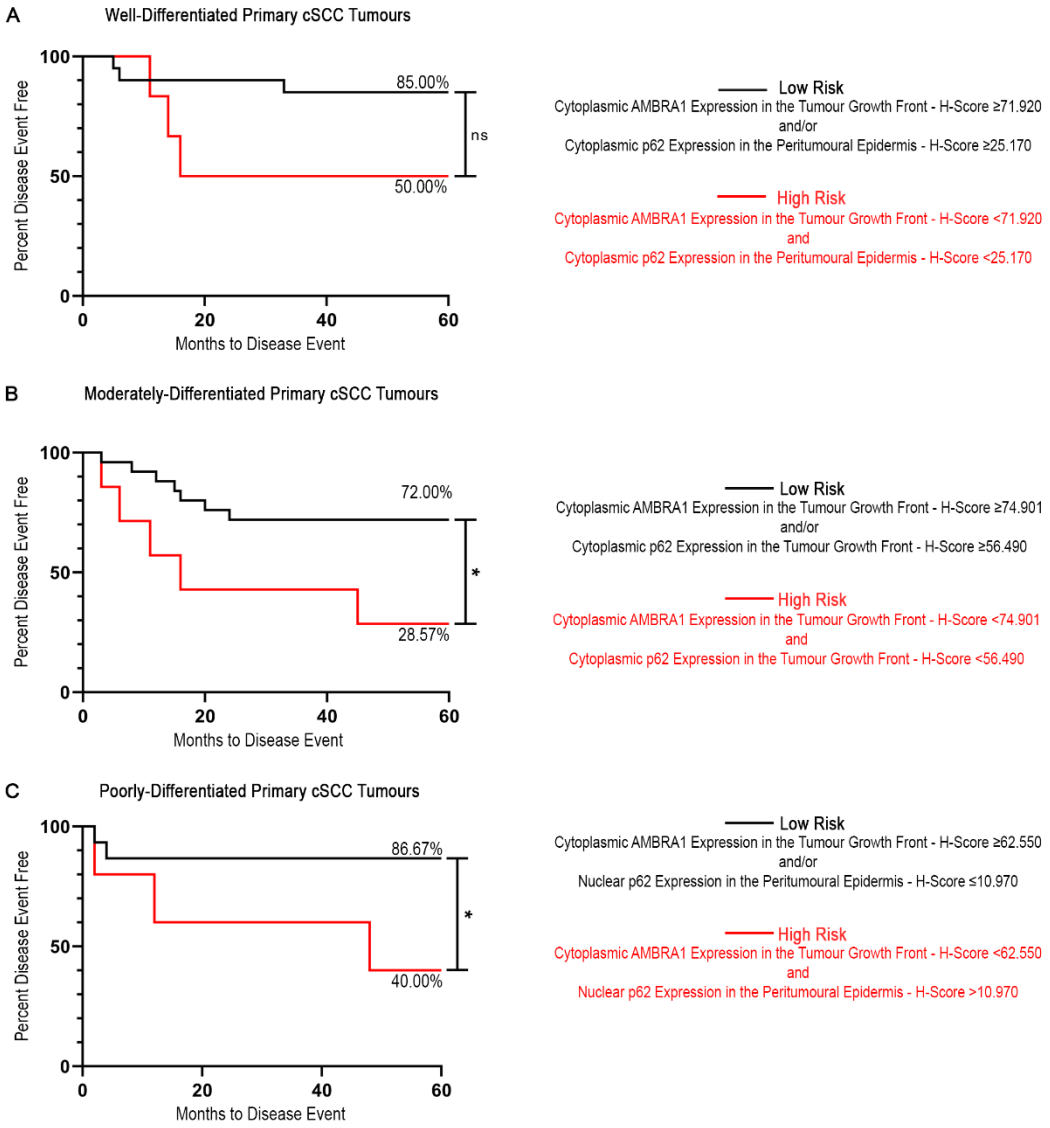

FIGURE A. 36. COMBINED TUMOUR GROWTH FRONT AMBRA1 AND PERITUMOURAL P62 EXPRESSION IS A PUTATIVE PROGNOSTIC BIOMARKER FOR MODERATELY AND POORLY DIFFERENTIATED CSCCS.

*(**A**) Kaplan-Meier survival analysis representing 60-month disease event free rate in 26 primary cSCC tumours stratified as low risk (n=20) and high risk (n=6) groups based on cytoplasmic AMBRA1 expression in the tumour growth front region and cytoplasmic p62 expression in the peritumoural epidermis. (**B**) Kaplan-Meier survival analysis representing 60-month disease event free rate in 32 primary cSCC tumours stratified as low risk (n=25) and high risk (n=7) groups based on cytoplasmic AMBRA1 expression in the tumour growth front region and cytoplasmic p62 expression in the tumour growth front region. (**C**) Kaplan-Meier survival analysis representing 60-month disease event free rate in 20 primary cSCC tumours stratified as low risk (n=15) and high risk (n=5) groups based on cytoplasmic AMBRA1 expression in the tumour growth front region and nuclear p62 expression in the peritumoural epidermis. Statistics acquired by Mantel-Cox log-rank test and Mantel-Haenszel test (ns=non-significant) (*P<0.05).*

List of Published Manuscripts and Abstracts arising from this Thesis

Abstracts

Michael Alexander, Jane Armstrong, Akhtar Husain, Niki Stefanos, Ashleigh McConnell, Rob Ellis, Marie Labus and Penny Lovat.
Defining the potential of AMBRA1 as a prognostic biomarker for cutaneous Squamous Cell Carcinoma.
British Journal of Dermatology, 2019. 180, 183-e215.
British Society of Investigative Dermatologists Annual Meeting, Bradford, UK (April 2019), Oral Presentation.

Michael Alexander, Jane Armstrong, Akhtar Husain, Niki Stefanos, Ashleigh McConnell, Rob Ellis, Marie Labus and Penny Lovat.
Defining the Impact of TGF-β Signalling on AMBRA1 Expression and cSCC Progression.
British Society of Investigative Dermatologists Annual Meeting, Cardiff, UK (March 2021), Poster Presentation